PhD Thesis

Tribological and Vibro-acoustic Behaviour of a Lubricated Contact Subjected to the Stick-Slip Phenomenon: The Case of the Spring-Brake System

Jointly awarded at the

Institut National des Sciences Appliquées de Lyon, École doctorale N°162:
Mécanique, Energétique, Génie Civil, Acoustique (MEGA)
Spécialité: Génie Mécanique

and at the

La Sapienza - Università di Roma
Dottorato di ricerca in Meccanica Teorica e Applicata XXXIII ciclo

By

Ilaria Ghezzi

On December 14th, 2020

PhD Committee:

Reviewer	N. Hoffmann,	Professor	Hamburg University of Technology
Reviewer	A. Meziane,	Professor	Université de Bordeaux
Examiner	M. Fillon,	Research Director	Institut Pprime, CNRS
Examiner	L. Baillet,	Professor	Université Grenoble Alpes-IsTerre
Co-director	Y. Berthier,	Research Director	CNRS Lyon
Co-director	F. Massi,	Professor	La Sapienza – Università di Roma
Invited	C. Le Cœur,	Engineer	SOMFY SASA
Invited	D. Tonazzi,	Ph.D.	La Sapienza – Università di Roma

Département FEDORA – INSA Lyon - Ecoles Doctorales – Quinquennal 2016-2020

SIGLE	ECOLE DOCTORALE	NOM ET COORDONNEES DU RESPONSABLE
CHIMIE	**CHIMIE DE LYON** http://www.edchimie-lyon.fr Sec. : Renée EL MELHEM Bât. Blaise PASCAL, 3e étage secretariat@edchimie-lyon.fr INSA : R. GOURDON	**M. Stéphane DANIELE** Institut de recherches sur la catalyse et l'environnement de Lyon IRCELYON-UMR 5256 Équipe CDFA 2 Avenue Albert EINSTEIN 69 626 Villeurbanne CEDEX directeur@edchimie-lyon.fr
E.E.A.	**ÉLECTRONIQUE, ÉLECTROTECHNIQUE, AUTOMATIQUE** http://edeea.ec-lyon.fr Sec. : M.C. HAVGOUDOUKIAN ecole-doctorale.eea@ec-lyon.fr	**M. Gérard SCORLETTI** École Centrale de Lyon 36 Avenue Guy DE COLLONGUE 69 134 Écully Tél : 04.72.18.60.97 Fax 04.78.43.37.17 gerard.scorletti@ec-lyon.fr
E2M2	**ÉVOLUTION, ÉCOSYSTÈME, MICROBIOLOGIE, MODÉLISATION** http://e2m2.universite-lyon.fr Sec. : Sylvie ROBERJOT Bât. Atrium, UCB Lyon 1 Tél : 04.72.44.83.62 INSA : H. CHARLES secretariat.e2m2@univ-lyon1.fr	**M. Philippe NORMAND** UMR 5557 Lab. d'Ecologie Microbienne Université Claude Bernard Lyon 1 Bâtiment Mendel 43, boulevard du 11 Novembre 1918 69 622 Villeurbanne CEDEX philippe.normand@univ-lyon1.fr
EDISS	**INTERDISCIPLINAIRE SCIENCES-SANTÉ** http://www.ediss-lyon.fr Sec. : Sylvie ROBERJOT Bât. Atrium, UCB Lyon 1 Tél : 04.72.44.83.62 INSA : M. LAGARDE secretariat.ediss@univ-lyon1.fr	**Mme Sylvie RICARD-BLUM** Institut de Chimie et Biochimie Moléculaires et Supramoléculaires (ICBMS) - UMR 5246 CNRS - Université Lyon 1 Bâtiment Curien - 3ème étage Nord 43 Boulevard du 11 novembre 1918 69622 Villeurbanne Cedex Tel : +33(0)4 72 44 82 32 sylvie.ricard-blum@univ-lyon1.fr
INFOMATHS	**INFORMATIQUE ET MATHÉMATIQUES** http://edinfomaths.universite-lyon.fr Sec. : Renée EL MELHEM Bât. Blaise PASCAL, 3e étage Tél : 04.72.43.80.46 infomaths@univ-lyon1.fr	**M. Hamamache KHEDDOUCI** Bât. Nautibus 43, Boulevard du 11 novembre 1918 69 622 Villeurbanne Cedex France Tel : 04.72.44.83.69 hamamache.kheddouci@univ-lyon1.fr
Matériaux	**MATÉRIAUX DE LYON** http://ed34.universite-lyon.fr Sec. : Stéphanie CAUVIN Tél : 04.72.43.71.70 Bât. Direction ed.materiaux@insa-lyon.fr	**M. Jean-Yves BUFFIÈRE** INSA de Lyon MATEIS - Bât. Saint-Exupéry 7 Avenue Jean CAPELLE 69 621 Villeurbanne CEDEX Tél : 04.72.43.71.70 Fax : 04.72.43.85.28 jean-yves.buffiere@insa-lyon.fr
MEGA	**MÉCANIQUE, ÉNERGÉTIQUE, GÉNIE CIVIL, ACOUSTIQUE** http://edmega.universite-lyon.fr Sec. : Stéphanie CAUVIN Tél : 04.72.43.71.70 Bât. Direction mega@insa-lyon.fr	**M. Jocelyn BONJOUR** INSA de Lyon Laboratoire CETHIL Bâtiment Sadi-Carnot 9, rue de la Physique 69 621 Villeurbanne CEDEX jocelyn.bonjour@insa-lyon.fr
ScSo	**ScSo*** http://ed483.univ-lyon2.fr Sec. : Véronique GUICHARD INSA : J.Y. TOUSSAINT Tél : 04.78.69.72.76 veronique.cervantes@univ-lyon2.fr	**M. Christian MONTES** Université Lyon 2 86 Rue Pasteur 69 365 Lyon CEDEX 07 christian.montes@univ-lyon2.fr

*ScSo : Histoire, Géographie, Aménagement, Urbanisme, Archéologie, Science politique, Sociologie, Anthropologie

Acknowledgements

This thesis has been developed in the framework of the collaboration between the INSA of Lyon, La Sapienza-University of Rome and the company SOMFY; my first thanks goes then to the institutions and the company which have supported this research and to the French National Association of Research and Technology (ANRT) for its support to this work through the CIFRE convention N. 2017/0998. I would like to warmly thank my Italian and French supervisors and co-supervisors: Professor Francesco Massi, Dr. Davide Tonazzi and Professor Yves Berthier for their professional guidance and help. I would like also to express also my gratitude to Francesco Massi for his encouragement and for the constant support. Sincere thanks go to my industrial supervisor Cedric Le Coeur and to Jeremy Chorier and Michael Rovere for their careful supervisor, for their collaboration and contribution to the research work during these years. Sincere thanks go also to the reviewers and all the Ph.D committee, Professor Norbert Hoffmann, Professor Anissa Meziane, Professor Michel Fillon and Professor Laurent Baillet for their comments, suggestions and questions that allowed for improving this work. I would like to finish extending my greeting to all friends, colleagues, professors, people that I had the opportunity and pleasure to meet during these years, at the LaMCoS at the DIMA as well as at the company SOMFY. Special thanks go to Davide, Alessandro, Riccardo, Gael, Francesco Adriana, Lucas, Pierrick, Gregorio, with them I felt like home anywhere. Concluding, a last but certainly not least thanks to my family to whom this thesis is dedicated.

Cotutelle agreements

ACCORD DE COOPERATION POUR LA MISE EN ŒUVRE D'UNE COTUTELLE DE THESE

L'Université de Rome "La Sapienza" ayant son siège à Rome (Italie), Piazzale Aldo Moro 5, représentée par son Recteur Professeur Eugenio GAUDIO agissant en-qualité et en vertu des pouvoirs qui lui sont conférés d'une part

ET

L'INSA de LYON, représenté par Monsieur Eric MAURINCOMME, Directeur de l'établissement, agissant en-qualités et en vertu des pouvoirs qui lui sont conférés, d'autre part

Pour la partie italienne :

- Vue la délibération du Sénat Académique du 2 octobre 2003 ;
- Vue la Loi 240/2010 art. 19 – dottorato di ricerca;
- Vu le D.M. 45/2013 relatif aux normes en matière de doctorat de recherche ;
- Vu le Règlement de l'Université en matière de doctorat de recherche ;

ET

Vu pour la part française :

- Vu le code de l'éducation, notamment ses articles L.612-7, L. 613-1, D. 613-3, D. 613-6, D613-18 et D613-19 ;
- Vu le code de la recherche, notamment son article L.412-1 ;
- Vu le décret n° 2015-127 du 5 février 2015 portant approbation des statuts de la communauté d'universités et établissements « Université de Lyon »
- Vu l'arrêté du 25 mai 2016 fixant le cadre national de la formation et les modalités conduisant à la délivrance du diplôme national de doctorat
- Vu la charte du doctorat de l'Université de Lyon avec avenant INSA Lyon
- La convention cadre franco-italienne entre la Conférence des Présidents d'Université (CPU) et la Conferenza dei Rettori delle Università Italiane (CRUI) sur la reconnaissance des diplômes et validation des titres universitaires signée en date 18 janvier 1996;
- La convention cadre franco-italienne entre la Conférence des Présidents d'Université (CPU) e la Conferenza dei Rettori delle Università Italiane (CRUI) sur la co-tutelle de thèse signée le 13 février 1998;

désireux de contribuer à l'instauration et/ou au développement de la coopération scientifique entre équipes de recherche italiennes et étrangères en favorisant la mobilité des doctorants, sont convenu(e)s des dispositions suivantes :

Titre I – Modalités administratives

Art. 1 – L'Université de Rome "La Sapienza" et L'INSA de Lyon désignées ci-après "les établissements", décident dans le respect des lois et des règlements en vigueur dans chacun des pays et/ou établissements, d'organiser conjointement une cotutelle de thèse au bénéfice de l'étudiante désigné ci-après:
Prénom et nom : Ilaria GHEZZI
Spécialité : Ingenieur Mecanique – Doctorat en Meccanica Teorica ed Applicata
Sujet de thèse : **Etude du comportement tribologique et vibro-acoustique d'un frein à ressort pour moteurs électriques tubulaires**

La dynamique d'un contact frottant est une problématique ancienne, mettant en jeu plusieurs disciplines comme la tribologie, la mécanique vibratoire ou la mécanique de la rupture. Une branche importante des problématiques scientifiques et industrielles est liée aux instabilités vibratoires engendrées par les contacts. Dans plusieurs disciplines et champs d'applications, l'analyse et les contrôles des instabilités de contact, telles que le « stick-slip » macroscopique et le couplage modal, est un sujet au cœur de la recherche actuelle. Ces phénomènes vibratoires, souvent non désirés car avec des répercussions négatives, sont les résultats des différents phénomènes physiques ayant lieu à l'échelle du contact et à celle du système, et dont les couplages complexes nécessitent une phase de compréhension. Dans ce contexte, ce travail de thèse propose de comparer et d'approfondir ces approches afin de proposer une méthodologie de prise en compte du couplage entre la dynamique du système frein à ressort et les interfaces flottantes des contacts entre le ressort à spires circulaires et le cylindre du frein, ainsi que l'ensemble des contacts concernés par le fonctionnement du frein. Les objectifs scientifiques de ce travail sont de deux ordres. Dans un premier temps, l'analyse des interfaces de contact ainsi que les mesures vibratoires du système mettront en évidence les interactions entre les conditions de chargement à l'échelle locale et la réponse acoustique du système. Ensuite, la formalisation et la simulation de ces interactions seraient une avancée majeure dans la prédiction des émissions acoustiques induites par un contact frottant. L'objectif central de la thèse est donc d'identifier et de formaliser le comportement tribologique et dynamique du système « frein à ressort » des moteurs tubulaires, afin d'identifier l'origine des bruits induits par les contacts.

- Contexte de l'étude :

o Conditions de financement :
La doctorante est salariée dans le cadre de la convention de formation par la recherche CIFRE n° 2017/0998 (France).

o Calendrier préliminaire du projet de recherche est indiqué pour les trois années :
La première année sera dédiée à l'étude bibliographique du comportement tribologique et vibro-acoustique de systèmes mécaniques proches du système concerné, accompagné par des simulations numériques préliminaires et caractérisations expérimentales.
La deuxième année, des simulations numériques du comportement tribologique du système frein seront accompagné par des campagnes d'essais expérimentales afin d'aider l'interprétation des données expérimentales.
La troisième année sera dédiée à la validation des scenarios des instabilités dynamiques identifiées et la validation des propositions de design sur frein, puis actionneur complet. Les derniers six mois seront principalement dédiés à la rédaction du manuscrit de thèse.

o Les modalités d'encadrement, de suivi de la formation et d'avancement du doctorant :
Les rencontres avec les directeurs de thèse (Francesco MASSI et Yves BERTHIER) auront une périodicité d'une fois toutes les deux semaines minimum. Tout le longue de la durée de la thèse le doctorant produira des rapports et présentations intermédiaires pour le suivi du travail. Chaque année, une présentation en face du collège des professeurs du doctorat en « Meccanica Teorica ed Applicata » est obligatoire pour l'inscription à l'année suivante.

o Conditions matérielles de réalisation du projet :
Le projet sera développé principalement sur les sites du LaMCoS de l'INSA de Lyon et du département DIMA de l'Université de Rome La Sapienza. Les bancs d'essais, déjà présents dans le locaux des deux établissements, seront dédiés à l'exécution des campagnes

expérimentales, Une ordinateur et les licences des codes numériques nécessaires seront mise à disposition du doctorant.

Les principes et les modalités administratives et pédagogiques de cette cotutelle sont définis par le présent accord.

Art. 2 - La durée de préparation de la thèse est normalement de trois ans. La durée de préparation du doctorat peut être au plus de six ans.
Un avenant sera rédigé au moins 6 mois avant la date de fin prévue initialement. Des périodes de recherche alternées auront lieu dans chacun des établissements. Le calendrier et la durée des séjours seront détaillés à l'article 8 de la présente convention. La durée minimale de préparation effectuée dans un établissement ne peut normalement être inférieure à une année.
La durée prévue pour la préparation de la thèse en cotutelle est de 3 ans, à partir de l'année scolaire 2017/2018

Art. 3 - La préparation de la thèse s'effectue par périodes alternées, à peu près équivalentes, dans chacun des deux établissements partenaires. La durée de ces périodes sera déterminée de commun accord par les deux directeurs de thèse.

Art. 4 – Le (la) doctorant(e) est inscrit(e) en thèse dans chacun des deux établissements co-contractants sous le régime de la collaboration internationale à partir de l'année universitaire **2017-2018**.
Le doctorant sera inscrit administrativement dans chacun des deux établissements dès que toutes les conditions nécessaires à son inscription seront réunies.
Le (la) doctorant(e) est inscrit(e) en thèse de doctorat de l'Université de Lyon, opéré au sein de l'INSA Lyon, au sein de l'Ecole Doctorale MEGA à compter de la rentrée universitaire 2017-2018.

Art.5 – Le (la) doctorant(e) acquitte, chaque année, ses droits d'inscription dans un des établissements. Il est exempté de ces droits dans l'autre établissement. Sur la durée de la thèse, la doctorante doit obligatoirement s'acquitter de ses droits d'inscription au moins une fois dans chaque établissement; l'acquittement desdits droits est une condition de validité de la cotutelle internationale. Le doctorant doit fournir chaque année les justificatifs d'inscription, s'ils existent, en doctorat à l'établissement pour lequel il en est exonéré.

Art.6 – Le (la) doctorant(e) est soumis à la réglementation en vigueur sur la couverture sociale dans le pays où il acquitte les droits d'inscription. Dans celui où il est exonéré, il doit justifier également d'une couverture analogue, et doit en produire les justificatifs au moment de son inscription administrative dans chaque établissement. Il s'engage par ailleurs à souscrire une « responsabilité civile vie privée » obligatoire en France. Ces assurances conditionnent l'inscription administrative.
Une assurance couvrant ses déplacements entre les deux pays est par ailleurs vivement conseillée.

Art.7 – Lors de son inscription, le (la) doctorant(e) devra fournir les justificatifs relatifs à ses ressources, à sa couverture sociale ainsi qu'à son assurance relative aux accidents du travail, dans chacun des pays,
Conformément à la Charte du Doctorat de l'UdL avec avenant INSA, un revenu minimum pendant les périodes de séjour en France, conforme à celui mentionné dans la Charte du

doctorat conditionne l'inscription en doctorat à l'INSA Lyon. Ce revenu doit être au moins équivalent au SMIC.
Dans le cas où le (la) doctorant(e) serait dans l'incapacité de présenter les justificatifs de financement nécessaires à son inscription, l'INSA Lyon pourra prononcer de plein droit la résiliation de la présente convention.

Art. 8 –Pour les périodes d'études effectuées en France et pour la soutenance, la doctorante bénéficie de l'ensemble des dispositions de l'arrêté du 7 août 2006 susvisé, et de la charte des thèses de l'INSA de Lyon.

Titre II – Modalités pédagogiques

Art. 1 – Le travail de thèse de l'étudiante sera réalisé sous la supervision commune de deux directeurs de thèse :

- Francesco MASSI (Professeur au Dipartimento di Ingegneria Meccanica e Aerospaziale), directeur de thèse à l'Université "La Sapienza" ;
- Yves BERTHIER (Professeur au Laboratoire de Mécanique des Contacts et des Structures), directeur de thèse à l' INSA de Lyon ;

qui s'engagent à exercer pleinement la fonction de tuteurs de la candidate ainsi qu'à formuler chacun un avis écrit sur la thèse de Doctorat.
L'avis favorable des deux Directeurs de Thèse est une condition nécessaire à l'admission à l'examen final.

Art. 2- La thèse donnera lieu à une soutenance unique, reconnue par les deux établissements concernés. La soutenance aura lieu à l'INSA de Lyon. Le jury de soutenance est composé sur la base d'une proportion équilibrée de membres de chaque établissement désigné conjointement par les établissements contractants et comprend, en outre, des personnalités extérieures à ces établissements. Il comprendra au moins quatre membres et au maximum huit, dont la moitié au moins sont des personnalités extérieures aux établissements signataires de la cotutelle. Les autres membres sont désignés sur la base d'une proportion équilibrée de membre de chaque établissement désigné conjointement par les établissements contractants. La parité homme/femme devra se conformer aux conditions requises par les deux établissements contractants. Conformément à l'arrêté du 25 mai 2016, "le directeur de thèse participe au jury, mais ne prend pas part à la décision". Le directeur de thèse, comme les co-encadrants, n'ont pas à sortir pendant les délibérations, ils peuvent prendre part aux discussions préliminaires mais doivent s'abstenir lors de la délibération et du vote final.

Art. 3 - La thèse sera rédigée et discutée en Anglais. Elle comportera un résumé substantiel rédigé en Français et en Italien.

Art. 4 – En cas de rapport favorable du Jury, chacun des deux établissements s'engage à conférer le titre de docteur de recherche pour la même thèse.
L'Université de Rome "La Sapienza" s'engage à conférer le grade de docteur de recherche en en Meccanica Teorica e Applicata.
L'INSA de Lyon s'engage à conférer le grade de docteur de recherche en Mécanique.

Art. 5- Lorsque le (la) doctorant(e) doit valider des formations complémentaires (scientifiques ou visant à son insertion professionnelle), les établissements (l'Ecole Doctorale (nom) pour l'INSA LYON) préciseront les modalités de reconnaissance mutuelle de ces formations, en

accord avec les directeurs de thèse et le doctorant. Les obligations de formation pour l'ED MEGA seront au prorata de la durée des séjours prévus dans le laboratoire de l'INSA Lyon, avec au minimum : au moins 14 heures de formation scientifique et au moins 10 heures de formation à l'insertion professionnelle. Le volume total de formation est de 20 heures.

Titre III – Conclusions

Art. 1 – L'étudiante est tenue de respecter les règlements et les usages de l'établissement d'accueil.

Art. 2 – Par l'intermédiaire de leurs directeurs de thèses respectifs, les établissements signataires s'engagent à se communiquer toutes les informations et la documentation utiles à l'organisation de la cotutelle de thèse faisant l'objet du présent accord.

Art. 3 – Les modalités de présentation, de dépôt et de reproduction de la thèse seront établies dans chaque pays dans le respect de la réglementation en vigueur.
La protection du sujet de thèse, ainsi que la publication, l'exploitation et la protection des résultats issus des travaux de recherche du doctorant dans les deux établissements signataires seront assujetties à la réglementation en vigueur et assurées conformément aux procédures spécifiques à chacun des pays impliqués dans la cotutelle.
Sur demande, les dispositions concernant la protection des droits de propriété intellectuelle pourront faire l'objet de protocoles ou de documents spécifiques.

Art. 4 – Le présent accord entre en vigueur à partir de la date de signature du représentant légal de chaque établissement signataire et le reste jusqu'à la fin de l'année universitaire au cours de laquelle la thèse ou les travaux seront soutenus. Dans le cas où l'étudiante ne serait pas inscrite dans l'un et/ou l'autre des établissements signataires, ou bien renoncerait par écrit à poursuivre, ou bien n'est pas autorisée à poursuivre la préparation de sa thèse en vertu de la décision de l'un au moins des deux directeurs de thèse, les deux établissements signataires mettront fin conjointement et sans délai, aux dispositions du présent accord.

Art. 5 – Le présent accord est rédigé en quatre exemplaires originaux, dont deux en italien et deux en française, faisant également foi.

Roma, li _____

Pour le Recteur de l'Université
La Sapienza de Rome

_____

Villeurbanne, li _____

Pour le directeur de l'INSA de Lyon
DR Marie Christine BAIETTO
Directrice Adjoint de la Recherche
Et des Etudes Doctorales

_____

Il Coordinatore del Dottorato di Ricerca
Antonio CARCATERRA

_____

Le Responsable de l'Ecole Doctorale
Philippe BOISSE

_____

Le Directeur du laboratoire
Daniel NELIAS

INSA de Lyon
Daniel NELIAS
Directeur
LaMCoS

_____

Il Co-direttore di tesi
Francesco MASSI

_____

Co-directeur (s) de thèse
Yves BERTHIER

_____

La Doctorante
Ilaria GHEZZI

_____

Tribological and Vibro-acoustic Behaviour of a Lubricated Contact Subjected to the Stick-Slip Phenomenon: The Case of the Spring-Brake System

Résume étendu

Ce travail a été développé dans le cadre de recherches sur les vibrations induites par le frottement, à cheval entre la mécanique du contact, la tribologie et la dynamique. En mécanique classique, le frottement est défini comme la force de réaction tangentielle qui se produit lorsqu'un corps glisse sur un autre corps. La définition peut être étendue au mouvement de deux corps solides séparés par un lubrifiant.
Toutefois, l'interaction locale à l'interface (impacts locaux et ruptures d'aspérités et jonctions) produit la libération d'énergie élastique sous forme d'ondes acoustiques, qui se propagent à la fois dans l'interface et à l'intérieur des solides en contact. Ces ondes se propagent depuis l'interface au volume des solides en mouvement relatif qui, à leur tour, répondent à cette excitation au contact en vibrant selon leur dynamique propre, produisant ainsi les vibrations induites par le frottement. La réponse dynamique du système peut à son tour modifier la réponse en termes de frottement du système. Les travaux présentés ici se focalisent sur un type particulier de vibrations induites par le frottement: le phénomène de stick-slip.
Tant dans la nature que dans les systèmes artificiels, il existe plusieurs exemples de stick-slip, à la fois dans le cas de contacts secs et lubrifiés. Tels que les sons produits par des instruments comme les violons et les violoncelles, le son produit lors du mouvement des pattes/ailes des sauterelles, les bruits produits lors du ponçage, le freinage brusque et le crissement des pneus ou de la craie sur un tableau noir, le mouvement progressif des glissières lesquelles , le bruit dérivant de vérins hydrauliques dans les simulateurs d'aéronef ou dérivant du filage dans la production textile sont quelques-uns des exemples les plus courants du phénomène de stick-slip. Le rôle du frottement et sa dépendance à la vitesse sont l'un des paramètres clés nécessaires pour comprendre ce phénomène.
Dans ce contexte, la présence d'un lubrifiant à l'interface entre les corps en contact peut, d'une part, améliorer les performances et la durée de vie du système mécanique, mais, d'autre part, augmenter la complexité et l'apparition d'instabilités des contacts, en ajoutant un paramètre difficile à maîtriser du point de vue tribologique et dynamique. En focalisant l'attention sur le phénomène du stick-slip dans les contacts lubrifiés, la compréhension de ce phénomène nécessite une approche multidisciplinaire et multi-échelles, qui prenne en considération les interactions complexes de divers phénomènes aux différentes échelles. A ce jour, l'intérêt scientifique et industriel croissant pour l'analyse de ces phénomènes a conduit à une forte croissance des travaux sur ce sujet, proposant différentes méthodes

d'analyse à la fois expérimentale et numérique. Ces travaux sont développés dans différentes disciplines, allant des sciences de la terre, de la physicochimie, à la mécanique appliquée. Cependant, la littérature présente un fort manque de travaux sur le comportement tribologique du contact lubrifié et sur la manière dont cela peut influencer directement la réponse vibrationnelle du système, étape fondamentale pour comprendre les conditions locales qui peuvent conduire à l'instabilité du stick-slip. De plus, lorsque le lubrifiant est une graisse, sa rhéologie complexe, fonction de l'épaississant, des additifs et de l'huile de base, devient un point clé pour analyser l'apparition et l'évolution du stick-slip. Une approche complémentaire est donc nécessaire pour prendre en compte le couplage entre le comportement local du contact (réponse en frottement du contact lubrifié) et la réponse dynamique et vibrationnelle du système.
Dans ce contexte, le travail présenté, développé dans le cadre de la collaboration entre SOMFY SASA, le laboratoire LaMCoS de l'INSA de Lyon et le Département de Mécanique Théorique et Appliquée (DIMA) de l'Université La Sapienza de Rome, propose une approche systématique du problème de stick-slip dans les contacts lubrifiés, et vise à améliorer la compréhension et à apporter des possibles solutions industrielles. Le travail a été développé en faisant référence à un cas industriel, afin d'analyser les résultats obtenus dans un contexte le plus réaliste possible. Le sujet est un frein à ressort mécanique, utilisé dans les actionneurs électriques tubulaires. Ces freins peuvent présenter une instabilité de frottement, générée par le contact graissé entre les deux composants principaux du frein (ressort de torsion et tambour).
Le travail a été divisé en trois parties principales, après documentation, la plus rigoureuse possible, de la littérature scientifique existante sur le sujet décrit ci-dessus: i) une analyse tribologique et dynamique de l'apparition du stick-slip dans les freins à ressort; ii) une analyse expérimentale du comportement de frottement local, en accordant une attention particulière au rôle de la rhéologie du lubrifiant; iii) une analyse numérique pour l'étude de la réponse dynamique du système mécanique.
En tenant compte de la production de plusieurs types de freins, des analyses tribologiques et dynamiques ont été effectuées sur des freins bruyants et silencieux. Ces analyses ont permis d'identifier que l'émission sonore du système de freinage est une conséquence du phénomène de stick-slip. En focalisant l'attention sur l'analyse du signal vibrationnel et sur la topographie des surfaces, les excitations impulsives périodiques, dues à la succession des phases d'adhérence et de glissement, au contact graissé entre le ressort et le tambour, conduisent à une excitation périodique de la dynamique du système et s'accompagnent de la présence de traces de mouvement axial du ressort.
Par ailleurs, il a été mis en évidence que l'apparition du stick-slip est prédominante après les premiers cycles de fonctionnement, c'est-à-dire lorsque le frein atteint des températures supérieures à la température ambiante, avec des valeurs de température interne égales à environ 80 °C. Les observations dynamiques et tribologiques sont reproductibles et caractéristiques de tous les freins bruyants analysés. De plus, l'ouverture

axial du ressort provoque un désalignement des composants, une modification de la raideur du ressort et une localisation de la pression de contact. Tous ces facteurs pourraient contribuer à l'apparition d'instabilité.
Comme expliqué précédemment, l'apparition de l'instabilité est due à l'interaction entre la dynamique du système et le comportement en frottement du contact au niveau local. Plusieurs paramètres peuvent affecter la réponse du système dynamique, tels que la charge normale, la vitesse, la rugosité de surface, la géométrie des composants, les propriétés du matériau, le type et les conditions de lubrification, les interactions physico-chimiques entre le lubrifiant et les interfaces, etc. Chaque modification des paramètres de contact peut affecter directement la réponse de frottement local et, par conséquent, la réponse dynamique globale du système. Pour cette raison, après avoir identifié la présence du stick-slip sur le système de freinage et après avoir analysé les caractéristiques tribologiques et dynamiques dues à l'apparition d'instabilité lors d'un freinage, une analyse approfondie de la réponse de frottement local a été réalisée avec de tests tribologiques spécifiques.
En tenant compte du système de freinage réel et en concentrant l'attention sur le contact lubrifié entre le tambour et le ressort de torsion, un système tribologique a été développé pour mesurer la réponse de frottement locale du contact (Image I) en fonction des conditions de fonctionnement imposées (charge normale, vitesse et température).

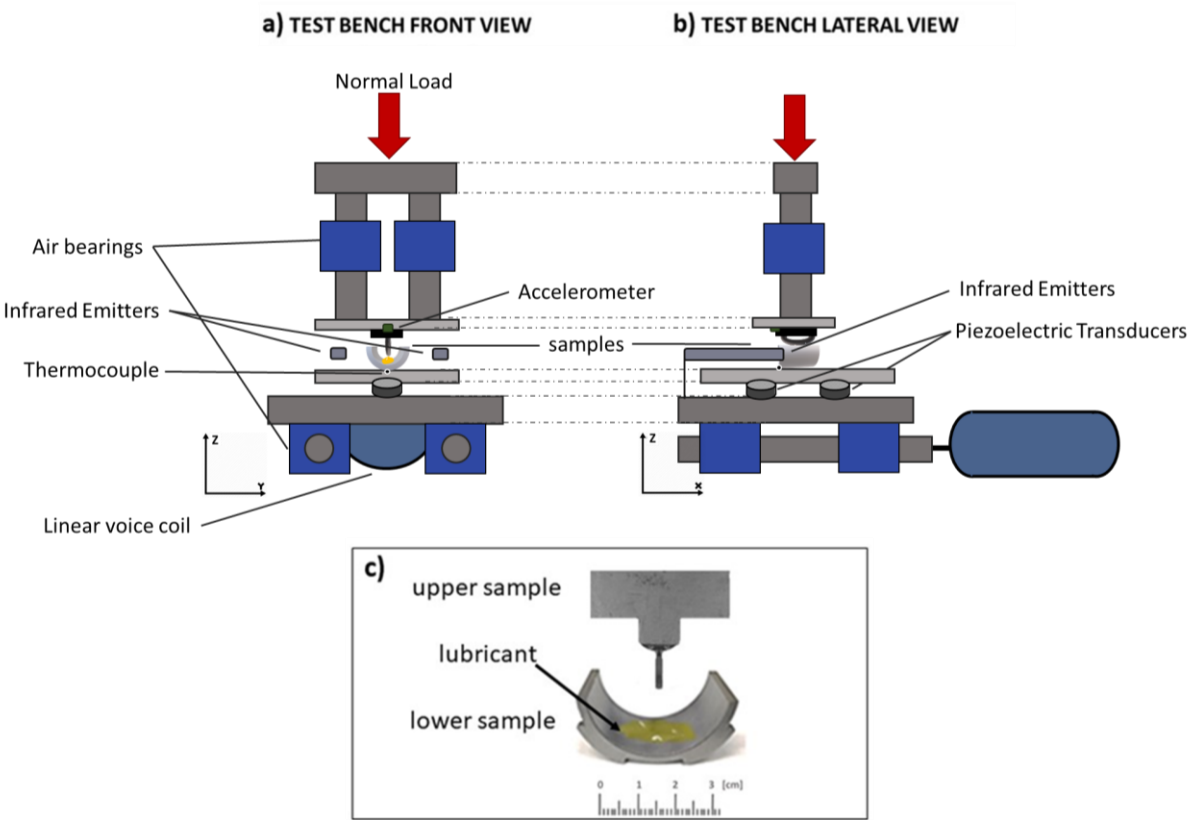

Image I: Schéma du banc d'essai utilisé pour les essais expérimentaux pour l'analyse du frottement du contact lubrifié. a) vue de face b) vue de côté c) détail des éprouvettes testées.

Le but de la campagne expérimentale était de caractériser la réponse en de frottement du contact lubrifié avec de la graisse, afin de comprendre comment les différentes conditions opérationnelles imposées et les différents paramètres de conception peuvent influencer la réponse au niveau local.
Les tests expérimentaux ont été réalisés dans un premier temps en prenant en considération une configuration de référence, le frein à ressort, où le lubrifiant est une graisse au lithium complexe (LiCPAO) et le ressort de torsion est revêtu d'un film de Diamond-Like-Carbon (DLC). En analysant les résultats obtenus (Image II), une tendance particulière du coefficient de frottement en fonction de la vitesse a été mise en évidence. Cette tendance ne suit pas la courbe classique de Stribeck. Au départ, le coefficient de frottement statique est suivi d'une forte baisse, passant au coefficient de frottement dynamique calculé aux conditions de vitesse les plus basses (0.1 mm/s). Après ce point, le coefficient de frottement augmente avec la vitesse, suivant une tendance presque logarithmique, et se stabilise lorsque la vitesse est d'environ 2 mm/s. Ce comportement particulier est accentué à haute température (80 °C), ce qui conduit à une plus grande différence entre le coefficient de frottement statique et dynamique. Cette différence est l'un des principaux promoteurs de l'apparition du stick-slip.

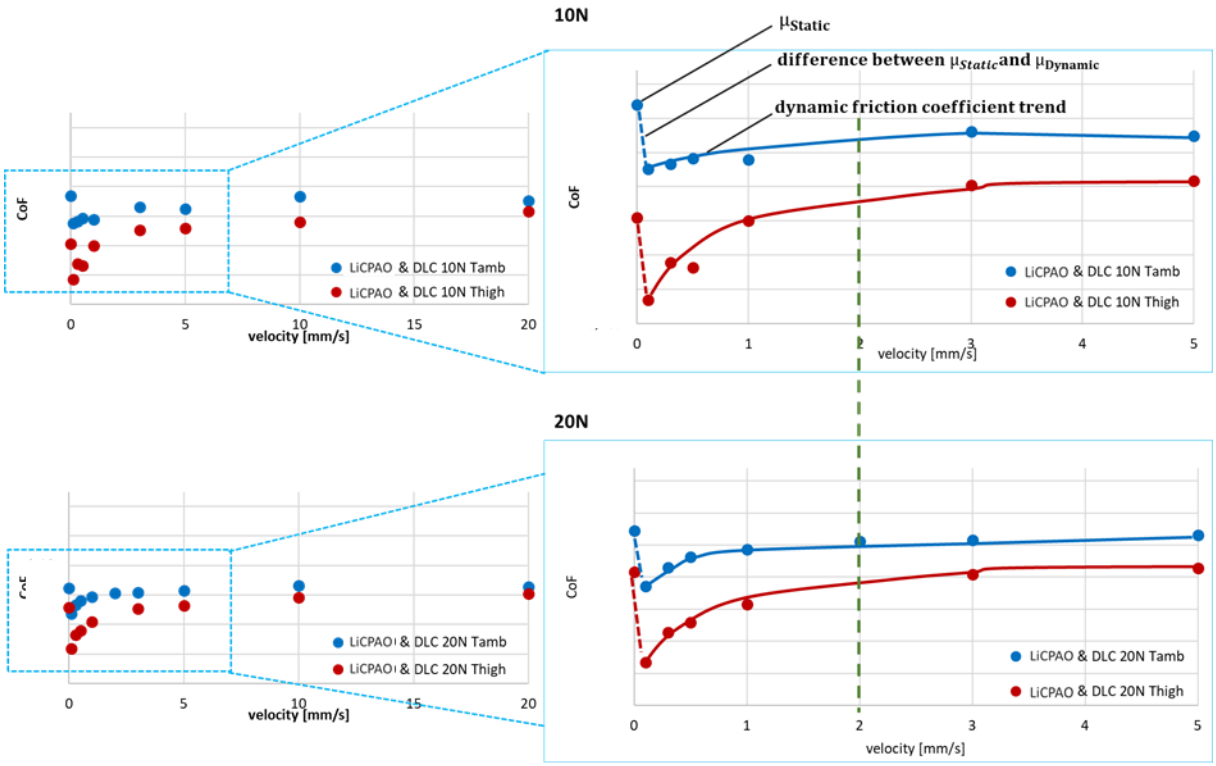

Image II: Evolution du coefficient de frottement en fonction de la vitesse pour la configuration standard, imposant une charge normale égale à 10N (haut) et 20N (bas) et deux températures différentes égales à 25°C (points et courbes bleus) et 80°C (points et courbes rouges).

En outre, après avoir analysé les freins actuellement en production, certains des principaux paramètres tels que le revêtement de surface du ressort, l'angle entre les stries de rodage du tambour, la rugosité et le matériau du tambour ont été testés. La réponse de frottement a été analysée en fonction

de la vitesse imposée; de plus, le coefficient de frottement statique et la différence entre le coefficient de frottement statique et dynamique ont été calculés en considérant la valeur obtenue en imposant une vitesse de 0,1 mm/s.
De plus, afin d'analyser l'influence effective des paramètres susmentionnés sur la propension du frein au stick-slip, un modèle numérique à paramètres concentrés de l'actionneur électrique tubulaire a été créé. Le but est de reproduire la réponse dynamique de l'ensemble du système mécanique, en introduisant les paramètres réels du frein et les courbes de frottement obtenues expérimentalement. Une fois le modèle validé, des simulations paramétriques ont été réalisées pour identifier le rôle des principaux paramètres sur l'apparition de stick-slip. La propension au stick-slip de chaque configuration a été évaluée en termes de vitesse critique, c'est-à-dire la vitesse en dessous de laquelle le système montre la présence de stick-slip. Les principaux résultats peuvent être résumés comme suit:

- En augmentant la rigidité ou en diminuant la valeur d'amortissement du frein, la propension au stick-slip diminue. Cependant, un changement substantiel de C et/ou K n'est pas en raison de la grande dépendance d'autres paramètres sur le système de freinage lui-même, comme le dimensionnement du moteur électrique.
- En faisant varier la valeur de l'angle de l'angle entre les stries de rodage de la surface interne du tambour, il n'y a pas de changement significatif sur la réponse dynamique du système. Au contraire, le changement de matériau, passant du matériau de référence à un autre matériau, produit une réduction significative de la valeur de vitesse critique.
  L'analyse paramétrique réalisée sur différents revêtements de surface du ressort de torsion (lubrifiant solide) a montré que le revêtement CW est celui qui garantit la moindre propension du système au stick-slip. En particulier, par rapport au lubrifiant solide DLC (configuration de référence), le CW montre une réponse de frottement locale caractérisée par une plus petite différence entre statique et dynamique, surtout à températures élevées Au contraire, le revêtement NiP et les tests réalisés sans lubrifiants solides ont montré une réponse dynamique largement influencée par la présence de stick-slip. Ces conclusions sont en accord avec les résultats obtenus sur des freins complet, lors d’une campagne expérimentale menée sur le système de freinage.

En conclusion, la campagne expérimentale, ainsi que les résultats obtenus par les simulations numériques, ont montré que la valeur de la courbe de frottement à vitesses élevées n'affecte pas significativement la réponse dynamique du système. Au contraire, la tendance à faible vitesse (de 0 à 1 mm/s) du coefficient de frottement en fonction de la vitesse a été identifiée comme un facteur clé. Lorsque la différence entre le frottement statique et dynamique est réduite et/ou la pente de la courbe est réduite, une diminution effective de la propension au stick-slip est observée.
De plus, les résultats expérimentaux ont mis en évidence la complexité de la réponse tribologique du contact, fonction à la fois des caractéristiques rhéologiques du lubrifiant et des caractéristiques mécaniques des corps en

contact. Les différentes conclusions ont conduit à la nécessité de comprendre l'influence des composants de la graisse (épaississant, huile de base et additifs) sur la réponse de frottement. A cet égard, une campagne expérimentale a été menée pour tester expérimentalement les différentes conditions de lubrification, avec et sans revêtement DLC.
Les tests et les résultats réalisés ont été analysés et discutés dans le but de fournir des informations sur la manière dont les différents composants du lubrifiant influencent le comportement de frottement local. Un diagramme des différentes courbes de frottement en fonction de la vitesse, dans les différentes configurations testées, est présenté dans la Image III.

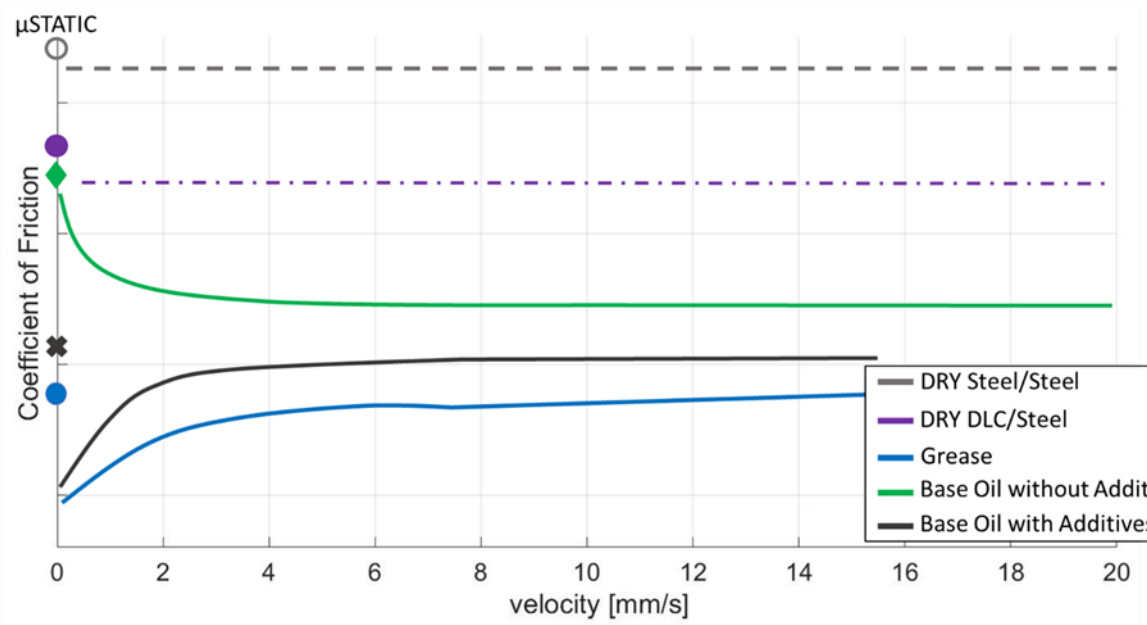

Image III: Schéma récapitulatif de l'évolution du coefficient de frottement en fonction de la vitesse, pour les différentes configurations testées.

La contribution de l'huile de base contenue dans la graisse s'est avérée être dominante aux vitesses élevées. En augmentant la vitesse, en effet, le coefficient de frottement en cas de lubrification avec graisse tend à atteindre le comportement de l'huile de base, qui suit la courbe typique de Stribeck.
Les additifs affectent la réponse de frottement à la fois à haute et à basse vitesse, conduisant à des contributions différentes en termes de réponse de friction locale. A vitesse élevée, les additifs provoquent une légère baisse du coefficient de frottement. Au contraire, pour les faibles vitesses, les additifs et l'épaississant (dans ce cas le « lithium complexe ») jouent un rôle fondamental. La courbe de frottement en fonction de la vitesse, aussi bien avec la graisse qu'avec l'huile plus les additifs, montre toujours un comportement caractérisé par une forte différence entre le coefficient de frottement statique et dynamique et par une forte pente négative du frottement en fonction de la vitesse. Les valeurs de frottement, pour les plus basses vitesses, sont bien inférieures à celles de l'huile de base seule.

Par conséquent, alors que l'épaississant et les additifs ont un effet positif en abaissant le coefficient de frottement statique, la diminution drastique du coefficient de frottement dynamique à bas vitesses favorise le stick-slip. De plus, comme indiqué précédemment, en, augmentant la température, le coefficient de frottement du contact graissé présente des valeurs de frottement inférieures à celles calculées à température ambiante, quels que soient les charges et les revêtements testés, ainsi que des valeurs plus élevées de la différence entre le frottement statique et dynamique. Cette diminution du frottement à des températures plus élevées a été associée à la fois à une diminution de la viscosité de l'huile de base et à une augmentation de la libération d'huile par l'épaississant qui compose la graisse.
Enfin, il a été démontré comment les lubrifiants solides à base de carbone, tels que le DLC et en particulier le CW, améliorent les performances tribologiques du contact, notamment en termes d'usure et de stabilité du coefficient de frottement, apportant une lubrification solide supplémentaire entre les surfaces de contact et en créant un troisième corps solide, à la fois dans des conditions sèches et lubrifiées. En présence du revêtement DLC, une forte diminution du coefficient de frottement statique et dynamique a été mise en évidence.

De manière générale, ce travail de thèse a mis en évidence la complexité du phénomène de stick-slip dans les contacts lubrifiés, l'interaction complexe entre la réponse locale (contact) et globale (système) du système et le rôle clé joué par la rhéologie du lubrifiant dans l'évaluation de la propension d'un système mécanique à l'instabilité. Par ailleurs, une analyse spécifique a permis d'identifier les différentes contributions des composants de la graisse au frottement en fonction de la vitesse. Les résultats obtenus ont mis en évidence la nécessité d'une approche multidisciplinaire, comprenant à la fois des analyses expérimentales et numériques, mécaniques et physico-chimiques, pour comprendre les mécanismes à l'origine des instabilités stick-slip dans les contacts graissés.

Tribological and Vibro-acoustic Behaviour of a Lubricated Contact Subjected to the Stick-Slip Phenomenon: The Case of the Spring-Brake System

Riassunto sostanziale

Il presente lavoro è stato sviluppato nel contesto della ricerca sulle vibrazioni indotte dall'attrito, a cavallo fra la meccanica del contatto, la tribologia e la dinamica. In meccanica classica, l'attrito è definito come la forza di reazione tangenziale che si verifica quando un corpo scorre su un altro corpo. La definizione è estesa al moto di due corpi solidi interposti da un lubrificante. In generale, l'interazione locale all'interfaccia (impatti locali e rotture di asperità e giunzioni) determina il rilascio di energia elastica sotto forma di onde acustiche, che si propagano sia lungo l'interfaccia sia all'interno dei solidi a contatto. Tali onde si propagano dalle superfici al volume dei solidi in movimento relativo che, a loro volta, rispondono all'eccitazione dal contatto vibrando secondo la loro dinamica, producendo così le cosiddette vibrazioni indotte dall'attrito. Il lavoro qui presentato focalizza l'attenzione su un particolare tipo di vibrazioni indotte dall'attrito: il fenomeno di stick-slip.

Sia in natura sia nei sistemi artificiali esistono diversi esempi di stick-slip, sia nel caso di contatti secchi che lubrificati. I suoni prodotti da strumenti come violini e violoncelli, il suono prodotto durante il movimento delle cavallette, i rumori prodotti durante la levigatura, frenate brusche e lo stridore di pneumatici o il gesso su una lavagna, dal movimento graduale di guide di scorrimento, il rumore derivante dai cilindri idraulici nei simulatori di aerei o quello derivante dalla filatura nella produzione tessile sono alcuni degli esempi più comuni del fenomeno dello stick-slip. Il ruolo dell'attrito e la sua dipendenza dalla velocità sono uno dei parametri chiave necessari per comprendere tale fenomeno.

In tale contesto, la presenza di un lubrificante all'interfaccia tra i corpi a contatto può, da un lato, migliorare le prestazioni e la durata del sistema meccanico, ma, dall'altro, può aumentare la complessità e l'insorgenza di instabilità di contatto, aggiungendo un parametro difficilmente controllabile sia dal punto di vista tribologico che dinamico. Focalizzando l'attenzione sul fenomeno dello stick-slip in contatti lubrificati, la comprensione di tale fenomeno richiede un approccio multi-disciplinare e multi-scala, coinvolgendo complesse interazioni di vari fenomeni a scale diverse, che si influenzano reciprocamente. Al giorno d'oggi, il crescere dell'interesse scientifico ed industriale nell'analisi di tali fenomeni ha portato ad un rapido aumento di lavori che propongono diversi metodi di analisi sperimentale e numerica. Questi lavori sono sviluppati nell'ambito di diverse discipline, che vanno dalla scienza della terra, alla fisico-chimica ed alla meccanica applicata. Tuttavia, la letteratura presenta una forte carenza di informazioni sul comportamento tribologico macroscopico del contatto lubrificato e su

come questo possa influenzare direttamente la risposta vibrazionale dell'intero sistema, passaggio fondamentale per comprendere le condizioni locali che posso portare ad instabilità di stick-slip. Inoltre, quando il lubrificante è un grasso, la sua complessa reologia, funzione sia dell'addensante che degli additivi e dell'olio di base, diventa un punto chiave per l'analisi dell'insorgenza e l'evoluzione dello stick-slip. È quindi necessario un approccio complementare per tenere conto dell'accoppiamento tra il comportamento locale del contatto (risposta d'attrito del contatto lubrificato) e la risposta dinamica e vibrazionale del sistema.
In questo contesto, il presente lavoro, sviluppato nell'ambito della collaborazione tra SOMFY SASA, il laboratorio LaMCoS dell'INSA di Lione e il dipartimento di Meccanica Teorica ed Applicata (DIMA) dell'Università La Sapienza di Roma, propone un approccio sistematico al problema dello stick-slip nei contatti lubrificati e mira a migliorarne la comprensione e a fornire possibili soluzioni industriali. Il lavoro è stato sviluppato facendo riferimento ad un caso industriale, al fine di analizzare i risultati ottenuti in un contesto il più realistico possibile. Oggetto dell'indagine è un freno meccanico a molla, utilizzato negli attuatori elettrici tubolari. Tali freni possono presentare instabilità di attrito, generate al contatto lubrificato con grasso tra i due componenti principali (molla torsionale e tamburo).
Il lavoro è stato suddiviso in tre blocchi principali, a seguito di uno scrupoloso lavoro di indagine della bibliografia scientifica esistente sull'argomento sopra descritto: i) una analisi tribologica e dinamica dell'insorgenza dello stick-slip nei freni meccanici a molla; ii) una analisi sperimentale del comportamento locale d'attrito, riponendo particolare attenzione al ruolo della reologia del lubrificante; iii) una analisi numerica per l'investigazione della risposta dinamica del sistema meccanico.
Prendendo in considerazione diversi freni in produzione presso la società SOMFY, sono state svolte analisi tribologiche e dinamiche permettendo l'identificazione fenomeno di stick-slip. Focalizzando l'attenzione sull'analisi del segnale vibrazionale e sulla topografia delle superfici osservate, le eccitazioni impulsive periodiche, dovute al susseguirsi di fasi di adesione e di strisciamento, al contatto tra molla e tamburo lubrificato con grasso, portano ad una periodica eccitazione della dinamica del sistema e sono accompagnati dalla presenza di tracce di movimento assiale della molla.
Inoltre, é stato evidenziato come l'apparizione dello stick-slip é preponderante a seguito dei primi cicli di funzionamento, cioè quando il freno raggiunge temperature maggiori rispetto alla temperatura ambiente, con valori di temperatura interna pari a circa 80°C. Le osservazioni dinamiche e tribologiche sono ripetibili e caratteristiche di tutti i freni analizzati. Inoltre, il tentativo della molla di aprirsi assialmente causa un disallineamento dei componenti, una modifica della rigidezza della molla e una localizzazione della pressione di contatto. Tutti questi fattori potrebbero contribuire al verificarsi dell'instabilità.
Come spiegato precedentemente, il verificarsi dell'instabilità è dovuto all'interazione tra la dinamica del sistema e il comportamento del contatto al livello locale. Diversi parametri di contatto possono influenzare la risposta

del sistema dinamico, come il carico normale, la velocità, la rugosità superficiale, la geometria dei componenti, le proprietà dei materiali, la tipologia e condizioni di lubrificazione, le interazioni fisico-chimiche tra lubrificante e interfacce, ecc. Ogni modifica in uno dei parametri di contatto influenza direttamente la risposta d'attrito complessiva e, di conseguenza, la risposta dinamica dell'intero sistema. Per tale motivo, dopo aver individuato la presenza stick-slip sull'impianto frenante e analizzato le caratteristiche tribologiche e dinamiche dovute all'insorgenza dell'instabilità in fase di frenata su freno completo, è stata eseguita un'analisi approfondita della risposta d'attrito locale del contatto mediante specifiche prove tribologiche.
Prendendo in considerazione il sistema frenante reale e concentrando l'attenzione sul contatto lubrificato tra il tamburo e la molla torsionale, è stato sviluppato un sistema tribologico per misurare la risposta di attrito locale del contatto (Figura I) al variare delle condizioni operative imposte (carico normale, velocità e temperatura).

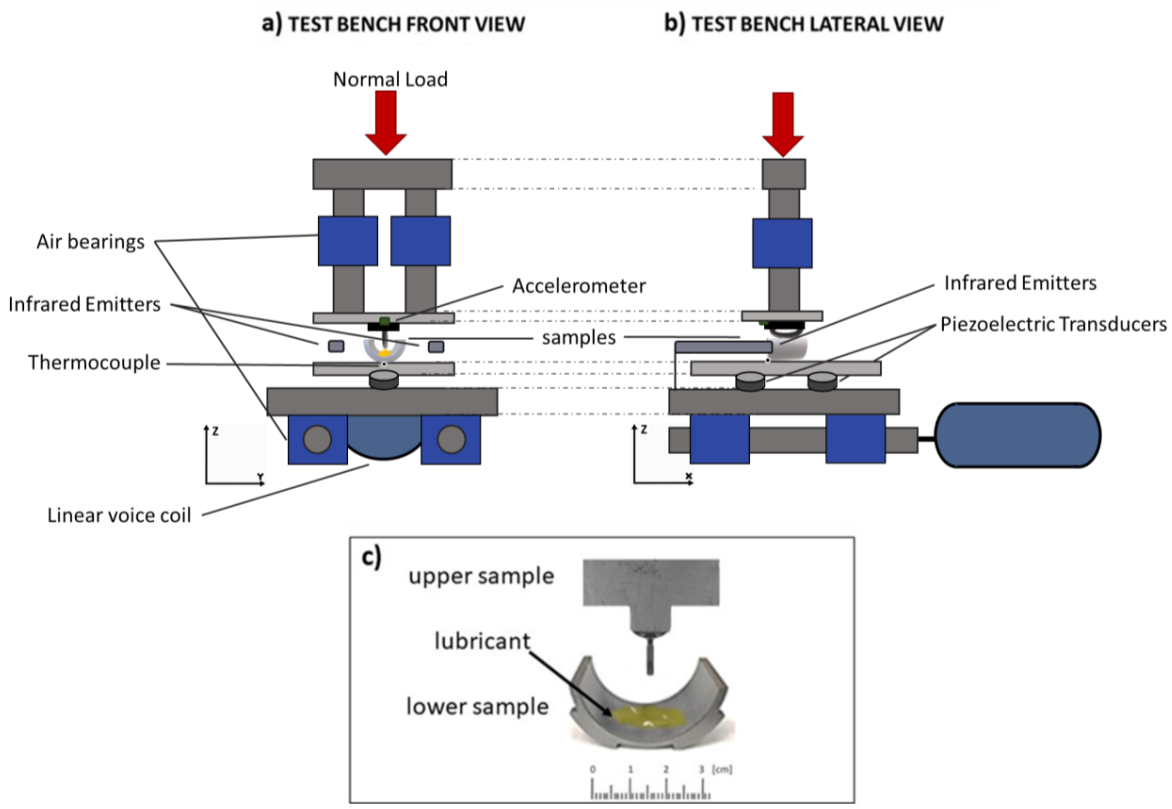

Figura I: Schema del banco prova utilizzato per le prove sperimentali per l'analisi del comportamento d'attrito del contatto lubrificato. a) vista frontale b) vista laterale c) dettaglio dei provini testati.

Scopo della campagna sperimentale è stata la caratterizzazione della risposta d'attrito del contatto lubrificato con grasso, al fine di comprendere come le diverse condizioni al contorno imposte, e i diversi parametri di progetto, possano influenzare la risposta al livello locale.
Le prove sperimentali sono stati svolti prendendo inizialmente in considerazione una configurazione di riferimento, dove il lubrificante è un grasso commerciale al litio complesso (LiCPAO) e la molla torsionale è rivestita con un film di Diamond-Like-Carbon (DLC). Analizzando i risultati

ottenuti (Figura II), è stato evidenziato un particolare andamento del coefficiente di attrito in funzione della velocità, che non segue la curva tipica di Stribeck. Inizialmente, il coefficiente di attrito statico è seguito da un forte calo, passando al coefficiente di attrito dinamico calcolato alle condizioni di velocità più bassa. Successivamente il coefficiente d'attrito aumenta con la velocità, seguendo un andamento quasi logaritmico, e si stabilizza quando la velocità è di circa 2 mm/s. Questo particolare comportamento viene enfatizzato nel caso delle prove eseguite ad alta temperatura (80°C), dando luogo ad una maggiore differenza tra coefficiente di attrito statico e dinamico. Tale differenza è uno dei principali promotori della comparsa di stick-slip.

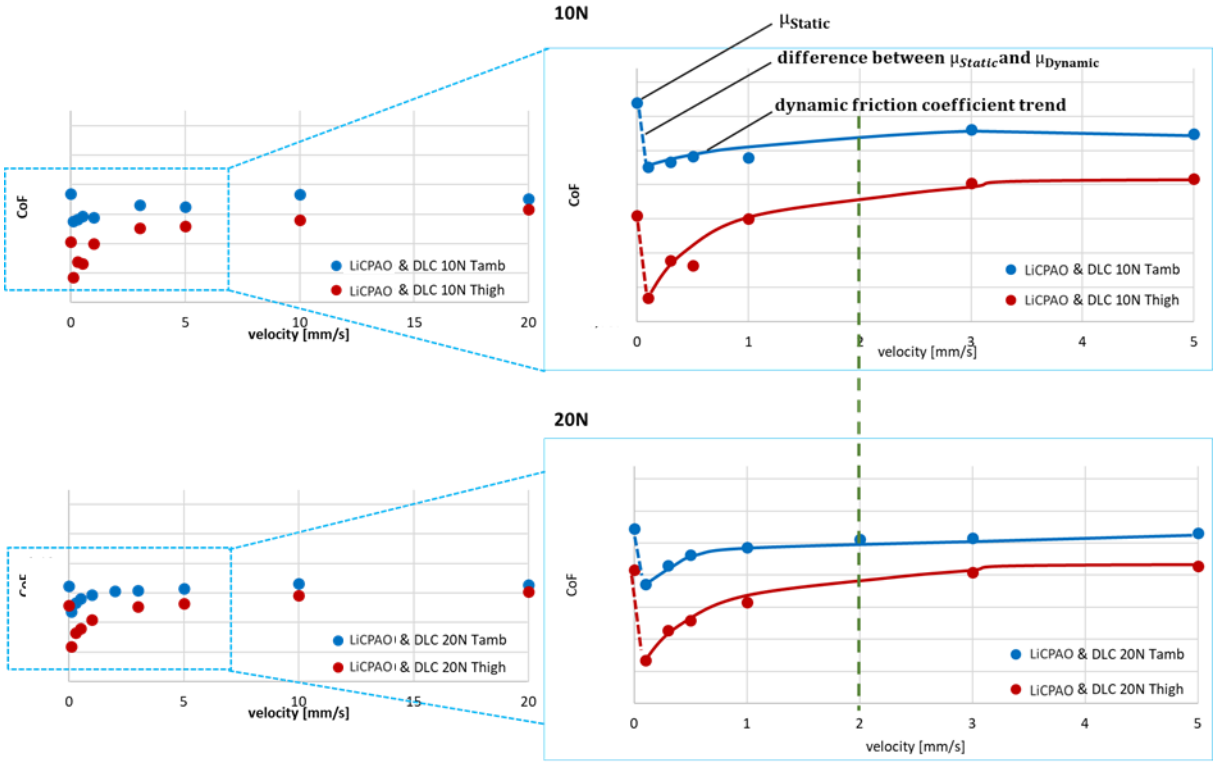

Figura II: Andamento del coefficiente d'attrito in funzione della velocità imposta per la configurazione standard, imponendo un carico normale pari a 10N (in alto) e 20N (in basso) e le due diverse temperature pari a 25°C (punti e curve blue) e 80°C (punti e curve rosse).

Inoltre, basandosi sui freni attualmente in produzione, sono stati individuati e testati alcuni dei parametri principali come il rivestimento superficiale della molla, l'angolo di rodaggio del tamburo, la rugosità ed il materiale del tamburo. La risposta di attrito è stata analizzata al variare della velocità imposta; inoltre sono stati calcolati il coefficiente d'attrito statico e la differenza tra coefficiente d'attrito statico e quello dinamico, calcolato considerando il valore ottenuto imponendo una velocità pari a 0.1mm/s.
Inoltre, al fine di analizzare l'effettiva influenza dei parametri sopra citati sulla propensione dell'intero sistema meccanico allo stick-slip, è stato creato un modello numerico a parametri concentrati dell'intero attuatore elettrico tubolare. L'obiettivo è quello di riprodurre la risposta dinamica dell'intero sistema meccanico, introducendo in ingresso i parametri reali del freno meccanico e le curve d'attrito ottenute sperimentalmente. Una volta

validato il modello, sono state effettuate le simulazioni parametriche per identificare il ruolo dei principali parametri chiave rispetto all'occorrenza dello stick-slip. La propensione allo stick-slip di ciascuna configurazione é stata valutata in termini di velocità critica, ossia la velocità al disotto della quale il sistema mostra presenza di stick-slip. I principali risultati possono essere riassunti come segue:

- Aumentando la rigidezza o riducendo il valore di smorzamento del sistema frenante, la propensione allo stick-slip diminuisce. Tuttavia, un cambiamento sostanziale di C e/o K non è applicabile in fase di progettazione del freno a causa dell'ampia dipendenza di altri parametri dal sistema frenante stesso, come ad esempio il dimensionamento del motore elettrico.
- Variando l'angolo di rodaggio della superficie interna del tamburo non si hanno cambiamenti rilevanti sulla risposta dinamica del sistema. Al contrario, il cambio di materiale e di rugosità superficiale produce una significativa riduzione del valore di velocità critica.
- L'analisi parametrica eseguita su diversi rivestimenti superficiali della molla torsionale (lubrificante solido) ha evidenziato che il rivestimento CW è quello che garantisce la minor propensione dell'intero sistema allo stick-slip. In particolare, rispetto al lubrificante solido DLC, si nota una risposta locale d'attrito caratterizzata da una minore differenza tra statico e dinamico, soprattutto ad alta temperatura. Al contrario, il rivestimento NiP e le prove eseguite senza la presenza di lubrificanti solidi hanno mostrato una risposta dinamica che è largamente influenzata dalla presenza di stick-slip.

In conclusione, la campagna sperimentale, insieme ai risultati ottenuti tramite le simulazioni numeriche, ha evidenziato che modificando la curva di attrito alle alte velocità non si influisce in modo significativo sulla risposta dinamica del sistema. Al contrario, è stato identificato come fattore chiave l'andamento a bassa velocità (da 0 a 1mm/s) del coefficiente d'attrito in funzione della velocità. Quando si riduce la differenza tra attrito statico e dinamico e/o si riduce la pendenza della curva, si osserva un'effettiva diminuzione della propensione allo stick-slip.
Inoltre, i risultati sperimentali hanno evidenziato la complessità della risposta tribologica del contatto, funzione sia delle caratteristiche reologiche del lubrificante che delle caratteristiche meccaniche dei corpi a contatto. Le diverse conclusioni hanno portato alla necessità di comprendere l'influenza che hanno i componenti del grasso (addensante, olio di base ed additivi) sulla risposta d'attrito locale. A tal proposito, è stata condotta una campagna sperimentale testando sperimentalmente le diverse condizioni di lubrificazione, con e senza rivestimento DLC.
I test eseguiti ed i conseguenti risultati sono stati analizzati e discussi con l'obiettivo di fornire informazioni su come i diversi componenti del lubrificante influenzino il comportamento di attrito locale. Uno schema delle diverse curve di attrito in funzione della velocità, nelle diverse configurazioni testate, è riportato in Figura III.

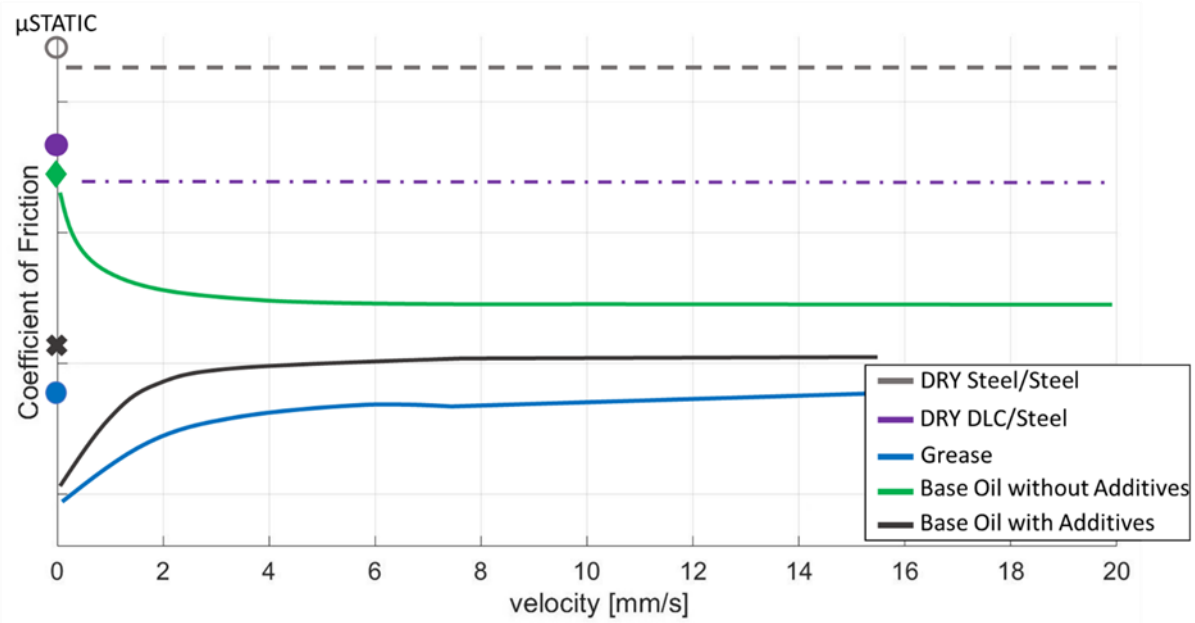

Figura III: Schema riassuntivo dell'andamento del coefficiente d'attrito in funzione della velocità imposta per le differenti configurazioni testate.

Il contributo dell'olio di base contenuto nel grasso è risultato essere dominante ad alte velocità. Aumentando la velocità, infatti, il coefficiente di attrito in caso di lubrificazione con grasso tende a raggiungere il comportamento dell'olio di base, che segue la curva tipica di Stribeck.
Gli additivi influenzano la risposta di attrito sia ad alte sia a basse velocità, portando a diversi contributi in termini di risposta d'attrito locale. Ad alta velocità, gli additivi provocano un leggero abbassamento del coefficiente d'attrito. Al contrario, per basse velocità, sia gli additivi che l'addensante (in questo caso litio complesso) giocano un ruolo fondamentale. La curva d'attrito in funzione della velocità, sia in caso di lubrificazione con grasso sia con olio ed additivi, mostra sempre un comportamento caratterizzato da un'elevata differenza tra coefficiente d'attrito statico e dinamico e da forte una pendenza attrito-velocità negativa. I valori d'attrito, per le più basse velocità, risultano molto più bassi rispetto a quelli del solo olio di base.
Dunque, mentre l'addensante e gli additivi hanno un effetto positivo nell'abbassare il coefficiente di attrito statico, la drastica diminuzione del coefficiente di attrito dinamico alle velocità più basse favorisce lo stick-slip. Inoltre, come precedentemente affermato, all'aumentare della temperatura, il coefficiente di attrito del contatto lubrificato con grasso mostra valori più bassi rispetto a quelli calcolati a temperatura ambiente, indipendentemente dai carichi e rivestimenti testati, nonché valori maggiori della differenza tra attrito statico e dinamico. Questa diminuzione dell'attrito a temperature più elevate è stata associata sia ad una diminuzione della viscosità dell'olio di base sia ad un aumento del rilascio di olio da parte della matrice di grasso, con l'aumento della temperatura.
Infine, è stato dimostrato come i lubrificanti solidi a base di carbonio, come DLC ed in particolare CW, migliorano le prestazioni tribologiche del contatto, soprattutto in termini di usura e stabilità del coefficiente di attrito, fornendo una ulteriore lubrificazione solida tra le superfici a contatto e creando un

terzo corpo solido, sia in condizioni asciutte che lubrificate. In presenza del rivestimento DLC è stata evidenzia un'elevata diminuzione del coefficiente d’attrito sia statico sia dinamico.

In generale, il presente lavoro di dottorato ha evidenziato la complessità del fenomeno di stick-slip nei contatti lubrificati, la complessa interazione tra la risposta locale (contatto) e globale (sistema) del sistema ed il ruolo chiave svolto dalla reologia del lubrificante nella valutazione della propensione di un sistema meccanico allo stick-slip. Inoltre, una analisi specifica ha permesso di identificare i vari contributi dei componenti del grasso nell’attrito riscontrato tra le due superfici in contatto. I risultati ottenuti hanno evidenziato come sia necessario un approccio multidisciplinare, comprendente analisi sia sperimentali sia numeriche, meccaniche e fisicochimiche, per comprendere i meccanismi all'origine delle instabilità di stick-slip nei contatti lubrificati con grasso.

Abstract

The main objective of the PhD thesis is the analysis of stick-slip phenomena in lubricated contacts, by merging the physical, experimental and numerical points of view and proposing a novel methodological approach, applied here to an industrial case. Nowadays, in the field of applied mechanics and tribology, one of the most important challenges is the ability to predict and reduce surface damages, failure of machine components and undesirable frictional and dynamic characteristics. In particular, the appearance of friction-induced vibrations at the contact is hardly controllable and can result in high local contact pressure, elevated stresses, system oscillations, discontinuous motion and premature failure [1]. Understanding the conditions for which the system is more predisposed to the stick-slip phenomenon may allow preventing the appearance of such instabilities, and the related vibrations and noise emission. Friction-Induced Vibrations are a phenomenon that engages multiple scientific challenges, due to the complexity of their physics. Focusing the attention on stick-slip phenomena, these are generally characterized by a saw-tooth displacement-time evolution [2]. Each change in the contact parameters influences directly the dynamic and frictional response of the system, due to the mutual influence of the local scale (contact) and the system scale (macroscopic frictional and vibrational response). Moreover, the presence of a lubricant, and in particular of grease, at the contact interface, increases the complexity of the phenomenon, from both a tribological and dynamic point of view. Lubricated systems are supposed to reduce the frictional losses and wear, but they can also collaborate in the appearance of dynamic contact instabilities, due to the friction-velocity characteristics when passing from boundary to mixed contact regimes [3]. The complex rheology of a grease, function of both the matrix, additive and oil responses, becomes then a key point for the occurrence and evolution of stick-slip. Despite the great importance of this phenomenon, from both scientific and industrial points of view, a lack emerges into the literature about stick-slip of lubricated interfaces. The few works are manly focused on molecular dynamics simulations and numerical modelling of the dynamical response of the system. The different role of the grease components, during the sliding, is nowadays still not clear. Nevertheless, the complex rheology of a grease, function of both the thickener, the base oil and the additives, is a key point for understanding and controlling the occurrence and evolution of stick-slip. Moreover, a general approach is needed to account for the coupling between the local phenomena (e.g. lubricated contact response) and the system dynamic response. Aiming to improve the understanding of stick-slip in lubricated contacts, the present Ph.D. work proposes a novel methodological approach to the stick-slip problem of a lubricated contact, referring to a real industrial case, in order to deploy the obtained results in a more realistic and detailed manner. The subject of the investigation is a mechanical brake used in tubular electric actuators [4, 5], which can present frictional instabilities originated at the lubricated contact between

the two main brake components. The methodology used is twofold: i) on one hand, experimental tests are carried out to understand the local frictional response of the lubricated contact; ii) on the other hand, a lumped model is created in order to simulate and analyse the system dynamic response. Introducing the information about the local lubricated contact behaviour (friction law), achieved experimentally, into the numerical model, it is possible to investigate the parameters for which the system is more predisposed to the stick-slip phenomenon and recreate a representative scenario of its appearance. Particular attention has been placed on the analysis of the lubricant rheology, dealing with different types of lubricants and regimes of lubrication, with both oils and greases. The frictional response has been thus related to the different contributions of the grease components (i.e. thickener, base oil and additives) on the rheology at the interface. The obtained local information has been then integrated in the lumped model to evaluate the unstable dynamic response of the entire system (i.e. the stick-slip phenomena) and identify the lubrication parameters that most influence its appearance. The numerical analysis had the dual objective of understanding the role of the local contact response in the system instability and investigating the stick-slip occurrence as a function of the key system parameters. The obtained results allowed to identify the lubrication components, and the respective friction-velocity curves, more favourable for the stick-slip occurrence. Combining the grease rheology evolutions with the stick-slip dynamic response represents a further challenge in both the domains of research. The Ph.D. thesis has been developed in collaboration between the Sapienza University of Rome, Department of Mechanical and Aerospace Engineering (Rome, Italy), the Institut National des Sciences Appliquées (INSA) of Lyon, laboratory LaMCoS (Lyon, France), and the company SOMFY S.A. (Cluses, France).

Index

Introduction and work objectives

Tribology is defined as the science and technology of interacting surfaces in relative motion, or, in other words, the study of friction, wear and lubrication. Friction forces between sliding surfaces arise due to varied and complex mechanisms and can be responsible for undesirable dynamic characteristics in many mechanical systems. The presence of a lubricant at the interface between the bodies in contact can, on one side, improve the performances and the lifetime of the mechanical system, but, on the other side, can also increases the complexity and the occurrence of contact instabilities, adding a parameter hardly controllable from both a tribological and a dynamical point of view. More in detail, understanding the stick-slip phenomena in greased contacts requires a multi-scale and multi-physical approach and involves complex series and interactions of various phenomena at different scales, which mutually influence each other's. Nowadays, the development of experimental and numerical simulation methods for investigating frictional problems have produced a sudden growth in the number of research activities considering not only the contact aspects but also the response of the system to which the contact surfaces belong. These works are developed in the framework of different disciplines, ranging from the earth science and chemistry to the applied mechanics.
Into this manifold framework, this work is placed in the context of the existing bridge between tribology and dynamics, dedicating this study to the analysis of a Friction-Induced Vibrations (FIVs) related issue.
Focusing the attention on the stick-slip phenomenon in lubricated systems, the literature presents a lack of information about the macroscopic tribological behavior of the lubricated contact and how this can influence directly the vibrational response of the entire system, fundamental step to understand the local conditions that can lead to stick-slip instability. Moreover, when the lubricant is a grease, its complex rheology, function of both the thickener, the additives and the oil, becomes a key point for the occurrence and evolution of the stick-slip, by driving the overall frictional response as a function of velocity. A general approach is then needed to account for the coupling between the local contact contributions (i.e. the greased contact response) and the system dynamic response.
In this context, the present Ph.D. work aims to improve the understanding of stick-slip instability in greased contacts and provide possible industrial solutions, answering to some of the main questions:

- How does the local frictional behavior, at the contact interface, drastically affect the dynamic response of the system and influence the stick-slip propensity of the mechanical system?
- Does the presence of a lubricant at the interface worsen the appearance of the stick-slip phenomenon?
- Which are the parameters that most influence the appearance of stick-slip in lubricated contacts?

- Is the overall friction-velocity characteristic of a grease the complex result of the synergy between rheological and physiochemical contributions?
- What is the role of each grease components (i.e. thickener, base oil and additives) in the frictional response of the lubricated contact and how they can affect the appearance stick-slip instability?

The PhD, developed within the framework of a collaboration between SOMFY Activity SASA, the LaMCoS laboratory of the INSA of Lyon and the DIMA of the Sapienza University of Rome, proposes a systematic approach to the stick-slip issue in lubricated contacts. Specifically, the work has been developed referring to a real industrial case, in order to deploy the obtained results in a more realistic and applied context. The subject of the investigation is a mechanical spring-brake used in tubular electric actuators, which can present frictional instabilities, generated at the greased contact between the two main brake components.

First, to detail the nowadays context on the subject, Chapter I presents a review on the major works on friction, stick-slip and lubricated contact interfaces, as well as the industrial case study of the mechanical spring-brake system under investigation. Then, the identification of the stick-slip dynamic and tribological signatures has been performed on different brake systems, by dynamic analysis and the tribological observations, in Chapter II.

Having therefore highlighted the presence and the conditions of appearance of the stick-slip phenomenon in the investigated greased contact, focusing the attention on the case study, the work has been divided into three different sections. The first part (Chapter III) presents the experimental investigations on the local frictional contact. The results from the parametric experimental investigation are presented, with focus on the frictional response as a function of the imposed boundary conditions. The second part (Chapter IV), illustrates the numerical simulations carried out to reproduce the dynamic response of the entire mechanical system. A lumped model of the entire tubular actuator has been developed and the different system and contact parameters are investigated to study stick-slip propensity of the system. The results obtained in Chapter III (i.e. the local frictional response) are here coupled with the dynamic response of the system, by introducing them as input of the numerical model.

The analysis reported in Chapter IV has led to the necessity of understanding how the grease rheological response affects the stick-slip propensity of the system. This subject has been discussed in Chapter V, aiming to provide information on how the different lubricant components affect the local frictional response and, consequently, the occurrence of the stick-slip dynamic instability.

Finally, Chapter VI is dedicated to the summary of the main contributions, obtained from the present work, as well as the work outlines.

I. Frictional Contacts and Friction-Induced Vibrations

In a classic mechanical approach, "friction" is defined as the tangential reaction force that occurs when one body slides over another. The definition is extended to the motion of two solid bodies interposed by a lubricant. The resistive force acting in the opposite direction of the relative motion is known as the friction force.

The force required to initiate sliding is defined as the static friction force and the force necessary to maintain the sliding is called the kinetic friction force [6]. If the force to initiate motion between the bodies is F_s and the force to maintain the relative motion at a given relative velocity is F_k, the corresponding coefficient of static friction $\mu_s = F_s/N$ and coefficient of kinetic friction $\mu_k = F_k/N$ are defined, where N is the normal contact reaction. In some cases, these coefficients are approximately equal; in most cases $\mu_s > \mu_k$ [7].

While this simplified approach and notation is useful for preliminary dimensioning and mechanical design, this is not sufficient for the investigations about friction related problems that, instead, require a multi-scale and multi-physical approach and involve complex series and interactions of various phenomena at different scales, that mutually influence each other. The dimensionless itself of such coefficient attests its physical meaningless.

A more inclusive approach of the contact issues is proposed by the tribological triplet [8, 9] and the third body concept [10, 11]. This approach allows for accounting the different scales and influencing parameters, mainly linked to:

- the dynamic response of the mechanical system that includes and drives the contact;
- the two solids in contact, their stress and strain distributions, their topographical evolution and the possibility to promote tribological transformations of the surfaces (TTS) [12];
- the third body, including all the matter at the interface, more or less continuous or discrete, fluid or solid, cohesive or powdery, and its complex rheology [13].

This approach includes an evolutive representation of the flows of the third body at the contact between two first bodies [14], represented in Figure 1. In addition to the framework of the dry contact condition and the solid lubrication, this notion of tribological triplet is clearly representative of fluid lubrication too.

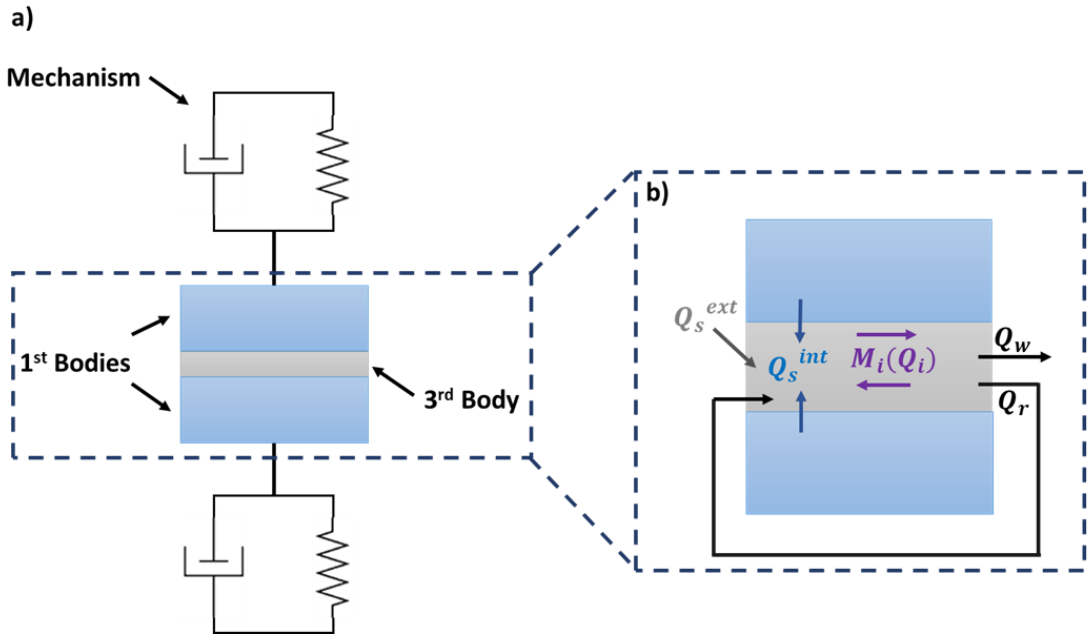

Figure 1: a) Scheme of the tribological triplet and the tribo-system, b) Third body flows thought and out of the contact, defining the tribological circuit.

Q_s^{int} represents the internal source flow caused by the formation of a third body due to the natural degradation of the first bodies in contact. Q_s^{ext} symbolizes the introduction of external third body, either artificial or natural, into the contact, such as an artificial lubricant. At the output from the contact, the flow can be divided into two main components: a part of the flow, schematized with Q_r , is reinjected and recirculate into the contact; a part of third body, the wear flow Q_w, is definitively expelled from the contact and can no longer participate to the accommodation mechanisms [15]. The amount of particles circuiting inside the contact is referred as the internal flow Q_i. The mass equilibrium of the system involves that the amount of particles M_i of the third body per unit of time have to be equal to the difference between Q_s and Q_w [13].

Moreover, when considering the interaction between solid surfaces, it is necessary as well to focus on the surface topography, the determination of the real area of contact and the understanding of the mechanism of mating contacts [16]. In fact, when two rough surfaces are in contact, the real contact area is made by the local areas of the asperities in contact [17]. Because of such discontinuity in the contact interface, the high concentration of elastic and adhesive energy at the real contact areas and the micro-impacts between asperities or local ruptures between local surface junctions are sources of waves generation and propagation into the solids (Figure 2). These local excitations, distributed all around the contact interface, excite the system dynamics and result in the so-called Friction-Induced Vibrations (FIV) [18, 19, 20]. These phenomena, combined with the dynamic response of the system, can largely affect the nominal functioning of the contact, modifying the operational conditions and leading to excessive wear of components, surface damage, fatigue failure and noise [21, 22, 23, 24].

Within this context, it is clear that the definition of the coefficient of friction (CoF) is nothing else that a macroscopic parameter used to describe the overall effects of an innumerable combination of phenomena and parameters. Nevertheless, when considering the macroscopic friction coefficient, as a results of all the local phenomena, its overall value and evolution, with respect to macroscopic boundary conditions such as sliding velocity or temperature, can be useful for the preliminary design of mechanical systems and the investigation of related dynamic instabilities of the system (mode coupling, stick-slip, etc.).

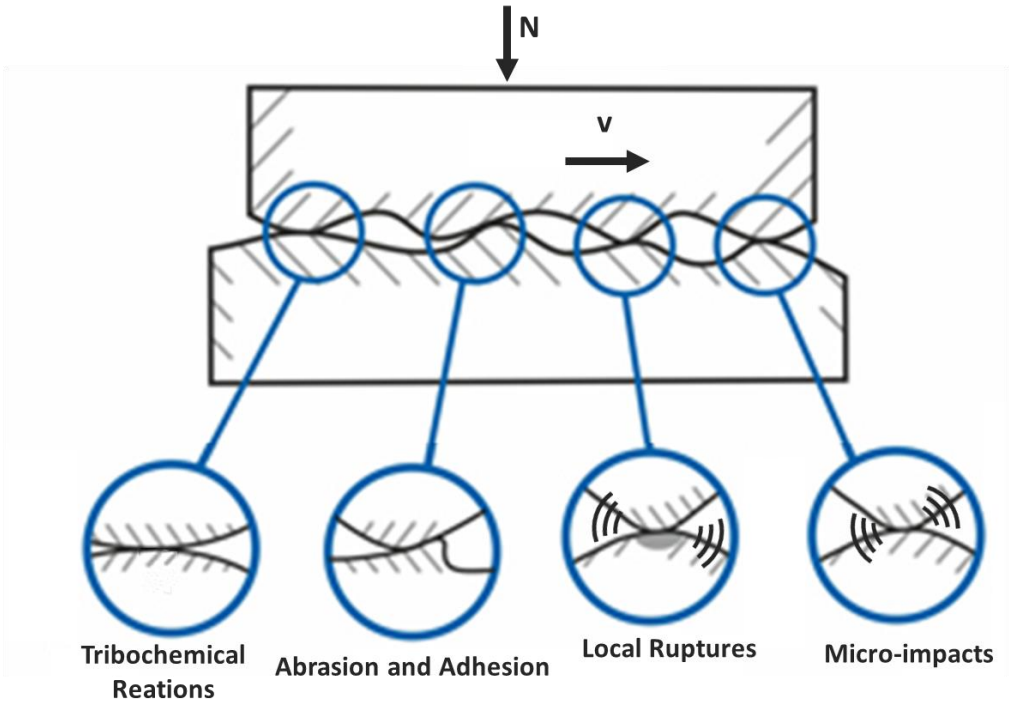

Figure 2: Scheme of the contact asperities during the sliding motion of one body over another.

1.1. Frictional contact generalities: dry and lubricated interfaces

As mentioned before, in dry sliding contacts between flat surfaces, friction can be modeled as the result of elastic and plastic strain of microscopical asperities in contact. For instance, considering some of the more commonly used friction empirical theories, frictional force at the contact interface is often attributed to [16]:

- the force necessary to shear adhesive junctions formed at the real area of contact between asperities;
- the deformation force, due to the ploughing of the asperities of the harder metal through the asperities of the softer one;
- the asperity deformation.

These forces and these three different effects are not independent. Friction can be then treated as the result of adhesion interactions, plowing interactions and asperity deformations.

Nevertheless, in this picture, a main actor is missing in determining the frictional response of a dry contact, i.e. the third body. As stated by Godet [11], the direct contact between two solid surfaces does not exist, and the presence of the third body (oxides, wear particles, external contaminants…) and its rheology drastically affect the overall frictional response of the system.

When an artificial third body (lubricant) is present at the interface, other physical mechanisms are added to the tribological system. A lubricant is a substance used to reduce friction and wear and to provide smooth running and satisfactory lifetime for machine components [25]. Lubricants, according to their physical state, may be solid (graphite, molybdenum disulfide, diamond-like carbon or polytetrafluoroethylene), liquid (oils) and gaseous (air, nitrogen, inert gases). There are also intermediate types, like semisolid/semiliquid (grease) lubricants. The main role of a lubricant is to accommodate contact stresses and relative velocities within its thickness, while separating the solid surfaces and evacuating energy (heat flows). When dealing with fluid lubricants, the Stribeck curve (Figure 3) illustrates schematically the different types of lubrication regimes, as a function of lubricant viscosity, η, sliding velocity, v, and applied pressure, p [26].

When the load is fully supported by a fluid film, the surfaces are completely separated by the lubricant and there are not asperities in contact. This is generally referred to as the *hydrodynamic* lubrication regime [27]. For high contact pressures (non-conforming contacts), the solids may be subjected to elastic deformation under the contacting conditions; this condition is generally referred to as the *elasto-hydrodynamic* lubrication (EHL) [28]. The hydrodynamic or hydrostatic pressure may not be sufficient to fully support the load, and the surfaces can come into contact. When the contact occurs between asperities of the surfaces, the amount and the extent of the asperities in contact depend on the lubricant viscosity, surface roughness, fluid film pressure, normal load, hardness, elasticity of the asperities, etc [29].

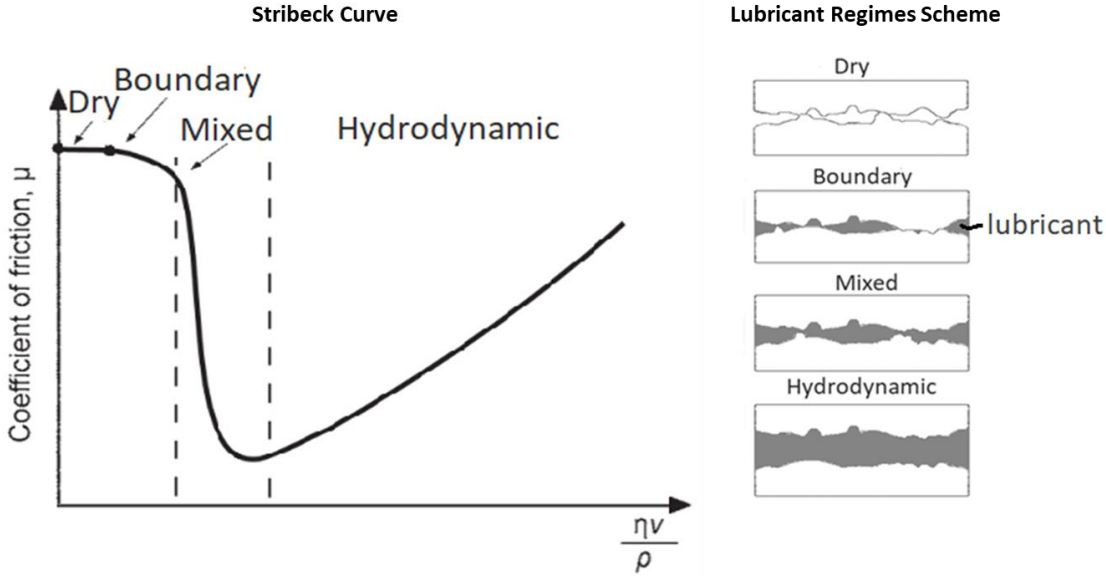

Figure 3: Stribeck curve and illustrations of the lubricant regimes.

A further increase in the contact pressure causes the plastic deformation of the asperities, the peaks in contacts increase and the fluid film thickness starts decreasing. When the average fluid film thickness falls below the average relative surface roughness, the asperities become the prevalent load supporting system. The contact is in a *mixed* lubrication regime. The intensification of this situation, due to a lower sliding velocity or a higher load, emphasizes the mechanical interactions of the asperities, leading to wear, deformation, abrasion, adhesion and fatigue [30, 31]. In this context, chemical reactions between the lubricant molecules and the contact surface can produce a boundary chemical film [32]. The combination of the load sharing by the asperities and the occurrence of chemical reactions constitutes the lubrication regime referred to as the *boundary* lubrication regime [29].

The performance of a lubricated contact is generally described, from a macroscopic point of view, considering the average film thickness, which is established at the contact interface [31]. In literature, the Hersey number ($\eta\, v/p$) is considered proportional to the effective lubricant film thickness between rubbing surfaces. When the thickness of the lubricant film, between the contact surfaces, is comparable with the surface roughness, contact asperities become in contact and the load is shared between the asperities in contact and the lubricant film. As a result, the friction coefficient (CoF) in boundary and mixed lubrication regimes is function of both the surface characteristics and the nature of the lubricant. Then, friction is largely influenced by the complex interaction between the surface topography, the lubricant pressure and the chemical reactions at the interface [33]. In general, the frictional response of such confined layers under shear will depend as well on the operating conditions (contact pressure, sliding velocity, and temperature), the nature of the surfaces in contact and their mechanical and topographic characteristics. The identification of the operating regime and the dynamic of transitions between boundary and mixed lubrication is a complex tribological problem, since the details of surface roughness and topography strongly influence the lubricant rheology and its ability to separate the contact surfaces. Moreover, in these two regimes of lubrications, collisions of asperities can cause deformation (elastic or plastic) and/or fracture, produce solid third body particles, severe wear and heat, resulting in a further evolution of the contact interface and its frictional response

Finally, when considering the interaction of a lubricated interface, in either boundary or mixed regime, with the dynamic response of the mechanical system, two main scales of observation can be considered:

- looking at the local phenomena, i.e. impacts and ruptures between asperities, these are sources of waves generation and propagation into the solids, which provide a broadband dynamic excitation that will result in Friction-Induced Vibrations (FIV);
- looking at the overall macroscopic effects of the local phenomena, as the resulting higher friction coefficient in boundary regime, or the negative friction-velocity slope within the mixed regime, the macroscopic frictional

characteristics can bring to dynamic instabilities (unstable FIV), such as mode coupling (due to high friction) or stick-slip (due to negative friction-velocity slope).

1.2. Friction-Induced Vibrations and stick-slip instability

Friction-induced vibrations involve a wide range of phenomena and applications. A general classification can be made, in agreement with previous studies [23, 24], as a function of the dynamic response of the system, in stable and unstable vibrations. In general terms, the local interaction at the interface (local impacts and ruptures of asperities and junctions) results in the release of elastic energy under the form of acoustic waves, generated and propagating along the interface and inside the solids in contact.

In case of stable vibrations, such broadband excitation at the interface excites the system dynamics, which remains stable and the induced vibration amplitude stays low, being damped by the material damping and the energy dissipation at the contact interface. The overall vibrational response of the system is a low amplitude large band vibration, modulated by the system dynamics (natural frequencies and mode of vibrations) [18].

Nevertheless, the dynamic of the mechanical system can be destabilized by the interaction with the overall frictional forces at the interface. In this case, the dynamic excitation from the interface can trigger a mode of the system that results to be unstable, due to either mode coupling [34], negative friction-velocity slope [35], or sprag-slip geometrical configuration [36]. The unstable system dynamics leads to feed the unstable mode with the energy from the contact interface, giving origin to high amplitude unstable vibrations [36, 37, 35].

In this case, friction-induced vibrations (FIV) can change drastically the relation between the remote stress applied at the boundaries of the bodies and the stresses distribution at the interface, with transient modifications of the tribological state of the contact interface itself. Unstable FIV are a main issue in mechanics, because they can cause excessive wear of components, premature failure and fastidious noise emission [1].

According to [37], from a vibrational point of view, the generation of unstable vibrations in systems with frictional contacts can be understood in terms of self-excited vibrations. From a kinetic point of view, an energy flow from the contact interface feeds into the dynamic system. Three different macroscopic instability mechanisms, occurring in sliding contacts, have been mainly described in literature [36, 38, 39]: sprag-slip, mode-coupling and stick-slip. All these mechanisms are amply described into the literature [6, 16, 1, 40, 41, 42]. Many works are focused on specific issues on complex systems, like brake squeal [43, 44], joint squeaking [45], earthquake faults [46] or tactile perception [47], in order to control or predict the effects of friction induced vibrations in each particular case, both in dry and lubricated contacts.

One of the most frequent, and most well-known way to generate unstable FIVs is when the coefficient of sliding friction decreases with the relative sliding velocity [48], leading to unstable oscillations, up to stick-slip phenomena.
Both in nature and in artificial systems, several examples of stick-slip instabilities exist, both in the case of dry and lubricated contacts. The sounds made by bowed instruments (violins and cellos) and grasshoppers, noises made during honing, heavy braking and screeching tires or chalk on a blackboard, the behaviour of some seismically active faults, the stepwise motion of slideways, hydraulic cylinders in aircraft simulators and the spinning of yarns in textile manufacturing are some of the most common examples of the stick-slip phenomenon [49, 50]. The role of friction and its dependence on speed are one of the key parameters necessary to understand the phenomenon.
Bowden and Tabor [51] suggested that the static friction coefficient is higher than the kinetic coefficient, owing to molecular bonding adhesion between the surfaces. Kaidanovsky and Haiken [52] noted the existence of a negative slope region in the friction-velocity curve for rubbing surfaces. So, one of the most widely accepted cause for stick-slip is that the static friction coefficient is markedly greater than the dynamic friction coefficient or, more rigorously, that the dynamic friction coefficient drops rapidly at small speeds [22]. In [53], it was highlighted that a discontinuous static/dynamic friction transition, or a decrease in dynamic friction with an increase in velocity, generate saw-tooth like displacement that results from stick and slip states. An original apparatus used to study stick-slip phenomena was built by Bowden [17]. The complexity of the phenomena was underlined, while the stick-slip behavior was considered as always occurring on a microscopic scale due to the clinging, elastic deformation, and shearing of surface irregularities, even though it may not be observable macroscopically. A more general view of stick-slip and its possible generation from the dynamic ruptures at the interface was discussed in [54].
By a macroscopic point of view, stick-slip instability is promoted whenever the coefficient of kinetic friction is lower than the coefficient of static friction, resulting in successive elastic energy releases in the system. When a driving force is applied to one of the solids in contact, high static friction prevents motion, until the force is enough to overcome it. Then, the surface starts to move and, with the change from static to dynamic friction, the elastic energy cumulated during the sticking phase is released and the sliding occurs [49]. The relative motion slows down due to friction, until the sticking is recovered again. The cycle starts all over again, defining the characteristic intermittent motion of the system.
One of the more widely spread models, based on the Coulomb's friction model, used to explain the stick-slip motion, is the lumped frictional system (mass-spring-damper-slider) sliding on a moving belt [55]. This single-degree-of-freedom model has been largely used to simplify the system dynamics and understanding the parameters that play a key role into the occurrence of stick-slip [56]. A solid of mass m at position x is attached to

a rigid foundation by a spring of stiffness *k* and a viscous damper with damping ratio *c*. The mass is riding on a driving belt, which is moving at constant velocity *v*, as shown in Figure 4.

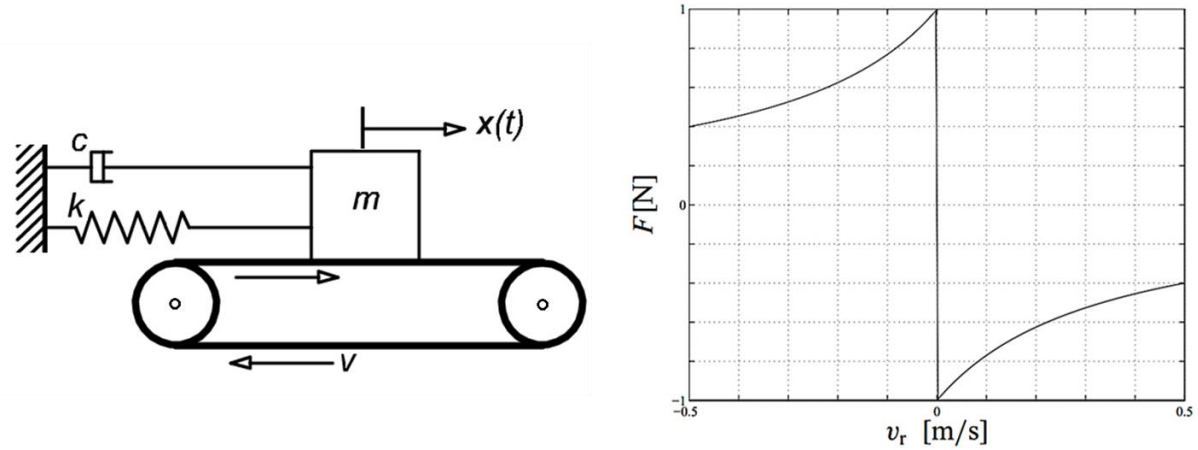

Figure 4: 1-DOF system with Coulomb friction and negative friction-velocity slope at the contact interface.

The equation of motion for the system is defined as follows:

$$m\ddot{x}(t) + c\dot{x}(t) + kx(t) = F(v_r) \qquad \text{Eq. 1}$$

Where, the relative velocity of the mass *m,* with respect to the belt is denoted by $v_{rel} = \dot{x}(t) - V$. The friction force *F*(v) is, in the slip phase, a function of the relative velocity v_{rel}; in the stick phase, it is a function of the externally applied force. So, the friction force can be read as:

$$F = \begin{cases} < \mu_s N & \text{in the stick phase} \\ sgn(\dot{x}(t) - V)\mu_k N & \text{in the slip phase} \end{cases} \qquad \text{Eq. 2}$$

The second equation applies whenever the relative velocity is non-zero, $\dot{x}(t) \neq V$ (slip condition), whereas the first equation applies if the sum of the external forces are lower than the static friction force and the relative velocity is nil (stick condition). The static friction coefficient μ_s is assumed to be larger than the kinetic friction coefficient μ_k. The difference between the two friction coefficients, $\Delta\mu$, becomes the driving source of stick-slip motion.

This simple spring-mass-damper system is useful to understand and simulate the unstable friction-induced vibrations related to the variability of friction with respect to the sliding velocity. Nevertheless, the local phenomena at the interface drive the overall resulting macroscopic force, and an accurate description of all these phenomena, and their interactions, requires refined contact models and rheological analyses.

The work from Ibrahim [15] depicts some aspects of the nature of friction, describing some of the main contact mechanics and the influence of the contact parameters on friction. Materials characteristics, sliding velocity [21], normal load [57], surface roughness [18] and temperature have to be taken into account as key parameters, and their effects into the resulting

macroscopic frictional forces have to be clarified. When accounting for the different physics and scales of a contact problem, recent works [23, 54, 58] reveal the presence of a mutual coupling between the local dynamics at the contact and the dynamics of the system. Each change in one of the contact parameters influences directly the contact dynamics and therefore the response of the system, due to the mutual influence of the local scale and the system vibrational response.
All these observations highlight the complexity of the stick-slip phenomena, which can result from both a macroscopic trend of the friction as a function of velocity and from the interaction of the system dynamic response with the interface local phenomena. In any case, what is macroscopically identified and described as stick-slip, is a result of several phenomena occurring at the interface: from the physiochemical reactivity of the surfaces to the rheology of the third body and the wave generation and propagation thought the real contact area, just to mention some of the several contributions to what is called "coefficient of friction (CoF)".

1.3. Stick-slip in lubricated contacts

Despite the use of lubricants has been promoted to reduce friction, stabilize the contact response and guarantee an adequate life of the components, lubricated contacts are not exempt from unstable FIVs. The presence of a lubricant introduces another parameter to the problem, which greatly influences the frictional contact response. Modeling friction and prevent the related vibrational problems (i.e. stick-slip) requires a then multiscale approach.
Considering FIV in lubricated contacts, in the case of mixed lubrication regime, with the lubricant's thickness decreasing, the asperities start to interact, promoting local impulsive excitations and generating waves that propagate along the interface and inside the bulk. Moreover, the overall frictional response changes, with no trivial dependence from the velocity.
In mixed or boundary conditions, the lubricant film can drop down to few layers of lubricant molecules (boundary lubrication regime) and the properties of the lubricant layer can change completely [59], increasing the complexity of the problem. Meanwhile, a full lubrication regime leads to a lower friction coefficient with constant or either increasing friction with velocity. Then, while mechanical systems working in full lubrication regime are less affected by FIVs, under specific conditions, the dynamic response of the fluid-structure system can bring to severe vibrational instabilities.
Dealing with stick-slip in lubricated contacts, several analytical macroscopic models [60, 61, 62, 63], simulations of molecular-scale processes [64, 65, 66, 67, 68] and experimental studies has been proposed in literature [69, 70, 71, 48, 72, 73]. Some of them deal with the theoretical and experimental challenging problems [19, 74, 75], others try to predict the stick-slip propensity as a function of the operating conditions [76, 77].
The first approaches proposed in literature were based on the empirical Amontons' Laws [60] and the Stribeck Curve [62]. Within this framework,

Armstrong-Helouvry [62] presented one of the first theoretical models to predict stable motion or instability at extremely low velocities, based on the Stribeck curve. The work focused the attention on the minimum velocity, below which stick-slip will occur, and the slip distance during the stick-slip motion.
Some works about the stick-slip in lubricated contacts [61, 71, 74, 78] asserted that the negative slope of the friction coefficient is not sufficient to completely explain the stick-slip motion, while the states, or phases, of the thin film during the motion must be taken into account.
Then, when dealing with lubricant films, diffused approaches are based on modelling a confined thin film at the molecular layer scale [79, 80] and investigate the molecular interactions between lubricant and solids in contact. One of the first molecular dynamic simulations about the stick-slip phenomenon in lubricated contact was performed by Robbins and Thompson's [81]. Their work showed that, when the thin film is confined statically (sticking), the molecules arrange in order, like in a solid state, and this order disappears in the following slip state. Even if the lubricant is a liquid, in such a confined geometry it might behave solid-like. They concluded that the stick-slip motion can involve periodic shear-melting transitions and recrystallization of the film. During the stick, a finite shear stress or static friction force is built up within the solidified film. When the maximum shear stress within the film is exceeded, shear melting of the film occurs. This slip process proceeds until the recrystallization of the film begins again [82, 83], as shown in Figure 5.
Aim of these molecular simulations is the analysis of the film behavior during the relative motion. In addition to the previously mentioned molecular dynamic simulations, based on atomically thin fluid films, other works [84, 85, 64] focused the attention on the energy lost during the stick-slip transition. Most of the results indicate that energy is lost due to the transition from a solid-like to a liquid-like state of the lubricant layer. Moreover, focusing the attention on the inability of the lubricant to refreeze during the final stage of slip, the results underlined a critical speed at which the system switches from steady sliding to an unstable behaviour.

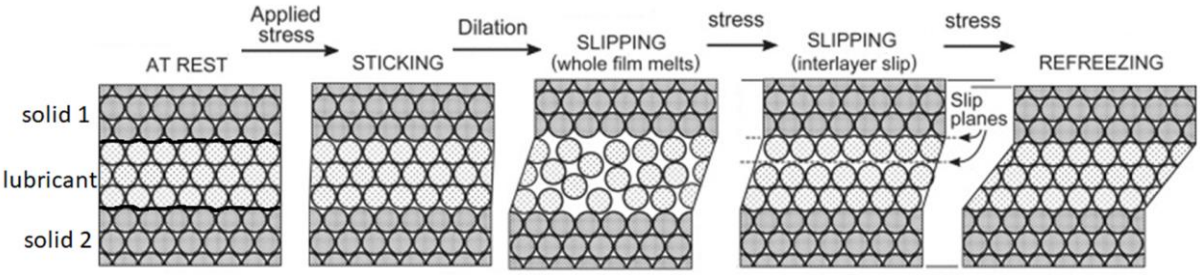

Figure 5: MD scenario of a lubricated interface between two solids during the sliding: i) the static loading, where the liquid film is ordered into quasi-solid-like layers; ii) under a shear force, the film dilates and partially melts and slips by viscous flow during sliding; iii) slipping can also occur intralayer; iv) the state at the end of each slip cycle is the recrystallization or refreezing, same as at the starting point.

This transition is typically discontinuous and sometimes hysteretic [86]. Nevertheless, Lei and Leng [64] showed that shear melting is one possible

scenario of the stick-slip mechanism in lubricated conditions, but not necessarily the only pathway for the energy dissipation during the slip state. Other proposed studies involve the development of a rate and state law to describe the macroscopic frictional properties of boundary lubricated systems, as in the case of dry contacts [87].
On the other side, some of the investigations on the stick-slip propensity in lubricated contacts are focused on experimental studies at different scales. Hess and Soom [63] performed a series of experiments that were run to examine friction-velocity characteristics of line contacts, operating under unsteady sliding velocities in the mixed, elastohydrodynamic and hydrodynamic lubrication regimes. Gao [78] analyzed the stick-slip propensity using a dynamic analysis for a pin-on-disk sliding system and considering the meniscus formation at the sliding interface. Rigaud [88] investigated the tribological response of a lubricated interface under free oscillating motion using a dynamic oscillating tribometer. He identified the instantaneous velocity-dependent and velocity-independent contributions to friction.
A restricted number of studies used a combined approach based on both experimental and numerical approach. Sinou [74] proposed a numerical model, constituted by a single-degree of freedom block on a moving belt, which incorporates the experimental results from local frictional behavior of confined monolayers of diamine at room temperature. The friction model used in the study is based on the formation and rupture of adhesive bonds between two shearing surfaces, considering that each junction can either be in a bonded state, contributing elastically to friction, or in a free state, participating to friction dissipation with a viscous contribution. He demonstrated the impact of the periodicity of velocity cycles and the values of minimum and maximum velocities reached by the belt, on the nonlinear behavior of the system, in terms of vibration amplitudes and frequency content. Nevertheless, in his work [74], the specific case of the evolution of the CoF, as a function of the sliding velocity, is analyzed for the confined monolayers of diamine at room temperature.
As evidenced by this overview of the main works dealing with stick-slip in lubricated contacts, the friction is largely dependent from the velocity. However, such dependence is largely affected by both the system (e.g. the contact surface geometry or the boundary conditions) and the rheology of the lubricant. For instance, lubricated systems under oil lubrication will not respond as the ones under grease lubrication. For this reason, there are still not clear generalized correlations between experimental and numerical analyses, necessary step to obtain a better understanding of the nonlinear stick-slip behavior of lubricated mechanical systems. While each single works can give relevant information on the specific investigated geometry and lubrication condition, providing some main information on the parameters leading to stick-slip, a general approach to fully investigate a stick-slip in a lubricated contact, under the effective operative conditions, is still missing. Moreover, while most of the works deal with stick-slip under oil lubrication, the effect of the complex rheology of a grease, including soap matrix, oil and additives, has not been investigated.

1.4. Lubricant Rheology

As mentioned above, lubricants are commonly used to reduce the friction and wear of surfaces in contact, but they can also collaborate to the appearance of FIV. Lubricants can be classified using a physical basis (aggregation state) or chemical criteria (chemical class or origin), the origin of the employed materials or in function of their viscosity. Usually lubricants are generally grouped as liquids (oils), semi-solids (greases), solids (surface coatings and powders) and gases (compressed air or other gases). In most of cases, liquid lubricants and greases are formed by a base oil to which additives and, for greases, a thickener are added.

1.4.1. Solid lubricants

A solid-film lubricant acts as a separating agent preventing metal-to-metal contact and lowering the CoF, having a low shear strength [89]. Such films are generated by tribologically activated reactions between lubricant additives and the metallic surfaces [90]. Usually they have a lamellar structure preventing direct contact between the sliding surfaces even at high loads. Examples of solid lubricants are graphite, molybdenum disulfide, tungsten disulfide, polytetrafluorethylene (PTFE), nickel-phosphorous alloy deposits (NiP) or diamond-like carbon (DLC) films. Depending of their composition, deposit technologies and physical characteristics, an extreme large variety of solid lubricants exists. For each of them, several works can be found in literature, addressing the overall tribological behaviour or the slight nuances that can bring to completely different rheological responses. In this thesis, DLC films and a NiP deposit will be investigated as possible surface treatments.

DLC films cover a wide range of coatings with different compositions and structures and therefore they also behave differently within a tribological contact. These coatings can be divided into two major groups, as a function of their hydrogen content: amorphous hydrogenated (a-C:H) and hydrogen-free carbon films (a-C). The two coating families have different mechanical properties and thermal stabilities. The a-C films have considerably higher hardness and higher elastic modulus compared to a-C:H films [91]. The difference in the structure and mechanical properties influences then the tribological performance of the coatings [90]. Anyway, in a general way, it can be asserted that DLC coatings are characterized by extreme hardness, high elastic modulus, excellent wear and corrosion resistance, high thermal and chemical stability, and low-friction characteristics [92, 93], but at a high production cost compared to others solid lubricant.

The NiP coatings, classified as solid lubricants, are the electroless nickel coatings. These are formed by an autocatalytic deposition of a nickel-phosphorous alloy (NiP), from an aqueous solution into a substrate, without the application of an electric current [94]. These coatings are widely used in the mechanical, chemical and electronic industries because of their corrosion and wear resistance, hardness, lubricity, uniformity of deposit regardless of geometries, solderability and nonmagnetic properties [95,

96]. These solid lubricants are largely used to reduce the CoF and are frequently associated to a fluid lubrication. Clearly the presence of a solid lubricant on the contact surfaces can change drastically the tribological properties and behaviour of the contact interfaces, even in the case of grease or oil lubrication.

1.4.2. Fluid lubricants

Fluid lubricants are often composed by a base oil to which additives are added. The base oil gives the general properties to the lubricant, such as viscosity, pressure-viscosity coefficient, density or thermal conductivity; on the other side, additives will confer specific properties to the lubricant, such as low friction, good wear resistance, enhanced viscosity at high temperature, good anti oxidation, etc. [97].
Base oils are mainly produced from mineral oils, synthetic Poly-A-Olefins (PAOs), synthetic esters silicones, vegetable oils, animal fats or mixtures of these. Mineral and synthetic oils are the most common lubricating oils utilised due to their availability, cost and compatibility with many engineering materials [30]. The efficiency of a lubricating oil is greatly influenced by its viscosity. Clearly, for any given application, the optimum lubricant viscosity depends on the relative velocities of the surfaces, on the material characteristics of the surfaces in contact and on the applied load. The physio-chemical reactions between the fluid lubricant and the solids in contact must be taken into account as well while choosing the appropriate lubricant.

1.4.3. Semi-solid lubricants

Greases are preferred in situations where low velocities/loads reduce the film thickness and when the lubricant could leak out of the contact under the action of gravity, load or accelerations. A grease is generally made of 85-80% base oil, 5-10% thickener, plus additives (~5%) [98]. The thickener traps the oil, maintaining the lubrication of the parts, and it determines the temperature operational window, while lubricity is governed mainly by the base oil and additives [99]. The consistency of the grease is a function of the thickener concentration and the manufacturing process [100]. A physical model generally used to explain some of the grease flow properties is a sponge impregnated by oil [101]. The base oil is kept inside the thickener structure by a combination of Van der Waals and capillary forces [102]. The effectiveness of these forces depends on how the fibers contact each other [103]. Calcium, Lithium and polyurea thickener are mostly used. In general, when a stress is applied to a grease, the lubricant response depends on the elastic and viscous properties of both the thickener fibers and the oil, respectively. The elastic characteristic prevents the grease from leaking, while its fluidity is essential to establish a lubricating film at the contact interface [104]. Thickening is the result of the physical interaction between thickener material and lubricating oil. In rheological terms, the elastic response to deformation is described by the storage modulus, and the viscous response is described by the loss modulus

[105]. With increasing thickener concentration, both the storage and the loss moduli will increase, but at a certain point, called the gel point, the storage modulus demonstrates a rapid increase by a few orders of magnitude. At this point the grease starts to lose its ability to flow freely. However, when the applied stress exceeds the yield stress, the internal structure of grease is broken and the grease acquires fluidity [105].

1.4.4. Additives

As reported above, both for fluid and semi-solid lubricants, additives are largely used to obtain the desired performances. A wide variety of chemical additives has been developed in the last decades. Some of the major classes are the anti-wear, friction modifiers, extreme-pressure additives, detergents, antioxidants, corrosion inhibitors and viscosity-index improvers [30]. The friction characteristics of a lubricant are largely affected by the use of additives. Wear and friction performances can be then controlled by the lubricant additives, which form tribofilms in the contacting surfaces, especially in boundary lubrication regime [106]. Then, in order to define and analyze the frictional behavior of a lubricated contact, the presence of additives must be taken into account too.

1.4.5. Influence of the grease rheology on the frictional response

The overall friction-velocity characteristic of a lubricated contact is a complex result of the synergy between several rheological and physiochemical contributions. The correlation between tribological properties and the chemical and structural nature of the lubricant has to be taken into account in the analysis of the frictional response of a lubricated contact [25]. More specifically, the role of the base oil, of the additives and of the thickener in the frictional behaviour of a greased contact is essential to understand the stick-slip propensity of the system under investigation.
The lubricating film formation is determined by the grease consistency and composition, i.e., thickener, additives and base oil type. As previously mentioned, the film thickness is an essential parameter to understand the frictional behaviour, but friction depends also on the history of the motion, the surfaces in contact and the operating conditions.
Few investigations on how grease composition, thickener type, additives, base oil type and viscosity affects the frictional behaviour, have been reported in literature. An interesting review can be found in [107]. Cousseau et al [108] noted a significant influence of the grease composition on the bearing friction torque and stated that the base oil properties and the interaction between the base oil and thickener are the dominant factors determining the tribological performance of greases in thrust bearings. De Laurentis et al. [98] noted marked differences in both grease friction and film thickness behaviour for different grease compositions. Moreover, they underlined a significant effect of the thickener in the low speed regime. Cann [109] conduced an experimental work with a ball-on-disc machine and fully flooded conditions showing the strong influence of the thickener type

on film thickness and friction. As an example, she demonstrated that Tetraurea greases produced higher films than the lithium-based greases, showing an 'inverse Stribeck' behaviour. More recently, Kanazawa et al. [107] investigated film formation and friction in grease (additive free), for lubricated rolling/sliding non-conformal contacts, under fully flooded conditions. The tests were performed imposing a driving speed range of 1000-1 mm/s. Both urea and lithium greases showed much lower thicker films compared to their base. The transition, from the thickener dominated low-speed behaviour to the oil dominated high-speed behaviour, occurred at a relatively constant film thickness for the tested greases. Moreover, under EHL regime, grease friction was entirely determined by the base oil viscosity, with no apparent influence of thickener type.
These studies clearly show that the grease composition, namely thickener type, additives, base oil type and viscosity have a significant influence on the frictional behaviour in grease lubricated contacts. A predominant role of either the thickener or base oil is often observed, respectively for low and high velocity regimes. However, most of the literature on the subject focus on the specific aspects of thickener structure or concentration, on the specific application case of bearings and in relative high velocity ranges. There are very few studies where the influence of each grease component is investigated in a systematic manner by considering the presence of solid lubricant, additives, thickener and base oil. Moreover, most studies overlook how the friction-velocity dependence of lubricants, in particular of greases, can drastically influence their tribological response at low velocities, which is the main range of interest when dealing with the propensity of the lubricated contact to promote stick-slip phenomena.

1.5. Concluding remarks and positioning of the work

As highlighted before, many studies can be recovered in literature either on contact instabilities or in lubricated contacts. Several works, when dealing with grease lubrication, are addressed to determine the rheological response in specific cases. Nevertheless, the literature presents few works [110, 111, 112, 113] available about the role of grease and its rheological response, related to the stick-slip contact instability.
The presence of lubricant at the interface increases the complexity of the stick-slip phenomenon from both a tribological and a dynamical point of view. The main works dealing with stick-slip in lubricated contacts are focused on molecular simulations or theoretical mathematical models, with the aim of understanding the phenomena, but rarely are then applied to a real case study. Then, there is a lack of information about the macroscopic tribological behavior of the lubricated contact and how it can influence directly the vibrational response of the entire system, fundamental step to understand the local conditions that can lead to stick-slip instability. Moreover, when the lubricant is a grease, its complex rheology, function of the thickener, the additives and the oil response, becomes a key point for the occurrence and evolution of the stick-slip, by driving the overall

frictional response as a function of velocity. The overall friction-velocity characteristic of a grease is a complex result of the synergy between several rheological and physiochemical contributions. A simple, reversible friction-velocity relation still does not exist and the different roles of the grease components during the sliding is nowadays still not clear. A general approach is then needed to account for the coupling between such local contact phenomena (i.e. the greased contact response) and the system dynamic response.
In this context, aiming to improve the understanding of stick-slip instability in greased contacts, the present Ph.D. work proposes a systematic approach to the stick-slip issues in lubricated contacts, addressing specifically to the greased frictional contact, within the low-velocity range, and its influence in the dynamic response of the system. The work has been developed referring to a real industrial case, in order to deploy the obtained results in a more realistic and detailed manner. The subject of the investigation is a mechanical brake used in tubular electric actuators, which can present frictional instabilities, generated at the greased contact between the two main brake components.

1.5.1. Case study: the spring-brake system

The used mechanical spring-brake is mounted on tubular actuators (Figure 6), which are subjected to many environmental and functional constraints. It must allow a strictly identical operation, along both directions of the engine rotation, and it must ensure the holding of the load.

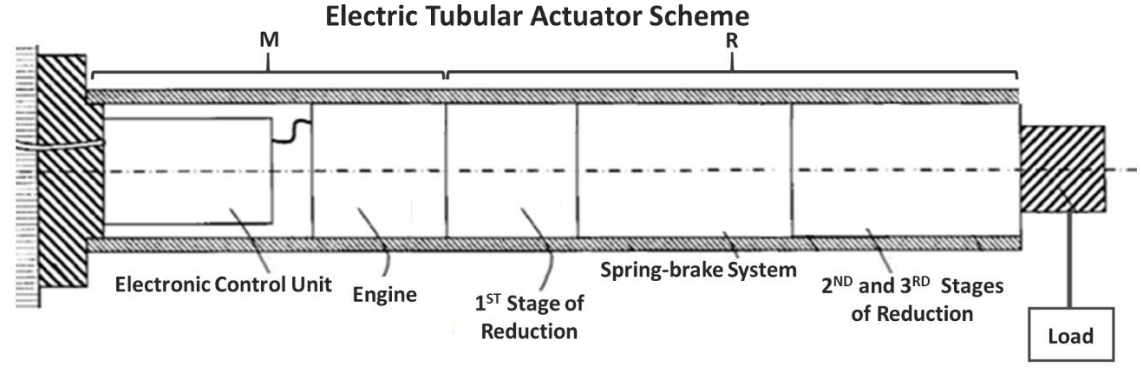

Figure 6: Detail of the electric tubular actuator containing the brake system under investigation.

The actuator is composed by an electric motor driven by a controller (block M in Figure 6) and a gearbox (block R in Figure 6), designed to transmit the movement from the engine to the output load, in which is included the mechanical spring-brake system.
During the operating conditions, two different configurations of the brake can be underlined: the *driving load configuration* (moving up the output load for a roller shutter application) and the *driven load configuration* (moving down the output load for a roller shutter application), depending on the case in which the output load (as example a store) is rising or falling.
The spring-brake concept is made up of four different components (Figure 7): the drum (a), the spring (b), the side frame (c) and the driver (d).

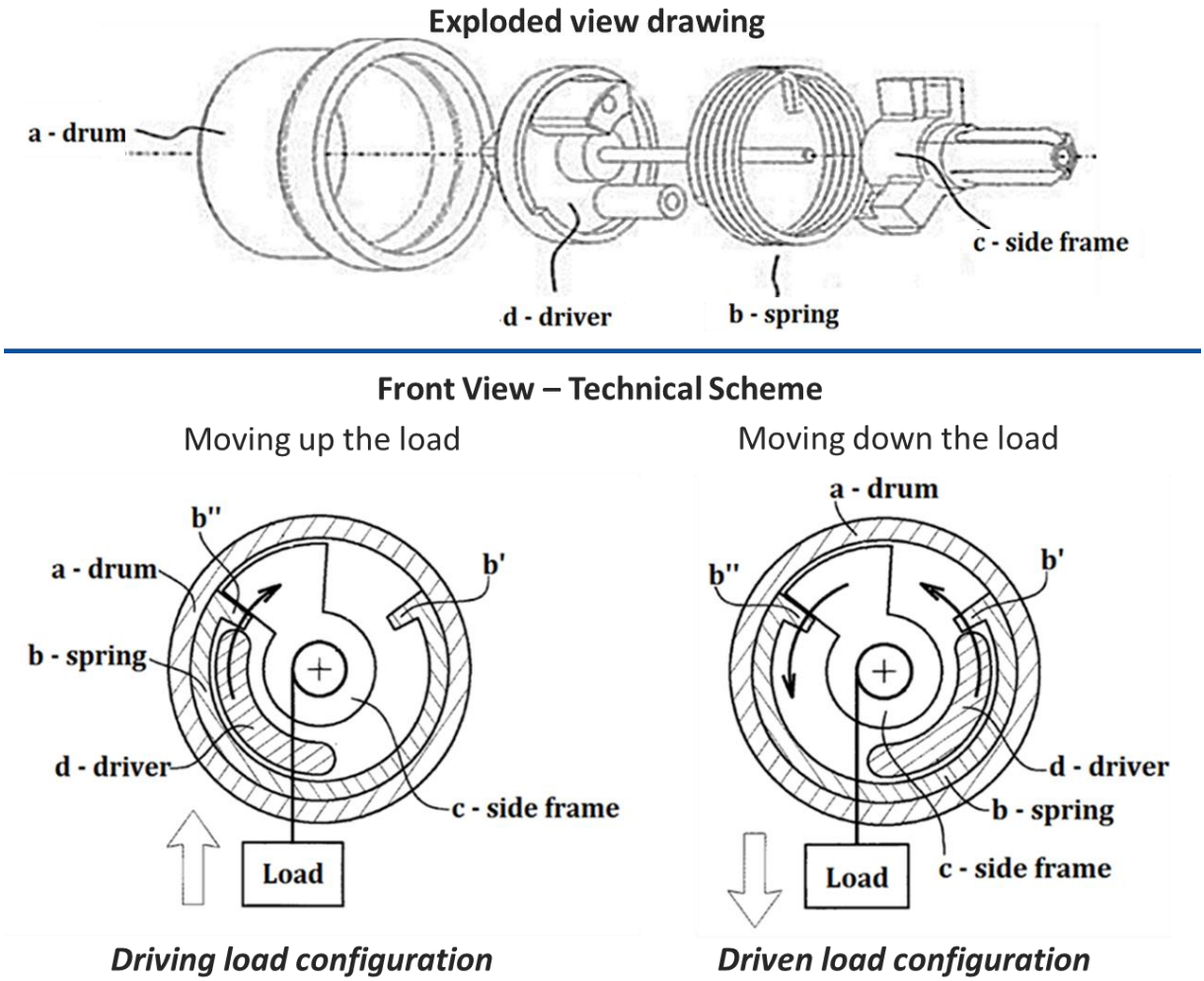

Figure 7: Scheme of the spring-brake system. Upper figure: exploded view of the assembly and identification of the brake components, drum (a), spring (b), side frame (c) and driver (d). Lower figure: technical scheme of the brake system functioning during the rising (moving up) and the driving down (moving down) of the load.

The external drum is fixed and a torsional spring is tightened inside it. The spring has both the ending parts bended towards the inside (*b′* and *b″* in Figure 7). The driver is stuck inside the drum and is directly connected to the engine, after the first stage of reduction. The driver transmits the rotation to the spring. The side frame (*c*) supports the output load. During rotation, the side frame is alternately in contact with the two spring end parts (*b′* and *b″*). In the moving down phase, the driver pushes the spring extremity b', in order to squeeze the torsional spring. When squeezing, the contact pressure between the external surface of the spring and the internal surface of the drum decreases, decreasing the frictional (brake) torque and allowing then the rotation (sliding) between the spring and the drum.
There are five different brakes, all working with the same principle, but with different geometries, materials, different drum and spring wire sizes, different lubricant, contact pressure, operating speeds and operating

temperatures. All these brakes can be affected by the presence of contact vibrational instabilities.
A specific brake geometry will be here taken into account as a reference, and it will be addressed to develop an in-depth analysis on the stick-slip occurrence under the greased contact. Nevertheless, a preliminary tribological analysis of the brake components of all the listed brake systems has been performed (see Chapter II), highlighting similarities on the tribological signatures of the contact instabilities observed in the different brake configurations. Then, the general approach and results, here proposed for a specific brake system, could be extended to the other systems and designs.
Focusing the attention on the brake under investigation, the drum is a sintered steel cylinder and the internal surface is machined with a defined honing angle (i.e. angle between the stripes produced by the honing tool that moves along the drum axis on its internal surface). The diameter of the spring is equal to 32.6mm in free condition, with a circular wire section of 1.6mm. The external surface of the spring is coated with a DLC film. The used DLC coating is a multilayer amorphous hydrogenated coating. The spring is tightened inside the drum and preloaded thanks to the interference between the drum and spring diameters. The contact interface, between the outer surface of the spring and the inner surface of the drum, is lubricated with a synthetic commercial grease (LiCPAO). The commercial grease is composed by a synthetic base oil (PAO) and a Lithium Complex thickener, plus the inclusion of additives. The grease aims to decrease wear and stabilize the friction between the components. During the braking phase the final part *b'* of the spring is constrained to the driver (*d*) while the final part *b''* of the spring is pushed by the side frame (*c*). The widening of the spring assures the braking, thanks to the increase of the contact pressure (and of the resulting frictional force) at the greased contact between the fixed cylinder and torsional spring.
The spring-brake described hereinabove will be used as a benchmark of the analysis. A typical stick-slip impulsive response has been identified (see Chapter II) after some completed cycles of the load (i.e. ascent and descent phases), when the temperature at the contact increases. and usually only during the descendent phase of the load. Because the unstable frictional response of the system is a consequence of the frictional contact response and its interaction with the system dynamics, an overall approach, accounting for both the scales of the problem, is here proposed.

1.5.2. Description of the proposed approach

The present work aims at investigating the stick-slip under greased lubrication, merging physical, experimental, rheological and numerical points of views and proposing an overall methodological approach, applied to an industrial case study (i.e. the spring-brake system).
As explained in the previous sections, the stick-slip phenomenon is influenced by the coupling of the local contact response and the dynamics of the whole frictional system. It is necessary then to have an in-depth

understanding of how the involved parameters affect locally and globally the system response. The PhD approach can be summarized by dividing the performed works into four mayor sections:

i. a first investigation, both tribological and dynamical, of the entire brake system and of the conditions affecting the stick-slip appearance (bock 1 in Figure 8);
ii. an experimental analysis, aiming to investigate the local frictional response of the greased contact, including a parametrical study on the main functional parameters of the real brake system (block 2 in Figure 8);
iii. a numerical analysis, aiming to simulate the dynamics of the overall system and its response to the local frictional behaviour (block 3 in Figure 8); a comparison and a generalization of the study on the framework of the real braking system is here performed;
iv. a focus on the role of the grease components in the local frictional response and then in the occurrence of the system dynamic instability (block 4 in Figure 8);

This overall approach will be accompanied by parametrical analyses, aimed to identify the role of the different working parameters on the stick-slip propensity.

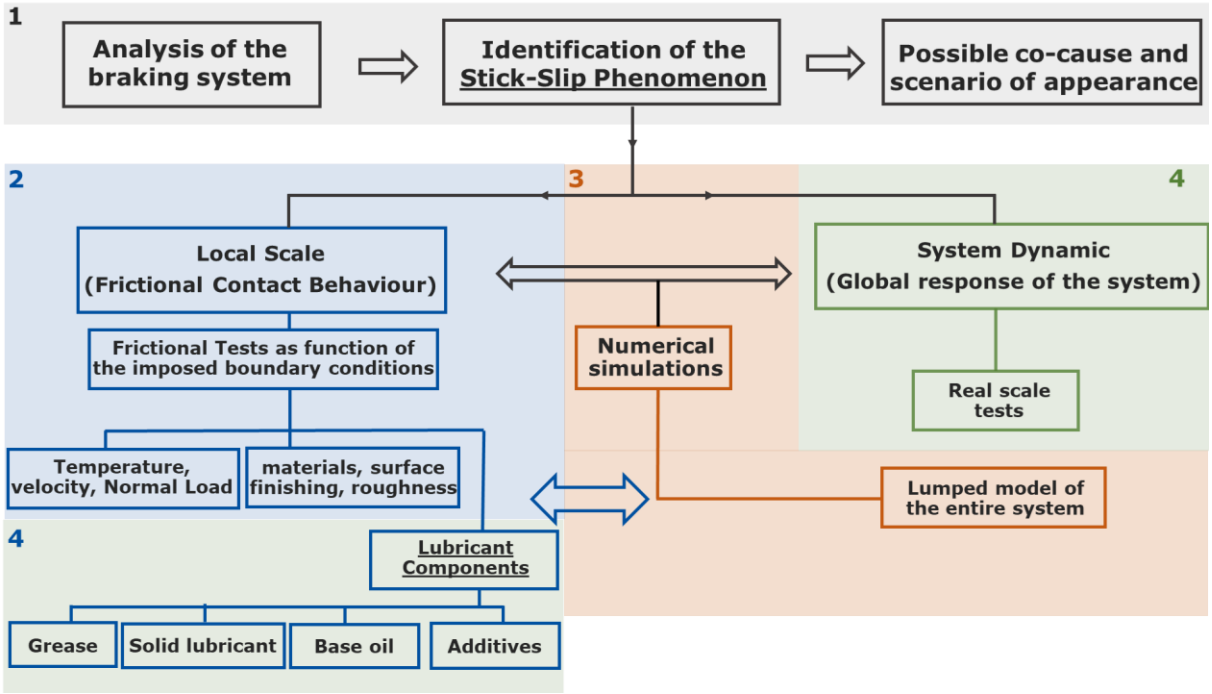

Figure 8: Schematization of the methodological approach investigate the stick-slip phenomenon in a greased contact.

- The starting benchmark of the analysis are the effective working conditions of the commercial mechanical brake, used in tubular electric actuators, which can generate frictional instabilities. The mechanical system has been analysed and the conditions for which the appearance

of the stick-slip instabilities may occur have been analysed from both a tribological and a vibrational point of view (ChapterII). Moreover, theoretical modelling, together with a finite element model, has been used to estimate the distribution of the contact pressure and the most stressed areas (see Chapter III). These data are necessary to determine the boundary conditions for the experimental tribological tests.

- Then, the local frictional contact response is reproduced and analysed on a dedicated tribometer (in Figure 8, block 2), in order to evaluate the trends of friction as a function of the imposed boundary conditions. The coefficient of friction is then analysed with respect to the sliding velocity, to retrieve a Stribeck-like curve. The same components of the real system (spring and drum) have been used, together with the same grease and DLC coating used for the application. The investigated parameters of influence are the surface roughness, the materials and the surface treatments of the bodies in contact. A deep analysis of the local behaviour in terms of the friction coefficient is a fundamental step to understand the contact conditions that could affect the stick-slip instability and its occurrence (see Chapter III).
- The coupling between the dynamic behaviour of the entire brake system and the local conditions at the contact has be performed thought numerical simulations. The numerical analysis has been performed by using a frictional lumped model (block 3 in Figure 8). The entire system (i.e. the tubular electric actuator in Figure 6) has been taken into consideration and the brake has been modelled with a nonlinear mass–spring–damper system with a confined frictional interface. As input of the model, the results of the experimental campaign have been used. The numerical analysis has the dual objective of understanding the role of the local contact frictional response (retrieved experimentally) and investigating the stick-slip phenomenon and its occurrence as a function of the key system parameters. Moreover, being representative of the whole actuator, the comparison with effective braking events on the commercial actuator allows for validating the results, obtained by the tribological experimental campaigns and the numerical simulations (see Chapter IV).
- Analyzing the results obtained thought the numerical lumped model, the influence of the grease frictional response has been identified as a key parameter. Aiming to isolate the influence of the grease components, the effect of the lubricant rheology on the frictional response is investigated (block 4 in Figure 8). Different types of lubrication, corresponding to dry contact, oil and grease, with and without additives, has been investigated though experimental tests (see Chapter V). The frictional response has been then related to the different contributions of the grease components (i.e. thickener, base oils and additives), analyzing the trends of the obtained frictional response as function of the sliding velocity, temperature and load.
- Finally, a conclusive chapter is presented. Goal of this block is the comparison of the experimental and numerical results obtained by this

study with the benchmark on the real industrial case of the spring-brake system and related frictional problems.

Understanding the conditions for which the system is more prone to the stick-slip phenomenon may allow preventing the appearance of such instabilities, and the related vibrations and noise emission, before its occurrence. This understanding is essential in order to establish the recommendations necessary for the development, industrialization and mass production of components, especially in the brake industry.

II. Stick-slip analysis in the lubricated spring-brake system

During the load descent phase, the widening of the spring ensures the braking, thanks to the contact pressure (and of the resulting frictional force) at the greased contact between the fixed cylinder and moving torsional spring. The operating conditions can induce unwanted noise emission. The presence of noise due to contact instabilities was detected in brakes of different sizes, materials, geometries of the spring coil, rotational speeds and output loads. The dynamic analysis of the system response during braking and the tribological analysis of the different contacting surfaces of the system have been here developed, in order to identify the signatures of the phenomena at the origin of the noise emission. This Chapter summarise then the dynamic analysis and the tribological observations performed on the different investigated brake systems.

2.1. Dynamic signature of the brake noise

Taking into account the reference brake systemin order to evaluate the dynamic response of the system, an accelerometer (B) has been placed on the external case (A) of the actuator (Figure 9).
The acceleration signal is then analysed to evaluate the presence and the features of vibrational instabilities arising from the braking system. The tests have been performed imposing an output nominal torque of 15Nm and a nominal speed regime of 337.8 rpm at the brake system.
The weight is fed up and down continuously for a total number of cycles equal to 10.

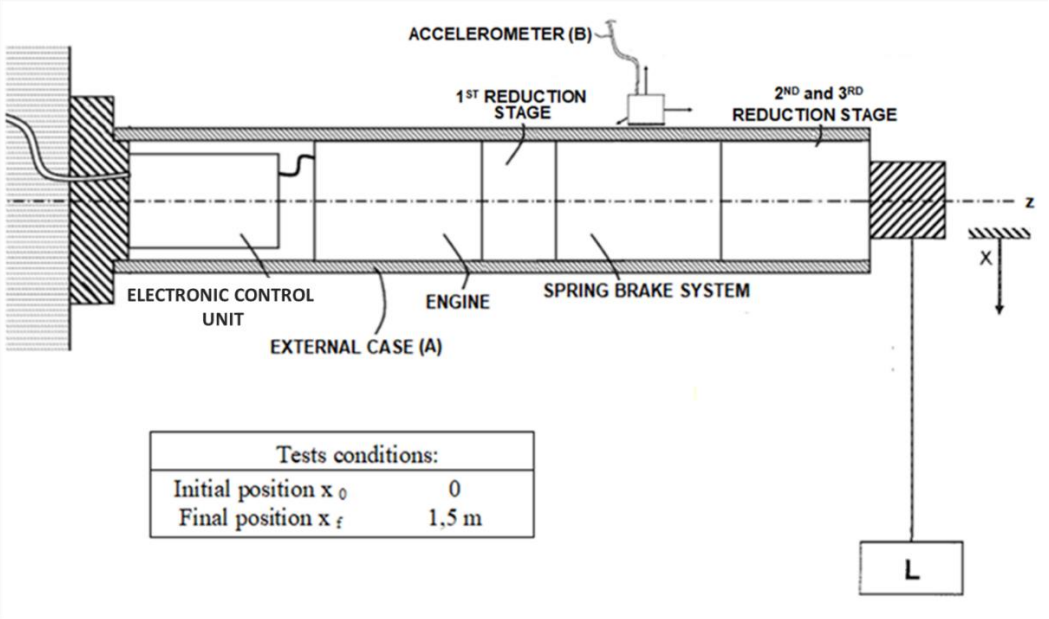

Figure 9: Schematic illustrations of the tests performed to evaluate the dynamic response of the system when imposing an output load L. The accelerometer (B) is placed on the external case (A) close to the brake system.

Analysing the acceleration as a function of the time (Figure 10), it is possible to highlight the vibrational response of the system, during the braking phase (descending phase). With the increase of the number of cycles, the internal temperature of the brake increases until reaching 80°C. In this situation, the response acquired by the accelerometer and the related spectrograms show the presence of impulsive periodic responses (Figure 10 b), due to the periodic excitation from the contact interface.

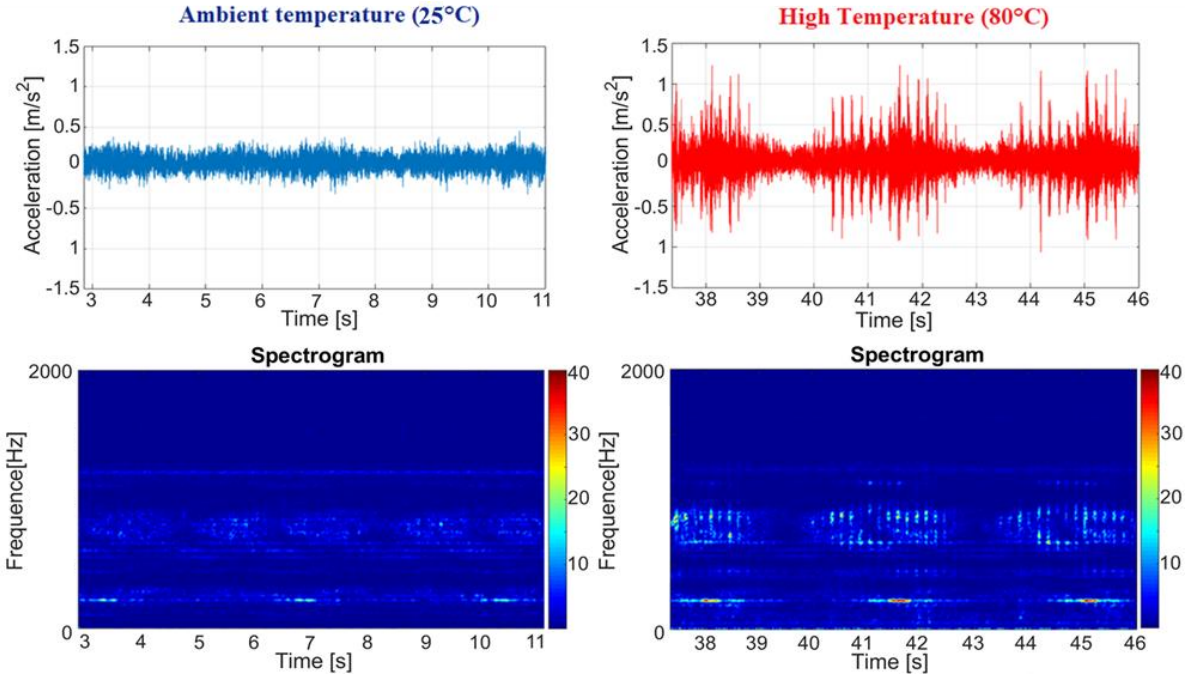

Figure 10: Time signals and the respective spectrograms of the acceleration, during the descent phase at ambient temperature, 25°C (blue signal), and higher temperature, 80°C (red signal). The colour-map is proportional to the amplitude of the vibration spectrum, as a function of the time.

Focusing the attention on the ambient temperature condition (at the first 2-3 cycles), the response of the system show the absence of contact instabilities. Analysing the corresponding spectrogram, the horizontal lines correspond to the natural frequencies of the system under analysis, which are the modes naturally excited during the normal functioning of the system. On the contrary, in the case of high temperature condition (80°C), the acceleration over the time, shown in Figure 10 (right), reveals the presence of periodical impulsive responses of the structure. Such response corresponds to the impulsive excitation of the entire structure due to the presence of a contact stick-slip instability. The analysis of the corresponding spectrogram enables the detection of the stick-slip phenomenon, characterized by the vertical lines, where all the natural frequencies of the system are excited periodically by the impulsive switch between sticking and sliding states.
Superposing the two signals and performing the Power Spectral Densities (PSD) of the acceleration, for the signals acquired during the load descent phase, at both room temperature (blue line) and 80°C (red line), it is possible to highlight the difference between the two dynamic responses (Figure 11).
In the first case (blue line), when the system is at ambient temperature (25°C), the braking phase proceeds without instabilities and the power spectral density (PSD) of the acceleration reveals exclusively low amplitude vibrations, due to the regular functioning of the system. On the contrary, analysing the PSD at high temperature (red line) we can notice that the spectrum of the acceleration shows an overall higher energy content. This is consequence of the impulsive excitations, due to the stick-slip intermittences, which excite all the system modes.

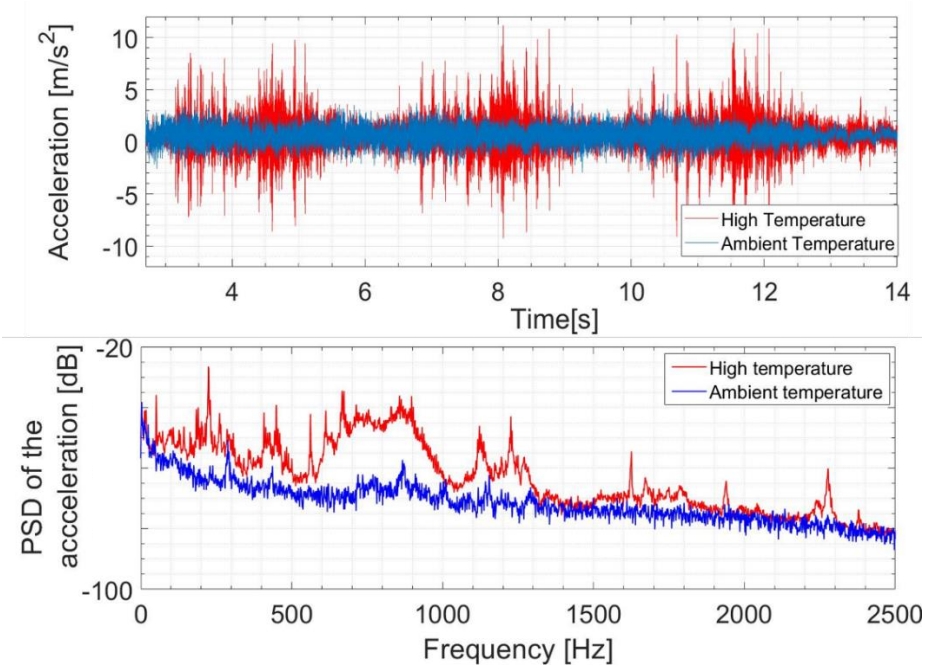

Figure 11: Acceleration in function of the time and Power Spectral Density (PSD) of the acceleration in function of the frequency, for the signals acquired during the load descent phase at 25°C (blue line) and 80°C (red line).

Moreover, observations of the braking system thought a slow-motion camera, highlighted the alternating movement, due to successive sliding and sticking phases, of the spring on the greased fixed cylinder, during the stick-slip appearance.
Other brake systems were analyzed, with the same operating method. The same conclusions can be made for all the tested brake systems:

- A typical stick-slip impulsive response can be measured at the corresponding position of the brake.
- The excitations are a succession of shocks whose occurrence frequency depends on the configurations.
- The impulsive excitations are repeated at each cycle of the brake system during the descendent phase of the output load.
- The stick-slip appears after some cycles of the load descend, when the brake internal temperature increases, reaching a temperature of about 80 degrees.
- The unstable frictional response of the system is a consequence of the greased frictional contact of the brake system. In fact, the same instabilities have been observed on the brake alone, separated from the other components of the actuator.

The interaction of the local contact response and the dynamics of the frictional system is at the origins of the stick-slip occurrence [2]. While the analysis of the acceleration signals allowed for identify a *dynamic signature* of the system response, coherent with a stick-slip instability, observations of the contact surfaces have been performed in order to identify the *tribological signature* of the phenomenon.

2.2. Tribological signature of the retrieved instability

Having therefore identified the different vibrational behaviours at ambient temperature and high temperature respectively, it is useful to analyse the topography of the contact surfaces both in absence and in presence of vibrational instabilities, in order to underline the tribological signature of the phenomena.
Both conditions have been analysed, by dismounting and observing two different sets of brakes subjected to the same operating conditions, one showing stable behaviour and another one presenting stick-slip instability. In fact, it should be noted that not all the brakes are affected by stick-slip instabilities, even in identical nominal working conditions. Only a reduced percentage of brake samples present the related noise emission, as often occurs when dealing with contact instabilities, which are a quite fugitive phenomenon [114].

2.1.1. Surface analyses on the reference brake system

The brake systems have been then dismounted and analysed with an optical microscope.

Figure 12 shows, from the top to the bottom, the side frame, the spring and the driver. Focusing the attention on the side frame, the contact zone here analysed is the area were the final part of the spring is in contact whit the side frame. This area is easily accessible, not affected by possible influence of dismounting and can give information on the spring movements. In fact, comparing the two analyzed configurations, silent and noisy brakes, it is clear how in the case of noisy brakes the contact area seems deeper and larger, suggesting a larger movement and possible axial displacement of the spring. Focusing the attention on the spring spires as well (middle images in Figure 12), in the case of the noisy brake, the spring show a misalignment of the spires that seems to be opened, due to an axial breath of the spring. The driver external surface show as well areas of contact more affected, with respect to the remaining contact surface, in the case of noisy brakes, compared to the silent ones.

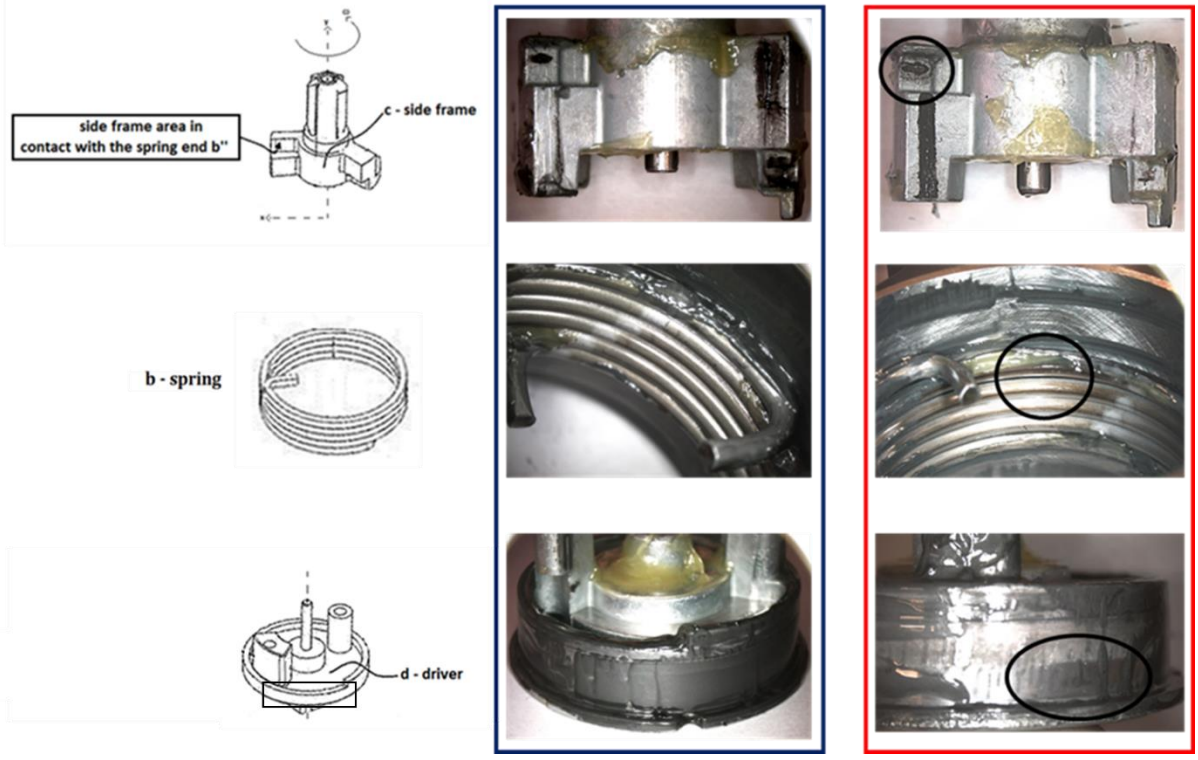

Figure 12: Surface analysis of the two tested braking systems showing respectively silent (blue) and noisy (red) behavior.

In conclusion, as highlighted in Figure 12, signs of both axial and radial displacement of the spring are clearly visible in the noisy brakes, highlighting a misalignment, or axial displacement, of the spires of the spring, with respect to the silent brake system. All the observations suggest that the spring tries to open axially inside the drum, falling out of alignment, with respect to the others brake components, and forming spaces between the single spires.

Therefore, the side frame and the drum surface show marks of axial displacements, where the pressure concentration is higher.

For a completed analysis, the surfaces were then cleaned with ethanol for 5 minutes and ultrasounds, allowing to remove wear particles and grease.

Then, the surfaces have been examined through a Scanning Electron Microscope (S.E.M.), model FP 2014/23 QUANTA 600, FEI, Brno, Czech Republic.
The contact surfaces between the side-frame and the spring and between the driver and the spring are shown in Figure 13.

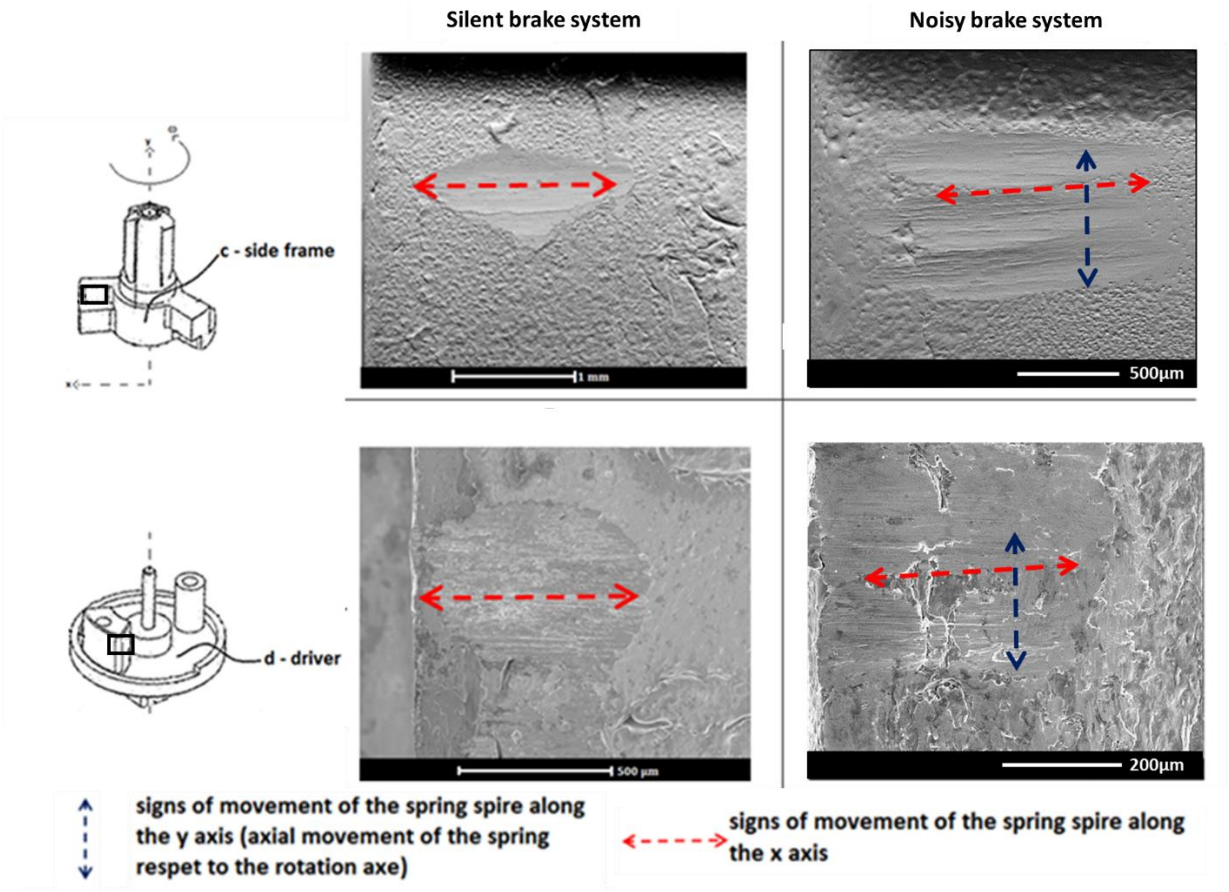

Figure 13: S.E.M images of the contact areas of the side frame (up) and driver (down) in contact with the end part of the spring (b'' and b' respectively), for a brake system that results not noising on the left and noisy on the right. The signs of movement along the radial direction (red) and along the axial direction (blue) are highlighted with arrows.

During the load descending phase, these contacts support the entire output load and are affected by all the movements of the ending part of the spring. For this reason, in the case of the presence of stick-slip instabilities, these contact zones will be largely affected by the relative motions (vibrations) between the spring and the rest of the brake components. For this reason, the traces of the presence of stick-slip are more evident at these zones, and these contacts have been chosen as representative to verify the movement of the torsional spring inside the drum during the braking phase.
Analysing the tests performed with the noisy brake, affected by the presence of stick-slip, vertical traces on the contact zone are observed (Figure 13 - right). These traces (blue arrows in Figure 13) are parallel to the drum axis. During the brake functioning, the stick-slip seems then to imply the breath of the torsional spring along the axis of the drum. The vertical traces identify therefore an axial displacement of the spring, which is not observed during braking in silent operating conditions (without stick-

slip). In the case of braking without stick-slip, there are only the traces of the radial movement of the ending pat of the spring, due to the normal operating conditions of the brake.
This behaviour is not dependent of the loading of the actuator. The same brake system, when imposing a lower output nominal torque, shows the same topological signature on the driver and side frame surfaces, in case of stick-slip appearance, as shown in Figure 14.

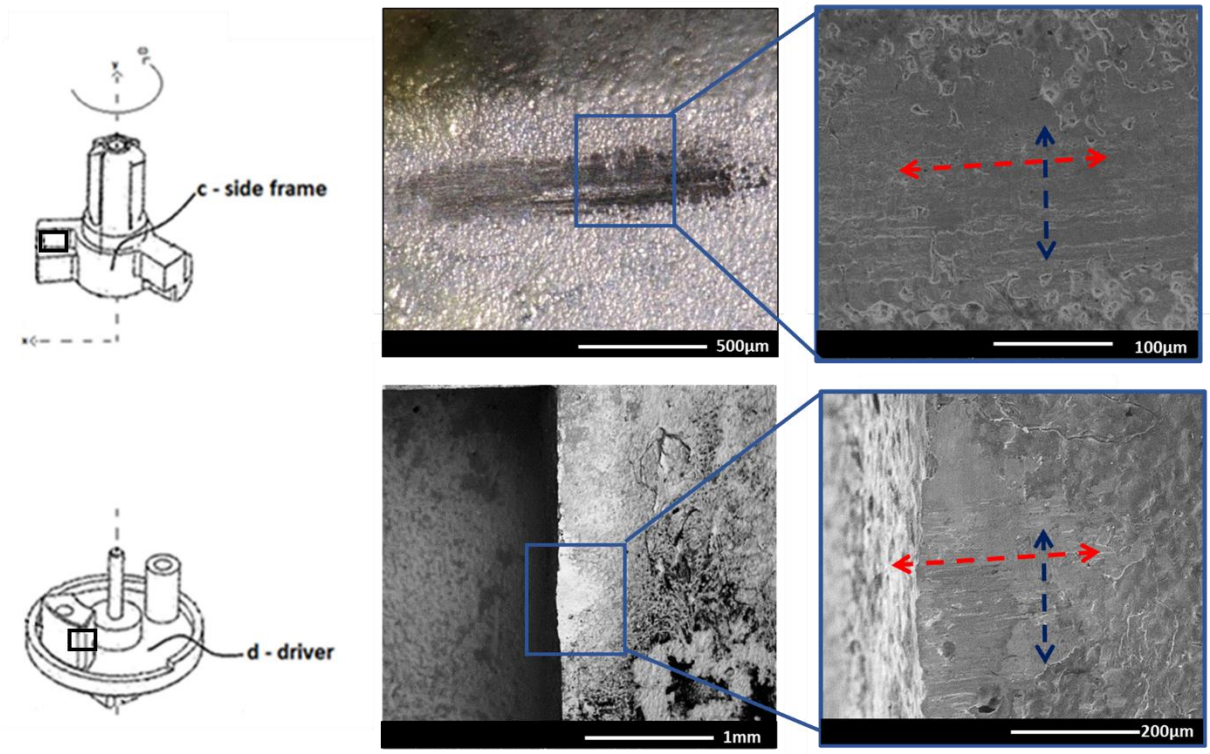

Figure 14: S.E.M. images of the areas of the side frame (up) and driver (down) in contact with the end part of the spring (b'' and b' respectively), for the noisy brake when applying 6Nm as the output nominal torque. The signs of movement along the x radial direction axis (red) and along the axial movement direction (blue) signs are highlighted with arrows.

Aiming to understand if the presence of these signs of axial movement of the spring can be generalized as independent from the spring-brake design, other brake systems has been analyzed.
First, considering the same brake design, another brake system has been taken into consideration (Figure 15), which has a similar conception but a larger dimensioning for larger loads.

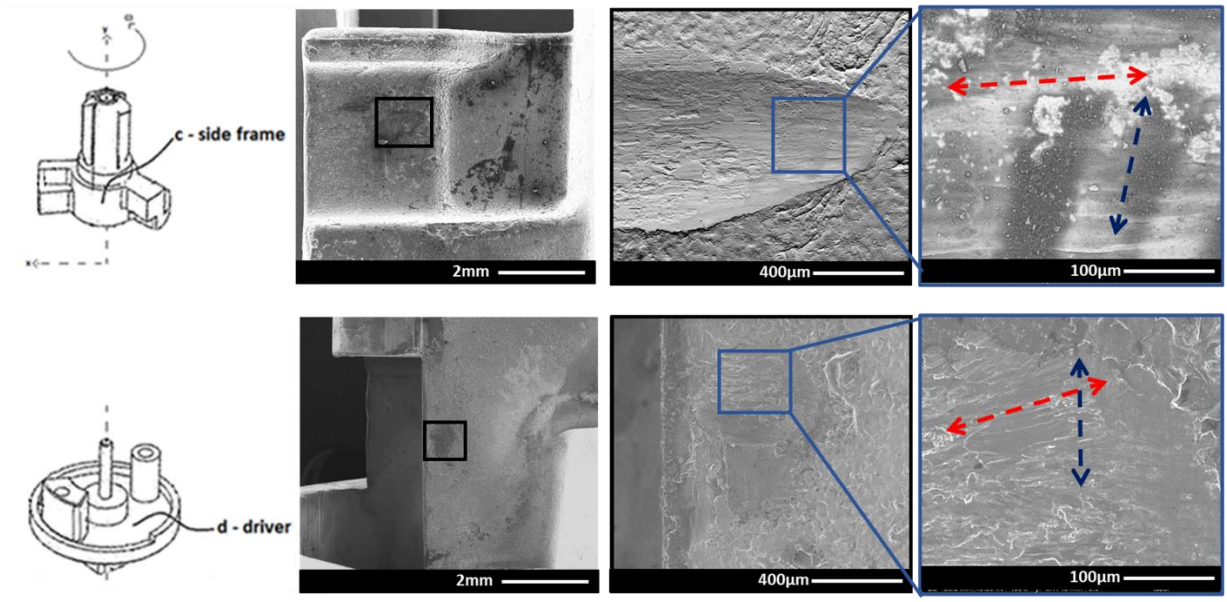

Figure 15: S.E.M images of the areas of the side frame (up) and driver (down) in contact with the end part of the spring (b'' and b' respectively). The signs of movement along the radial direction axis (red) and the axial direction (blue) are highlighted with arrows.

As in the previous analyzed cases, stick-slip seems to impose a breath to the torsional spring along the x-axis, leading to vertical traces on the driver and side frame contact surfaces (blue arrows in Figure 15). These vertical traces identify therefore an axial displacement of the spring, which seems independent from the applied output nominal torque. Again, in the case of braking without stick-slip, there are only the traces of the radial movement of the ending pat of the spring, due to the normal operating conditions of the brake (red arrows).

2.1.2. Generalization of the observed tribological signature

Aiming to clarify if this *tribological signature* of the stick-slip appearance is unique of the brake design or can be generalized for all the spring-brake systems subjected to the stick-slip phenomenon, others brake systems have been analyzed, taking into considerations different drum geometry and materials, different spring geometry and solid lubricant, and different nominal conditions. As an example, Figure 16 shows the complete analysis of the greased brake system named BS2, which presents a square spring spire, different design and dimensions of the components and different operating conditions, with respect to the reference one.

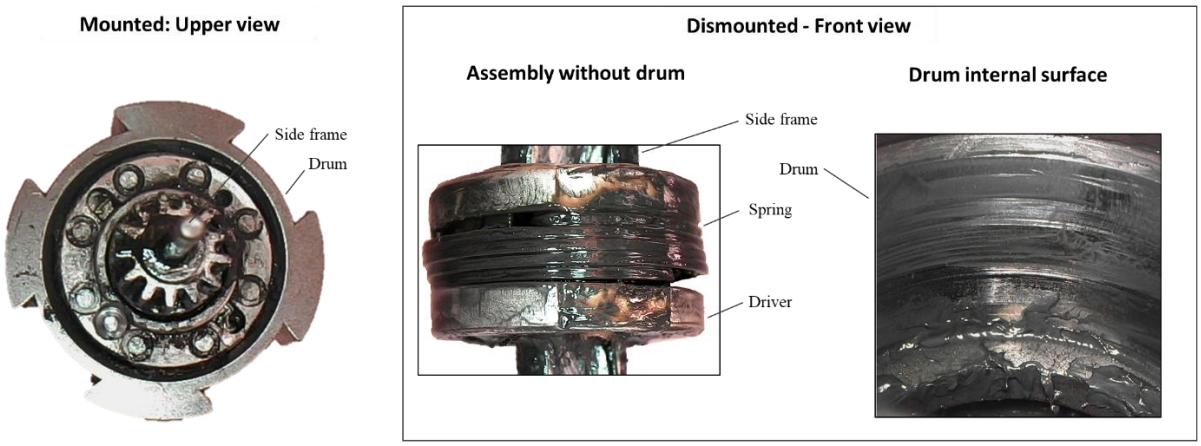

Figure 16: Optical microscope images of the BS2 noisy spring-brake system showing stick-slip appearance. On the left side the mounted view of the entire brake system. On the right side the images of the dismounted brake.

Focusing the attention on the dismounted assembly of the noisy brake system, without the drum, it is possible to underline that the spring is misaligned with respect to the original position and that there are areas of stress concentration on the outer surface of both the side frame and the driver.

Moreover, analyzing the internal surface of the drum, corresponding to the areas of contact with the external surface of the spring, there are some areas where signs of pressure and stress concentration are observed, probably due to the misalignment of the spires of the spring.

As in the case of the reference brake, the side frame and driver surfaces in contact with the end parts of the spring have been cleaned with the previously reported protocol and examined through the Scanning Electron Microscope (S.E.M.). Figure 17 shows the same tribological signature retrieved at the contact surface of the BS2 noisy brake system.

Traces along the axial direction are observed on the contact zone (blue arrows). Again, during the brake functioning at the imposed rotational speed, the stick-slip seems to imply the breath of the torsional spring along the x-axis also in the case of a brake system with a completely different design.

The identified tribological signature is independent from the spring-brake geometry, characteristic and operating conditions. The axial traces identify the axial displacement of the spring, which is not observed during braking in absence of stick-slip.

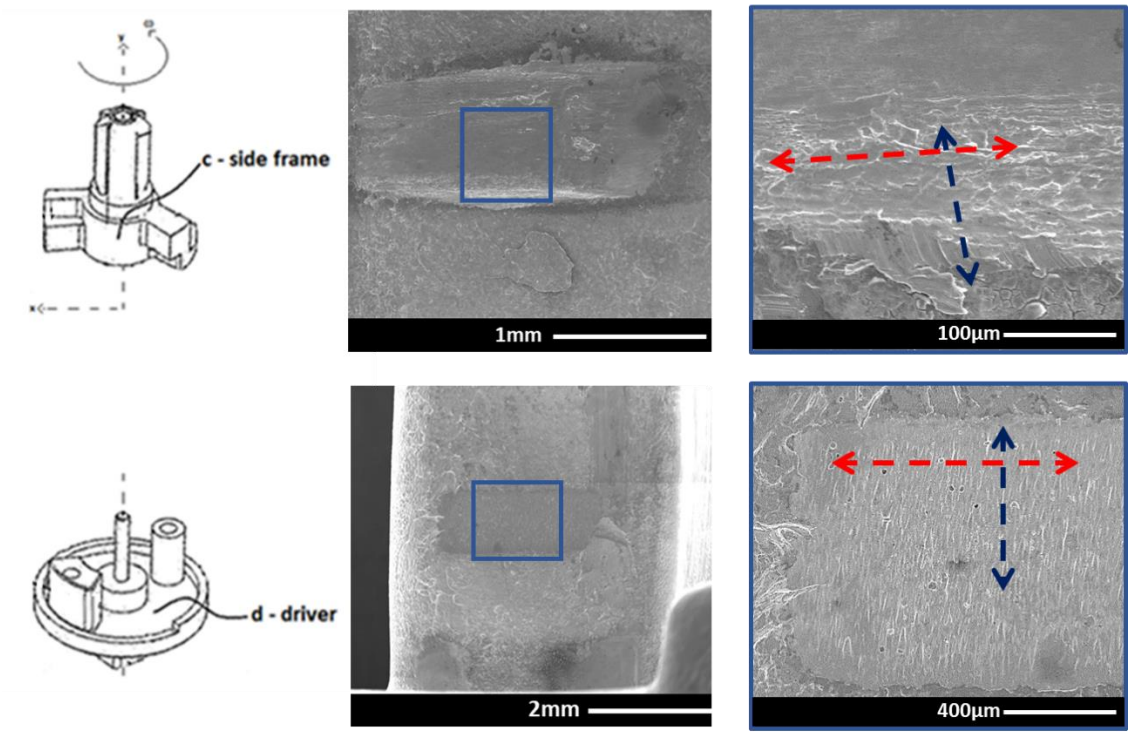

Figure 17: S.E.M images of the areas of the side frame (up) and driver (down) in contact with the end part of the spring (b'' and b' respectively), for the noisy BS2. The signs of movement along the radial direction (red) and the axial direction (blue) are highlighted with arrows.

The same observations have been made also for the BS3 brake system and the same result has been obtained. Finally, Figure 18 shows the S.E.M. images of four of the different analyzed brake systems (different nominal output torque, rotational speed, spring geometry, solid lubricant, drum material and geometry), all affected by the stick-slip phenomenon. All these brake systems have the same axial traces on the side frame and driver contact surfaces.

In conclusion, as observed above and highlighted trough the surface analysis, when considering noisy brakes (i.e. during braking with stick-slip instabilities) the torsional spring does not remain in the original axial position. The discontinuous motion, characterized by alternating phases of sliding and sticking of the spring on the cylinder occurs, inducing as well an axial displacement (breathing) of the spring, leading to a clear visible *tribological signature* on the contact surface of the side frame and driver.

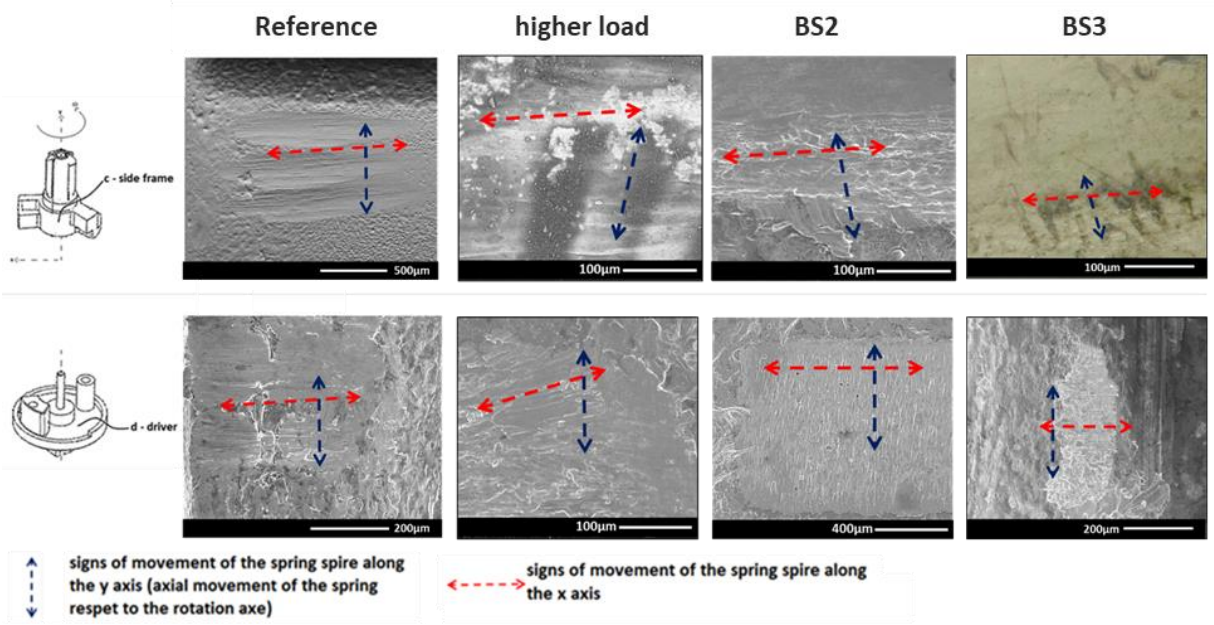

Figure 18: S.E.M. images of the areas of the side frame (up) and driver (down) in contact with the end part of the spring for different brakes, all affected by stick-slip.

This axial component of the displacement and the consequent misalignment of the torsional sprig can lead to modifications of the nominal working conditions, at both the system and contact scales: on one hand, the overall torsional stiffness of the spring could be drastically reduced, reducing the system stiffness; on the other hand, the contact pressure distribution between spring and drum, along the spire length, can be largely modified, leading to higher local pressure conditions.
These conclusions are independent from the applied output load, operating conditions and spring-brake design, but characteristic of the stick-slip appearance.

2.3. Concluding Remarks

The preliminary analysis, summarized in this Chapter, allowed to identify the stick-slip contact instabilities. Looking at the vibrational signal analysis and at the topography of the observed surfaces, the periodic impulsive excitations, due to the succession of sticking and sliding phases, at the greased contact between the spring and the drum, bring to a periodic excitation of the system dynamics and are accompanied by the presence of traces of axial movement of the spring. These dynamic and tribological observations are repeatable and characteristic of all the analysed noisy brakes, with respect to the silent ones.
While the impulsive dynamic excitation of the structure is a consequence of the stick-slip frictional response, the axial breathing of the spring during sick-slip could be either a cause or an effect of the instability. On one hand, during braking with stick-slip, the torsional spring does not remain in the original position. The attempt of the spring to open axially can cause a misalignment of the components, a modification of the spring stiffness, a

degradation of the grease role and a localization of the contact pressure. All these factors could then contribute to the occurrence of the instability.
On the other hand, the stick-slip movement of the spring can be associated as well to an alternation of static phases, in which the system accumulates potential energy, alternated with dynamic phases, in which the potential energy is released and could cause an axial component of the spring displacement. Thus, the kinetics of the system, due to the stick-slip phases, could be at the origin of the axial movements of the spring.
In any case, as explained in Chapter I, the occurring of vibrational instabilities is due to the interaction between the system dynamics and the local contact behaviour. Several contact parameters can affect the response of the vibrating system, such as normal load, sliding velocity, surface roughness, component geometries, material properties, types and conditions of lubrication, physio-chemical interactions between lubricant and interfaces, etc. Each change in one of the contact parameters influences directly the overall frictional response and, consequently, the dynamic response of the system. Moreover, as observed in the previous Chapter, the presence of a greased contact increases the difficulty of the problem.
For this reason, after having identified the stick-slip instability on the whole brake system, and analysed its tribological and dynamical signatures, an in-dept analysis has been performed to investigate the local frictional response of the greased contact by specific tribological tests.

III. Experimental analysis of the local frictional response

Understanding and controlling the stick-slip phenomenon needs an in-depth knowledge of how the involved parameters affect locally and globally the system behavior. In Chapter II, the presence of the stick-slip phenomenon has been identified and the investigations underlined that stick-slip occurs at the greased contact between the spring and the drum. Moreover, its occurrence is observed after some cycles of the system working protocol, when the contact is subjected to a higher temperature. Furthermore, this phenomenon has been emphasized on several brakes, including different drum or spring geometries, lubricants, speeds and normal loads.
Then, aim of the experimental campaign, presented in this Chapter, is the characterization of the frictional response at the contact scale, in order to understand how the contact parameters can affect the stick-slip instability. Starting from nominal working conditions, a parametrical analysis is then performed to investigate how the frictional behavior of the lubricated contact between spring and drum is affected by different design configurations.
The reference configuration is the one used in the braking application [115], with a commercial Lithium Complex grease and DLC coating at the interface. Based on the existing benchmarks of brake systems under production, some main parameters have been identified as the ones that could affect the frictional response of the greased contact and promote the stick-slip appearance. Starting from the reference configuration, the parametrical analysis has been then performed. The tested parameters are the surface coating of the spring, the drum roughness, the drum material and the lubricant composition and rheology.
The parameters of interest have been varied at each test campaign, maintaining constant the ranges of the operating conditions (load, velocity, temperature) where the frictional response has been analysed. While the effects of the topographical and material parameters of the solids in contact are reported here, Chapter V focuses on the response of the contact to the lubricant composition.

3.1. Experimental test bench

Taking into consideration the real brake system and focusing the attention on the greased contact between the drum and the spring, a simplified tribological system has been developed to measure the local frictional response of the contact, under well controlled boundary conditions, as illustrated in Figure 19. The frictional tests are performed on a drum, cut in two parts, and a sector of the spring coil, retrieved directly form the production line of the mentioned components of the spring-brake system. The components are all selected from the same production batch,

unassembled and ungreased (except possible residual grease from the sintering process).
In Figure 19, the upper sample is the coil section (semi-circular section) of the steel torsional spring. The external surface of the torsional spring is covered by a DLC layer. The used DLC coating is a multilayer amorphous hydrogenated. The spring coil section is loaded against the semi-cylindrical steel specimen (drum) by a constant normal load.

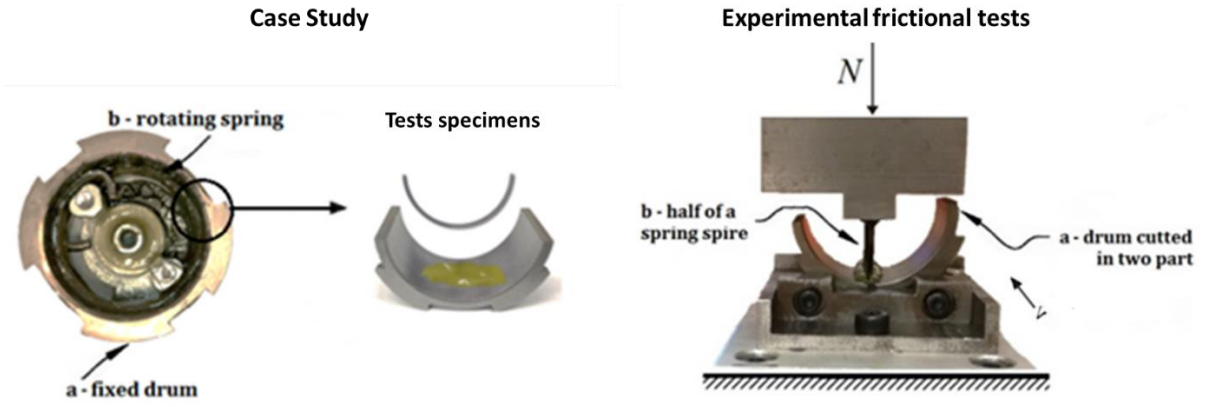

Figure 19: From the case study to the simplified frictional tests on the greased contact between drum and torsional spring.

The lower specimen is the half of the hollow drum cylinder, made of sintered steel. It is characterized by a defined honing crosshatch angle. The crossing canals of the honed surface allow to settle lubricant reserves, which can strongly influence the lubrication conditions at the contact..
Aim of the experimental tests is the analysis of the local behaviour of the lubricated contact, in terms of friction coefficient. For this reason, the tests are performed positioning the spring coil rotated of 90 degrees with respect to the real operating configuration of the brake system. The rotation has been necessary to allow the reciprocating motion of the spring on the drum surface, imposed by the tribometer. Nevertheless, this position allows as well to localize the contact area (contact pressure) in a reduced contact zone, which is representative of the contact localization between the spring and drum during the operative conditions. In fact, as explained thereafter in Section 3.2.1, the deformation of the spring brings the pressure to be localized mainly on three or four contact zones.The reduction of the contact area (ellipse), obtained with the rotation of 90 degrees, allows approaching the contact geometry in these localized zones. Moreover, about the surface topography, the direction of the honing grooves has been accounted for when performing the tests in this configuration.
The principle of the experiments is shown in Figure 20, where the two specimens are tested trough a testbench called *TriboAir*.

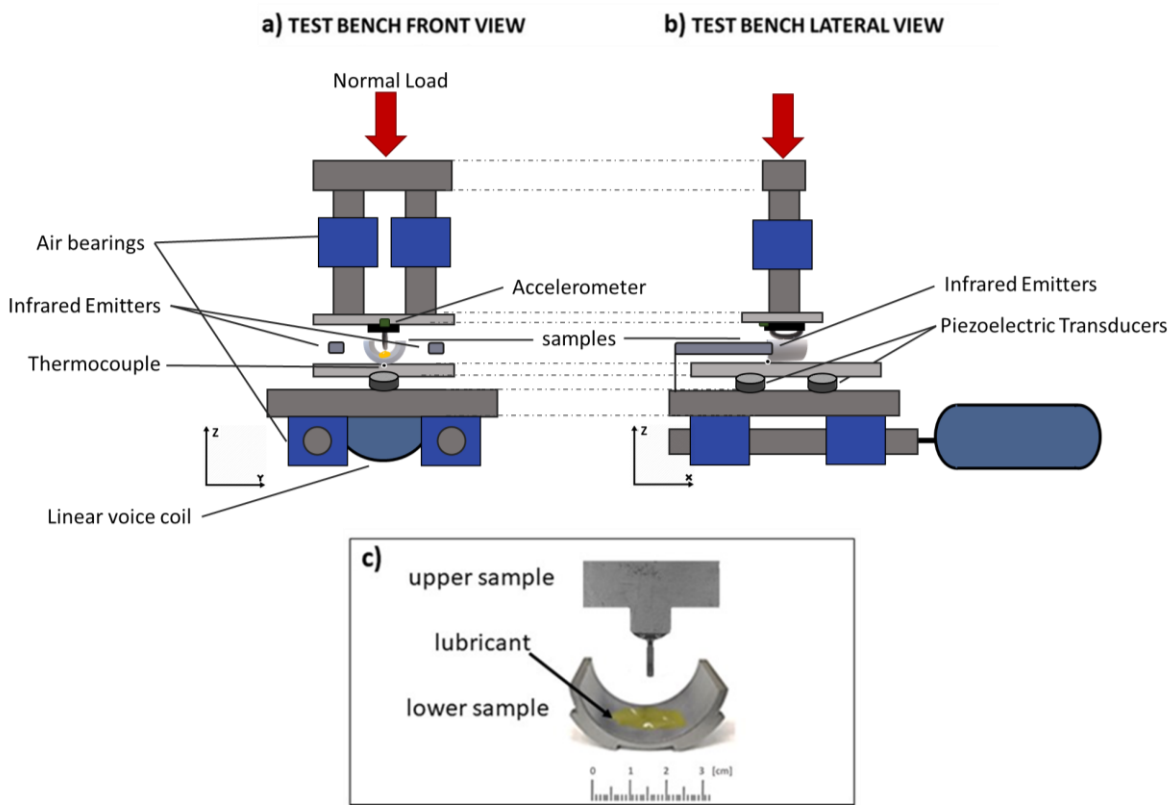

Figure 20: Test bench scheme. a) front view. b) lateral view. c) detail of the samples in contact.

The driving relative velocity, imposed to the lower sample, can ranges from 0.1 to 50 mm/s and is imposed driven by a linear voice coil (BEI KIMCO LA30-75-001A). The speed profile is regulated by a controller (ELMO Gold DC Whistle) and a linear optical encoder (MicroE OPS-200-1-1), which measures the instantaneous position with a resolution of 0.1μm. The normal force is applied by death weights along the z-axis and supported by a two air bearing system. The air bearings allow for avoiding frictional forces in the vertical direction, assuring a constant normal load. The tangential motion of the lower sample is allowed as well by air bushings, in order to avoid any parasitic noise coming from the set-up and allowing then high-resolution measurements. The contact forces are measured with two 3-axial piezoelectric transducers (Kistler 9017C). The two 3-axial force transducers are mounted on the translating base of the test bench, in order to measure the overall normal and tangential contact forces. The signals are acquired synchronously by an 8-channels analogue-to-digital data acquisition card (NI4472) at the sampling frequency of 5120 Hz and then post-processed using Matlab ©.
Infrared lamps have been used to regulate the temperature of the specimens, which is monitored by thermocouples positioned on the samples, close to the contact surfaces. The two infrared (IR) emitters are placed on the side of the samples in contact, allowing to perform tests at different temperatures. This allows to consider the heating that the real brake system undergoes during its operating, analysing how the

temperature affects the frictional response of the contact. Two ceramic plates thermally isolate this area, protecting sensitive test-bench parts from overheating and allowing to maintain a constant temperature during the whole test. During each frictional test, the applied normal load, the sliding velocity and the temperature are then controlled and maintained constant. A normal load *N* is imposed and the two surfaces are rubbed against each other at controlled sliding speed *v*. In the developed system, the spring spire is fixed and the drum is moved along the x-axis (Figure 20). In the reference configuration, the two contact surfaces are lubricated with grease, in quantities representative of the effective lubrication of the brake system, in order to assure a similar grease intake.

3.2. Definition of the contact boundary conditions

The experimental test bench has been designed to measure the contact frictional behaviour under well controlled boundary conditions. The tests have been here performed to characterize the local frictional response at the greased contact, by identifying the evolution of the friction coefficient as a function of sliding velocity, temperature and contact pressure.
The values and the ranges of the controlled boundary conditions (sliding velocity, temperature and normal load) have then been first identified to be representative, as much as possible, of the real operative conditions of the brake systems under investigation.

3.2.1. Normal Load and Contact Pressure

Due to the complexity of the spring-brake systems, a simplified tribological system has been developed to control the boundary conditions and measure the local frictional response, taking into account the real case study.
The effective maximum contact pressure between the real brake components is not easily identifiable, due to its dependence from the output loads, the complex contact geometry and pressure distribution that characterize the spring-drum contact interface(s). During the load descent phase and during the braking phase, the contact between the rotating torsional spring and the drum undergoes a pressure distribution depending on the position of the torsional spring and its overall deformation. Moreover, as explained before, during the load descent phase, stick-slip instability could appear leading to misalignment of components and contact pressure localizations, with consequent higher values.
Starting from the technical planning and design of the brake systems [116], during the load descent in nominal operation conditions (i.e. without stick-slip presence), four main contact zones are identified between the spring and the drum surfaces (, where the maximum pressure is applied. These four areas are reduced into three in the extreme case in which one of the ends of the spring coil is completely detached from the internal surface of the drum [116]. The contact forces have been calculated by a semi-analytical model for the pre-dimensioning of the brake system [4].

Analyzing the forces calculated for the brake system, when imposing different nominal torque values at the output , the resulting maximum forces are within a range that goes from 3.73N to 16.38N (without stick-slip appearance). Then, by a semi-analytical model based on Hertzian theory, the theoretical maximum contact pressure has been calculated in previous work [117]. It should be kept in mind that the obtained values of contact pressure are a rough estimation of the real contact pressures. In fact, when applying the analytical model and the Hertzian theory, several hypotheses have been accounted for.
Starting from the pressure range estimated on the real application [117], it is possible calculate the equivalent normal load (*N*) that must be applied on the TriboAir test bench, in order to obtain the same range of contact pressures. Then, following the Hertzian theory [118], the normal load has been calculated, as shown in the Figure 21.
Imposing the normal load N, the resulting contact area is an ellipse, function of the radii of curvature of the solids and their mechanical characteristics (Young's modulus and Poisson's Ratio).
The contact can be geometrically described by the radii of curvature, derived from the size and the shape of each body. Considering the curvature radii of the Triboair test configuration, the normal load range that have to be applied during the experimental tests, in order to cover the contact pressures calculated on the real brake system, goes from 5N to 18N.

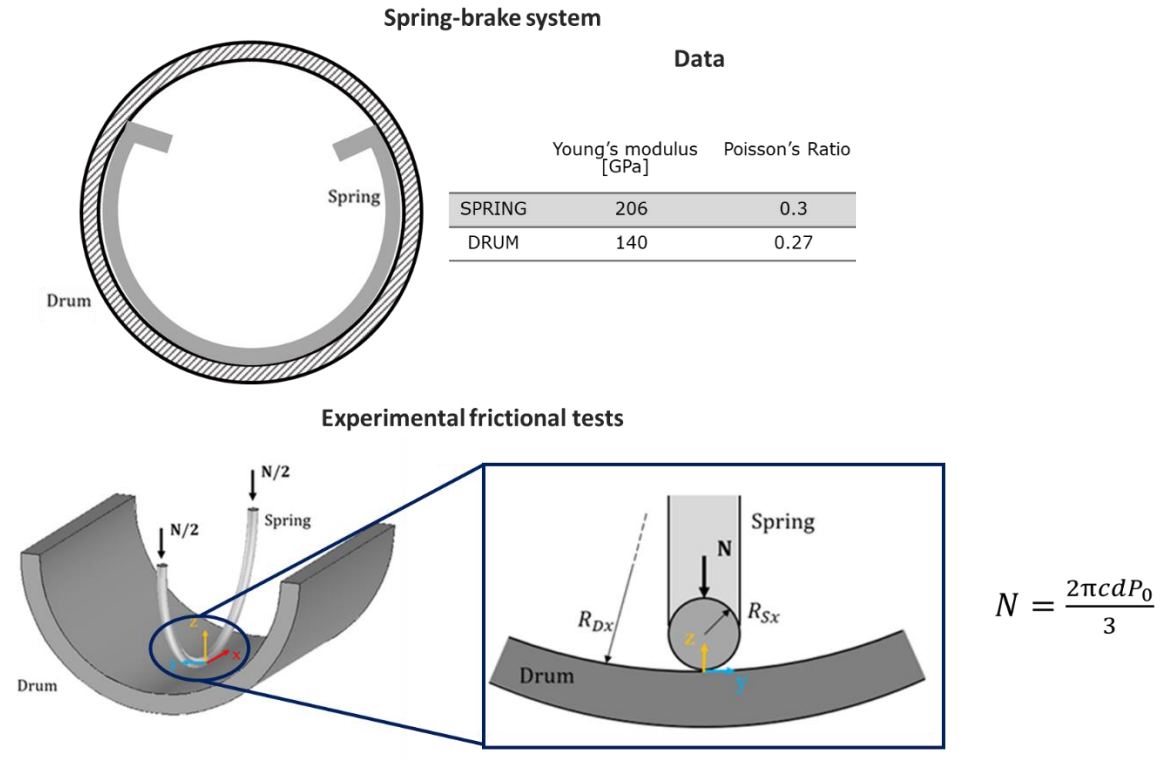

Figure 21: Determination of the Normal Load that must be imposed during the frictional tests to obtain the equivalent contact pressure as in the case study.

Nevertheless, during braking, the actual overall deformation and misalignment of the torsional spring, can differ from the expected one, bringing to higher maximum contact pressures. Consequently, when

reproducing the contact pressure conditions on the tribological tests hereafter, the pressure range to be investigated has been opportunely enlarged. Moreover, aiming to account as well the stick-slip instability, and the consequent contact pressure localizations, the normal load range chosen for the preliminary frictional tests goes from 5N to 50N.
The analysis of the contact area and the maximum contact pressure has been performed first using the Hertz's theory. Then, the same geometry has been implemented in ANSYS in order to perform a finite element analysis (F.E.M) of the contact to calculate the contact pressures and the stress distributions. Aim of this step is to confirm, excluding several of the hypothesis from the Hertz theory, that the chosen normal loads are representative of the considered operating conditions. In order to perform the Finite Element analysis, the target body was defined as the drum and the contact body as the spring. The spring and the drum have been divided into several body layers progressively smaller towards the contact area, as shown in Figure 22. Then, an element size gradually smaller was imposed, starting from the outer body (A) to the inner one (D).

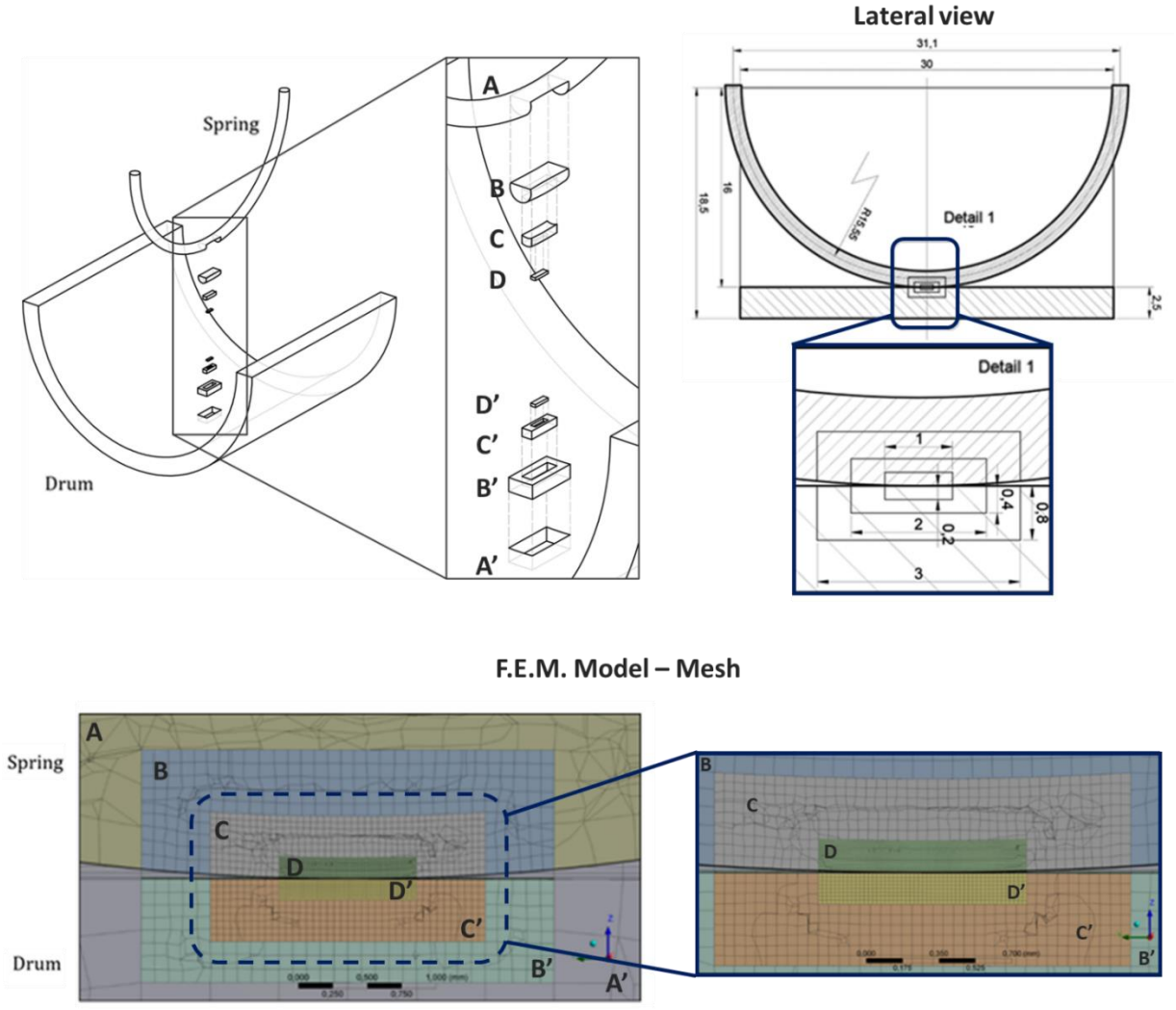

Figure 22: Detail of the slice in three different body layers of both the spring (A, B, C, D) and the drum (A', B', C', D') used for refining the mesh size, as shown on the lower part of the image.

The dimension ratio between the elements of the contact are chosen to correctly implement the Lagrange method [119] [120]. To define the correct element size for the target (i.e. drum) and the contact (i.e. spring) surfaces and to have the minimum percentage of nodal overlapping, the sizes of the contact element and the size of the target element have been imposed. As explained in detail by L. Baillet and T. Sassi in [121], reducing excessively the ratio between the elements size of the contact pair, below the value of the discretization parameter *h*, the analysis can present numerical errors.
Then, an analysis of mesh convergence, both on the target and contact bodies, has been performed.
The contact areas (element D for the spring and element D' for the drum) have been refined with a mesh sizing initially equal to 400μm and 600μm, respectively. Then, the mesh has been imposed gradually smaller and each simulation has been defined as design point (DP).
The different steps to obtain the correct mesh size of both the target and the contact body, according to the convergence of the results in terms of maximum contact pressure, are reported in Table 1. All the numerical simulations were performed using an increasing normal load, starting from 0 and reaching the maximum value of 50N.

Test number	Spring (contact body) [μm]				Drum (target body) [μm]				Mesh Nodes
	A	B	C	D	A'	B'	C'	D'	
DP1	600	500	400	400	600	800	600	600	167413
DP2	600	300	300	300	600	500	400	400	186159
DP3	600	300	200	200	600	400	400	400	188737
DP4	300	100	100	100	300	200	200	200	210704
DP5	300	100	50	50	300	100	80	80	252804
DP6	300	100	50	40	300	100	80	60	263980
DP7	300	100	50	25	300	100	80	50	282508
DP8	300	100	50	20	300	100	50	50	297085
DP9	300	100	50	15	300	100	50	20	355463
DP10	300	100	50	12	300	100	50	20	418952
DP11	300	100	50	10	300	100	50	23	487339
DP12	300	100	50	10	300	100	50	20	497530
DP13	300	100	50	8	300	100	50	20	694587
DP14	300	100	50	6	300	100	50	20	1213194

Table 1: Simulations with different contact and target element sizes, to obtain the convergence of the results.

Plotting the maximum pressure as a function of the number of nodes (Figure 23) it is possible to underline that the convergence of the results in terms of maximum contact pressure can be considered as reached with the mesh sizing DP9. Then, increasing the number of elements, lowering the mesh size, the computation time significantly increases.

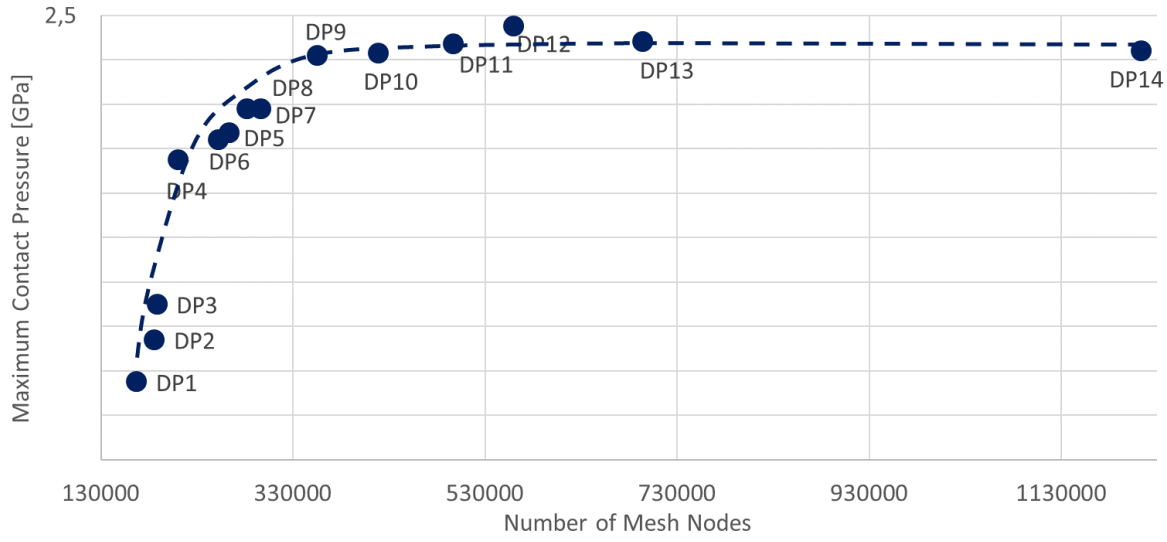

Figure 23: Maximum Contact Pressure vs Number of Mesh Nodes for the estimation of contact convergence.

When considering the contact area and pressure distribution, as an example, Figure 24 shows the results obtained for the simulations DP4, DP11 and DP13. An increase in the maximum pressure values and stress distribution is obtained in simulations with progressively smaller mesh size.

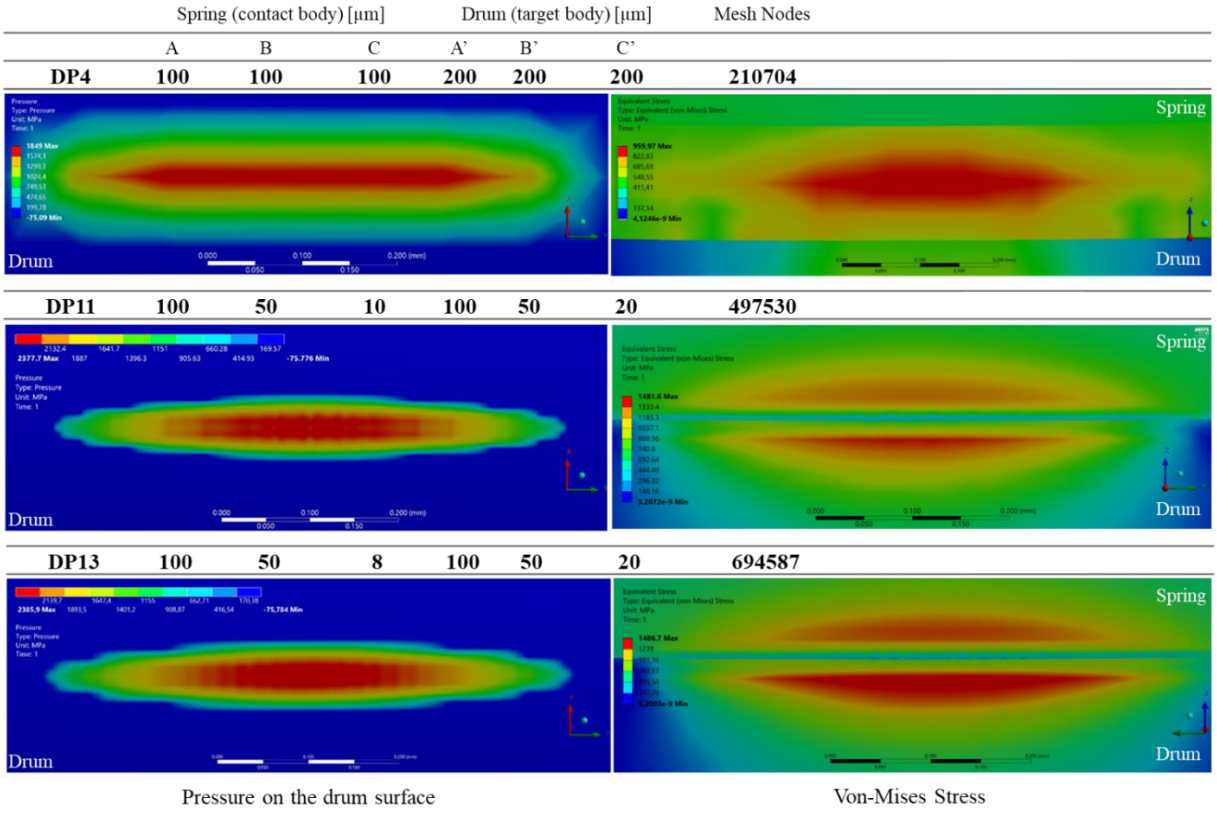

Figure 24: Pressure distribution on the drum surface and equivalent Von-Mises stress for the design points (DP) number 4, 11 and 13 shown in Table 1.

Analyzing the pressure distribution on the drum surface (Figure 24 – left images), the difference in the pressure and stress distribution between the DP4 and DP11, before reaching the convergence, is evident. For the finer meshes (DP11 and DP13), the maximum stress values, calculated by Von-Mises theory, are localized in the subsurface of the drum.
Finally, the result from the FE simulations, with an appropriate elements size (as in the case of the PD14) is compared with the values obtained with the Hertzian theory, as a function of the normal load. The difference between the pressure obtained with Hertz and the pressure obtained by the FE simulations goes from 0.5% to a maximum of 6%.

theory.

Finally, considering the results presented above, has been decided to perform the frictional tests applying a normal load from 5N and up to 50N (5N, 10N, 20N and 50N).
Each normal load will be obtained by adding weight (for 20N and 50N) or subtracting weight by a pully (for 5N and 10N) from the total weight of the loading system, including the two upper air bearing system, the ceramic isolating plate and the upper sample, as shown in Figure 25.

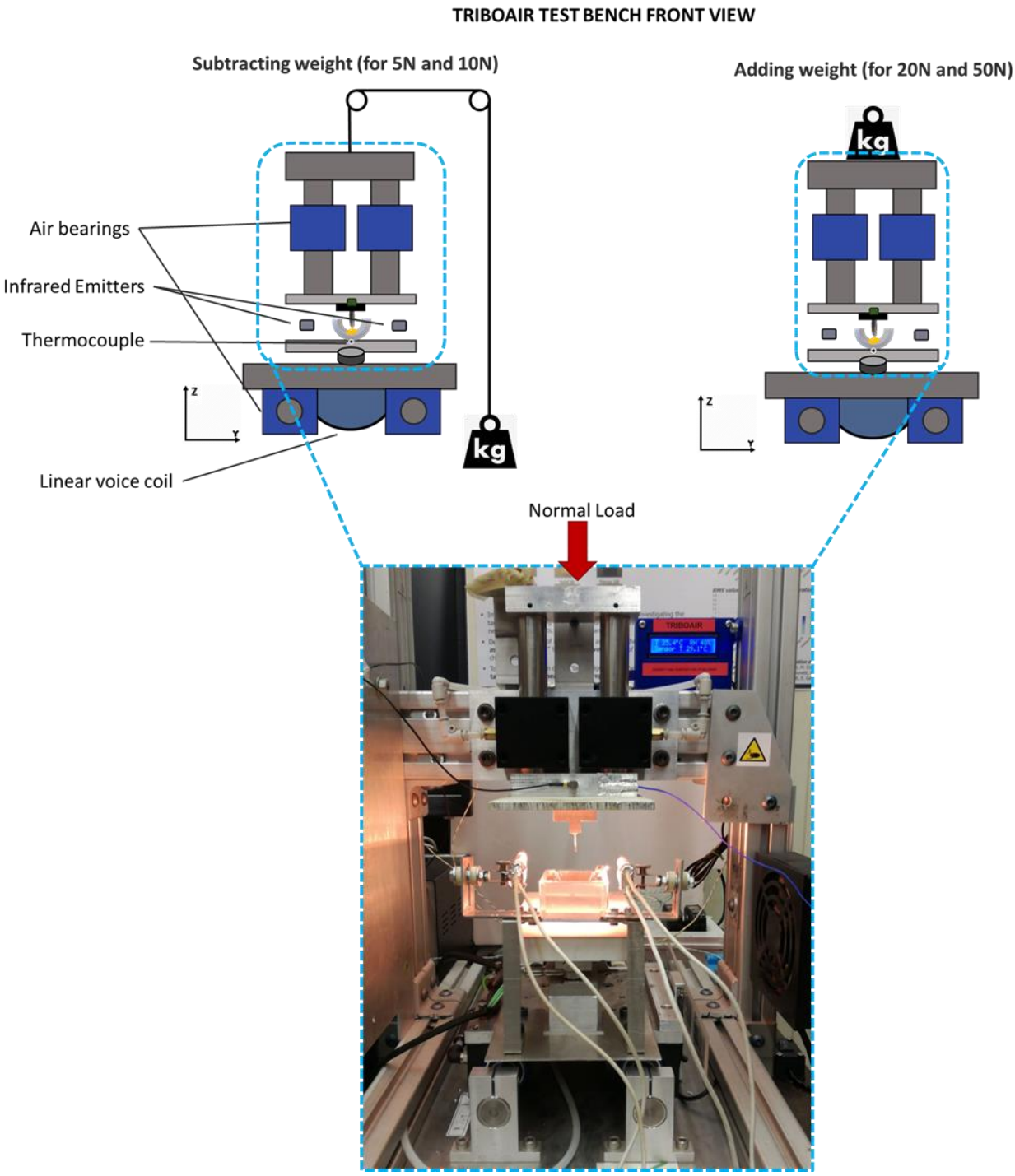

Figure 25: TriboAir test bench loading system.

3.2.2. Sliding Velocity

As mentioned before, the TriboAir test bench is equipped by a linear voice coil (BEI KIMCO LA30-75-001A), able to impose a velocity profile, regulated by a controller (ELMO Gold DC Whistle). A linear optical encoder (MicroE OPS-200-1-1) measures the instantaneous position with a resolution of 0.1µm. The brake system, object of the study, is characterized by a torsional spring that rotates inside a fixed drum with a rotational speed.

However, in the experimental tests, the sliding velocity is imposed on the lower support of the drum sample, and the maximum velocity is limited by the inertia of the mobile assembly of the alternative tribometer.
Nevertheless, as shown in previous studies [36, 35, 62], the stick-slip phenomenon is mainly influenced by the friction force variation at low speeds, particularly when lubrication is present and the lubricated contact is mainly affected by mixed contact conditions, showing negative friction-velocity slope. For all these reasons, the experimental tests have been performed within a low sliding velocity range, i.e. between 0 and 20mm/s. These assumptions will be then verified when, obtaining the trend for the friction coefficient at the higher velocities, it shows a constant or slightly increasing trend with the velocity (see Sections 3.3. and 3.4.).
This velocity range has been thus selected in order to analyse the trend of the dynamic friction coefficient within the velocity range where a negative slope can be expected, due to the operating regime of lubrication. To have robust results, because of the expected low friction and its variation, the tests have been performed with an imposed constant velocity. Therefore, successive tests at different velocities are performed, to identify the evolution of the friction coefficient. Thus, in all the performed tests the velocity is maintained constant. The displacement is characterized by a sliding distance on the internal drum surface. In order to verify the repeatability ad robustness, all tests are conducted for 4 cycles, where a single cycle consists of a round trip (back and forward) of the spring on the lubricated surface of the drum.

3.2.3. Temperature

In the real brake system, as the number of operating cycles increases, the internal temperature at the greased contact increases from ambient temperature to a higher operative temperature, up to 80 °C. Both the conditions, room temperature and high temperature, have been then taken into consideration during the frictional tests, in order to investigate the lubricant behaviour and its interactions with the spring surface coating (the DLC layer). To reach the wished temperature, two infrared emitters heat the contact pair gradually, in order to have a homogeneous heating of the solids in contact, with a fix thermal gradient of 0.1° C/s by an automatic controller (Figure 26).
When the temperature, monitored by the thermocouple, placed close to the contact area on the drum sample, reaches the desired value (80 °C for the high temperature tests), the tests are carried out. Each heating phase is followed by a period of time equal to 10 minutes, in order to let the system temperature stabilize.

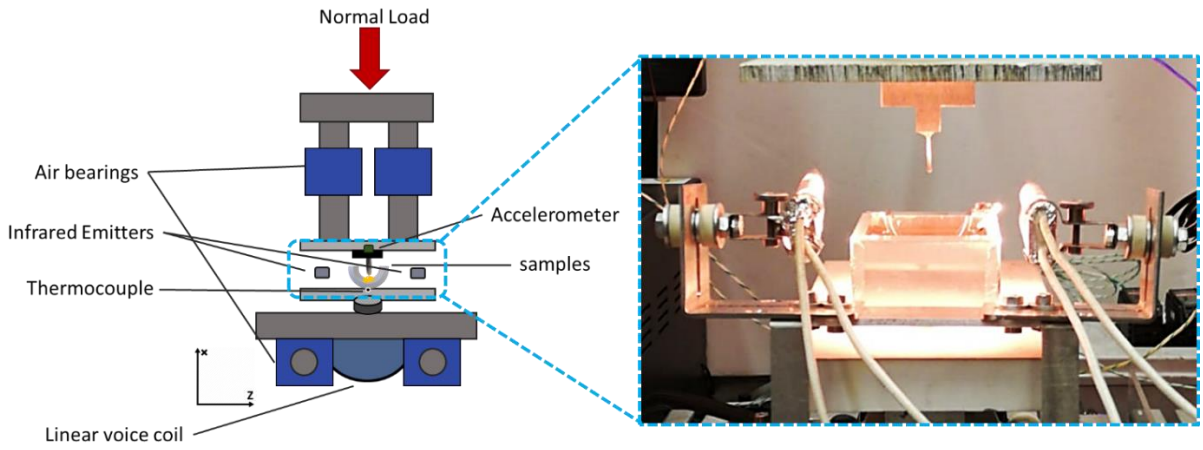

Figure 26: Heating system based on the two infrared (IR) emitters.

3.2.4. Measurement protocol

Once evaluating the boundary conditions (sliding velocity, temperature and normal load) to be tested, a measurement protocol has been defined and applied to retrieve the frictional response under the different tested configurations. For each configuration, the contact response has been retrieved at both ambient temperature (25°) and high temperature (80°), for the different defined normal loads (5N, 10N, 20N and 50N) and a set of sliding velocities (from 0.1 to 20 mm/s). The complete test protocol, performed for each tested configuration, is shown in Table 2.

Before each complete protocol, a running-in period is performed, in order to accommodate the contact surfaces and let a lubricant (grease) layer establish properly at the interface. Nevertheless, for some configuration, it is possible that the first measurement (test number 1 in Table 2) is still not in stabilized contact conditions, due to the surface wear, especially if the tests are performed without the presence of grease at the contact interface or without the presence of the solid lubricant (DLC layer) on the upper sample. For this reason, for each combination of tested load and temperature the first measurement (speed 0.1 mm/s) has always been repeated at the end of the set, before heating or cooling the samples (in Table 2 the tests number V 1^{ST}, V 2^{ND} and V 3^{RD}), in order to verify that the contact surface conditions have not changed. If the contact conditions, and then the coefficient of friction is changed, the upper and lower samples must be changed with new ones and the running-in has to be repeated.

Additional tests have been performed to ensure that the tests order, in terms of normal load, temperature and sliding velocity, doesn't influence the coefficient of friction. Moreover, all the tests reported and discussed hereafter have been repeated tree times for each configuration. In all the tests, the same behaviour of the friction coefficient was underlined and the values obtained have a dispersion of the results lower than 8%.

5N

Tests	Cycles	Normal Load [N]	Velocity [mm/s]	Temperature [°C]
Running-in	15	20	0.5	25
1	4	5	0.1	25
2	4	5	0.3	25
3	4	5	0.5	25
4	4	5	1	25
5	4	5	3	25
6	4	5	5	25
7	4	5	10	25
8	4	5	15	25
9	4	5	20	25
V 1^{ST}	4	5	0.1	25
heating				
10	4	5	0.1	80
11	4	5	0.3	80
12	4	5	0.5	80
13	4	5	1	80
14	4	5	3	80
15	4	5	5	80
16	4	5	10	80
17	4	5	15	80
18	4	5	20	80
V 2^{ND}	4	5	0.1	80
cooling				
V 3^{RD}	4	5	0.1	25

10N

Tests	Cycles	Normal Load [N]	Velocity [mm/s]	Temperature [°C]
1	4	10	0.1	25
2	4	10	0.3	25
3	4	10	0.5	25
4	4	10	1	25
5	4	10	3	25
6	4	10	5	25
7	4	10	10	25
8	4	10	15	25
9	4	10	20	25
V 1^{ST}	4	10	0.1	25
heating				
10	4	10	0.1	80
11	4	10	0.3	80
12	4	10	0.5	80
13	4	10	1	80
14	4	10	3	80
15	4	10	5	80
16	4	10	10	80
17	4	10	15	80
18	4	10	20	80
V 2^{ND}	4	10	0.1	80
cooling				
V 3^{RD}	4	10	0.1	25

20N

Tests	Cycles	Normal Load [N]	Velocity [mm/s]	Temperature [°C]
1	4	20	0.1	25
2	4	20	0.3	25
3	4	20	0.5	25
4	4	20	1	25
5	4	20	3	25
6	4	20	5	25
7	4	20	10	25
8	4	20	15	25
9	4	20	20	25
V 1^{ST}	4	20	0.1	25
heating				
10	4	20	0.1	80
11	4	20	0.3	80
12	4	20	0.5	80
13	4	20	1	80
14	4	20	3	80
15	4	20	5	80
16	4	20	10	80
17	4	20	15	80
18	4	20	20	80
V 2^{ND}	4	20	0.1	80
cooling				
V 3^{RD}	4	20	0.1	25

50N

Tests	Cycles	Normal Load [N]	Velocity [mm/s]	Temperature [°C]
1	4	50	0.1	25
2	4	50	0.3	25
3	4	50	0.5	25
4	4	50	1	25
5	4	50	3	25
6	4	50	5	25
7	4	50	10	25
8	4	50	15	25
9	4	50	20	25
V 1^{ST}	4	50	0.1	25
heating				
10	4	50	0.1	80
11	4	50	0.3	80
12	4	50	0.5	80
13	4	50	1	80
14	4	50	3	80
15	4	50	5	80
16	4	50	10	80
17	4	50	15	80
18	4	50	20	80
V 2^{ND}	4	50	0.1	80
cooling				
V 3^{RD}	4	50	0.1	25

Table 2: Protocol for the experimental frictional tests for a given configuration.

3.3. Frictional response of the reference configuration

The friction coefficient is calculated, for each test, as the ratio between the tangential force and the imposed normal force, acquired through the force transducers. A generic test, corresponding to the test V 2ND in Table 3, is presented here to show the trend of the friction coefficient as function of time. Figure 27 presents the sliding velocity, imposed to the drum sample with the linear voice-coil, and the consequent drum displacement acquired by the encoder, together with the normal and tangential contact forces, acquired by the two 3-axial force transducers.

Tests	Cycles	Normal Load [N]	Velocity [mm/s]	Temperature [°C]
V 2ND	2	20	0.1	80

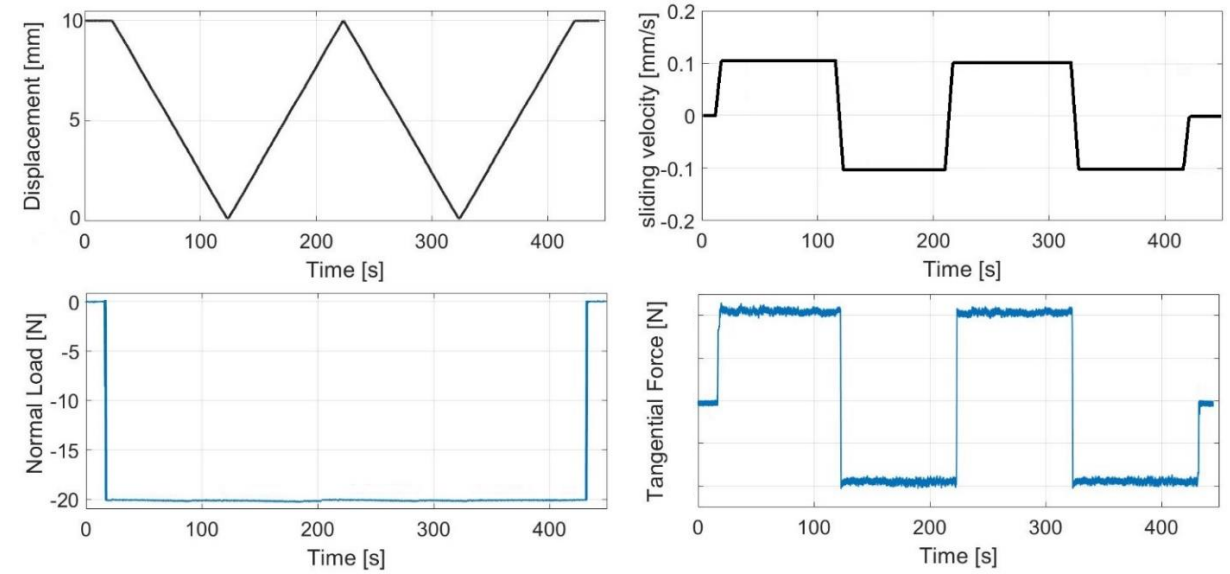

Figure 27: Imposed displacement and sliding velocity as a function of time (upper plots); Normal Load and Tangential Force as a function of time (bottom plots).

Figure 28 shows the corresponding trend of the friction coefficient as a function of time. The trend of the friction coefficient is similar to a square wave, coherently with the imposed displacement.

As shown in Figure 28 (black continuous line), the dynamic friction coefficient is calculated as the average value of the friction coefficient curve, in the time interval where the velocity is maintained constant. The static friction coefficient (black cycle in Figure 28) is retrieved at the beginning of the sliding, corresponding to the peak in the friction coefficient curve, just before the sliding occurs. This peak represents the frictional resistance at the first detachment between the two surfaces in contact.

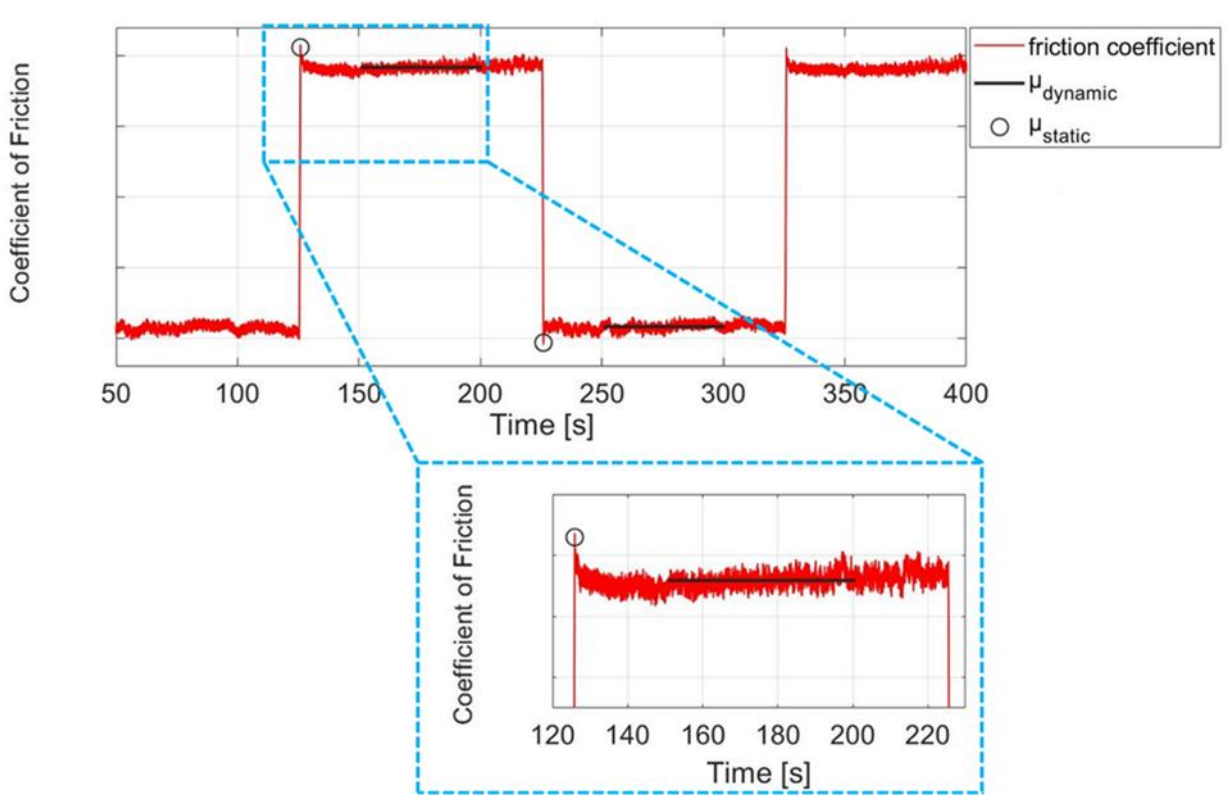

Figure 28: Resulting coefficient of friction (CoF) in function of time.

The static friction coefficient has been calculated always within the tests performed at a sliding velocity of 0.1mm/s, in order to neglect the contribution of the inertia when the system accelerates. A test without contact between the upper and the lower samples has been performed to verify that the inertia contribution can be neglected.
The dynamic friction coefficient has been then retrieved for all the tested sliding velocities and configurations. It has been then evaluated as function of the imposed sliding velocity, as presented in detail in the following.
The experimental protocol has been settled to give a general overview of the local system response at different speeds, contact pressures and temperature conditions. The case study configuration used as a reference is the one of the previously described brake system [115].
The two main components are a sintered steel cylinder (the drum) and a torsional spring, coated with the DLC solid lubricant. The contact interface, between the outer surface of the spring and the inner surface of the drum, is lubricated with the synthetic commercial grease. This grease is composed by a synthetic base oil (PAO) and a Lithium Complex thickener, plus the presence of additives.

The experimental frictional tests have been performed, using the TriboAir tests bench, applying different loads (5N, 10N, 20N, 50N) and velocities (from 0.1mm/s to 20mm/s), at both ambient and high temperature (25 °C and 80 °C). The overall friction coefficient results are evaluated as a function of sliding velocity over the applied normal load. The recovered frictional responses, obtained from the complete protocol (Table 2), are

analysed with respect to the ratio between sliding velocity and load, in order to reproduce a Stribeck-like curve (Figure 29). The dynamic friction coefficient (continuous line in Figure 28) calculated for a single frictional test (for a given combination of velocity, temperature and load) is represented by a single point of the graph in Figure 29.

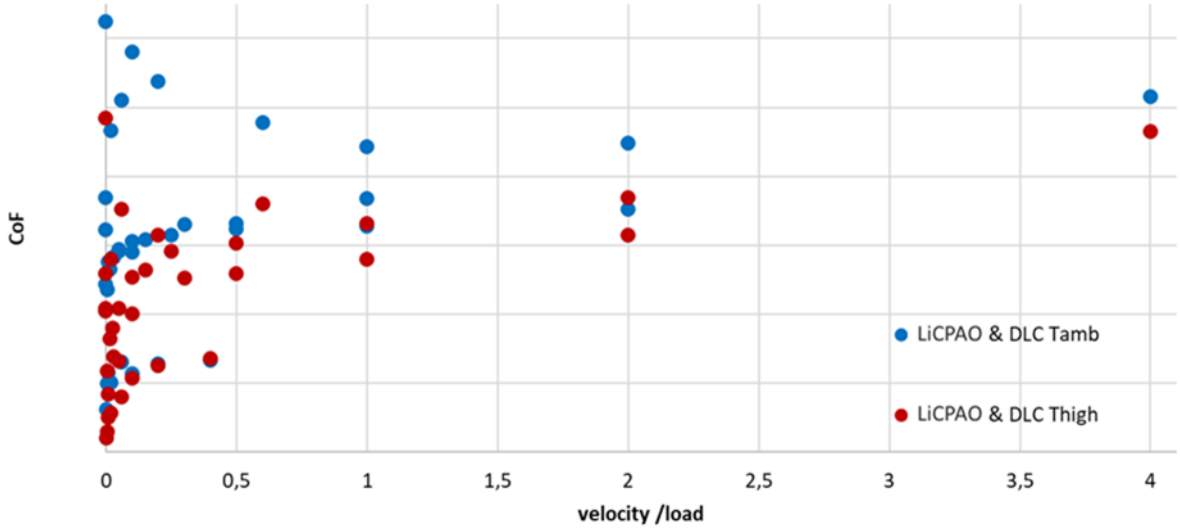

Figure 29: Coefficient of friction (CoF) of the Reference configuration as function of the sliding velocity over the normal load, applying different normal loads (5N, 10N, 20N and 50N) both at ambient temperature (25°C) and high temperature (80°C).

The experimental results, in presence of the grease and the DLC coating of the spring, shows that the measured friction does not follow a classic Stribeck-like curve [62], mainly at low velocities. A clear trend is not easily identifiable when analysing the frictional response as function of the velocity/load ratio. For this reason, the obtained friction coefficients have been plotted separately with respect to either the load or to the velocity. When the load increases, it is possible to see how, for each of the tested sliding velocity, the friction coefficient decreases. This trend could be attributed to a higher release of oil from the thickener matrix when the local pressure increases. This monotonically decreasing, as function of the applied normal load, is more evident at ambient temperature compared to the higher one, where the CoF values are slightly lower and the variation with the load is reduced.

It is then useful to analyse the coefficient of friction (CoF) as function of the imposed sliding velocity, for each applied normal load (5N, 10N, 20N and 50N).

Focusing the attention on the sliding velocity, Figure 30 shows the CoF values as a function of the sliding velocity, for each applied normal load (5N, 10N, 20N and 50N). The results at ambient temperature (blue dots) and high temperature (red dots) are compared.

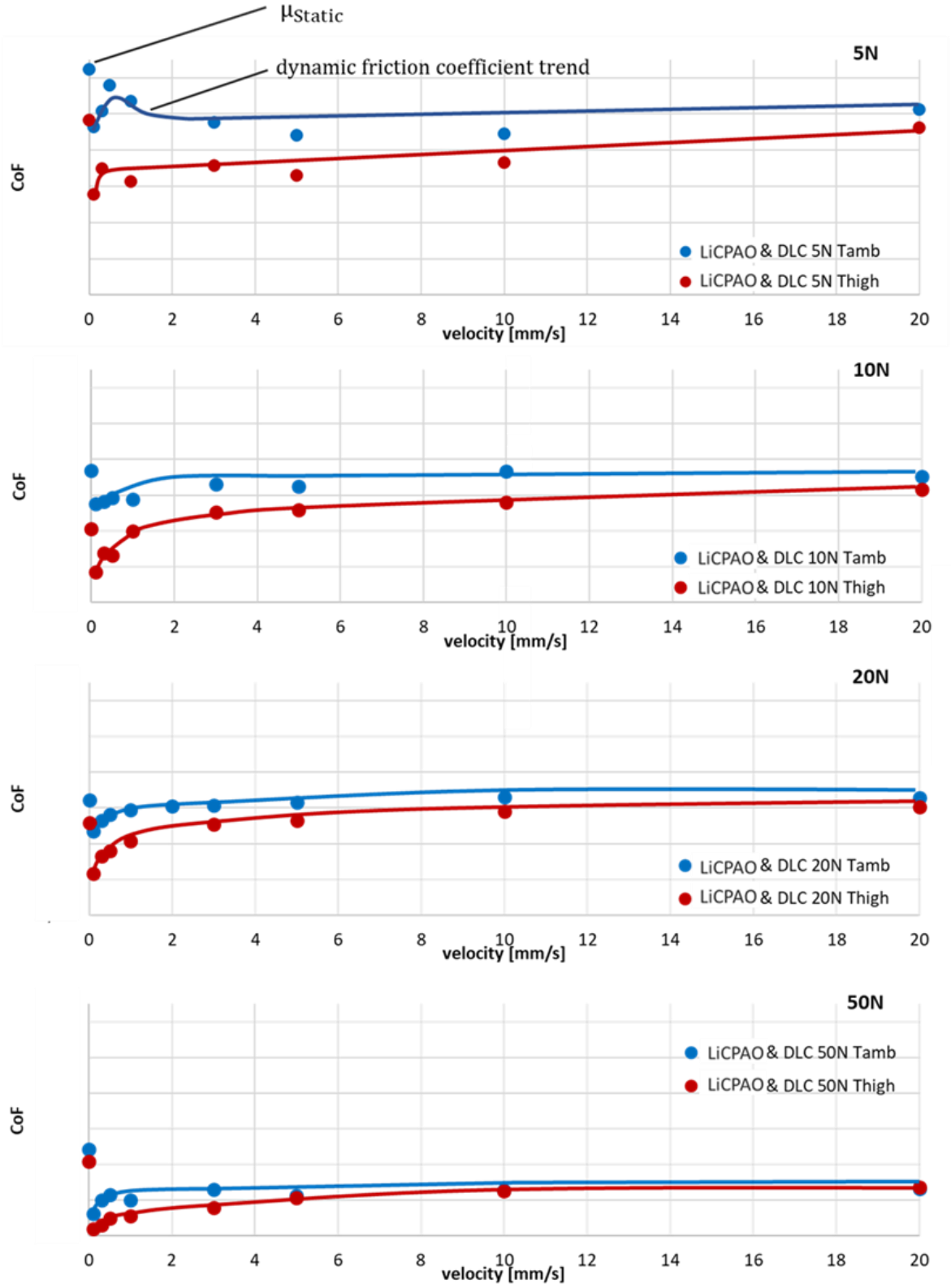

Figure 30: Coefficient of friction (CoF) of the Reference configuration, as a function of the sliding velocity, when applying different normal loads (5N, 10N, 20N and 50N) both at ambient temperature (25°C) and high temperature (80°C).

Some considerations on the obtained results are here reported:

- After a high static friction coefficient, a large drop to the dynamic friction coefficient is observed at the smallest values of the dynamic friction,

obtained for the lowest imposed sliding velocity. Then, from its lowest value at 0.1mm/s, the dynamic friction coefficient rises again relatively quickly, at low values of the sliding velocity, until reaching an almost stable value.

- The trend of the dynamic friction coefficient is always similar and does not depend from the applied normal load and temperature. As observed above, the friction coefficient generally decreases as the imposed normal load increases.
- The larger fluctuations of the CoF at 5N, both at high and ambient temperature, can be related to a not well-established lubrication regime. Low pressures may be not sufficient to assure a constant boundary condition at the greased contact interface, with the higher asperities in contact that can drive the frictional response.
- Comparing the frictional behaviour at different temperatures, as the temperature increases, the greased friction coefficient shows a similar trend but lower values, independently of the tested loads. This decrease of dynamic friction at higher temperature can be associated to both a decrease in oil viscosity and an increase of oil release by the grease matrix, when the temperature increases.

Analysing in detail the trend of the friction coefficient, as shown in Figure 31, it is evident that it exhibits two main operating regions: the relatively high-speed region (from 2mm/s to 20mm/s), where the frictional behaviour results almost stable, and the low-speed region (from 0.1mm/s to 2mm/s), where friction first drops from the high static to the lowest dynamic values and then increases as the sliding velocity increases.
More in detail, in the low velocity range, the static friction coefficient is suddenly followed by the smallest dynamic friction coefficient, measured at 0.1 mm/s. The curve rises then as the sliding velocity increases, stabilising after 2mm/s.
In all cases, large differences between static and dynamic friction coefficients have been observed. Since one of the most accepted cause of the stick-slip occurrence is an high difference between static and dynamic friction coefficient ($\mu_S - \mu_D$ in Figure 31), i.e. the higher is the difference, the higher is the propensity of the brake system to promote stick-slip vibrations, it can be interesting to underline this difference as function of the imposed normal load and temperature.

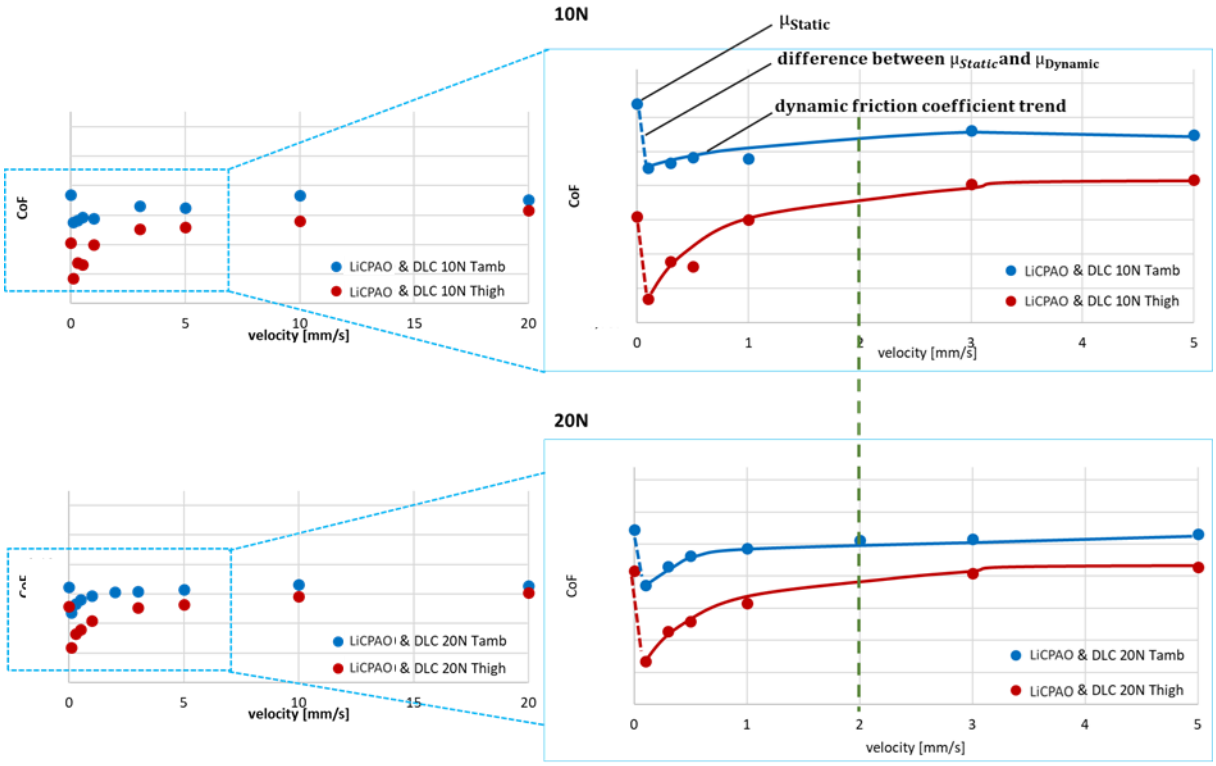

Figure 31: Frictional behavior of reference configuration applying a normal load of 10N (upper figure) and 20N (lower figure) both at ambient (25°C) and high (80°C) temperature. On the right part of the image, zoom of the CoF as function of the sliding velocity from 0 to 5mm/s. Two operating regions are identified (vertical dashed line).

Then, Figure 32 shows the difference between static and dynamic friction coefficients as function of the applied normal load for the reference configuration, for both ambient (25°C) and high (80°C) temperature.

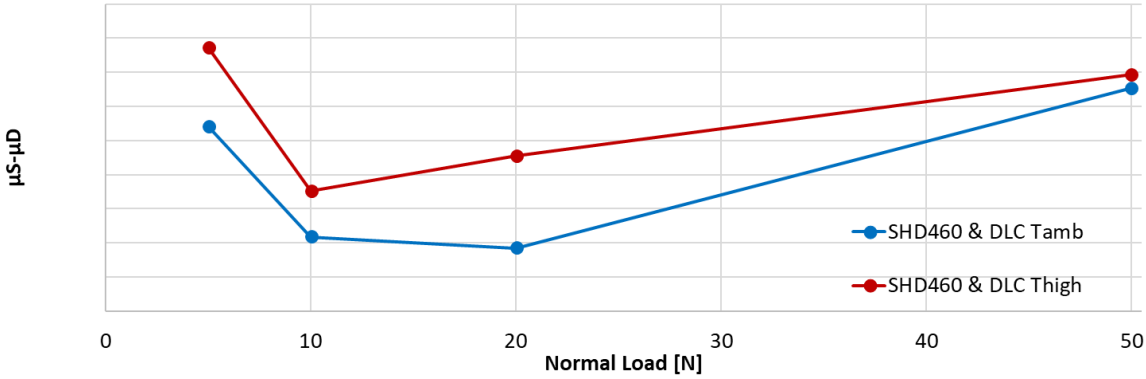

Figure 32: Difference between static and dynamic (at 0.1mm/s) friction coefficient with respect to the imposed normal load, at ambient (25°C) and high (80°C) temperature.

The evolution with respect to the load is qualitatively similar for both the temperatures, but the difference between the friction coefficients is significantly larger at high temperature. With higher temperature conditions, the dynamic friction coefficient values decrease more than the static ones, giving rise to a higher difference between them. As it will be investigated in the following (Chapter IV), this condition may increase the propensity to the stick-slip occurrence and justify the different behaviour

(respectively stable of unstable) registered by the brake system at ambient and high temperatures.

3.4. Influence analysis on some main functional parameters

In the previous section, the frictional behaviour between the components of the reference configuration has been analysed and discussed. Because of the complexity of the stick-slip problem in greased contacts and its occurrence in spring-brake systems, and because of the different working conditions to which the brakes can be subjected and the great variety of involved factors, it is appropriate to carry out a parametric analysis to understand which factors affect most the local frictional behaviour. The main objective of this chapter is then the investigation of the effect that specific contact parameters can have on the frictional behaviour of the greased contact, in order to identify the conditions that could affect the stick-slip propensity of the system.
Because of the applicative nature of the investigated system, different applicative solutions (analysed here) have been tested, in order to both provide information on the operative design solutions and retrieve information useful for the understanding of the interface behaviour. Afterward, a more specific analysis on the role of the different components of the lubrication has been carried out and reported in Chapter V.
During the parametrical campaign, several configurations have been then tested (Table 3), using different surface coatings (DLC, CW, NiP and without solid lubricants) and different drum surface materials and finishing (different honing angle and roughness). Thus, these configurations allow to analyse how the frictional response at the local scale is affected by each design configuration and therefore evaluate the conditions for which the system is more predisposed to the stick-slip phenomenon. Each tested configuration differs from the standard condition (discussed in Chapter 4.3) by a single parameter change. Comparing the results, it is possible then to analyse the effect of the specific tested parameter on the local frictional response. The tested configurations are reported in Table 3. All configurations are named with the parameter change that characterizes the configuration with respect to the reference one.

Tested configuration	Grease type	Lower Sample (i.e. drum)	Upper sample (i.e. spring)
Reference	LiCPAO	Drum reference	Solid lubricant: DLC
Drum 2	LiCPAO	Drum reference with different honing angle	Solid lubricant: DLC

Drum 3	LiCPAO	Drum 3 with lower roughness	Solid lubricant: DLC
CW	LiCPAO	Drum reference	Solid lubricant: CW
NiP	LiCPAO	Drum reference	Solid lubricant: NiP
Steel	LiCPAO	Drum reference	Without solid lubricant

Table 3: Tested configurations.

3.4.1. Drum surface finishing

During the experimental campaign, two types of drum finishing with different honing angles (i.e. angle between the grooves caused by the honing process of the drum internal surface) and roughness have been tested.
The reference drum and the drum number 2 are made of sintered steel and honed with a defined honing angle. The drum number 2 is characterized with a higher honing angle.
The experimental protocol is the one shown in Table 2. The results in terms of CoF trends are shown in Figure 34, as function of the sliding velocity. As an example, in Figure, the trends for 10N and 20N of the applied normal load, and both temperatures, are compared to the reference configuration. The same results are found in the case of 5N and 50N.

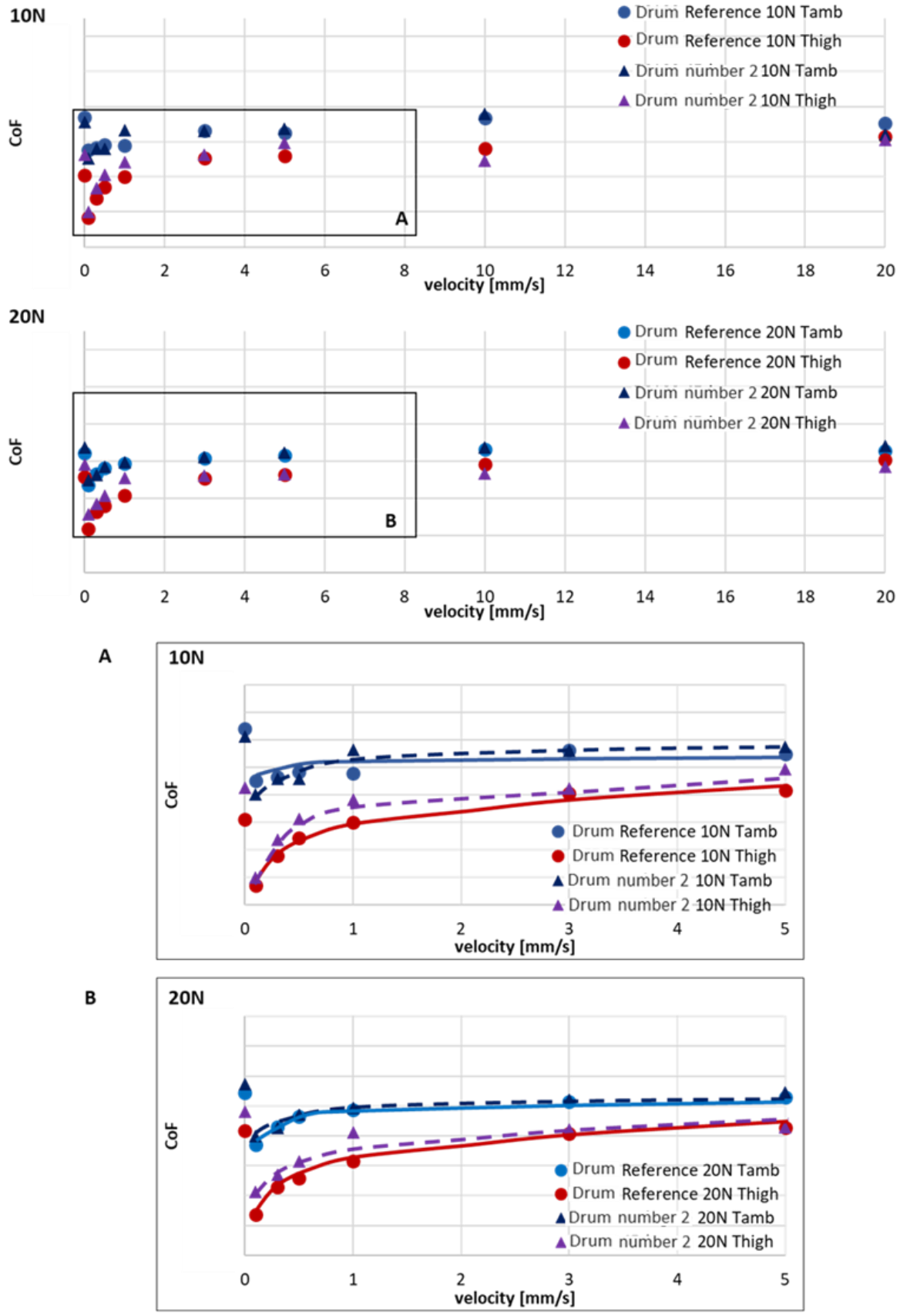

Figure 33: Comparison between the friction coefficient trends and values, as function of the imposed sliding velocities. The lower images show a detail of the configurations for 10N (A) and 20N (B), at both at ambient (25°C) and high (80°C) temperature.

As shown in the Figure 33, the increase of the honing angle (Drum number 2) did not produce significant changes on the trend of the friction coefficient. The same considerations reported for the reference configuration in Section 3.3. can be made for the configuration with increased honing angle. Again, the trend of the frictional response exhibits two operating regions: the relatively high-speed region (from 2mm/s to 20mm/s), where the frictional behaviour results almost stable, and the low-speed region (from 0.1mm/s to 2mm/s), where friction first drops from the high static to the lowest dynamic values and then increases as the sliding velocity increases.
Regarding the difference between static and dynamic friction coefficient, in the configuration under examination, similar results are found with respect to the reference configuration.

3.4.2. Drum material

Another design configuration regard the complete modification of the drum material. Then, the influence of the drum material, and respective different topography, on the frictional response has been analysed by comparing the results with the standard configuration. The drum 3 is made of machined steel, having a surface and bulk porosity, without superficial milling and lower surface roughness.
The drum number 3 configuration is characterized by a different drum, the spring covered by a DLC layer and the grease LiCPAO. The results in terms of CoF trends are shown in Figure 34, as function of the sliding velocity. For each applied normal load and temperature, the drum 3 trends are compared to the reference configuration.
The tests carried out with the drum 3 show more stable friction coefficient values than one carried out with the reference drum (Figure 34). A lower dispersion of the results is observed, specially at lower loads. This is due probably to the lower and more isotropic roughness, due to the material porosity, rather than to the surface finishing.

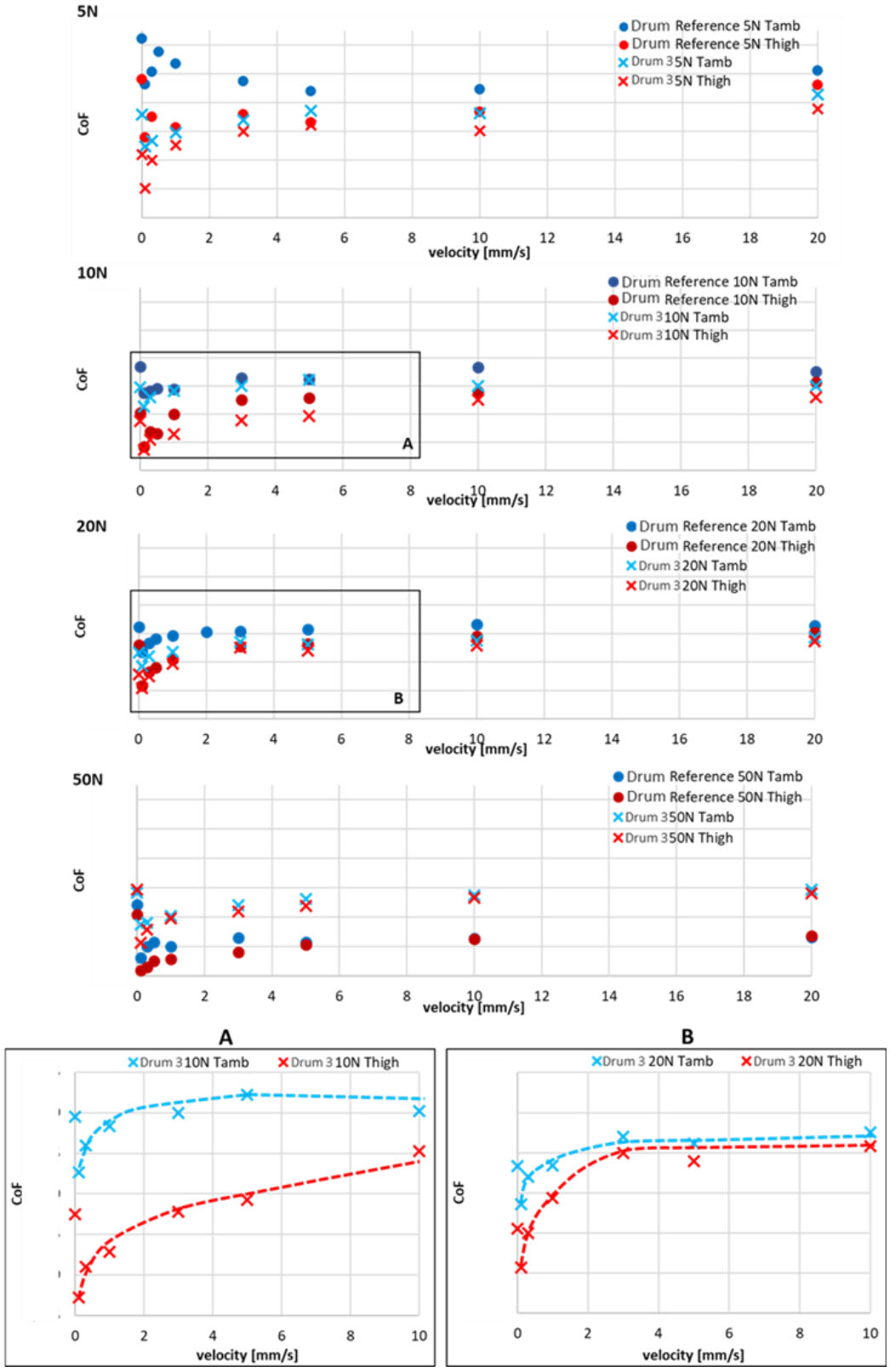

Figure 34: Comparison between the friction coefficient trends and values between the drum 3 configuration and the reference configuration, as function of the imposed sliding velocities. The lower images show a detail of the drum 3 configuration for 10N (left side) and 20N (right side), at both at ambient (25°C) and high (80°C) temperature.

It is worth underlining that, changing the drum, the friction coefficient remains always in the same range of values.

The evolution the friction coefficient with respect to velocity, at different loads, is very similar to the reference one, with slightly lower values, probably dues to the lower roughness and then a better established lubricant film. This behaviour is more accentuated at low loads, and then the two configurations converge for higher loads.
Moreover, changing the drum, the difference between static and dynamic friction coefficient ($\mu_s - \mu_d$) decreases, as shown in Figure 35. This is mainly due to the decreasing in the static friction coefficient, with respect to the dynamic one, which is probably a consequence of the lower roughness, which allows for maintaining the lubricant at the interface and decreasing the adhesion between the asperities at the static contact.

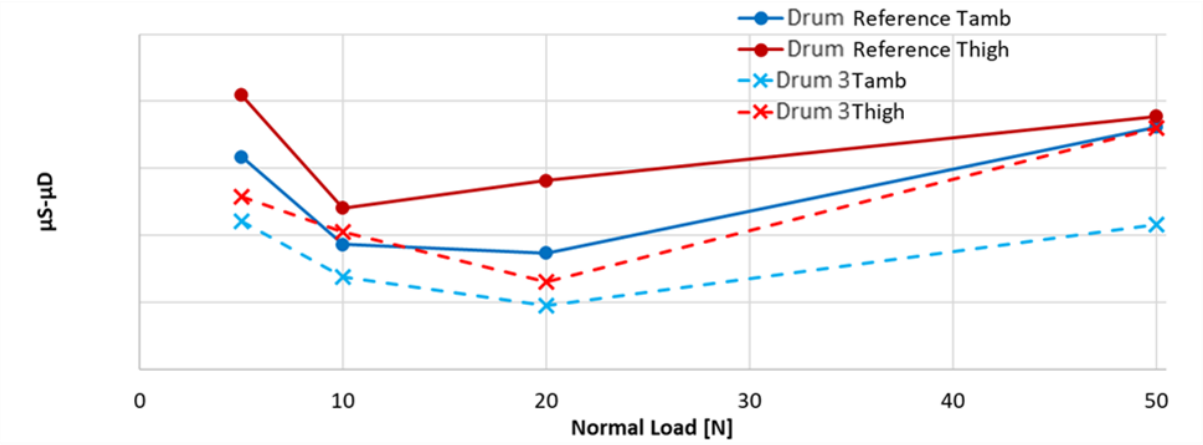

Figure 35: Difference between static and dynamic friction coefficient ($\mu_s - \mu_d$) as function of the applied normal load sliding velocities, for both the drum number 3 configuration and the reference configuration, at ambient and high temperature.

3.4.3. Spring coatings and solid lubrication

Aiming to perform the analysis of how the spring surface coating (solid lubrication) affects the frictional response at the contact, four different spring coating conditions have been tested: DLC (reference configuration), CW, NiP and absence of solid lubricant (coating). A detailed analysis of the frictional response of the four cases has been performed and reported in the following.

- **CW**

The CW (tungsten carbide) is a coating generally classified in the DLC-like solid lubricants. The tested CW coating covers the upper sample (i.e. the spring). The tested CW configuration is characterized by the spring coated with a CW layer, the reference drum and the grease LiCPAO. The results, in terms of CoF trends, are shown in Figure 36, as function of the sliding velocity.

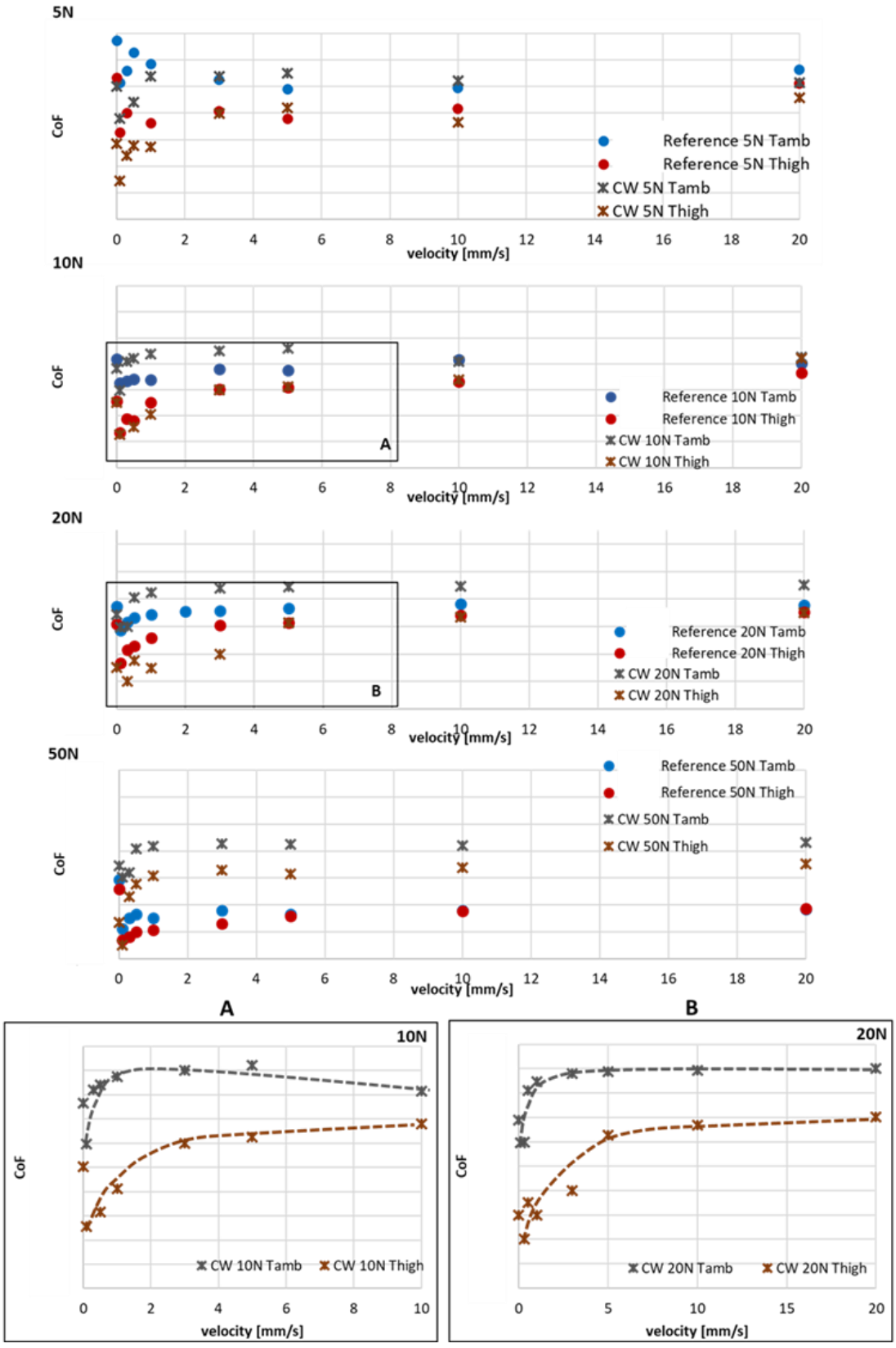

Figure 36: Comparison between the friction coefficient trends of the CW configuration and the reference configuration, as function of the imposed sliding velocities. The lower plots show a detail of the frictional trend for the CW configuration for 10N (left side) and 20N (right side) and both at ambient (25°C) and high (80°C) temperature.

For each applied normal load and temperature, the CW trends are compared to the reference configuration.
The evolution of the friction coefficient with respect to velocity (crosses in Figure 36), at different loads, is very similar to the reference one, with a slightly higher friction at ambient temperature and a decrease of the friction coefficient as the temperature increases. As in the case of the reference configuration, the CW trend exhibit two operating regions: the relatively high-speed region, where the frictional behavior results stable, and the low-speed region, where friction increases as the sliding velocity increases. Increasing the temperature, the friction coefficient behaviour shows lower values in the case of CW, independently of the tested loads. However, in the case of the CW solid lubricant a more stable behaviour is underlined, both considering the different normal applied load and the increase of temperature. In fact, looking at the values of the CoF retrieved with the CW, these are more constant as function of the sliding velocity and the normal load. Moreover, for all the applied normal load and tested temperatures, the static friction coefficient of the CW is lower.
Therefore, due to a more stable behaviour and lower static friction coefficient values, the difference between static and dynamic friction coefficient ($\mu_s - \mu_d$) in the case of CW is lower, compared to the reference configuration. Figure 37 shows the comparison between DLC (dots) and CW (crosses), as function of the applied normal load.

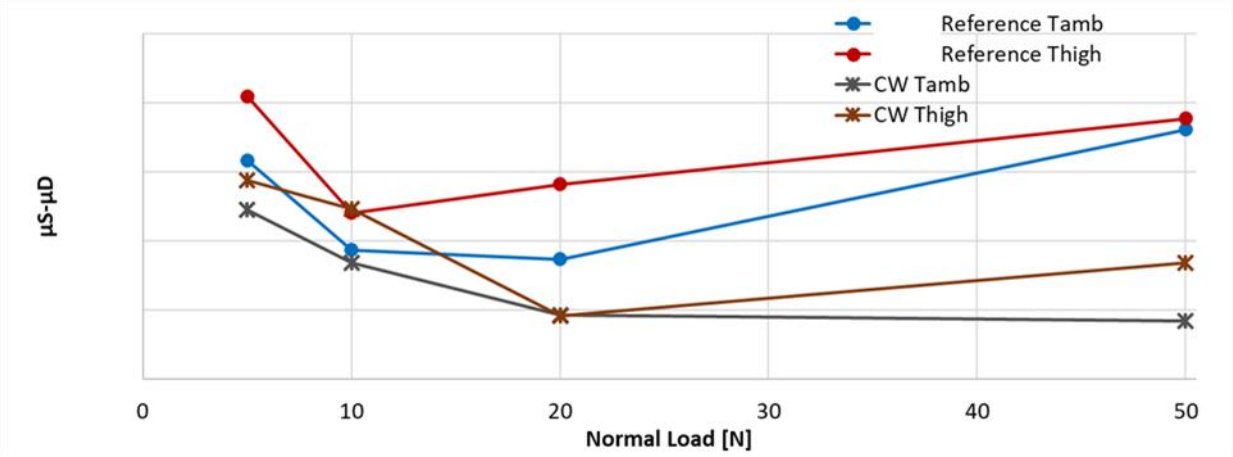

Figure 37: Difference between static and dynamic friction coefficient (μ_s-μ_d) as function of the applied normal load sliding velocities, for both the CW configuration and the reference configuration, at ambient and high temperature.

The CW results in a solid lubricant that could bring an advantage in terms of stick-slip propensity of the system, due to the lower difference between static and dynamic friction coefficient and a more stable overall frictional behaviour at the greased contact. However, the low static friction coefficient, at low sliding velocity conditions, must be taken into consideration during the spring-brake design. An excessively low value of the static friction coefficient could in fact lead the brake system to not hold the output load in static condition. This situation could lead to the sliding of the output load and to not support the nominal output torque, functional requirement necessary for these brake systems.

- **NiP**

This type of solid lubricant is widely used in engineering applications, owing great properties against corrosion and wear. The NiP configuration is characterized by the spring coated with a NiP, the reference drum and the grease LiCPAO.
Before looking at the obtained overall frictional trends, a phenomenon observed during experiments with this configuration is here addressed: during the tests, localized drops in the friction coefficient have been observed. This behaviour is recurrent for low values of sliding velocity and high loads, in particular at high temperature. These *friction drops* are observed at each sliding cycle in the same spatial position of the drum surface, as show in Figure 38. Under the same test conditions (normal load equal to 20 N, sliding velocity equal to 0.1 mm/s and high temperature), the friction coefficient signals of the NiP and the standard configuration are compared, underlining the stable behavior of the reference configuration and the friction drops observed with the NiP configuration.

Tests	Normal Load [N]	Velocity [mm/s]	Temperature [°C]	Solid lubricant (spring surface)
Reference	20	0.1	80	DLC
NiP	20	0.1	80	NiP

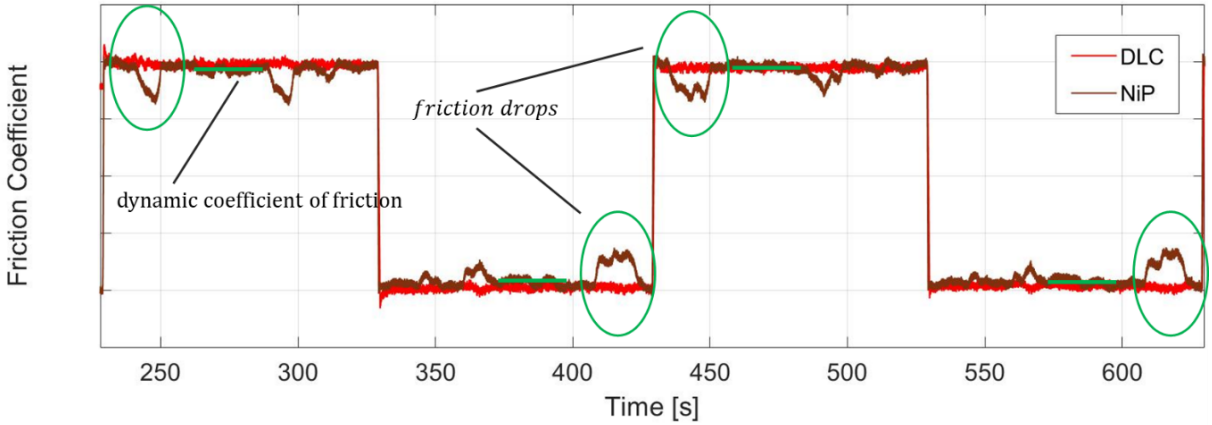

Figure 38: Coefficient of friction as function of the time for both the Reference configurationand the NiP configuration. During the CoF evolution, in the NiP configuration, *friction drops* are observed (green circles).

Aiming to understand the *friction drop* phenomenon, figuring out the causes of its occurrence and the possible effects on the frictional response at the contact, an in-depth analysis of the frictional behavior of the two configurations has been conducted together with a surface topography analysis. The configurations have been tested under the same boundary conditions (i.e. sliding velocity, imposed normal load, temperatures) and are characterized by same drum, same grease, but different spring treatments.
At the end of the complete test protocol, the contact area of both drums and spring coils has been analyzed with the aid of an optical microscope, to compare the surface topographies between the two tested configurations. The topography has been investigated focusing the attention on the contact

areas of both the spring and the drum. The bodies in contact have been cleaned following a cleaning protocol, consisting in 5 minutes in ethanol and 5 minutes in heptane, in a ultrasounds cleaning machine and dried whit compressed air, in order to analyze the topography of the solids in contact without the grease.
Figure 39 shows the contact surfaces of the reference configuration, where the spring coil coated with a DLC coating. The surface of the drum is first showed with the presence of grease (before the cleaning protocol), in order to investigate the 3rd body distribution at the contact.

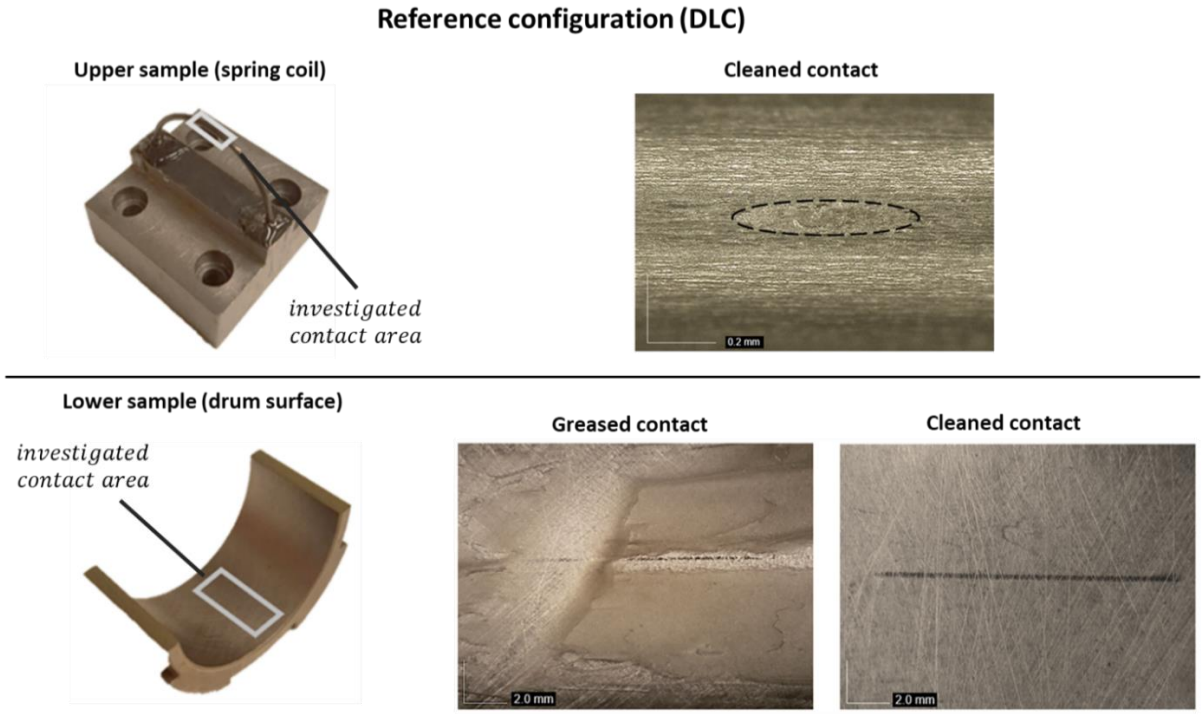

Figure 39: Optical microscope contact surfaces topographies of the Reference Configuration (DLC solid lubricant on the spring external surface). Upper figure: spring coil. Lower figure: Drum surface before and after the cleaning protocol.

The grease seems to be homogenously distributed and partially discarded from the contact, by the passage of the spring. Moreover, the drum contact surface (lower sample) shows the presence of solid third body on the drum surface, both before and after the cleaning protocol, due to the presence of the DLC coating on the spring. This 3rd body layer remains on the surface of the drum even after the cleaning protocol, due to a material transfer from the spring to the drum surfaces. According to several studies [90, 92, 122], it may strongly contribute to the tribological performances at the contact, due to the establishment of a DLC - DLC contact, or more correctly, DLC–DLC plus lithium complex grease contact and DLC solid third body, able to assure a more stable frictional behavior. Moreover, the DLC layer protects in such a way the spring surface, which does not show remarkable wear.
In fact, focusing the attention of the spring contact surface, the upper image in Figure 39 shows that the surface coating does not seem to be significantly damaged. A deposit of cohesive and protective third body, probably

composed by a mixture of DLC particles and grease, appears on the contact area.
On the contrary, analyzing the NiP configuration (Figure 40), at the end of the complete tests protocol, the contact area of the drum shows the presence of localized areas with grease accumulation (circle in figure) along the contact track. The area where the accumulation of grease is observed corresponds to the zone where the friction drop occurs in the friction curve (Figure 40). This grease accumulation on the sliding area of the drum leads thus to a drastic modification in the lubrication condition at the contact, during the displacement of the spring on the drum.

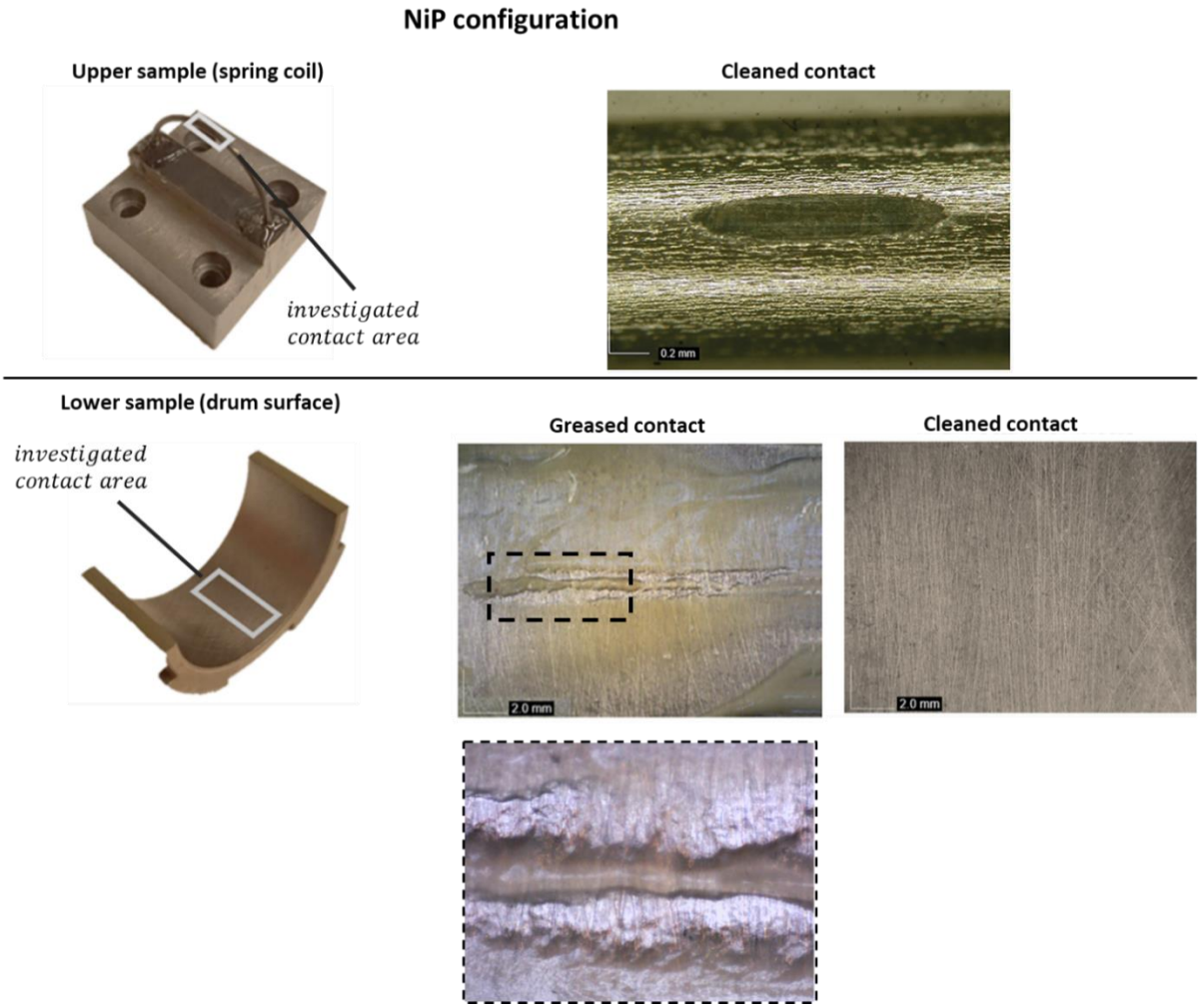

Figure 40: Optical microscope contact surfaces topographies of the NiP Configuration (NiP solid lubricant on the spring external surface). Upper figure: spring coil. Lower figure: Drum surface before and after the cleaning protocol, whit the zoom on the grease accumulation on the drum contact surface (lower image).

After the cleaning protocol, neither third body or surface wear are observed on the drum contact area. Only the honing marks due to the production process are visible. From what concerns the NiP coated spring, its contact area is extremely visible, as reported in the upper image in Figure 40. The surface coating seems completely removed, although the number of cycles of the complete protocol is not high, compared to the real application. The

longitudinal sliding marks on the contact area, along the sliding direction of the spire, are visible too. No cohesive and/or protective third body appears on both the contact areas of the spring and the drum. Moreover, the flattened surface of the spring could explain the drop of the friction coefficient when encountering grease accumulation, providing a flat-to-flat contact with instauration of a temporary hydrodynamic lubrication regime (lower friction).
However, analyzing the Figure 41, the overall friction coefficient behavior of the NiP configuration (green and violet squares) shows a quite similar evolution compared to the DLC one (blue and red dots). In order to compare the results between the two different configurations, the dynamic friction coefficient has been calculated taking into account the stable part of the signal for the NiP condition, without considering the presence of the *friction drops*, whose values can be up to 50% smaller than average value of the CoF.
Again, the trend of the coefficient of friction, as function of the sliding velocity, does not represent the typical Stribeck-like curve. Starting from an high static friction coefficient, the CoF drops significantly at small values of the imposed sliding velocity, as in the case of the reference configuration. The trend of the dynamic friction coefficient is always similar and does not depend from the applied normal load and temperature.
Increasing the operating temperature (80°C), the NiP friction coefficient trend shows lower values compared to the ambient temperature condition, independently of the tested loads. This decrease is accentuated in the case of the tests performed with NiP, compared to the reference configuration.

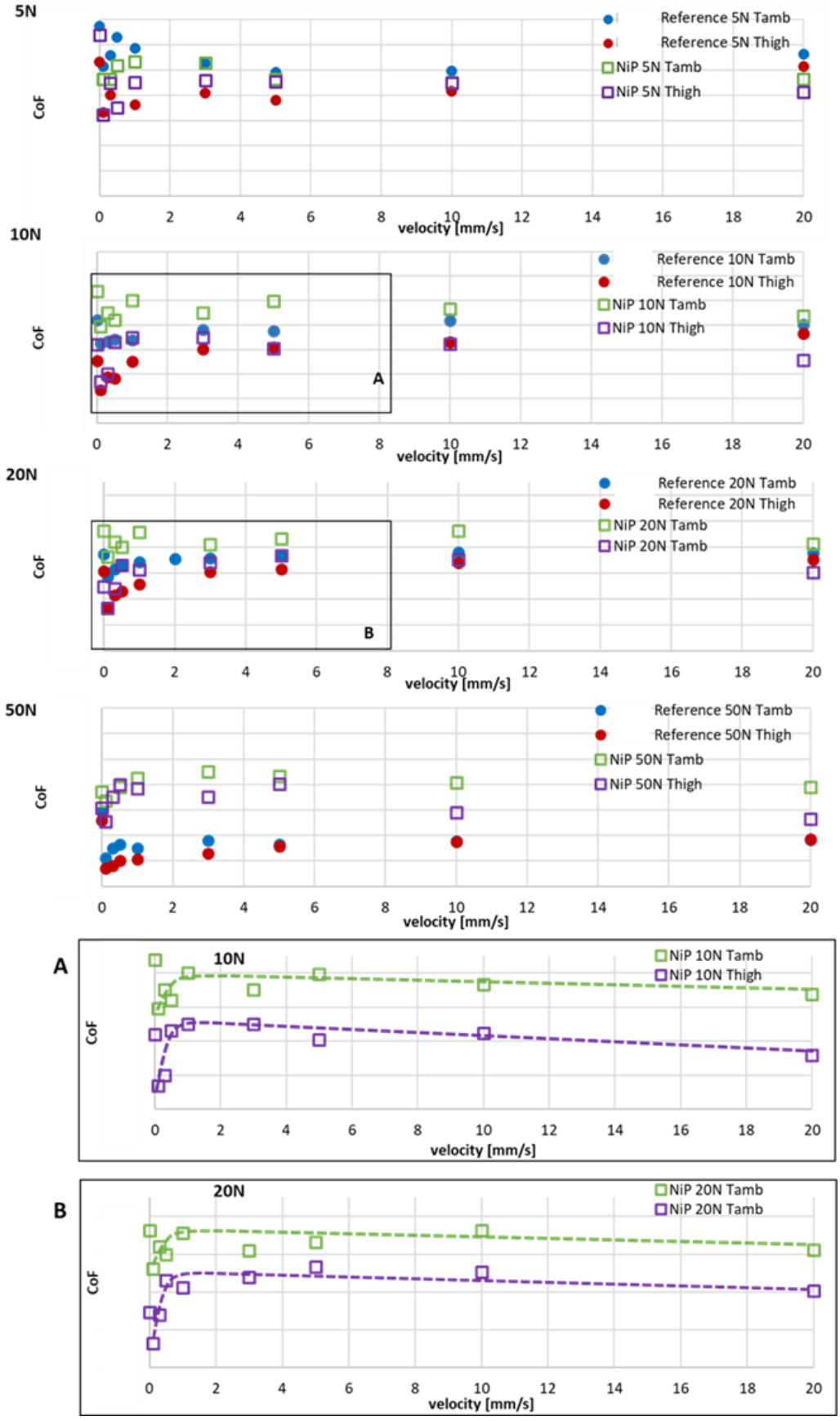

Figure 41: NiP configuration VS Reference configuration. The coefficient of friction (CoF) is analyzed as function of the sliding velocity, at ambient and high (lower figure) temperature, for different imposed normal loads (5N, 10N, 20N and 50N). A detail of the CoF trend for both 10N and 20N are shown in the lower plots (A and B).

Considering the difference between the static and dynamic friction coefficients ($\mu_s - \mu_d$), for low normal load (5N and 10N) the NiP configuration presents a higher difference compared to the DLC configuration. While the difference is lower when considering the higher loads. At high temperature, the NiP shows as well a larger difference for the lowest loads.

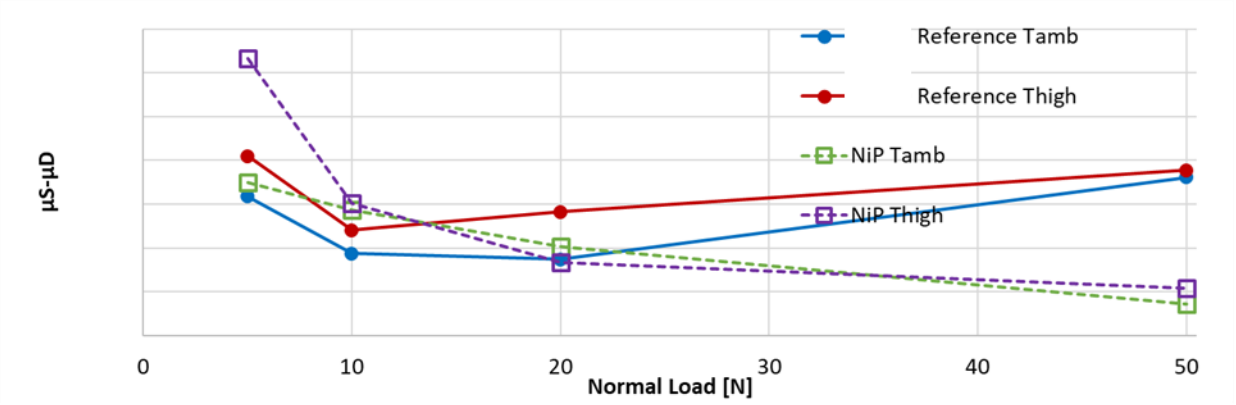

Figure 42: Difference between static and dynamic friction coefficient with respect to normal load, at ambient and high temperature for both the Reference configuration (circles) and NiP configuration (square).

While the general trend of the friction curves is maintained with both the coatings, the difference in amplitude of the dynamic and static friction coefficient are due to the different properties of the surface coatings and their abilities to form protective tribo-films between the contact surfaces and prevent wear and higher static friction.

- **Without Surface coating**

The tested configuration is characterized by the reference drum, the grease LiCPAO and the harmonic steel spring without any coating. The spring has undergone a surface finishing. The finishing consists in being submerged in a vibratory finishing machine, with distilled water and small grains of sand. Vibratory finishing produces a smoother finished surface thanks to laps produced by the small media.
As in the NiP case, the investigated configuration with absence of solid lubricant gives rise to the presence of *friction drops*. Considering, as an example, the test performed imposing a normal load of 20 N, a sliding velocity equal to 0.1 mm/s and high temperature condition, the *friction drops* presence is shown in Figure 43, in comparison with the stable behavior of the reference configuration.
Again, this behaviour is recurrent for low values of sliding velocity and high loads, in particular at high temperature. As in the NiP configuration, also in the case of absence of solid lubricant, these *friction drops* are repeated each cycle in the same position, as underlined with the green circles in Figure 43.

Tests	Normal Load [N]	Velocity [mm/s]	Temperature [°C]	Solid lubricant (spring surface)
Reference	20	0.1	80	DLC
Without solid lubricants	20	0.1	80	None

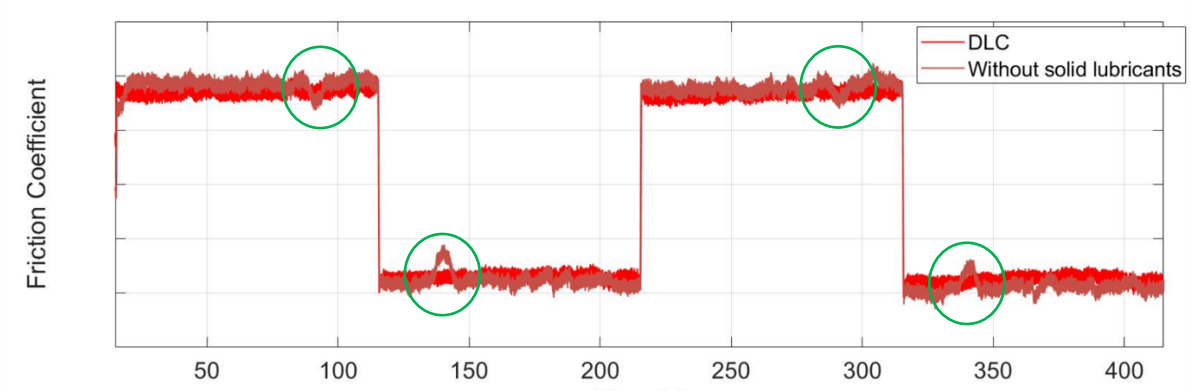

Figure 43: Coefficient of friction as function of the time for both the Standard configuration (DLC) and without solid lubricants (harmonic steel). During the CoF evolution, in the configuration without solid lubricants, friction drops occurs (green circles).

The contacting surfaces has been observed by an optic microscope, as reported in Figure 44.

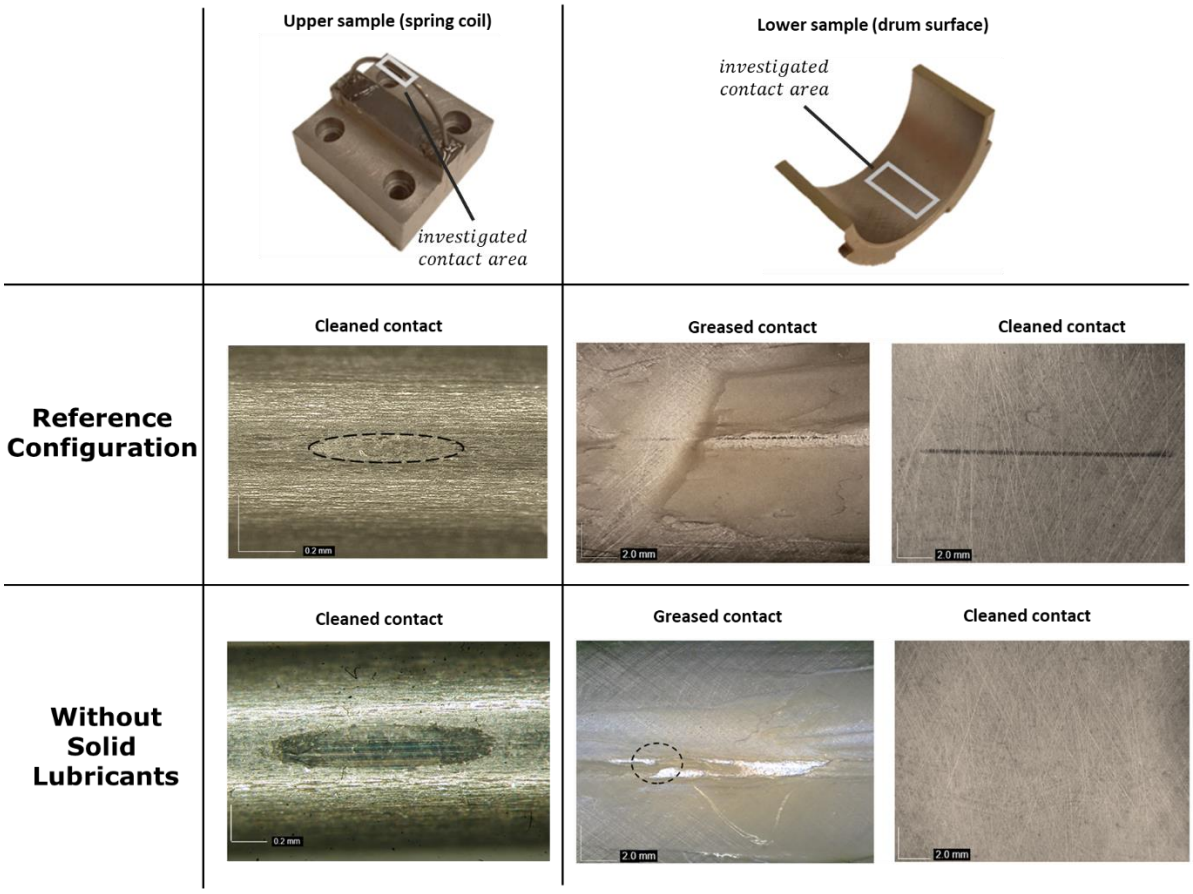

Figure 44: Comparison between Reference configurations and tests performed Without any solid lubricant on the spring surface. Optical microscope contact surfaces topographies. Upper figures: spring and drum in the reference configuration. Lower figures: Spring and drum without coating. The drum surface is observed before and after the cleaning protocol.

As in the case of NiP, the absence of solid lubricant results in a contact area of the spring strongly worn after the test protocol with a flattened zone. Not observable third body layer or surface wear on the drum contact area is underlined, comparing the two configurations.
The spring contact surface, in absence of solid lubricants, is affected by severe localized wear, more than in the case of the NiP coating, and characterized by a smoothed and flattened surface.
Again, in order to compare the results between the two different configurations (presence of DLC and absence of any solid lubricant on the spring surface), the dynamic friction coefficient has been calculated considering the stable part of the signal, without considering the presence of the *friction drops*.
As for all the other tested configurations, the coefficient of friction, as a function of the sliding velocity, does not represent the typical Stribeck-like curve. For all the tested configurations (DLC, CW, NiP and without solid lubricants), the two operating region can be underlined: a low-velocity region and a high-velocity one. The trend of the dynamic friction coefficient is always similar and in the same range values. It does not depend from the applied normal load and temperature.
In the case of absence of any solid lubricant, the CoF assume slightly higher values, compared to the reference configuration, if subjected to the same boundary conditions. This is coherent with the role of the DLC solid lubrication, which decreases the frictional force between the two contacting surfaces, providing a DLC-DLC contact pair with solid (and grease, in this case) lubricant.

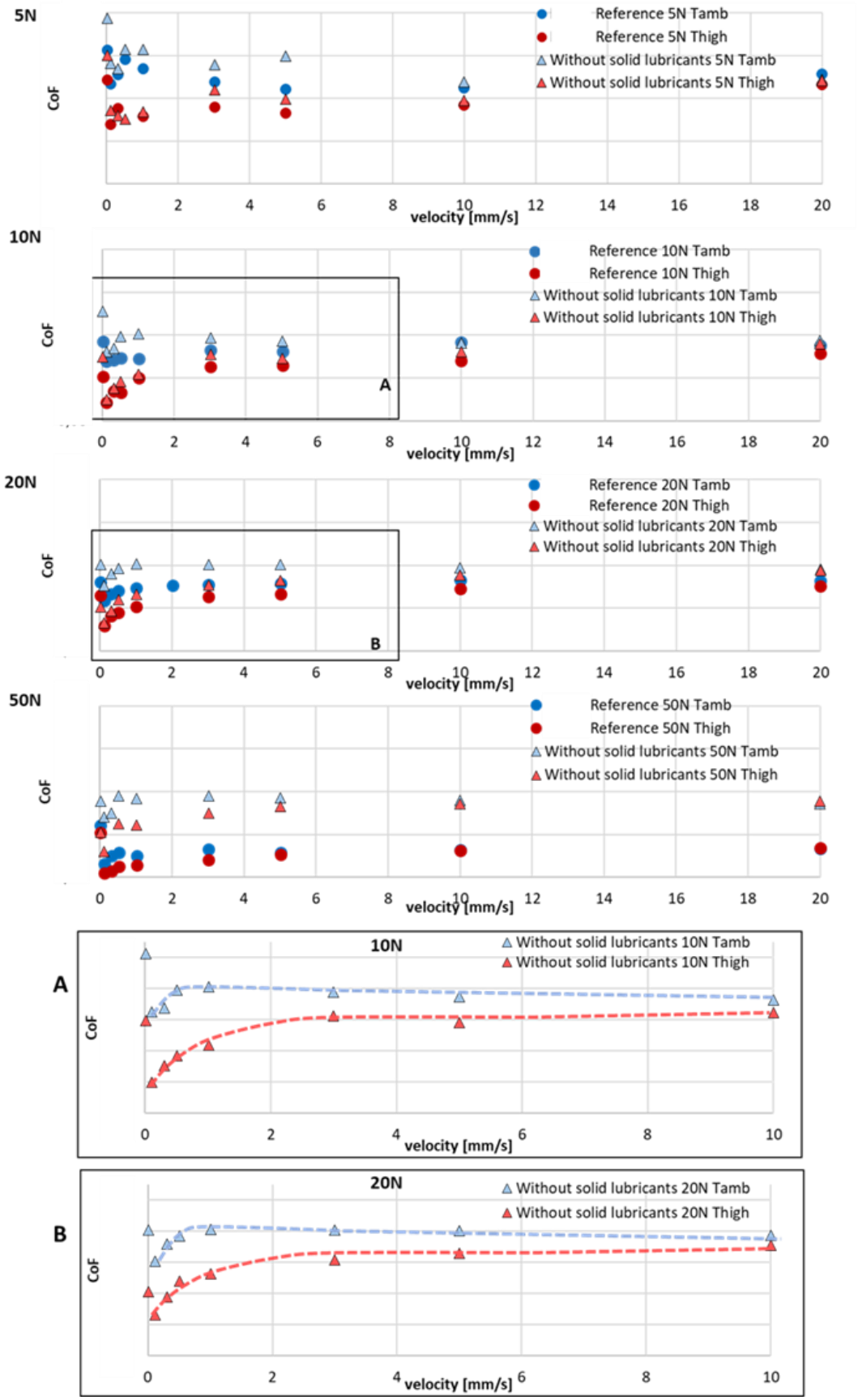

Figure 45: Absence of solid lubricants VS Reference configuration. Coefficient of friction (CoF) as a function of the sliding velocity, at ambient and high (lower figure) temperature, for different imposed normal loads (5N, 10N, 20N and 50N). A detail of the CoF trend in the case of absence of solid lubricants, for both 10N and 20N, are shown in the lower plots (A and B).

Analysing the difference between static and dynamic friction coefficients (Figure 46), this is higher for 5N and 10N, compared to the reference case, for both ambient and high temperature conditions. On the contrary, at higher applied normal load (20N and 50N) the $\mu_s - \mu_d$ values are lower, probably due to the flattened profile of the spring, which allows a local permanence of the grease and then a lower static friction coefficient. .

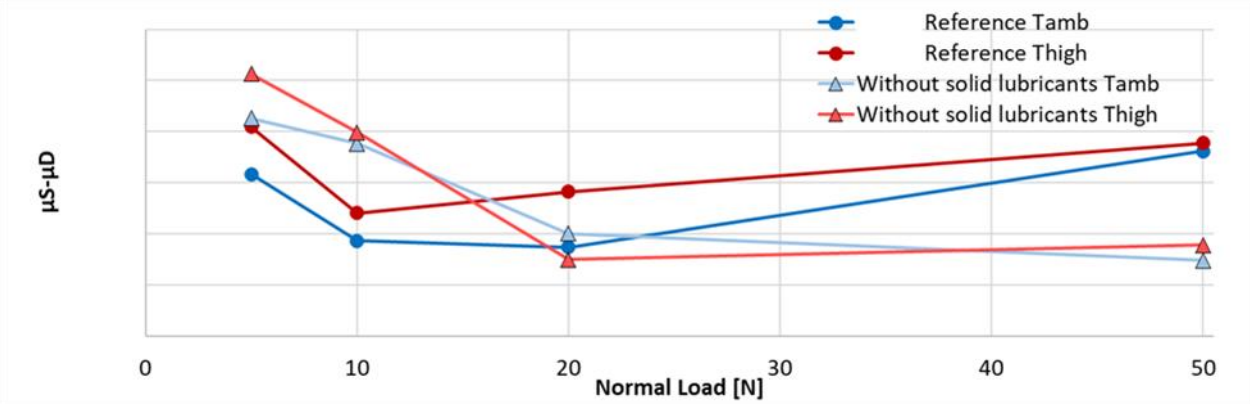

Figure 46. Difference between static and dynamic friction coefficient with respect to normal load, at ambient and high temperature for both the Reference configuration (circles) and absence of solid lubricants (triangles).

3.5. Concluding remarks

The local frictional contact response has been reproduced and analysed on a dedicated test bench, in order to evaluate the trends of friction as a function of the imposed boundary conditions. The experimental results have highlighted the complexity of the tribological response of the contact, function of both the rheological characteristics of the lubricant and the mechanical characteristics of the bodies in contact. It has been possible to identify some of the relative influences on the frictional behaviour of the involved design parameters, with respect to the sliding velocity.

First, a test protocol has been established and the ranges of the boundary conditions to be tested, i.e. contact pressure, sliding velocity and temperature, have been identified.

Then, an experimental campaign has been conducted to analyze the frictional response in terms of friction coefficient, at the contact scale, in the reference configuration. Analyzing the frictional behavior of this configuration, it has been underlined a particular trend of the friction coefficient, as a function of the sliding velocity, that does not follow the typical Stribeck-like curve. Initially, the static friction coefficient is followed by a sudden large drop, passing to the dynamic friction coefficient calculated at the lowest-speed conditions. Then, the coefficient of friction increases following a quasi-logarithmic trend and stabilizes when the sliding velocity is at about 2mm/s. This behaviour is emphasized in the case of the tests performed at high temperature, giving rise to a higher difference between static and dynamic coefficient of friction. This difference is assumed to be one of the main promoters for stick-slip occurrence, and its large value is

mainly due to the specific trend of the friction observed in the low velocity range. Then, in the higher velocity range the friction either stabilize or increases slightly with the velocity.
Then, different design configurations have been tested, in order to both provide information on the suitability of the design solution for the commercial brake systems and retrieve information on the parameters that could mostly affect the frictional trend and thus influence the appearance of the stick-slip phenomenon.
The main outcomes from the parametrical experimental campaign can be summarized as follows:

- For all the tested configurations, the friction coefficient evolution does not represent the typical Stribeck-like curve, probably due to the lithium complex grease lubrication. The friction coefficient drops drastically at the lowest value of the velocity and then increases until a stabilization;
- The drop at low velocities is significantly larger at high temperature, compared to ambient temperature, evidencing how this condition can deeply affect the stick-slip occurrence;
- The increasing of the load leads generally to a decrease of the friction coefficient, probably due to a greater oil release from the grease, or to the contribution of the solid lubricant, which participate to the lubrication mechanisms;
- A change in the drum material largely affects the frictional response. The drum 3 seems to establish favorable frictional conditions at the contact, with respect to the reference one, lowering the static friction coefficient;
- The CW coating provides a more stable frictional behavior compared to the DLC coating and lower values of the difference μ_s-μ_d, due to a lower static friction coefficient.
- The NiP coating and the tests performed without the presence of solid lubricants showed a contact area topography strongly worn after the test protocol, while there is no presence of solid third body transfer on the counterpart. On the contrary, the DLC and CW spring topography does not seem to be significantly worn and the drum contact surface shows the clear presence of a DLC transfer, able to improve the tribological performances of the contact, especially in terms of wear and friction coefficient stability.
- Moreover, with the NiP coating and in absence of solid lubricants, presence of *friction drops* of the tangential force are observed. In such circumstances, both the configurations are characterized by a drum contact topography that shows localized accumulations of grease that probably lead, tougher with a flattened spring profile, to localized hydrodynamic contact regime and the consequent drops in the friction coefficient.

In a more general manner, the experimental results have highlighted the complexity of the tribological response of the contact under analysis, which includes both grease and solid lubrication. While the parametrical analysis gave some information on the tested design solutions, it allowed as well to focus the attention on the role of the LiCPAO grease in the trend of the frictional response. In fact, within all the configurations reported in this

Chapter, which showed the same friction trends with respect to the velocity, the sole common element at the interface is the used grease. For this reason, in Chapter V, an in dept analysis has been dedicated to the role of the grease and its components on the local frictional response.
Before, in order to identify the effect of the friction trends with respect to the sliding speed on the stick-slip instability, a lumped numerical model has been developed and presented in following Chapter. The frictional trend, retrieved here, have been then considered as an input for the evaluation of the dynamic response of the whole mechanical system. Whit this aim, the obtained information is integrated in the lumped numerical model, representing the entire system, to evaluate the unstable dynamic response (i.e. the stick-slip phenomena) and identify the parameters that most influence its appearance, specifically on the observed trends of the friction coefficient.

IV. From the local contact to the system response

Due to the mutual influence of the local contact frictional response and the dynamical response of the system, a lumped model of the entire tubular electric actuator has been developed to evaluate the parameters that most influence the stick-slip appearance. Aiming to represent the whole spring-brake system, a mass-spring–damper system has been considered and all the parameters of the real system have been reduced and introduced into the model. On one side, stiffness, damping and loads have been calculated on the real system, considering all the system components. On the other side, the coefficient of friction is not assumed to be a constant value (Coulomb-Amounts friction law), but the trends obtained by the experimental tests (presented in Chapter III) have been considered. The experimental results obtained on the local frictional behaviour of the greased contact are in fact introduced as an input of a numerical lumped model of the mechanical system. The choice of representing the entire system through a lumped model has been made aiming to simplify the description of dynamical system and approximate its behaviour to obtain a simple and qualitative analysis of the parameters that most influence the stick-slip appearance. Parametrical analyses are then developed in order to identify the key factors leading to the instability.

4.1. Numerical model of the Electric Actuator

Considering the Reference brake-system, the entire actuator has been taken into account [115]. In Figure 47, a scheme of the whole tubular actuator is shown. An electric engine drives the loading system, imposing a time varying rotational speed. The electric motor (block *M*), driven by a controller, transmits the rotational speed to the axis after a first stage of reduction ($R1$). The mechanical spring-brake system is located just after this first reduction stage. The driver, first component of the brake, transmits the rotation to the entire brake system. On the opposite side, the side frame component, followed by the second and third stages of reduction ($R2$ and $R3$ in Figure 47), supports the output load. The output load (m) is subjected to a linear displacement.
The speed imposed by the engine can vary between 0 and 3000rpm, as a function of the load and the imposed displacement law [4].

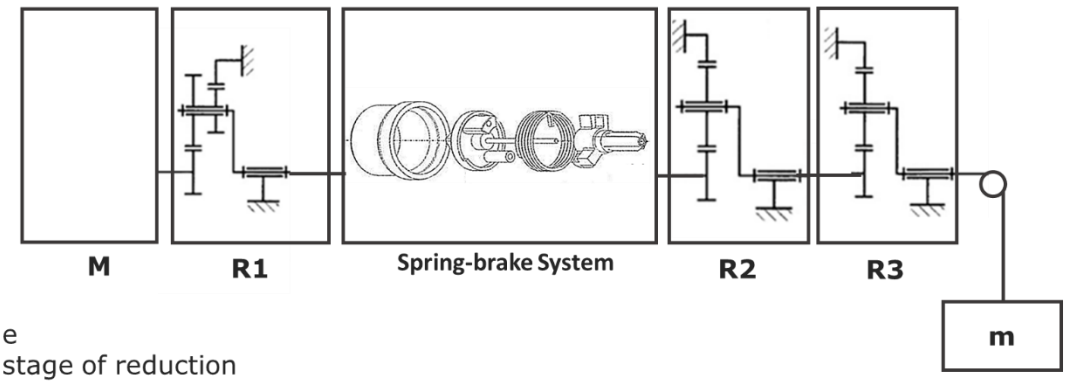

M – Engine
R1 – first stage of reduction
R2 – second stage of reduction
R3 – third stage of reduction
m – output load

Figure 47: Tubular actuator simplified view (upper image) and the corresponding scheme (lower image), including the view of the spring brake components.

Starting from the scheme in Figure 47, the lumped model has been created and the equation of motion determined. As shown in Figure 48, the spring-brake system is represented by a nonlinear slider-spring-damper system, where the contact load at the slider (representing the normal force between spring and drum contact surfaces), $N(x,y)$, is function of the spring elongation, as occurs in the real brake system.

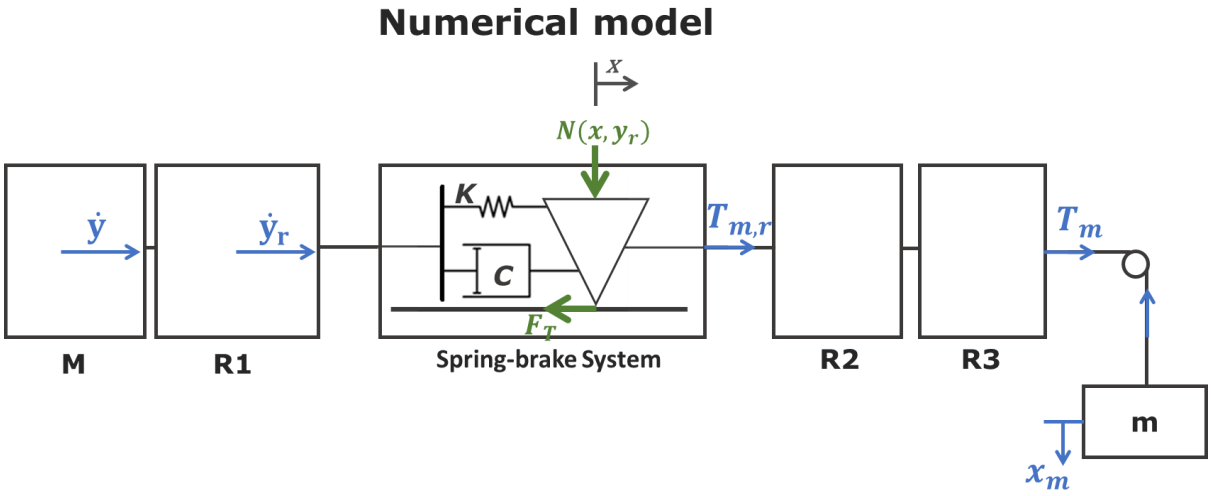

Figure 48: Scheme of the numerical lumped model implemented in Simulink of the reference tubular actuator.

The velocity, transmitted from the engine to the brake, is reduced by the first stage of reduction ($R1$) and expressed by $\dot{y}$ and $\dot{y}_r$ respectively (as shown in Figure 48). On the opposite side, the force term T_m contains all the information about the output load (m) and can be reported to the brake level by the term $T_{m,r}$. The mass (inertia) of the spring is neglected, compared to the mass (inertia) of the load.
It is possible to write the equation of motion as follow:

$$-k(x - y_r) - c(\dot{x} - \dot{y}_r) - F_T + T_{m,r} = 0 \quad \text{Eq. 3}$$

where k and c are the stiffness and the damping of the brake system, $T_{m,r}$ is the output load term, including the inertia of the mass m, and F_T is the friction force at the greased contact between the slider, representing the spring, and the ground, representing the fixed drum in the case study.
Considering the second and third stages of reduction ($R2$ and $R3$), the force generated from the output load at the brake level, $T_{m,r}$ can be written as:

$$T_{m,r} = T_m \tau_2 \tau_3 \eta_2 \eta_3 \frac{r_{pull}}{r_{brake}} \quad \text{Eq. 4}$$

Where r_{pull} is the radius of the pulley, which holds the load m, and r_{brake} is the radius of the brake system (drum internal circumference). τ_2 and η_2, τ_3 and η_3 are respectively the gear ratio and the reverse efficiency of the second and third reduction stages.
The force term T_m is function of the output load (m) and can be written as:

$$T_m = mg - m\ddot{x}_m \quad \text{Eq. 5}$$

where $\ddot{x}_m$ is the acceleration of the output load and can be calculated as the derivate of $\dot{x}_m$. Where, $\dot{x}_m$ is equal to:

$$\dot{x}_m = \dot{x} \tau_2 \tau_3 \quad \text{Eq. 6}$$

The friction force F_T is given by:

$$F_t = \begin{cases} sign(\dot{x}) \mu N(x, y_r) & if\ F_{sum} > F_{static}\ and\ v_x \neq 0 \\ k(x - y_r) + c(\dot{x} - \dot{y}_r) + T_{m,r} & if\ F_{sum} \leq F_{static}\ and\ v_x = 0 \end{cases} \quad \text{Eq. 7}$$

where F_{sum} is the sum of the external forces, while F_{static} is the maximum static friction force. If the sum of the forces applied on the spring is lower than the static friction force, and if the relative speed of the spring (v_x) is equal to zero, the friction force will be equal and opposite to sum of the external forces, and consequently the system is in sticking. On the contrary, if one of the two conditions are not respected, the friction force will be equal to the dynamic friction coefficient multiplied by the normal contact force $N(x, y_r)$ and the spring is sliding on the drum.

The normal force, $N(x, y_r)$, is function of the elongation of the spring. When the engine imposes the rotation to the axis, the torsional spring is compressed and the normal force at the greased contact decreases, decreasing the braking torque, until the sliding of the spring and the descent of the load. The normal force $N(x, y_r)$ is then given by an initial pre-load (N_{max}), due to the interference between the spring and drum radii and to the applied load, and decreases when compressing the spring, until it arrives at an equilibrium force, N_{eq}, for which the sliding of the mass occurs:

$$N(x, y_r) = N_{MAX} - N(x - y_r)$$ Eq. 8

The described lumped model allows to analyse the conditions for which the system is more predisposed to the stick-slip instability, by analysing the dynamic frictional response of entire system as a function of the system parameters and the local frictional law at the contact. The equation of motion, reported in Eq. 9, has been solved by a Simulink/Matlab code (represented in Figure 49).

$$-k(x - y_r) - c(\dot{x} - \dot{y}_r) - F_T + [mg - m\ddot{x}(\tau_2\tau_3)]\tau_2\tau_3\eta_2\eta_3\frac{r_{pull}}{r_{brake}} = 0$$ Eq. 9

In the developed model, the coefficient of friction is not assumed to be a constant value (Coulomb-Amounts friction law). The experimental frictional analysis, performed on the Triboair test bench (Chapter III), shows that the macroscopic friction coefficient undergoes relevant variations, as a function of imposed boundary conditions and mainly as a function of the sliding velocity. The used curves of the friction coefficient are then the ones obtained experimentally.
Moreover, the equation of motion takes into consideration all the mechanical parameters of the tubular electric actuator under investigation. Each input parameter has been treated separately, to obtain values as much as possible representative of the real system. In the present study, the numerical lumped model has been developed focusing the attention on the reference configuration. Nevertheless, the model allows an easy adaptation to the different configurations of other actuators.

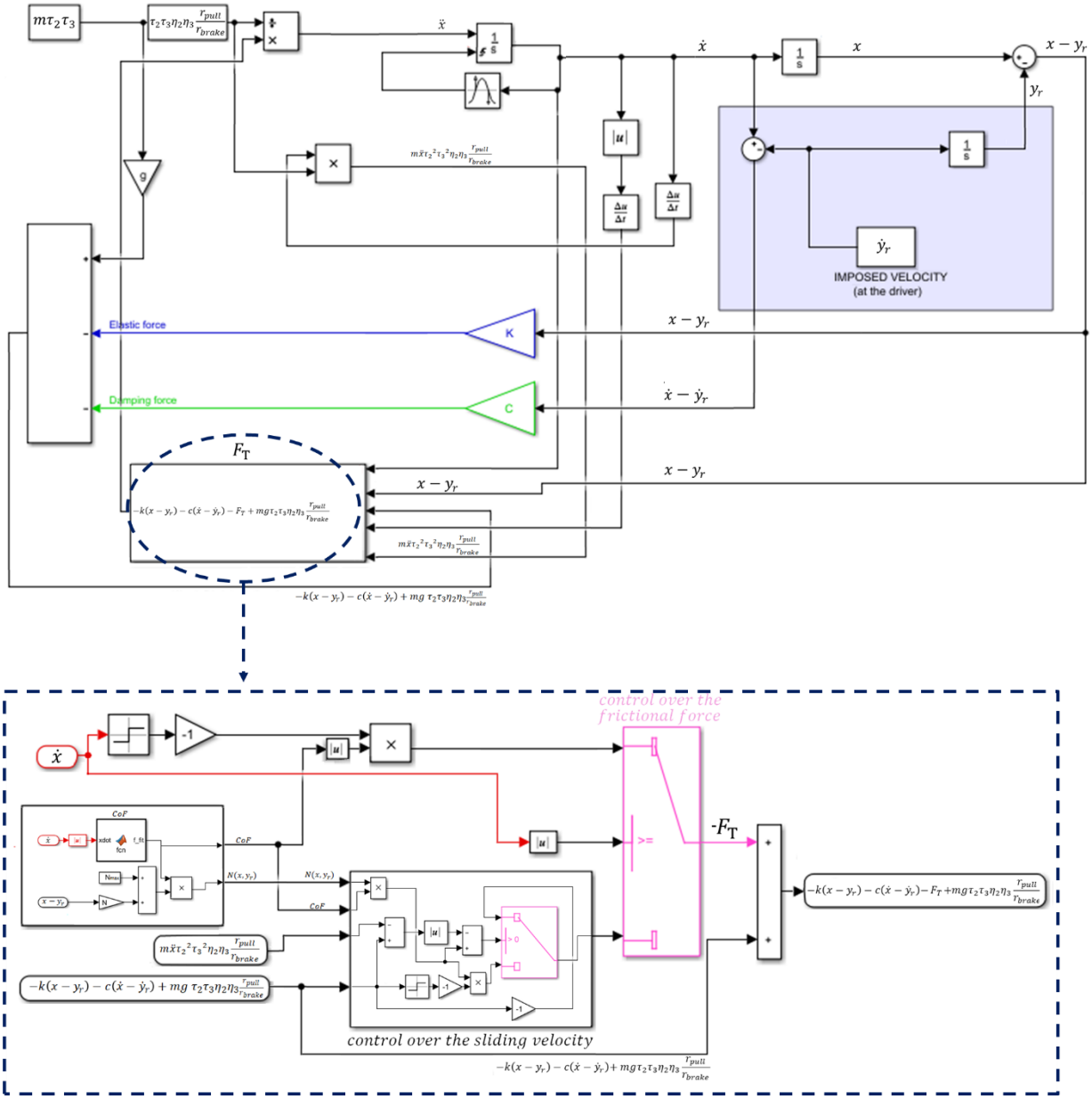

Figure 49: Simulink lumped model of the of the reference tubular electric actuator.

4.2. Identification of the system parameters

The numerical lumped model has been alimented by the data from the frictional tests, in order to recreate the scenarios that bring to the frictional instability. The reduction ratios and efficiency factors of the reduction stages, together with the imposed velocity and mechanical characteristics of the entire actuator have been introduced as inputs as well. The equation of motion has been then solved by a Simulink code and the outputs of the model are analyzed.

The inputs of the numerical model to be defined are:

- The mechanical properties of the stages of reduction, τ and η;
- The imposed velocity v and the output load m;

- The mechanical properties of the brake system, C and K;
- The normal force $N(x, y_r)$ between spring and drum;
- The trends of friction coefficients $\mu(v_{rel})$, as function of the different operative conditions and type of lubricants (see Chapter III).

4.2.1. Velocity profile and output load

The profile of the speed imposed by the engine ($\dot{y}_r$) has been defined as a trapezoidal curve of a total duration equal to 20 seconds, where the first and last 1 seconds are the acceleration and deceleration phases. During the rest of the time the velocity is constant. The rotational velocity, transmitted from the engine to the axis, can range from 0 up to a maximum value of 3000 rpm. In order to consider the equivalent translational velocity at the spring-drum contact interface, the rotational speed of the engine has been multiplied by the radius of the contact surface (inner radius of the drum):

$$v = \frac{2\pi\omega_r}{60} r_{brake} \quad \text{Eq. 10}$$

Where ω_r is the rotational speed at the output of the first stage of reduction ($R1$) and r_{brake} correspond to the internal radius of the drum.
On the opposite side of the electric actuator, an external load (m) is imposed. In order to be representative of the reference configuration, an equivalent load is applied in the numerical model. Willing to reproduce as close as possible the real condition, considering the nominal output torque equal to 15Nm, the output load that has to be imposed to obtain the same nominal torque has been calculated as follow:

$$m = \frac{C_n}{g\, r_{pulley}} \quad \text{Eq. 11}$$

where r_{pulley} is the radius of the pulley used to impose the output load, , g is the gravitational constant and C_n is the nominal torque. So, the output load applied in the numerical model, to be representative of the case study conditions, is represented by a mass.

4.2.2. Stiffness and damping of the brake system

Aiming to characterize the macroscopic mechanical properties of the brake system, experimental tests have been performed to define its stiffness and the damping at both ambient temperature (25°C) and high temperature (80°C).

- **Stiffness**

The brake has been used to build up an experimental set-up to measure the torsional stiffness of the spring at high temperature (80°C) and ambient temperature (25°C), when mounted on the brake components (driver and side frame). The results have been then compared with the theoretical stiffness value of the spring. The theoretical torsional stiffness [123] can be calculated as:

$$K_{torsional} = \frac{d^3 E\, n}{64\, {}^{d}/_{D}} \frac{\pi}{180}$$ Eq. 12

Where d is the spring coil diameter, D is the internal diameter of the spring, E is the Young Modulus and n is the number of spires.

Considering the reported values of the spring for the reference configuration.
The principle of the experiment for measuring the effective stiffness is shown in Figure 50.

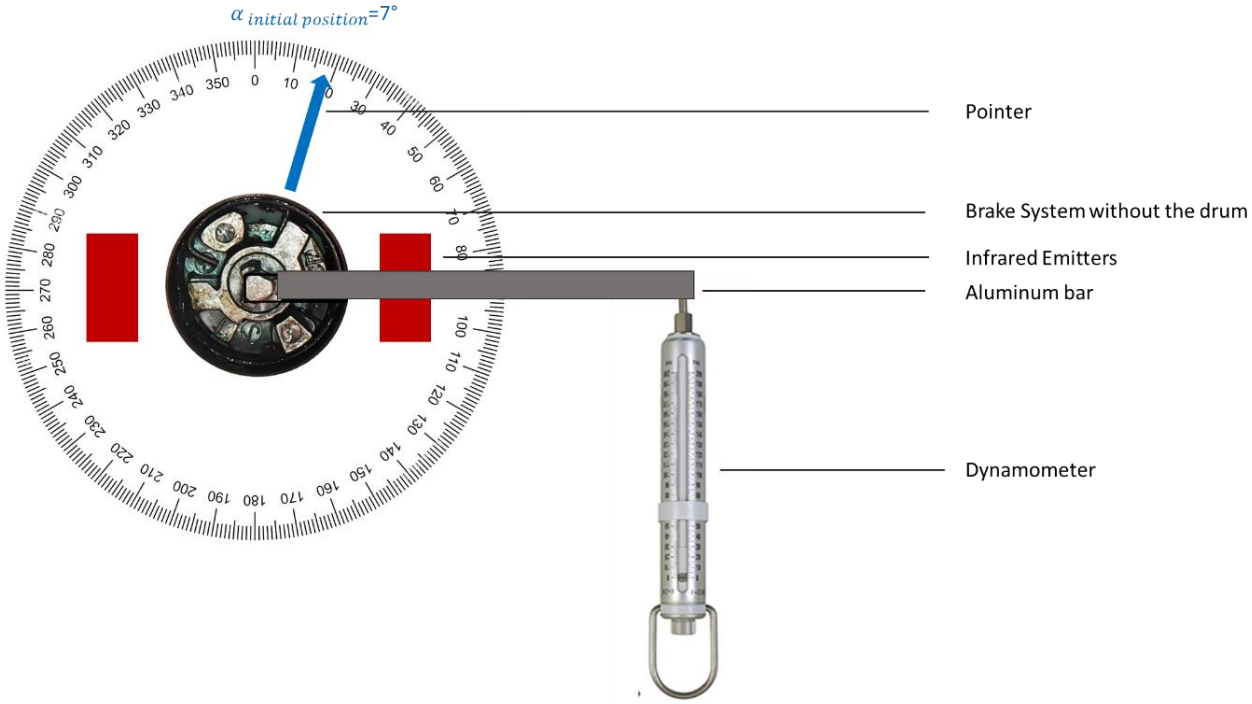

Figure 50: Principle of the experiment conducted to determine the spring torsional stiffness.

The brake, without the drum component, has been stuck, by the driver component, on a surface where a goniometer is positioned too. The two end parts of the spring have been constrained to the driver and to the side frame respectively. In this configuration the lower side of the spring, constrained to the driver, is unable to move; by imposing a rotation on the side frame, the spring upper end rotates accordingly. An aluminum bar is connected to the central part of the side frame and a dynamometer (Pesola Präzisionswaagen AG, Medio Line 3N) with a precision equal to ±0.3%, is fixed to its end in order to provide and measure the imposed torsional torque. On both sides of the brake system, two infrared emitters are placed to obtain the desired temperature.
When imposing a force ($N_{imposed}$), by means of the dynamometer, the side frame rotates, allowing the display of the walked degrees (α) through the pointer. Knowing the aluminum bar length (l_{bar}) and the applied force, the imposed torque can be computed ($C_{imposed} = N_{imposed} l_{bar}$). Then, the torsional

stiffness of the spring is calculated as the imposed torque divided the walked degrees (Eq. 13).

$$K_{torsional} = \frac{C_{imposed}}{\alpha} \left[\frac{Nm}{deg}\right] \quad \text{Eq. 13}$$

The tests have been performed both at ambient temperature (25°C) and higher temperature (80°C) conditions and considering two different aluminium bar lengths (85mm and 60mm), aiming verify the precision of the used method. The tests have been performed following the protocol reported in Table 4.

Protocol A (without the drum)				Protocol B (without the drum)			
Test	l_{bar} [m]	Temperature [°C]	α [degrees]	Test	l_{bar} [m]	Temperature [°C]	α [degrees]
1	0,085	25	14	1	0,06	25	14
2	0,085	25	21	2	0,06	25	21
3	0,085	25	28	3	0,06	25	28
4	0,085	25	35	4	0,06	25	35
5	0,085	25	42	5	0,06	25	42
6	0,085	25	49	6	0,06	25	49
7	0,085	25	56	7	0,06	25	56
8	0,085	25	63	8	0,06	25	63
9	0,085	25	70	9	0,06	25	70
Heating				Heating			
10	0,085	80	14	10	0,06	80	14
11	0,085	80	21	11	0,06	80	21
12	0,085	80	28	12	0,06	80	28
13	0,085	80	35	13	0,06	80	35
14	0,085	80	42	14	0,06	80	42
15	0,085	80	49	15	0,06	80	49
16	0,085	80	56	16	0,06	80	56
17	0,085	80	63	17	0,06	80	63
18	0,085	80	70	18	0,06	80	70

Table 4: Tests protocol to determine the spring torsional stiffness.

Starting from the initial position, a rotation is imposed to the bar through the dynamometer and every 7 degrees the corresponding force is registered, until reaching the 70 degrees.
Each protocol has been conducted three times. The results are compared with the theoretical stiffness value (Eq. 12) and are shown as a function of the walked degrees (α) in Figure 51.

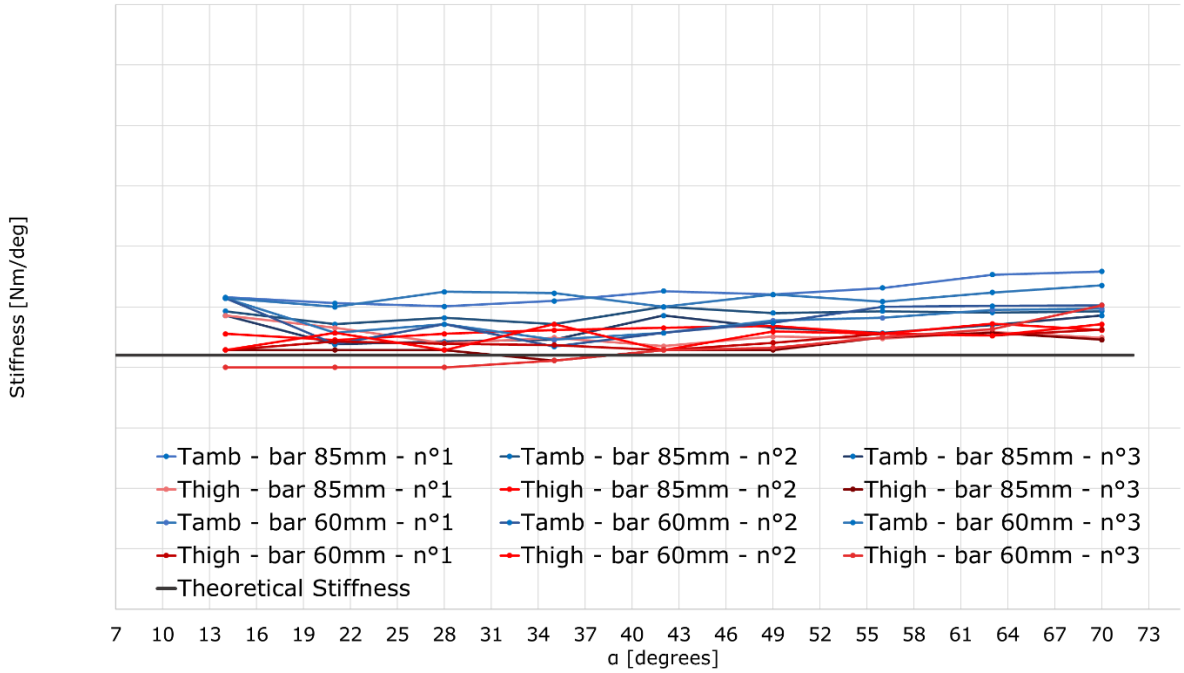

Figure 51: Measured stiffness as a function of the angle for the reference configuration without the drum, both at ambient (curves in shade of blue) and high temperature (curves in shade of blue), compared to the theoretical stiffness (grey line).

As shown in Figure 51, considering each point for each configuration, the stiffness values stay almost constant. The results obtained are not influenced by the aluminium bar length. At the ambient temperature (curve in shades of blue in Figure 51) the stiffness results slightly higher than the one obtained at high temperature (curves in shades of red in Figure 51). This slight difference is probably due to either the variation of the properties of the spring steel or the different behaviour of the grease between the spring spires, at the tested temperatures. As well, a slight increase is as well observed with the tightening angle, probably due to the contact between the spires of the spring and with the other brake components, when tightening the spires. Comparing the obtained results, with respect to the theoretical value, the theoretical stiffness value underestimates slightly the real values of the torsional stiffness of the spring.
Computing the average of the obtained results, the mean torsional stiffness of the spring has been calculated.
Considering that, in the numerical model, the spring-brake system is modelled on a translational system, the torsional stiffness has been converted as longitudinal stiffness, accounting for the radius of the drum contact surface (which drive the rotation of the spring), through the following formula:

$$K_{linear} = \frac{K_{torsional}}{{r_{spring}}^2} \frac{360}{2\pi} \left[\frac{N}{m}\right] \quad \text{Eq. 14}$$

The equivalent stiffness is then equal to $224\ \frac{N}{m}$ for the ambient temperature (25°C) condition and equal to $198\ \frac{N}{m}$ for the high temperature condition (80°C).

- **Damping**

Unlike the mass or stiffness, which can be measured by static tests, the damping cannot be determined by a static measurement. The damping ratio is a dimensionless term and describes how rapidly the oscillations of a structural system decay, which is a significant factor when analysing a structural dynamic response largely affected by energy dissipation [124], as in the case of stick-slip phenomena. In order to estimate the structural damping of the spring-brake system of the reference configuration specific dynamic tests have been then performed.

The experimental set-up is presented in Figure 52. As for the stiffness measurement, the driver is fixed to the ground, while the greased spring has the two ending parts fixed to the side frame and to the driver respectively. In this case, a massive disc (m) equal to 0.34 kg and external diameter equal to 64 mm has been fixed to the side frame (the mobile ending of the spring) in order to constitute a rotational one degree-of-freedom system, where the torsional spring is the one of the brake system and the moment of inertia is the one of the added mass. The damping of the rotational system is mainly due to the greased contact between the spires and the internal contact between the brake components (driver, axle, side frame), which are the same present in the spring-brake system. Moreover, in order to position the system in an equilibrium position, which is not at the complete extension of the torsional spring, and thus to obtain an oscillation around the equilibrium position, a longitudinal spring (i.e. added spring) is connected to the periphery of the massive disc.

On the upper part of the mass, an uni-axial accelerometer (PCB-352A24), with a mass equal to 0.8gr, is placed to retrieve the tangential acceleration. The torsional spring is preloaded thanks to the added spring, imposing an initial rotation to the mass. In this way, the torsional (brake) spring and the added spring are pre-stressed, and the system can oscillate around the equilibrium position. The mass is then rotated manually to give an initial condition (perturbation) on the position, different from the equilibrium. It finally is released and stars oscillate, while the accelerometer records its oscillations until the rest.

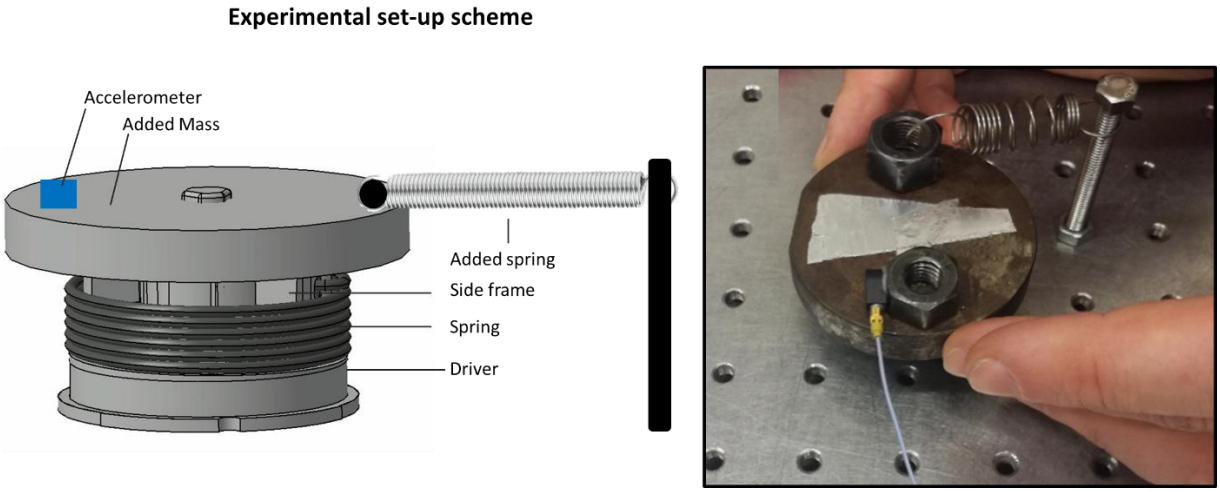

Figure 52: Principle of the experiment conducted to determine the damping.

The technique used to calculate the damping of the spring-brake system is based on the log-decrement method [124]. Considering a generic damped signal $x(t)$, the damping coefficient can be calculated taking into considerations any of the two successive peaks $x(t)$ and $x(t+1)$.
The logarithmic decrement, δ, is defined as the natural logarithm of the ratio of the amplitudes of successive peaks (Eq. 15).

$$\delta = \frac{1}{n} \ln \frac{x(t)}{x(t+1)} \qquad \text{Eq. 15}$$

where n is the integer number of successive positive peaks that have been considered [124].
Analysing the acceleration signal over the time, retrieved by the accelerometer, and considering the successive peaks in order to calculate δ, it is possible obtained the Damping Ratio, ζ, as:

$$\zeta = \frac{\delta}{\sqrt{4\pi^2 + \delta^2}} \qquad \text{Eq. 16}$$

In the performed experimental tests, from the acceleration signal, it has been possible to calculate the natural frequency of the signal as well, ω_n. The acceleration over time and the corresponding Fast-Fourier Transform (FFT) of one of the performed experimental tests are shown in Figure 53, as an example.

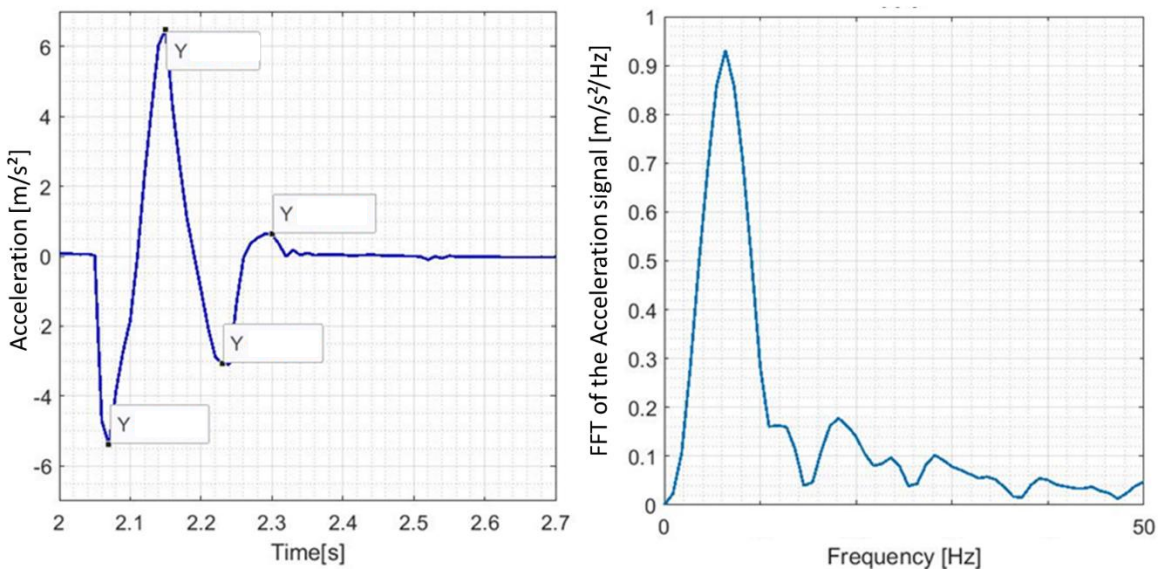

Figure 53: Acceleration over the time (left image) of a single experiment and the corresponding FFT of the signal (right image).

Knowing the moment of inertia of the mass, J, equal to $0{,}0001741\ kgm^2$ and the natural frequency,ω_n, the damping factor of the system has been calculated as:

$$c=2J\zeta\omega_n \qquad \text{Eq. 17}$$

The experimental tests have been performed rotating the mass, both clockwise and counterclockwise, and imposing an initial rotation to the brake system equal to 45 degrees. The system is then left free to return to the initial position. The tests have been performed three times for each rotation direction. The obtained results are reported in Table 5.

Tests	**Rotation Direction**	**Inertia J [kgm^2]**	**Damping Ratio ζ**	**Natural Frequency ω_n**
1	clockwise	0.0001741	0.0456	39.986
2	clockwise	0.0001741	0.0426	39.986
3	clockwise	0.0001741	0.0400	39.986
4	clockwise	0.0001741	0.0321	39.986
5	clockwise	0.0001741	0.0302	39.986
6	counterclockwise	0.0001741	0.0179	39.986
7	counterclockwise	0.0001741	0.0264	39.986
8	counterclockwise	0.0001741	0.0341	39.986
9	counterclockwise	0.0001741	0.0300	39.986
10	counterclockwise	0.0001741	0.0321	39.986

Table 5: Results of the tests conducted to determine the damping value.

It is clear that as the damping is affected by several parameters that cannot be fully controlled (positioning of the spires, status of the contacts between the components, …) and being one of the most difficult dynamic features to be measured, an interval of values is obtained, rather than an exact number. Nevertheless, for the scope of the dynamic analysis, it is here needed to have an estimation of the damping and its possible range of variation.
The damping of the translational model of the brake system, obtained experimentally without considering the contact with the drum, is then in a range between $0.8\ [\frac{Ns}{m}]$ and $2.5\ [\frac{Ns}{m}]$.
It should be noticed that the damping is here calculated considering the original configuration of the brake components, including the greased contact between the spires of the spring, but without the presence of the drum. This choice has been made considering that the contribution of the contact with the drum, in the numerical model, is accounted by the slider.

4.2.3. Normal Force

When the brake system is mounted, starting from the initial configuration of the torsional spring, the spring is tightened inside the drum. In the case of the brake system the tightening is equal to a defined value (i.e. difference between external diameter of the torsional spring and internal diameter of the fixed drum). Thus, an initial contact force (pressure distribution) is present at the contact between the spires and the drum. At this, the normal force (pressure) corresponding to the load on the side frame (which tends to open the torsional spring) must be added. Then, an imposed displacement at the driver side (y_r) is necessary to start the spring motion, and it is given by the engine that tightens the spring. By imposing this displacement, the spring is in fact compressed until the friction force (braking torque) between the spring and the drum decreases to the value of the torque given by the load, and a balance is reached.
The normal force at the greased contact between the spring and the drum is thus maximum when the angular displacement is equal to zero (corresponding to the mounting position of the spring inside the drum) and it decreases as the angular tightening of the spring ($x - y_r$) increases, until the equilibrium is reached.
Moreover, if the driver side of the spring is maintained fixed (imposed displacement by the engine, y_r, equal to 0), continuing to impose a load to the spring from the other side, the spring spires will detach, from the contact with the drum, and the normal force at the contact will arrive to zero.
Therefore, to be representative of the real situation, the imposed normal force, in the numerical model of the electric actuator, is defined as a decreasing curve that goes from the maximum value N_{max} (corresponding to the mounting position with the nominal load) until zero (corresponding to the spring coils detachment from the greased contact with the drum surface).

The maximum normal force N_{max} is equal to the tangential force (T) divided by the static CoF.
The tangential force, T, is calculated as follow:

$$T = \frac{C_n \tau_2 \tau_3 \eta_2 \eta_3}{r_{spring\ external}} \ [N] \qquad \text{Eq. 18}$$

where the C_n is the nominal torque given by the load on the actuator.
Thus, the corresponding normal force introduced into the numerical model (dashed line in Figure 54) is a curve that starts from N_{max} and decreases with the increase of the tightening of the spring ($(x - y_r)$ into the model), until reaching the null value, obtained for the tightening corresponding to the detachment between spires and drum.
When imposing such law of the normal force, $N(x, y_r)$, as a function of the time, the resolution of the equation of motion will result (when the system is stable) in an equilibrium value N_{eq}, corresponding to the frictional torque necessary for allowing the load (m) to move (descent) with a constant velocity. The normal load as a function of the time will the stabilize on the equilibrium value, as schematized by the continuous line in Figure 54.

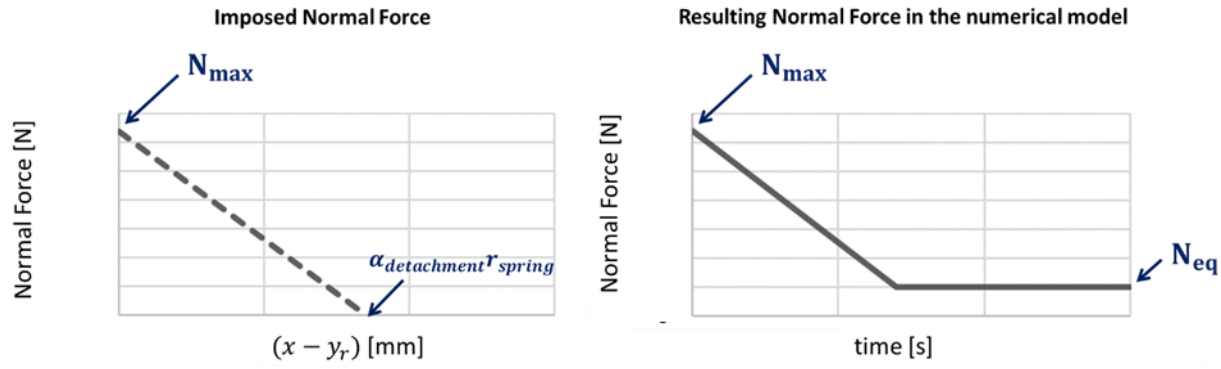

Figure 54: Left - Scheme of the imposed normal force N between the spring and the drum, as a function of the spring tightening $(x - y_r)$; Right - Trend of the resulting force in the lumped model obtained solving the equation of motion, as function of the time.

The curve of normal force, as a function of the spring tightening, has been then introduced as an input in the numerical lumped model and has been assumed equal to a straight line starting from the N_{max} and passing through the point equal to the value at which the detachment of the spire is reached (i.e. $\alpha_{detachment}$ multiplied by r_{spring}). Thus, to define the curve, two points are needed. At this aim, while the value of the N_{max} (at $(x - y_r) = 0$) has been calculated trough the value of the nominal load, the angular tightening needed to bring to the detachment has been measured by the set-up illustrated in Figure 50, with the drum mounted on the system. Comparing the measured force needed to tighten the spring, with and without drum, it is possible to retrieve the angular tightening corresponding to the spring/drum detachment.
Then for each iteration of the numerical simulation, the numerical model will take into consideration the corresponding normal force value, as a function of the actual tightening of the spring $(x - y_r)$. The value at which

the movement stabilizes (without stick-slip) will corresponds to the normal force value at the equilibrium.
For the sake of clarity, it is important to note that, as explained previously, the known points are the values of N_{max} and $\alpha_{detachment} r_{spring}$; the shape of the curve passing through these two points, introduced into the numerical model, has been assumed as a straight line. However, numerical simulations have been carried out, imposing the different normal force curves shown in Figure 55, to verify that the shape of this curve does not influence the dynamic response of the system.

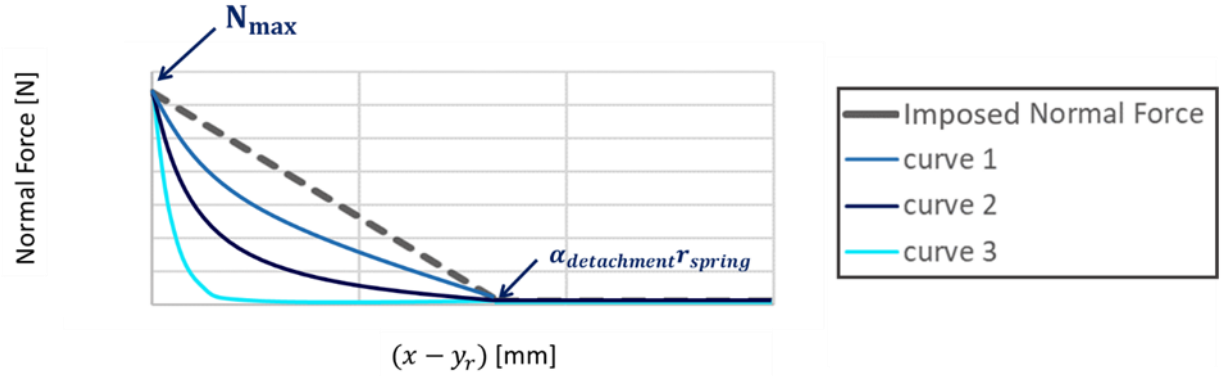

Figure 55: Scheme of four tested imposed normal force N (between spring and drum), as a function of the spring tightening $(x - y_r)$.

The results of the numerical simulations showed that, when introducing the different tested curves, the dynamic response of the system (i.e. stick-slip occurrence) is almost unvaried and the shape of the curve can be neglected.

4.2.4. Frictional contact law

The model has been designed aiming to provide the possibility of adding any trend of the friction coefficient, as function of the sliding velocity. In this way, it is possible to test both the classic Coulomb model and the real trends of the coefficient of friction, obtained experimentally. The curves of the friction coefficient, used as an input, are obtained by cubic interpolation of the experimental results presented in the Chapter III.
The numerical solver, at each iteration, will then choose the value of the CoF on the interpolated curve, with respect to the actual relative velocity between the slider and the frame (i.e. the spring and the drum).

4.3. Stick-slip simulation and model validation

A preliminary numerical evaluation of the lumped model has been necessary to validate the model. Aim of these simulations is to analyse the robustness of the lumped model by simulating and evaluating the system dynamic response in the reference configuration, both at ambient and high temperature. The results have been then compared to the experimental tests performed on the real tubular electric actuator, presented in Chapter II, Section 2.1.

4.3.1. Reference configuration

Introducing as an input the same operating conditions of the reference configuration, it is possible to simulate the dynamic response of the entire system both at ambient temperature (25°C) and high temperature (80°C). The input parameters are presented in Table 6.

Numerical model inputs

Configuration	Reference
Output load m	[kg]
Speed profile	Acceleration from 0 to 1 seconds, Constant for 19 seconds, deceleration for 1 seconds until reaching 0mm/s.
Stiffness K	200 N/m
Damping C	C=1 Ns/m
Normal Force	Figure 54
Frictional behaviour	Friction trends retrieved experimentally in Chapter III, Section 3.3.

Table 6: Inputs of the numerical simulation of the Reference configuration.

Figure 56 presents the results obtained when introducing the friction coefficient obtained thought the experimental tests (Chapter III, Figure 30), at ambient temperature. The velocity curve imposed by the engine, starts from 0 and reaches the maximum speed within 1 s. The imposed velocity is kept stable for 18s and subsequently reset to zero by a deceleration ramp lasting 1 s. As it is possible to see in Figure 56 – A, after some seconds the spring starts sliding, and the velocity starts to increase according to the imposed conditions. The spring displacement follow the imposed boundary conditions. In the meantime, due to the tightening of the spring (increasing of the $(x - y_r)$ term), the normal force decreases, reaching the equilibrium. After the first detachment, initial oscillations can be observed, during the acceleration phase. This is due to the initial impulsive excitation when passing from the sticking frictional contact condition to the sliding one, and the high difference between static and dynamic friction coefficients, due to the frictional trend retrieved experimentally. Nevertheless, in this case, the contact instability is observed only in the first seconds after the motion begin but disappears after the stabilization of the transient phase. As well, the instability is not observed when the imposed velocity decreases again to zero, at the end of the simulation.

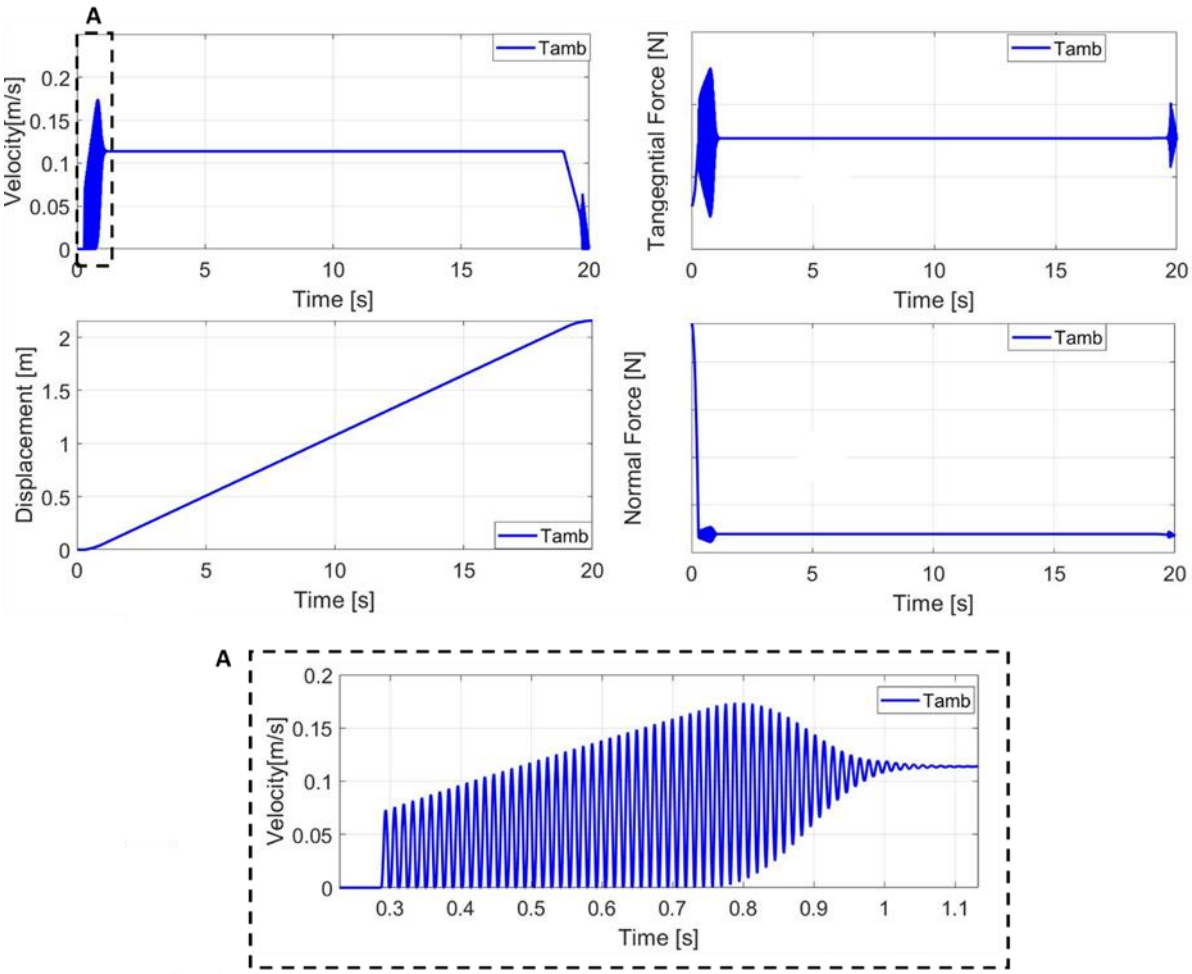

Figure 56: Numerical results of the simulation of the tubular electric actuator at ambient temperature condition.

Focusing the attention on the phase-plane plot of the results obtained at ambient temperature (Figure 57), the velocity $(\dot{x} - \dot{y}_r)$ is plotted as a function of the displacement $(x - y_r)$. This choice has been made to subtract the quasi-static movement imposed by the engine to the absolute motion of the slider (spring). The profile of the velocity imposed by the engine $(\dot{y}_r)$ has been defined as a trapezoidal curve, where the first and last 1 seconds are the acceleration and deceleration phases. During the rest of the time the velocity is constant. At the zero time the displacement y_r is imposed by the driver to the brake system, the spring is compressed until the first detachment occurs. The movement of the brake does not start at time zero but with a delay equal to the displacement necessary to reach static friction force and therefore the motion starts. After the sliding occurs, a transient oscillation of the system is observed, due to the shift from static to dynamic friction, with increasing and then decreasing of the system oscillations, represented by ellipses (harmonic oscillations) around zero. The same transient oscillation has been observed during the last seconds, in the deceleration phase. During constant velocity phase, the equilibrium is reached and the displacement of the spring is equal to the imposed displacement. This result in the velocity $(\dot{x} - \dot{y}_r)$ equal to zero (dot in the

lower zoom in Figure 57) and the corresponding relative displacement equal to the value of x_{gap}.

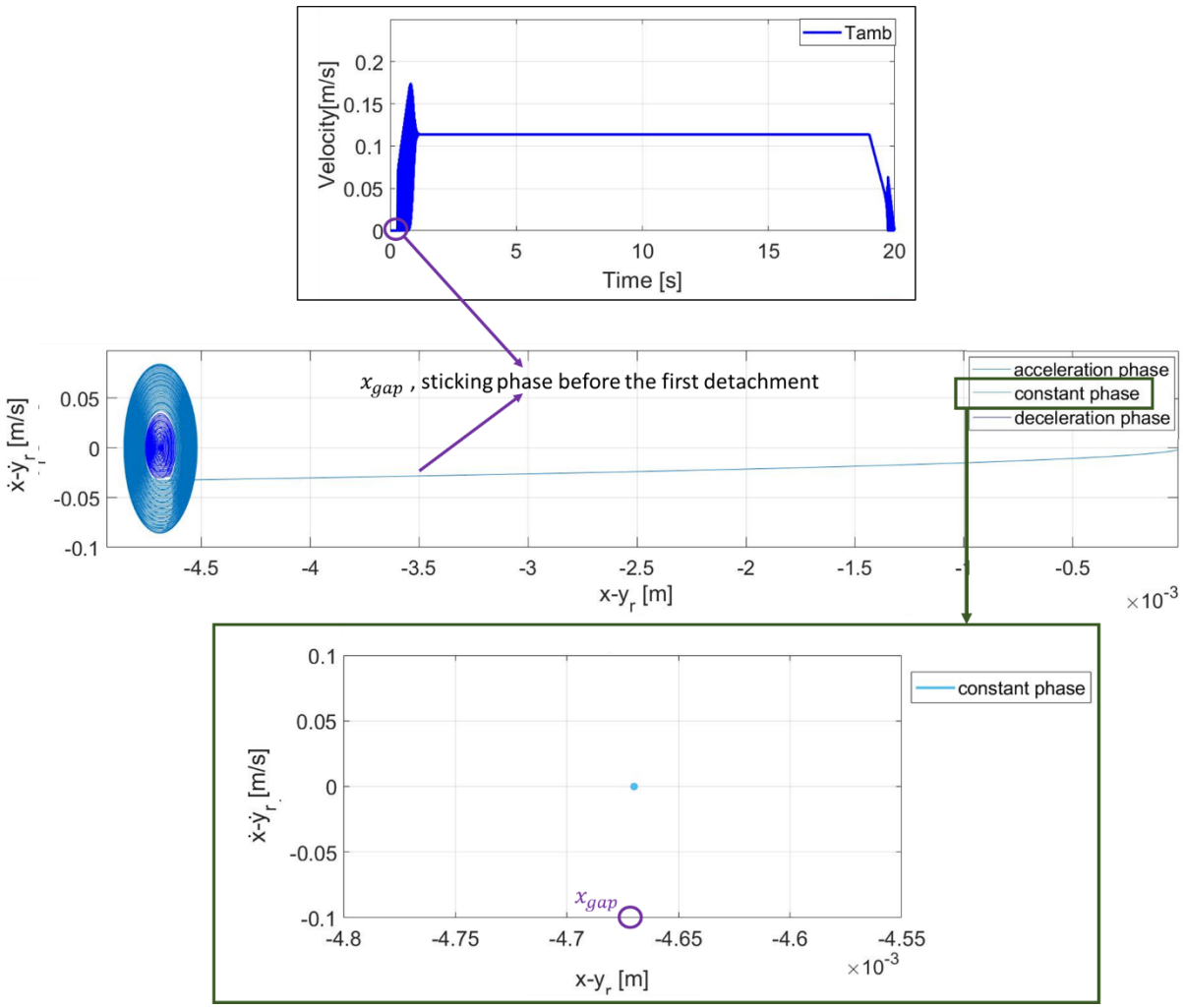

Figure 57: Phase-plane diagram of the dynamic system response at ambient temperature.

On the contrary, when performing the same numerical simulation by introducing the high temperature frictional behavior, but maintaining the same operating conditions, it is possible observe a clear occurrence of the stick- slip instability (Figure 58).
The contact status shift periodically between sticking and sliding. The speed (Figure 58- A) oscillates between zero, during the stick phases, and a maximum value, due to the system oscillation. The spring displacement is represented by the classic jerking motion, with a step-wise curve (Figure 58- B).The normal force oscillates around the equilibrium value, due to the periodic oscillation of the spring elongation during the instability (Figure 58- D). Consequently, the tangential force follows the normal load oscillation during the sliding phases (Figure 58- C), while it increases during the sticking phases, due to the imposed displacement by the engine, until shifting again in sliding.

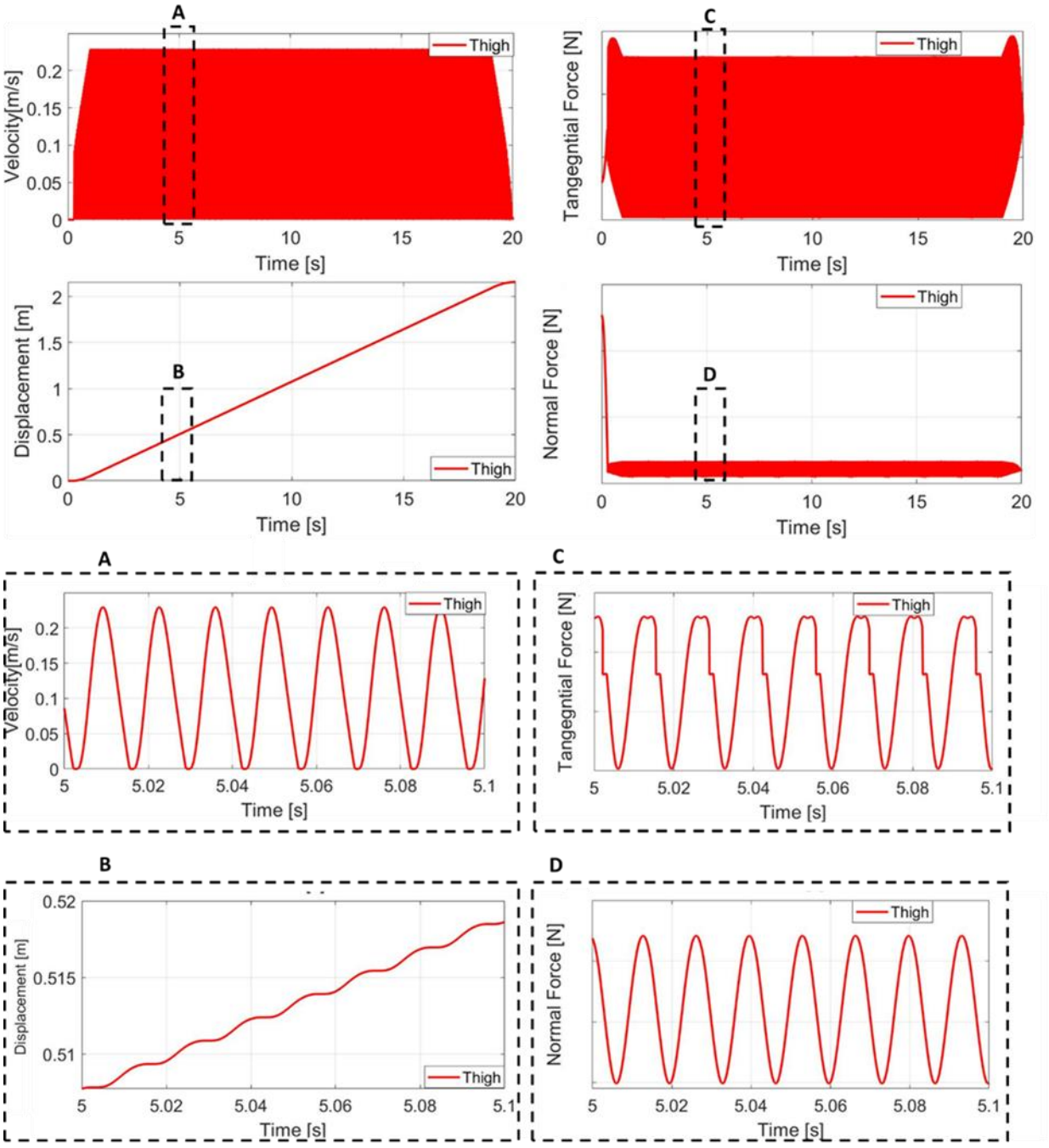

Figure 58: Numerical results of the simulation of the tubular electric actuator at high temperature (80°) condition.

As shown in Figure 58, it is possible to observe the occurrence of the stick-slip contact instability within the whole simulation time, i.e. within the whole range of imposed velocity, due to the local frictional behavior at the greased contact, measured at high temperature.

Focusing the attention on the phase-plane plot of the results obtained at high temperature (Figure 59), again, the velocity $(\dot{x} - \dot{y}_r)$ is plotted as a function of the displacement $(x - y_r)$. Analyzing the phase at constant imposed velocity by the engine (from 1s to 19s), the limit cycle with stick-slip appearance is observed.

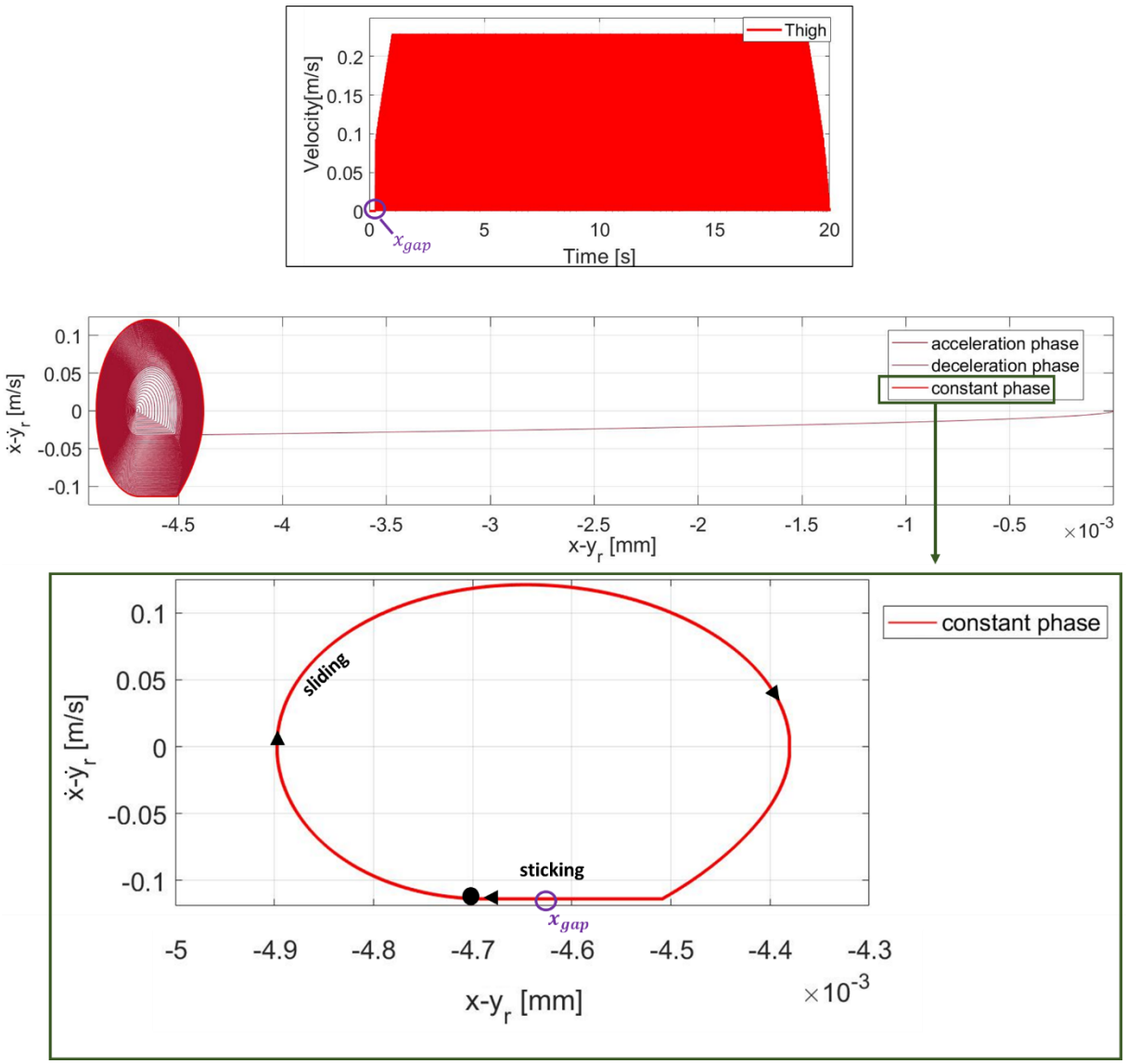

Figure 59: Phase-plane diagram of the dynamic system response at high temperature.

The stick-slip cycle represented in Figure 59 is repeated and superposed for each stick-slip cycle during this phase. The stick phase is represented by a segment parallel to the position axis ($x - y_r$) and lying on the straight line, corresponding to the value of the imposed velocity by the engine. In fact, during the stick phases the spring velocity ($\dot{x}$) is equal to zero and the plotted velocity will be equal to the imposed sliding speed (-$\dot{y}_r$). During the acceleration and deceleration phases, the value of the imposed velocity (horizontal line) translates then along the Y axis of the plot.
On the contrary, each sliding phase is represented by an elliptical sector (harmonic oscillation). Starting from the stick phase, with the change from static to dynamic phase, the elastic energy cumulated during the sticking phase is released and the sliding occurs [49].
In the presented reference case of the reference configuration, the developed numerical model predicts a stick-slip appearance for the higher

temperature condition, while the simulation at ambient temperature shows a stable response.

4.3.2. Numerical VS Experimental results

The results obtained by the numerical simulations (Figure 58) are here compared with the ones obtained through the experimental tests on the entire actuator, previously discussed in Chapter II-Section II.

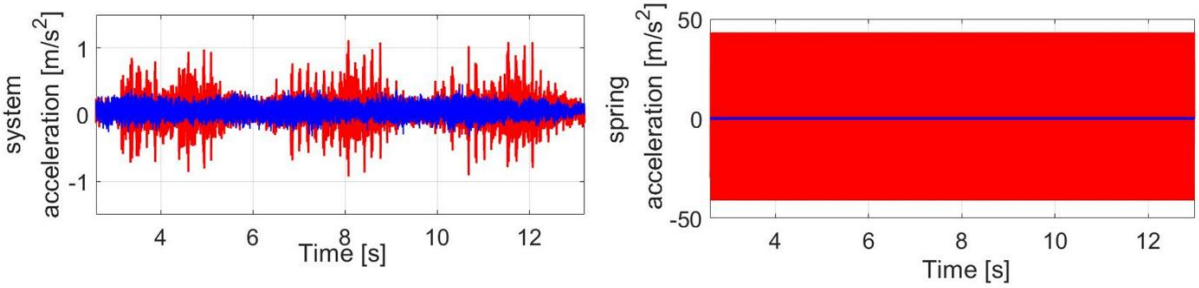

Figure 60: Comparison between the tests performed on the entire tubular actuator (left side) and the results of the numerical simulations (right side) both at ambient temperature (blue curves) and high temperature (red curves).

Analyzing Figure 60, the experimental system response of the entire actuator is reported on the left side, while on the right side the results obtained through the numerical simulations are reported, at both ambient (25°C) and high temperature (80°C). The results of the lumped model show a strong correlation with the dynamic response of the actuator, reproducing the difference observed at ambient and high temperature conditions.
The effect of the different frictional response of the greased contact, with respect to the temperature, (which is the only parameter varied in the simulations) leads to the appearance of stick-slip oscillations of the system at high temperature conditions, both from an experimental and numerical point of view. The increase in the friction-velocity slope (difference between static and dynamic friction coefficients) recovered experimentally on the greased contact, and implemented into the lumped model, is thus a key point to understand the appearance of the frictional stick-slip instability.

4.4. Parametrical analysis for identification of the key parameters

Aiming to understand which are the most influent parameters in the stick-slip appearance, a parametrical study on both the mechanical design parameter and the different tested frictional configurations (see Chapter III Section 3.4.) has been performed.
In order to compare the propensity of the system to get unstable, the critical velocity is here considered.
Figure 61 shows the typical trend of the system response when the imposed velocity start from zero and increase up to the maximum value. The instability will occur within a range of velocity, from zero up to a critical value (v_c).

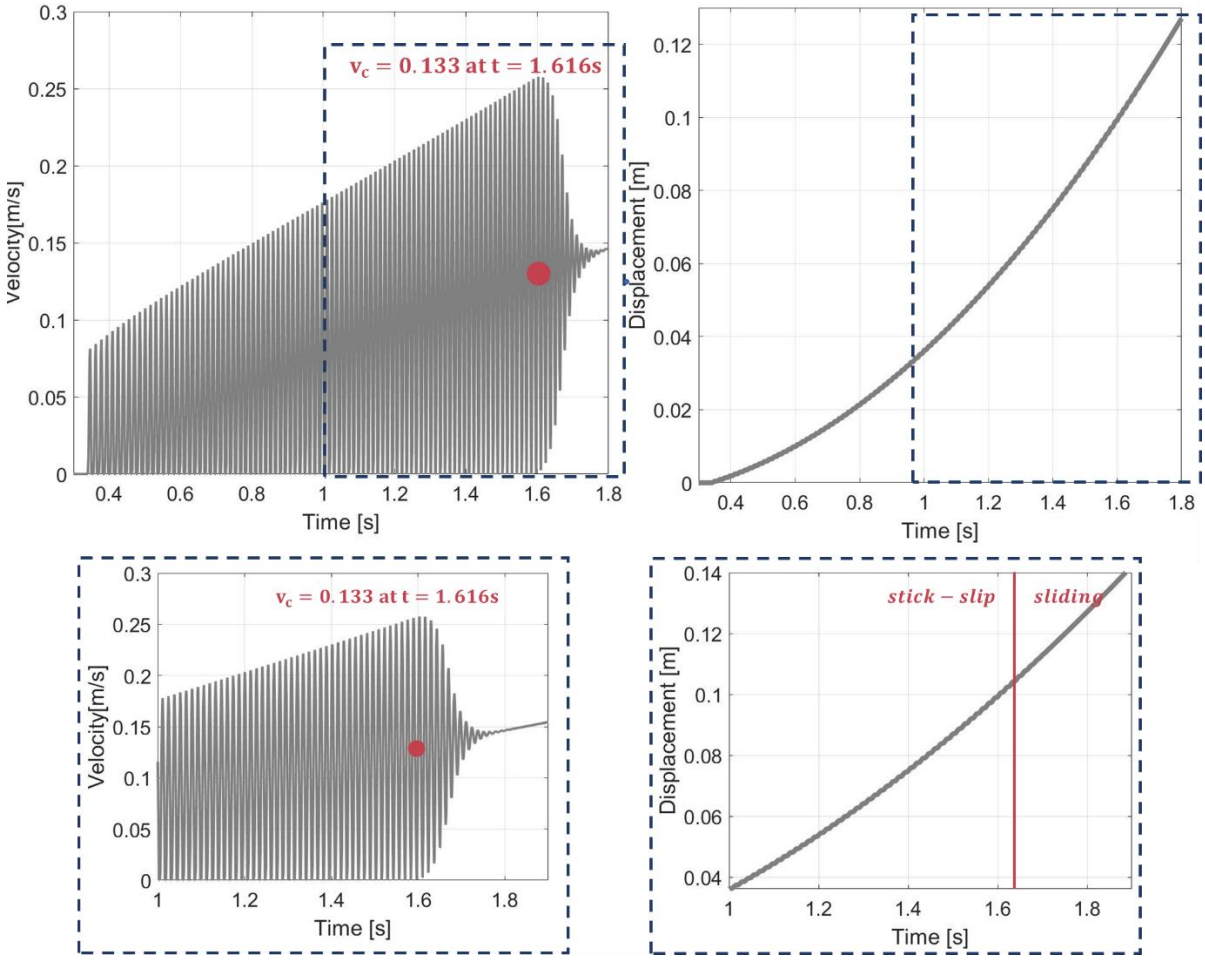

Figure 61: Definition of the critical velocity (v_c), as the numerical value for which the system switches from a stick-slip motion to the sliding.

The critical velocity (v_c) is thus defined as the velocity at which the system passes from an unstable behavior (stick-slip oscillations) to a stable one. The higher the critical velocity, the more the system is considered to be prone to the stick-slip phenomenon. This parameter is often used into the literature as an index of the propensity of the system to present stick-slip instability [125, 126]. In agreement with previous works [127, 128], the critical velocity, from stick-slip to the sliding condition and vice-versa, is higher in the acceleration phase with respect to the deceleration phase. To investigate and compare the propensity of each configuration to the stick-slip phenomenon, the critical velocity in the acceleration phase has been calculated and reported in the following for the different simulated configurations.

First, a parametrical analysis ranges the main mechanical properties of the system (stiffness and damping). Then, the friction curves obtained in Chapter III have been introduced into the model for comparing the different design configurations. Finally, a focus is placed on the main features of the measured frictional trends.

4.4.1. Influence of the mechanical parameters: stiffness K and damping C

In order to evaluate the propensity of the system to the stick-slip, as a function of the mechanical parameters of the brake system, the values of *K* and *C* have been varied by an order of magnitude, higher and lower, from the reference configuration, keeping the other conditions constant. For both the parameters, the ambient and high temperature conditions have been simulated and the obtained numerical results have been evaluated in terms of critical velocity.
Starting from the stiffness value (*K*), simulations have been then performed imposing *K* equal to 20, 200 and 2000 N/m, maintaining *C* equal to 1.

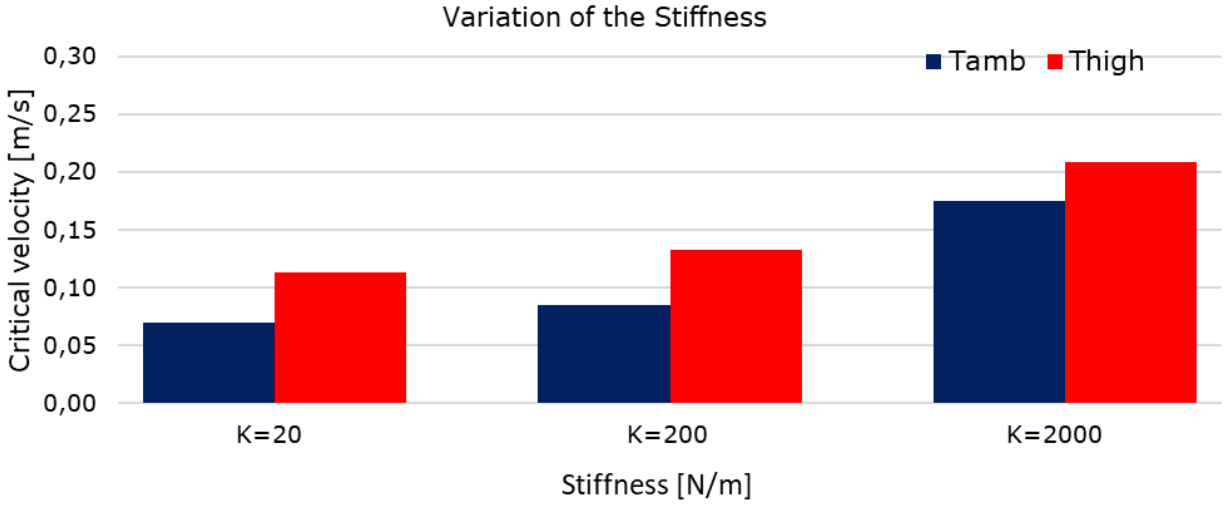

Figure 62: Stick-slip propensity histogram, in terms of critical velocity, as a function of the spring stiffness variation, at both ambient temperature (blue) and high temperature (red).

As shown in Figure 62, the higher the stiffness value, the higher the stick-slip propensity, both at ambient and high temperature.
On the contrary, other works [129, 130] dealing whit stick-skip show that as the system stiffness increases, the magnitude of the stick-slip decrease. The increase of the stick-slip propensity as the stiffness increase, obtained in the presented numerical results, is probably due to the strong link between the stiffness and the normal contact force variation. In the model of the spring-brake system, as the torsional spring expands, the contact force increase. Consequently, the variation of the spring stiffness in the numerical affect as well the normal and tangential force oscillation at the interface.

Then, aiming to evaluate the influence of the damping value (*C*), tests have been performed imposing *C* equal to 0.1, 1 and 10, maintaining *K* equal to 200 N/m (Figure 63).

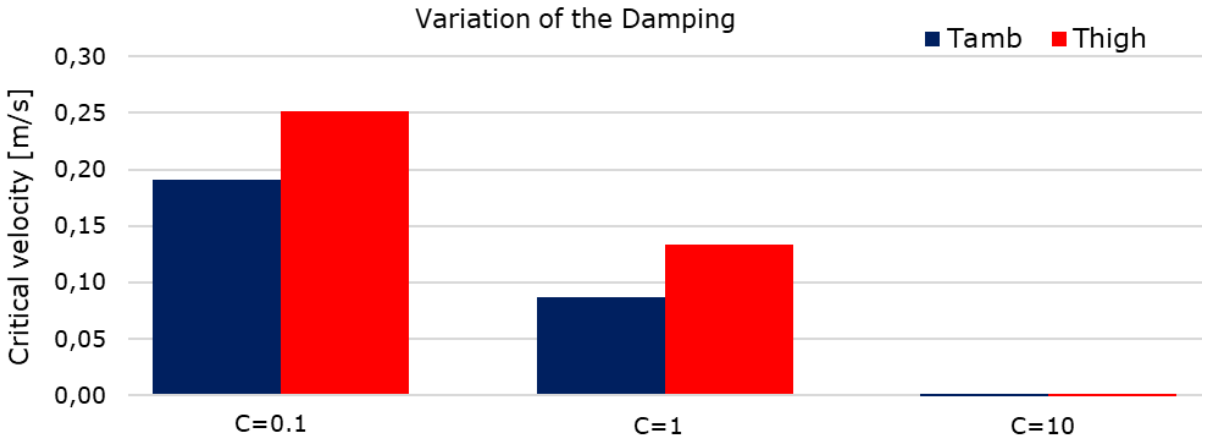

Figure 63: Stick-slip propensity histogram, in terms of critical velocity, as a function of the damping variation at both ambient temperature (blue) and high temperature (red).

As underlined in Figure 63, the higher the damping value, the lower the stick-slip propensity.
As expected, an increase of the damping, which has a stabilizing effect, is much more effective than a variation in the stiffness.
The results agree whit previous works [131, 132].
It should be noticed that the results seem as well to exclude a possible solution of the stick-slip occurrence by varying the system stiffness. In fact, while the decrease of the stiffness of an order of magnitude would be difficult to obtain technically, the decrease in the instability propensity is not so efficient.

4.4.2. Influence of the design configurations: drum material, roughness and solid lubricant

In the Chapter III, Section 3.4., the local frictional response of the reference configuration has been discussed and compared to several configurations, aiming to investigate the influence of different surface coatings (DLC, CW, NiP and without solid lubricants), different drum surface materials and surface finishing (different honing angle), both at ambient and high temperature.
The same configurations are here compared, introducing the experimental frictional curves (measured at 5N) as an input of the numerical model, to qualitatively compare the stick-slip propensity of each configuration. Each tested configuration differs from the standard condition only by the frictional law introduced at the contact. The operating conditions are unvaried with respect to the previously discussed reference configuration. All the configurations are named with the parameter change that characterizes the specific configuration, with respect to the reference one.

- **Drum surface finishing and material**

Considering the drum honing angle and material, Figure 64 shows the critical velocities obtained by the numerical simulations, compared to the reference configuration.

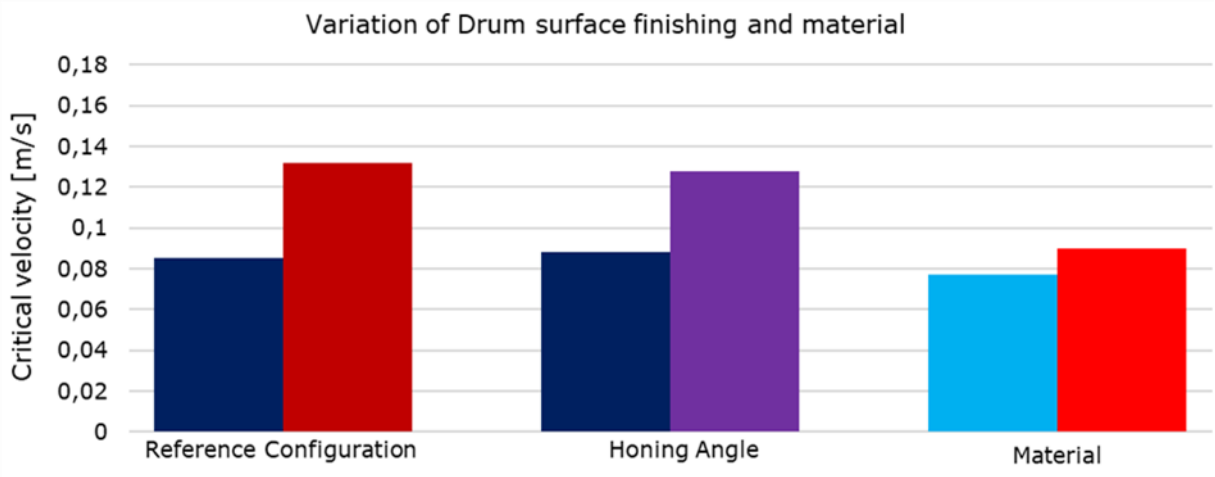

Figure 64: Influence of the drum surface finishing and material on the critical velocity (stick-slip propensity) of the electric tubular actuator.

Focusing the attention on the honing angle variation (i.e. drum 2) and comparing the results with the reference configuration, the increase of the honing angle did not produce significant changes on the propensity of the system to stick-slip. This is coherent with the measured frictional trends, where same trends and similar values of the difference between static and dynamic friction have been observed (see Chapter III Section 3.3). Moreover, the same results here obtained by numerical simulations, about the stick-slip propensity, are in agreement with the experimental tests conducted by on the entire brake system [133].
Considering the different tested material (i.e. numerical results of the drum 3 configuration), the critical velocity is remarkable lower compared to the reference configuration. This behaviour is mainly due to the lower difference between static and dynamic friction coefficient ($\mu_s - \mu_d$), as previously shown in Figure 35.
The lower roughness and the surface porosity of the drum 3 allows for maintaining the lubricant at the interface and decrease the adhesion between the asperities at the static contact. This leads to a decrease of the static friction coefficient, with respect to the dynamic one, and then to a lower difference between static and dynamic CoFs (see Chapter III Section 3.4.2). Thus, the change of the drum material positively affects the dynamic response of the system.
The drum 3 drum seems to establish favorable frictional and dynamical conditions, with respect to the reference configuration.

- **Spring coatings and solid lubrication**

Aiming to perform the analysis of how the spring surface coating (solid lubricant) affects the frictional response at the contact, four different spring coatings have been tested thought the experimental tests on the TriboAir test-bench: reference configuration, CW, NiP and absence of solid lubricant (coating). .
Introducing the retrieved frictional behaviours (Chapter III, Section 3.4.3), as an input of the numerical model, maintaining the operating conditions unvaried, it is possible to analyse the stick-slip propensity of each design

configuration and compare the results with the reference configuration (Figure 65).

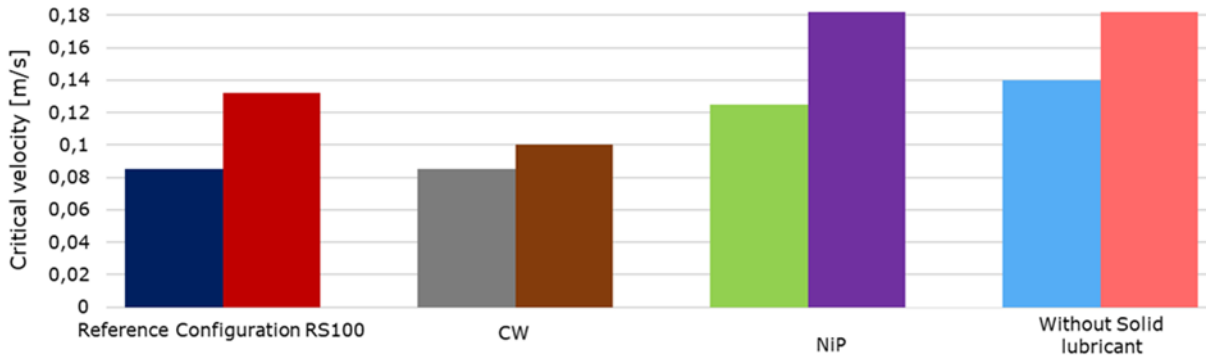

Figure 65: Influence of the solid lubricant used as spring surface coating on the critical velocity (stick-slip propensity) of the electric tubular actuator.

As shown by the histogram, the CW coating provides a more stable behavior, compared to the reference configuration, due to a more stable frictional behavior (as shown in Figure 36) and lower values of the μ_s-μ_d difference (as shown in Figure 37). The CW is the more favorable condition with respect to the stick-slip propensity. On the contrary, the NiP coating and the test performed without the presence of solid lubricants showed a dynamic response that is largely affected by the presence of stick-slip, with higher critical velocity values, compared to the reference configuration, both at ambient and high temperature conditions. This unfavorable dynamic behavior is due to the frictional trends at the lubricated contact. Indeed, as exhaustively discussed in Section 4.3.3., both the configurations are characterized by a high difference between static and dynamic CoF.
The same parameters have been tested on entire brake systems, in a Design of Experiment (DOE) plan [133]. The DOE has been based on testing 7 factors, including the same four solid lubrications presented here, and 36 configurations. All the configurations have been tested using the same protocol. The tests were based on imposing a rotation to the brake system, in both directions (i.e. moving up the load and moving down the load) for a period of 60 seconds and repeating the tests three times. One single operator evaluated qualitatively the noise produced by the brake system, assigning a color (i.e. green, yellow, orange and red) to each test. An automatic program classified each test according to the selected color, with a predefined noise level characterized by a number that goes from 0 to 50 [133].
The following Figure [133] shows the results obtained testing the different solid lubricants.

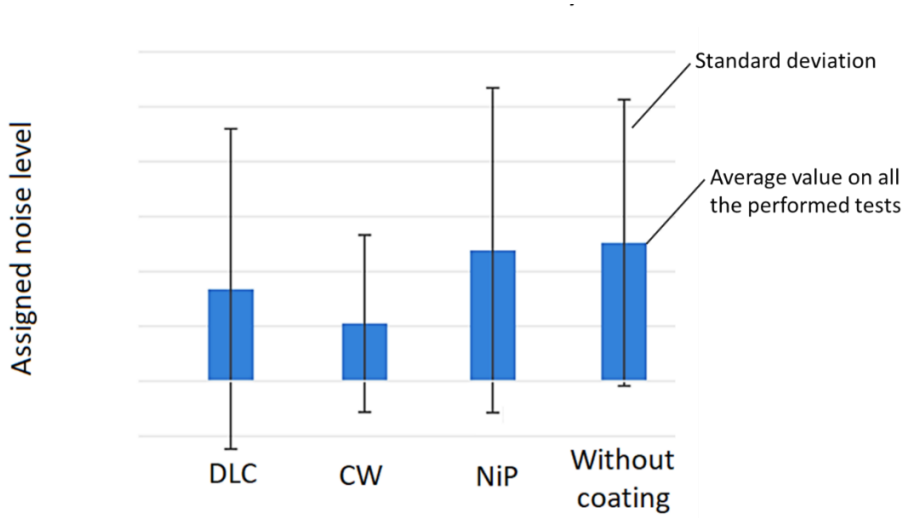

Figure 66: Average value and standard deviation of the assigned noise level on all the performed tests on the brake system.

The information extracted from the DOE highlights the trend of propensity of the instability of the brake system, as a function of the used coating. Because of the qualitative sensorial protocol, the standard deviations have high values for all the analysed configurations. However, it is clear that the CW configuration, with respect to the other configurations, presents a better behaviour in terms of noise emission. On the contrary, the NiP configuration and the tests performed without solid lubricants show the highest stick-slip appearance. Then, as shown in Figure 66, the results [133] are well in agreement with the ones obtained by the numerical model (Figure 65). The CW surface coating seems to be the better solution in terms of stick-slip appearance.

4.4.3. Influence of the frictional trend main features

As highlighted in the previous sections, the influence of the difference between static and dynamic friction coefficients seems to be a key point in the stick-slip appearance, together with the overall frictional trend of the greased contact. Then, aiming to better understand the role of the local frictional response on the dynamic system response, a parametrical analysis has been performed by varying the key features of the frictional trends, within both the low-velocity range and the high-velocity range, observed experimentally. Considering then the reference configuration, in the case of stick-slip appearance (i.e. high temperature condition), the dynamic response of the system has been simulated and evaluated as a function of the frictional trend characteristics.

- **High-speed range**

Focusing the attention on the high-speed range, from 1mm/s to 20mm/s, numerical simulations have been performed starting from the reference configuration (red curve in Figure 67) and modifying the trend, either increasing (green curve in Figure 67) and decreasing (light-blue in Figure 67) the dynamic CoF in the high-speed range. A further positive or negative

friction-velocity slope has been added, up to reach the respective higher or lower friction value.
Figure 67 reports as well the values of the critical velocity, obtained through the numerical simulations introducing the three frictional trends.

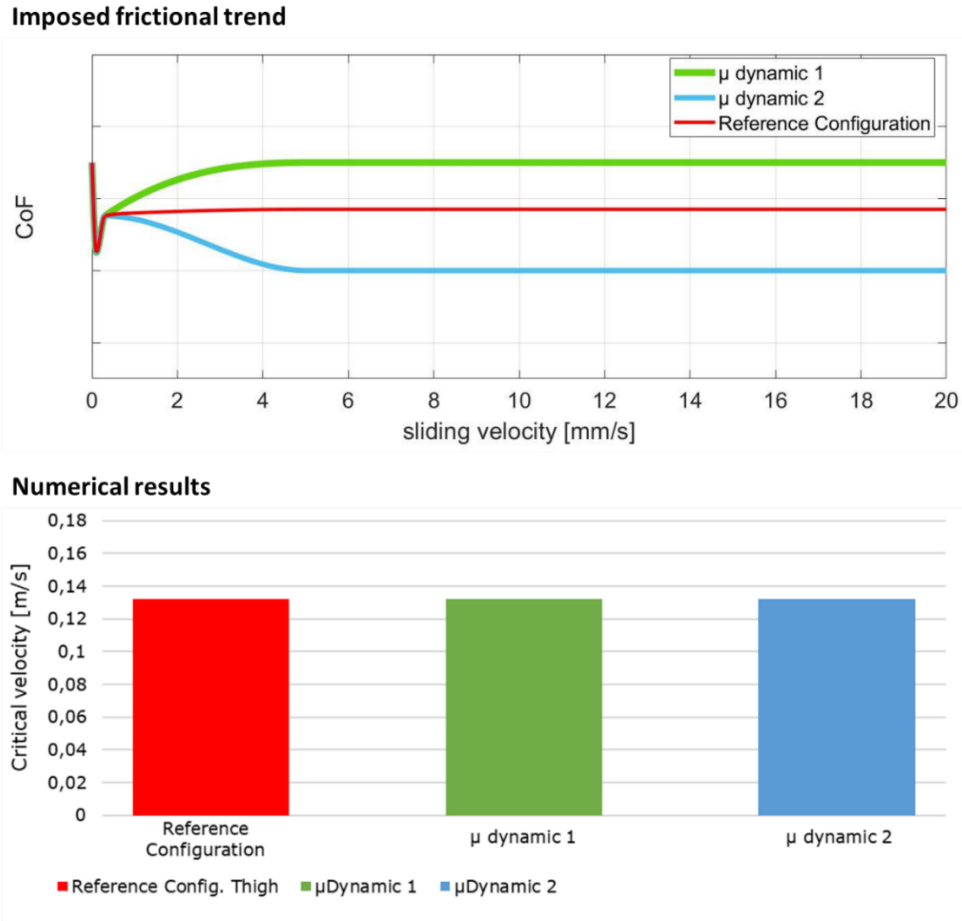

Figure 67: Upper figure: frictional trends imposed as an input in the numerical lumped model, aiming to analyse the dynamic response of the system as a function of the dynamic CoF in the high-speed range. Lower figure: obtained critical velocities.

The obtained critical velocities are extremely similar. Thus, no significant effect on the propensity to the instability can be appreciated when varying the frictional trend of the greased contact within the high-speed region. Even a further negative friction-velocity slope in such range does not affect the stability of the system.

- **Low-velocity range**

Focusing the attention on the low-speed range (from 0 to 1mm/s), two main features have been investigated: the influence of the difference between the static and the lowest dynamic friction coefficient, where the lowest dynamic coefficient is the one retrieved at 0.1mm/s, and the friction-velocity slope. Starting from the difference between static and dynamic friction coefficients (μ_S-μ_D), three cases have been tested and compared to the reference configuration.
Figure 68 reports the overall trends.

In all the reported tested cases, the only change is the μ_S-μ_D value, maintaining the initial friction-velocity slope unvaried. The imposed frictional trends are reported in Figure 68.

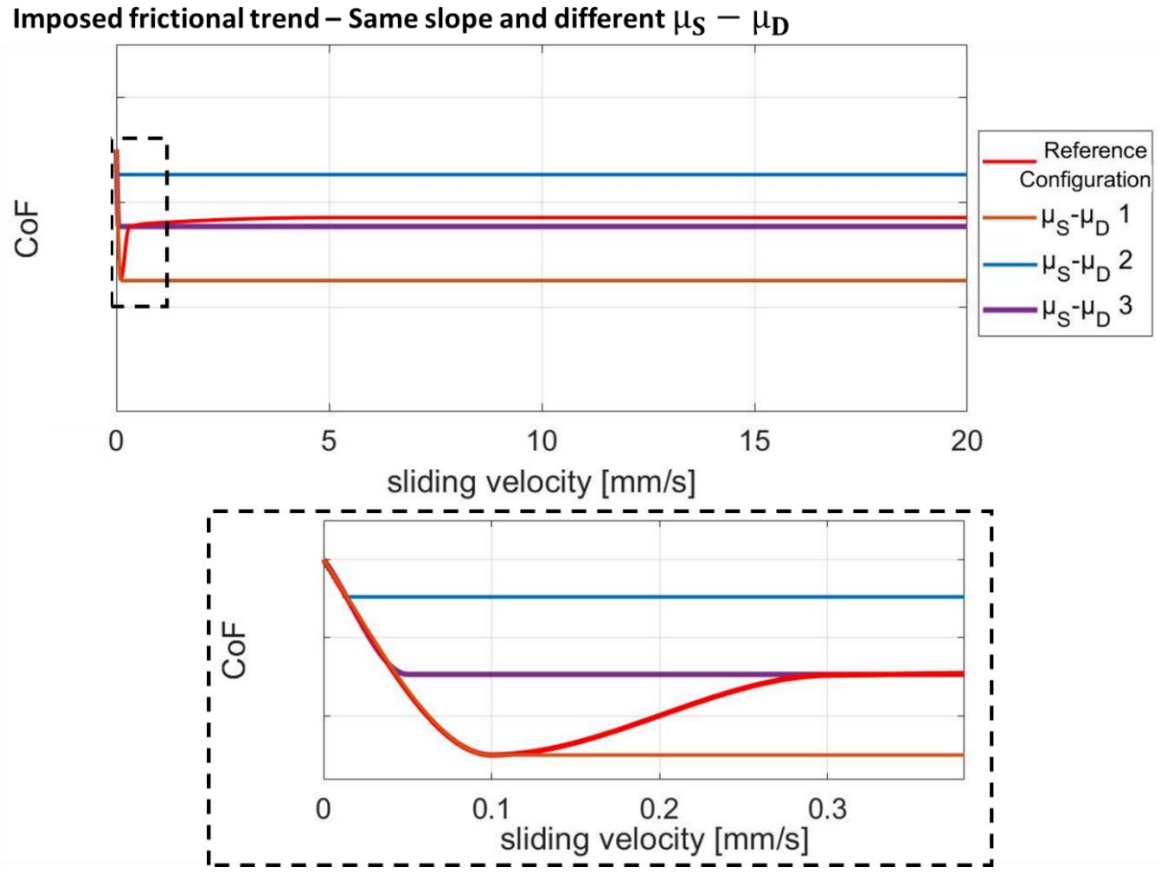

Figure 68: Frictional trends imposed as an input in the numerical model, aiming to analyse the dynamic response of the system as a function of the difference between static and dynamic CoF.

The first two configurations (Reference configuration in red and μ_S-μ_D 1 configuration in orange) present the same value of the μ_S-μ_D but a different dynamic friction coefficient at high velocity. On the contrary, the other two configurations have a difference in the μ_S-μ_D and the same slope, compared to the reference configuration.

The results of the numerical simulations, as critical velocities, are presented in Figure 69.

In the first two cases (red and orange bar), only a slight decrease of the critical velocity, and so of the stick-slip propensity of the system, can be observed, coherently with the previous results. This difference is mainly due to the change in the frictional trend in the speed range that goes from 0.1mm/s to 1mm/s.

Focusing the attention on the other two cases (violet and blue bar), a considerable decrease of the sticks-slip instability is observed. The critical velocity shows an increasing monotonic trend with the difference in static and dynamic friction (Figure 68-bottom).

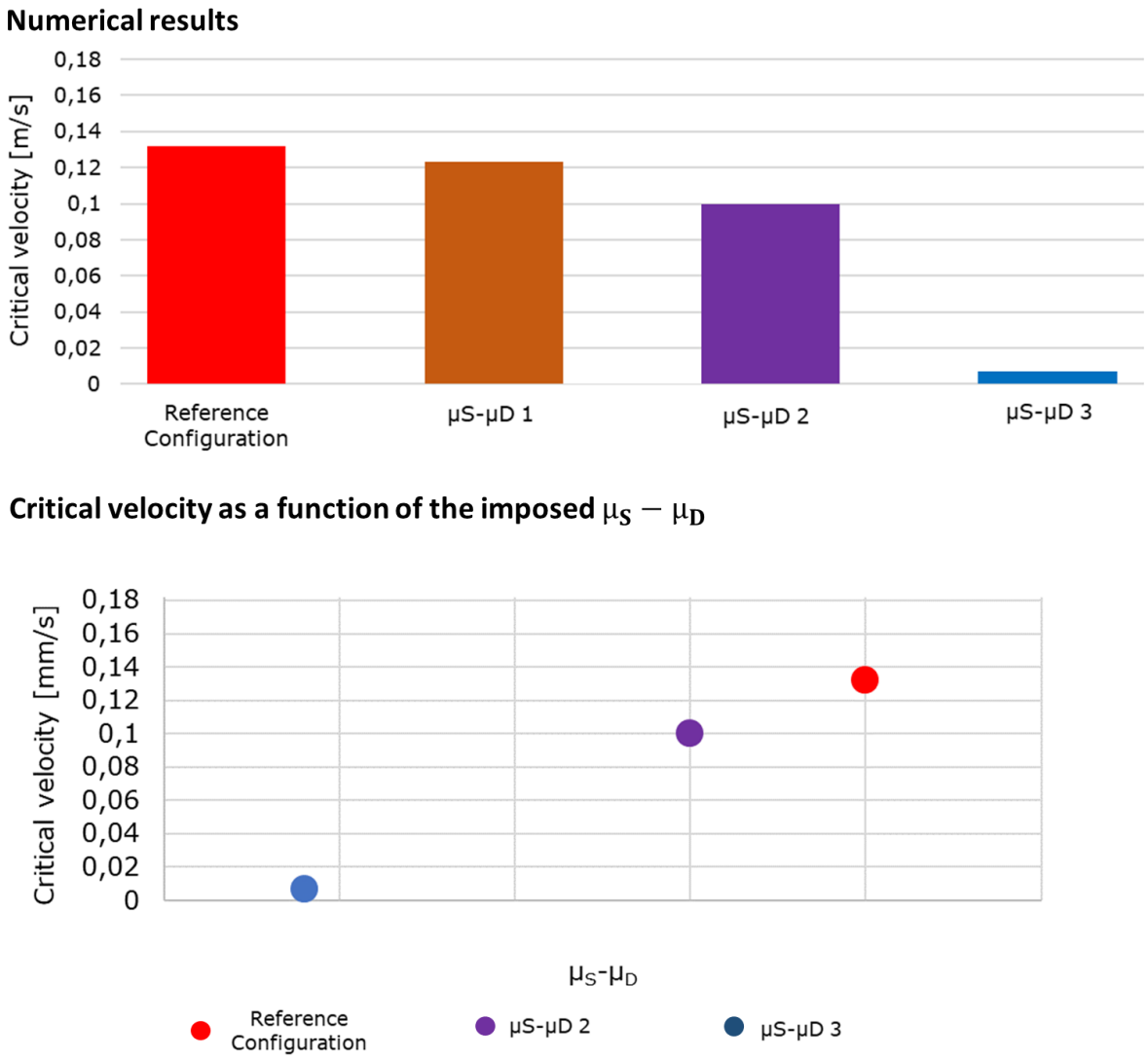

Figure 69: Numerical results of the lumped model introducing as an input the frictional curves with different values of the difference between static and dynamic CoF.

Then, focusing the attention on the initial friction-velocity slope, the frictional trends shown in Figure 70 have been investigated and compared. Three different slopes have been taken into account, maintaining the same difference between static and dynamic CoF.

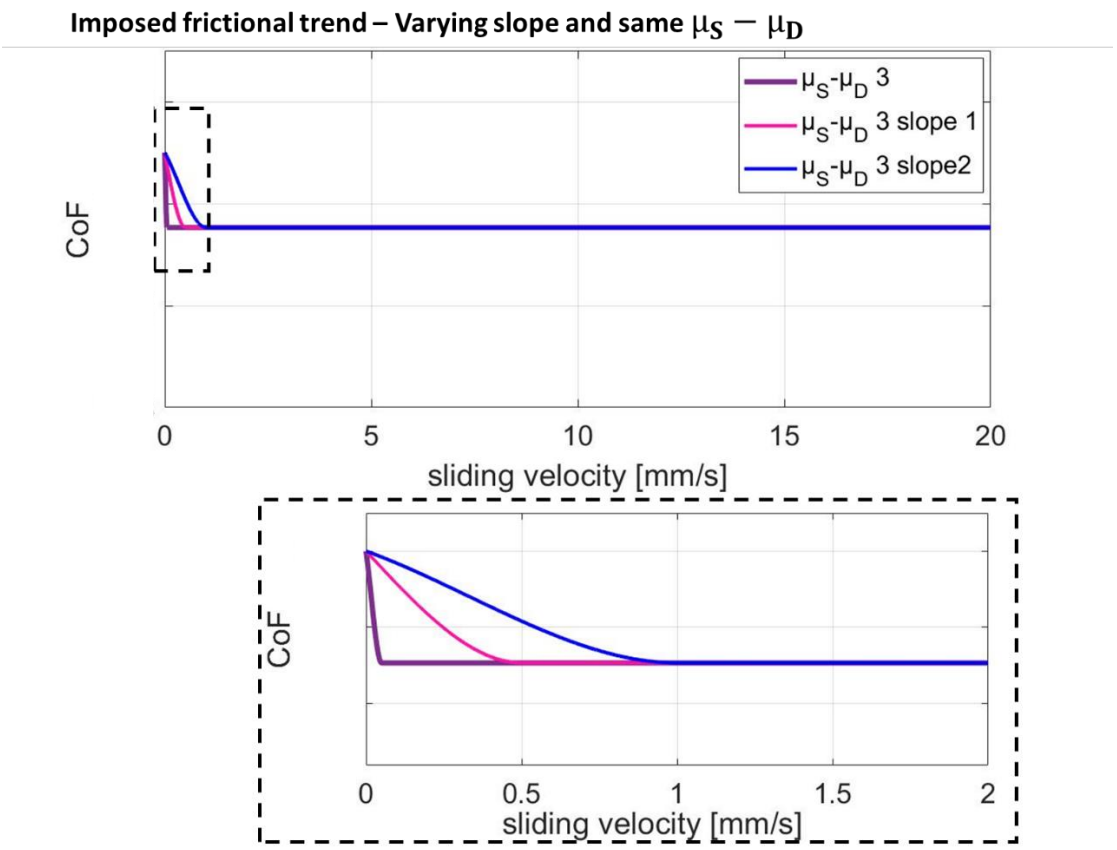

Figure 70: Frictional trends imposed as an input in the numerical lumped model, aiming to analyse the dynamic response of the system as a function of the friction-velocity slope in the low-velocity range.

The obtained numerical results are shown in Figure 71.
The dynamic response of the system is strongly affected by the slope characteristic of the frictional trend of the greased contact. A lower absolute value of the slope (sweeter slope) brings to the absence of the stick-slip instability. In fact, while the reference configuration is unstable, both the lower tested slopes give a stable response. Moreover, when comparing the trends of the system response for the two different tested slopes, it is evident as the initial vibrations (excited by the first detachment) are damped faster when the slope is lower. This highlights the overall effect of the negative friction-velocity slope, which contrasts (reduces) the dissipative effect of the damping, by feeding energy in the system oscillation.

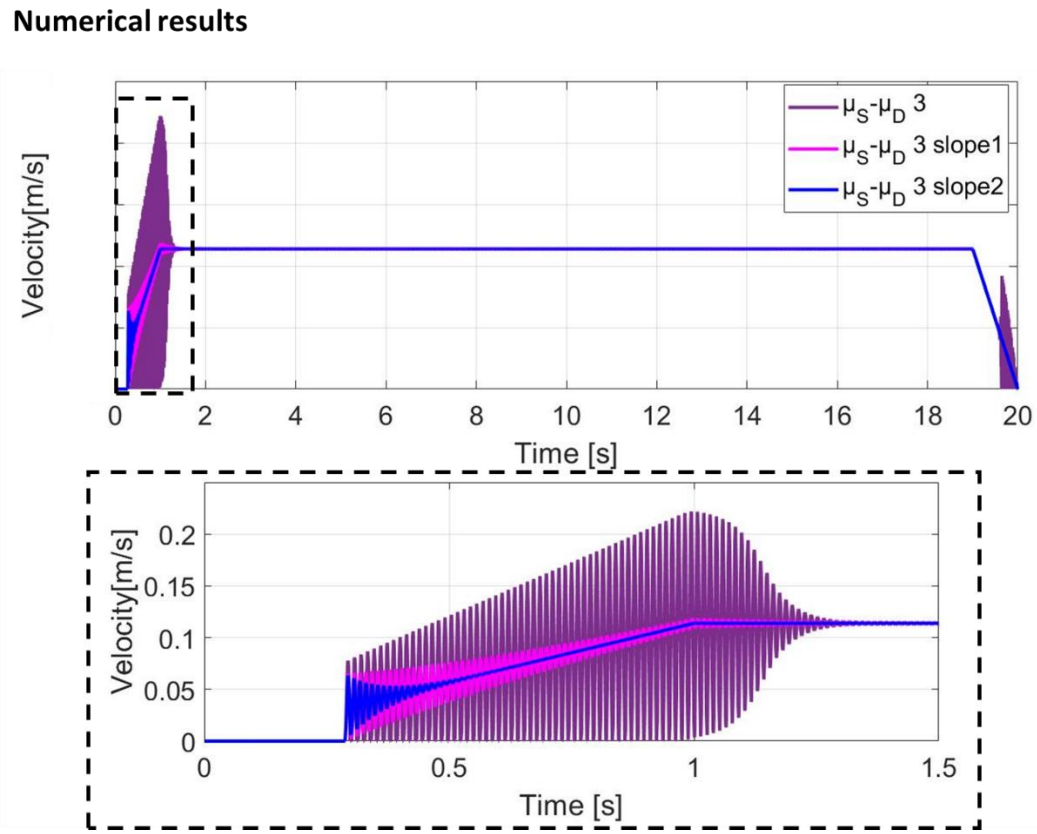

Figure 71: Numerical results of the lumped model introducing as an input the frictional curves with different friction-velocity slope.

From these results, it is evident how the frictional trend at the low-velocity range is the one affecting the occurrence of the stick-slip instability, and thus the focus should be kept on the response of the greased contact within this range.

4.5. Concluding remarks

Understanding the conditions for which the system is more predisposed to the stick-slip phenomenon may allow for preventing the appearance of such instabilities. Moreover, considering the applicative nature of the investigated system, it has been considered useful to test different applicative solutions, in order to both provide information on the operative design solutions and retrieve information necessary for the understanding of the dynamic response of the system.

A numerical lumped model of the actuator has been then developed and alimented by the data from both the real mechanical system and the experimental frictional tests. All the mechanical and functional parameter of the tubular actuator have been taken into consideration and introduced into the numerical model. The equation of motion has been then solved by a Simulink code and the outputs of the model have been analyzed and compared with respect to the reference configuration.

The model has been validated simulating the dynamic response of the system when introducing the frictional trend of the reference configuration,

obtained through the experimental tests, both at ambient and high temperatures. When introducing the two different frictional behaviours, the results of the numerical simulations show stick-slip at higher temperature, as observed experimentally on the real system. These results allow for asserting that the friction-velocity response of the greased contact is a key parameter in destabilizing the system, bringing to the stick-slip instability.
Once validated the model, parametrical simulations have been addressed for identifying the role of the main parameters of the brake system on the stick-slip occurrence.
The influence of different design parameters has been first investigated: different surface coatings, different drum surface materials and surface finishing, both at ambient and high temperature.
Then, the different features of the frictional trend of the greased contact have been investigated, focusing at both the high and low-velocity ranges.
The main outcomes from the parametrical campaign can be summarized as follows:

- Increasing the stiffness or reducing the damping value of the brake system, the stick-slip propensity increase. However, a substantial change of C and/or K is not achievable in the design of the brake system, due to the wide range of other functional outputs (e.g. braking torque), which depends from the stiffness and damping of the brake system. As an example, a change in the stiffness value of the spring imply drastic changes in the engine design and reduction stages.
- Increasing the honing angle of the drum and comparing the results with the reference configuration, did not produce significant changes on the dynamic response of the system. On the contrary, the material change, passing from the reference drum to the drum number 3, produces a significant reduction of the critical velocity value. This behaviour is due to the lower difference between static and dynamic friction coefficient. The drum 3 seems then to establish favorable frictional and dynamical conditions, with respect to the reference configuration.
- The parametrical analysis performed on the coatings (solid lubricant) showed that the CW is a more favorable condition, with respect to the stick-slip propensity, compared to the DLC solid lubricant (reference configuration). On the contrary, the NiP coating and the test performed without the presence of solid lubricants showed a dynamic response that is largely affected by the presence of stick-slip. The favorable dynamic behavior of the CW solid lubricant, compared to the others, is due to a more stable frictional behavior and lower values of the difference μ_s-μ_d. The same results have been obtained on an experimental DOE campaign performed on the entire brake system.
- Aiming to understand which are the characteristics of the frictional trend that most affect the stick-slip appearance, a parametrical analysis has been performed varying both the frictional behaviour in the low-velocity range (i.e. the μ_S-μ_D and the slope) and the behaviour in the high-velocity range. The high-speed range does not affect significantly the dynamic response of the system. On contrary, the trend at low-speed range (from

0 to 1mm/s) has been underlined as a key factor. When reducing the difference between the static and the dynamic CoF and/or reducing the slope of the curve, an effective decrease of the stick-slip propensity has been observed.

The different conclusions here reported have led to the necessity of understanding the role of the grease and its different components, with particular attention in the low-velocity range, when boundary and mixed lubrication conditions are expected.
Aiming to highlight the influence of the lubricant components, i.e. thickener, oil and additives, the frictional response has been then investigated by testing different types of lubrication conditions, both with and without Diamond-Like-Carbon (DLC) coating. The performed tests and results are discussed in the following Chapter, aiming to provide information on how the different lubricant components affect the local frictional behavior and, consequently, the occurrence of the stick-slip dynamic instability.

V. Role of lubricant components on the local frictional response

As explained in the previous Chapter, the presence of a lubricant at the interface increases the complexity of the phenomenon, from both a tribological and a dynamical point of view. Both the CoF-velocity slope and the difference between static and dynamic CoFs affect directly the system propensity to the stick-slip instability. The friction-velocity curve, characterized by a negative friction-velocity slope within the boundary and mixed contact regimes, collaborates then in the appearance of contact instabilities, increasing the possibility of the occurrence of the stick-slip phenomenon. In case of grease lubrication, the complex rheology of the grease, function of its different components (the thickener, the additives and the oil), becomes then a key point for the occurrence and evolution of the stick-slip phenomenon, by driving the overall frictional response as a function of the sliding velocity.
Aiming to understand the role played by the different lubricant components (thickener, oil, additives and solid DLC lubricant) the frictional response under low sliding velocity conditions has been here investigated by testing different types of lubrication conditions, corresponding to dry contact, oil lubrication and greased contact (with and without additives), both with and without Diamond-Like-Carbon (DLC) coating. The results are reported for the two different operational temperatures (25°C and 80°C).

5.1. Tested conditions

The experimental campaign has been performed on the same samples reported in Chapter III, Section 3.1., and on the same test bench. Aim of the experimental tests is to provide a better understanding of the role of the different lubricant constituents in determining the frictional response under the different selected boundary conditions (i.e. temperature and imposed normal load) within the low sliding speed range.
Two normal loads have been tested for each velocity, 10 N and 20 N, being the load range considered the most representative of the application. As well, the tests have been then performed at both ambient (25 °C) and high (80 °C) temperature. Compared to the previous cases (see Chapter III and IV), being interested in defining the contact behaviour in the low-speed range, tests were performed to obtain a better resolution (higher number of points) within the sliding velocity range that goes from 0 to 1mm/s.
The different tested lubrication conditions have been investigated to decouple, as well, the influence of the DLC coating from the influence of the grease components. The tested lubrication conditions are summarized in Table 7.

Test	Lubrication condition	Lubricant Composition	Quantity
Reference Configuration	LiCPAO & DLC	Lithium Complex, PAO and additives	5 ml introduced by a pipette on the contact zone & DLC coating on the upper specimen
LiCPAO without solid lubricant	LiCPAO	Lithium Complex, PAO and additives	5 ml introduced by a pipette on the contact zone
Dry without solid lubricant	-	-	-
Dry with DLC	DLC coating	-	DLC coating on the upper specimen
Base Oil	PAO without Additives & DLC coating	PAO	fully flooded condition & DLC coating on the upper specimen
Base Oil plus additives	PAO with additives & DLC coating	PAO plus additives	fully flooded condition & DLC coating on the upper specimen

Table 7: Tested conditions for the analysis of the influence of the different lubricant components on the frictional response.

As a preliminary analysis, the grease rheological features have been measured at both temperatures. Then, the reference configuration has been tested again, with a higher test point resolution, when both solid (DLC) and grease lubrications contribute to the overall measured friction coefficient (Reference configuration).
Then, the same contact boundary conditions have been tested on the grease lubricated contact, excluding the DLC solid lubricant. The comparison between the frictional responses, with and without DLC, is discussed for both dry and greased contact.
Afterwards, the base oil alone, with and without additives, has been tested. The different obtained curves have been discussed, aiming understand the influence of the different components on the overall frictional behaviour.

5.2. Grease rheological characterization

The grease used for the experimental tests is a commercial synthetic lithium complex grease (LiCPAO). It is based on a synthetic base oil (PAO), while an additive package is added to guarantee low and high temperature

performances, improve the mechanical efficiency and ensure a longer service life.
Rheological measurements have been then performed to characterize the grease, both at ambient (25°C) and high temperature (80°C), using an MCR 502 Anton-Paar rheometer with cone plate configuration.
The cone-plate system has been used to test the grease, with the upper plate diameter equal to 24.991mm. The principle of the performed tests on the grease is shown in Figure 72.

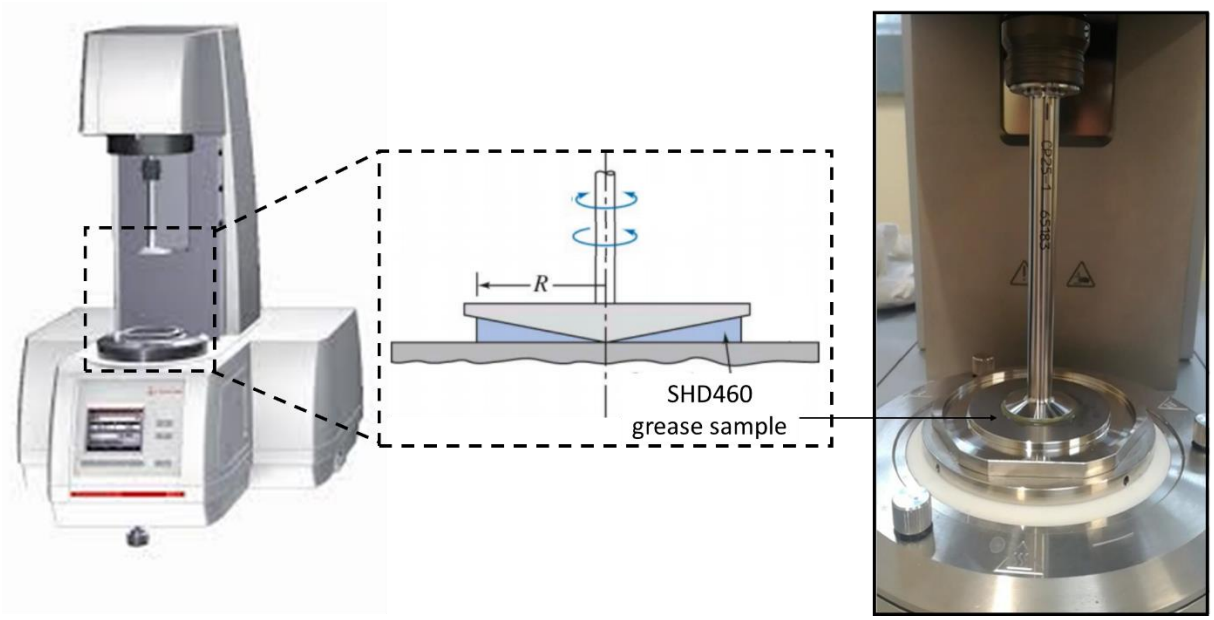

Figure 72: Principle of the experimental tests performed through the rheometer to investigate the rheological characteristics of the LiCPAO grease.

To minimize the initial deviation induced by the placing and loading procedure, the grease samples were first deposited on the bottom plate and the top plate descended at a controlled speed, until the wished measure position was reached, leaving a gap of 0.051mm [134]. Subsequently, the accumulated grease at the plate periphery was carefully removed with a spatula. Once the sample was prepared, following the procedure described above, rheological tests were conducted.
The viscosity has been measured by steady-state flow curve measurements. In addition, oscillatory strain sweep measurements were performed to measure the grease viscoelastic properties, imposing a frequency equal to 1Hz.
Figure 73 shows the obtained results in terms of the viscosity, as a function of the shear rate (image a), and in terms of the grease's viscoelastic properties G’ and G”, as a function of the applied strain (image b), imposing either a temperature equal to 25 degrees (blue dotted curves) and 80 degrees (red dotted curves).

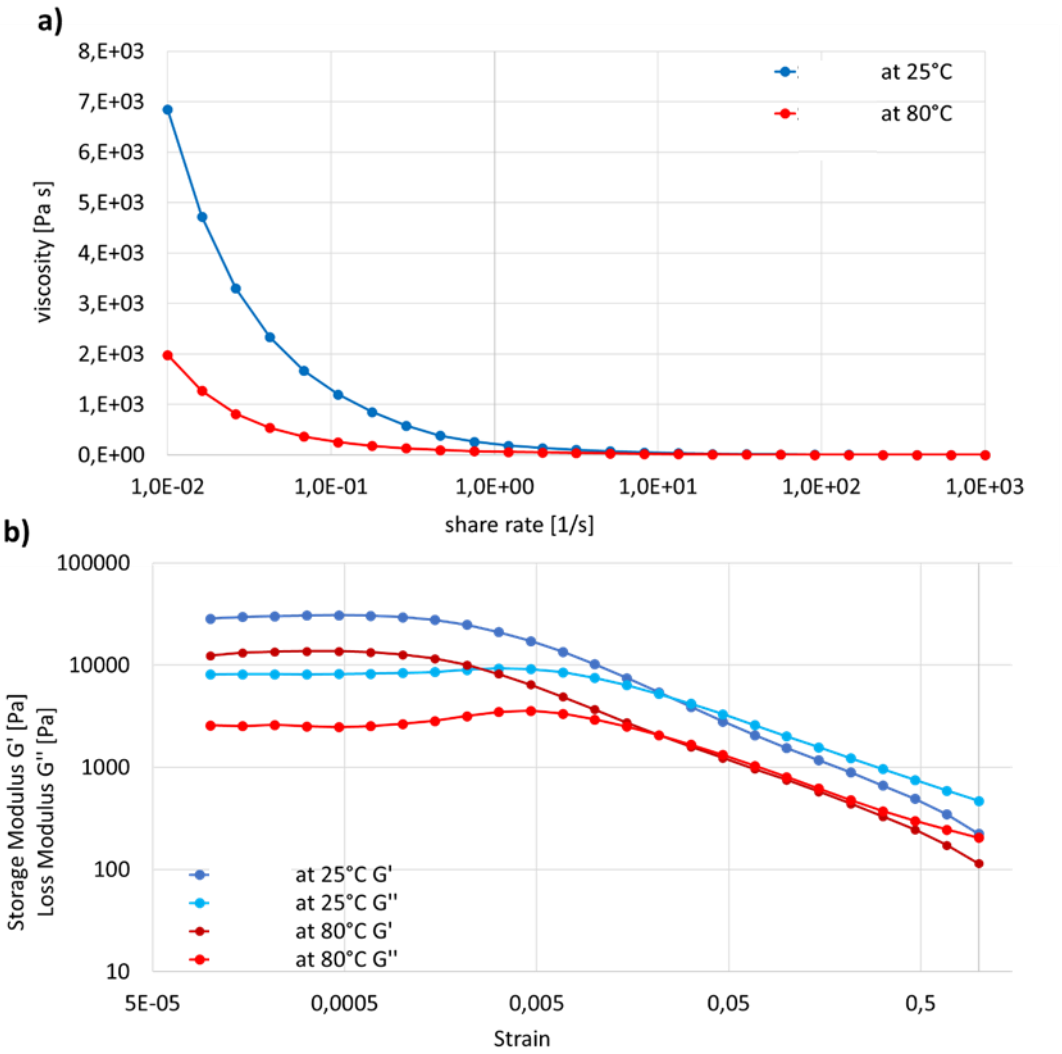

Figure 73: a) Viscosity versus shear rate and b) Storage Modulus G' and Loss Modulus G'' versus strain, measured at the frequency of 1 Hz, both at T=25°C and T=80°C, for the tested grease.

The flow curve (Figure 73-a) shows a high-viscosity region at lowest shear rates, followed by a sudden decrease and a stabilization region, with a consequent strong decrease of the viscosity at room temperature. This behaviour is much less pronounced for the higher temperature and the difference in viscosity between low and high shear rate is markedly lower. At low shear rates, a large difference between viscosities at ambient and high temperatures is observed.

The viscoelastic properties (i.e. the elastic modulus G' and the loss modulus G") were measured by oscillating shear at a frequency of 1 Hz (Figure 73-b). The storage modulus decreases, while the loss modulus stays almost stable, until a crossover point is reached. The crossover point is where G' is equal to G". Beyond this point, G' starts to faster decrease, with respect to G", indicating a structural breakdown within the grease microstructure.

Each test has been repeated three times, changing each time the grease sample with a fresh one. The results showed a variability less than 5%, allowing to confirm the reliability of the recovered results.

5.3. DLC role in the frictional response

The first element that has been considered in the investigated lubrication condition is the presence of DLC coating, which plays the role of solid lubricant. As previously discussed in Chapter 3.4.3., the DLC solid lubricant can affect the frictional response both directly, by modifying the contact rheology, and indirectly, by reacting with the grease components. Then, tests have been performed both with and without DLC coating in both greased and dry conditions.

5.3.1. Greased condition

Figure 74 shows the results of the tests performed on the Steel/Steel specimens (without DLC), under greased lubrication condition, compared to the reference configuration (DLC and LiCPAO grease), applying the same normal loads and temperatures.
Comparing the experimental results obtained in greased conditions (LiCPAO grease), both with DLC coating (Reference Configuration) and without DLC coating (LiCPAO without solid lubricant), the shape of the friction curves, with respect to velocity, does not follow the classic Stribeck-like curve, where an exponential decrease of friction with velocity would be expected. Moreover, in both cases, and applying both the normal loads (10N and 20N), an evident decrease of the frictional curve is obtained when increasing the temperature. This behavior is due to the viscosity characteristics of the grease, as previously discussed and shown in Figure 73. Looking at the frictional response of the two tested configurations, in both cases a first large friction drop, due to the shift between static and dynamic friction, is followed by an increase and stabilization with respect to the velocity. While the same overall trend is observed, the main effect provided by the DLC coating is an overall lower value. Its effect is mainly observed within the low velocity range (lower than 5mm/s), where boundary and mixed contact conditions are expected. This agrees with the role of DLC, which provides further solid lubrication between the contacting surfaces, when the contact moves toward more severe boundary lubrication.
As underlined in the zooms at the bottom of Figure 74, the difference between static and dynamic friction coefficients is higher in the case of absence of the DLC coating, both at ambient and high temperature, thanks to the solid lubricant layer that lower the static friction. The higher is the difference, the higher is the propensity of the brake system to promote stick-slip vibrations, as shown in Chapter 4.4.3.
After the first value of the dynamic CoF, calculated at 0.1mm/s, the friction curve is much steeper in the absence of DLC, toward a stabilization at higher values.

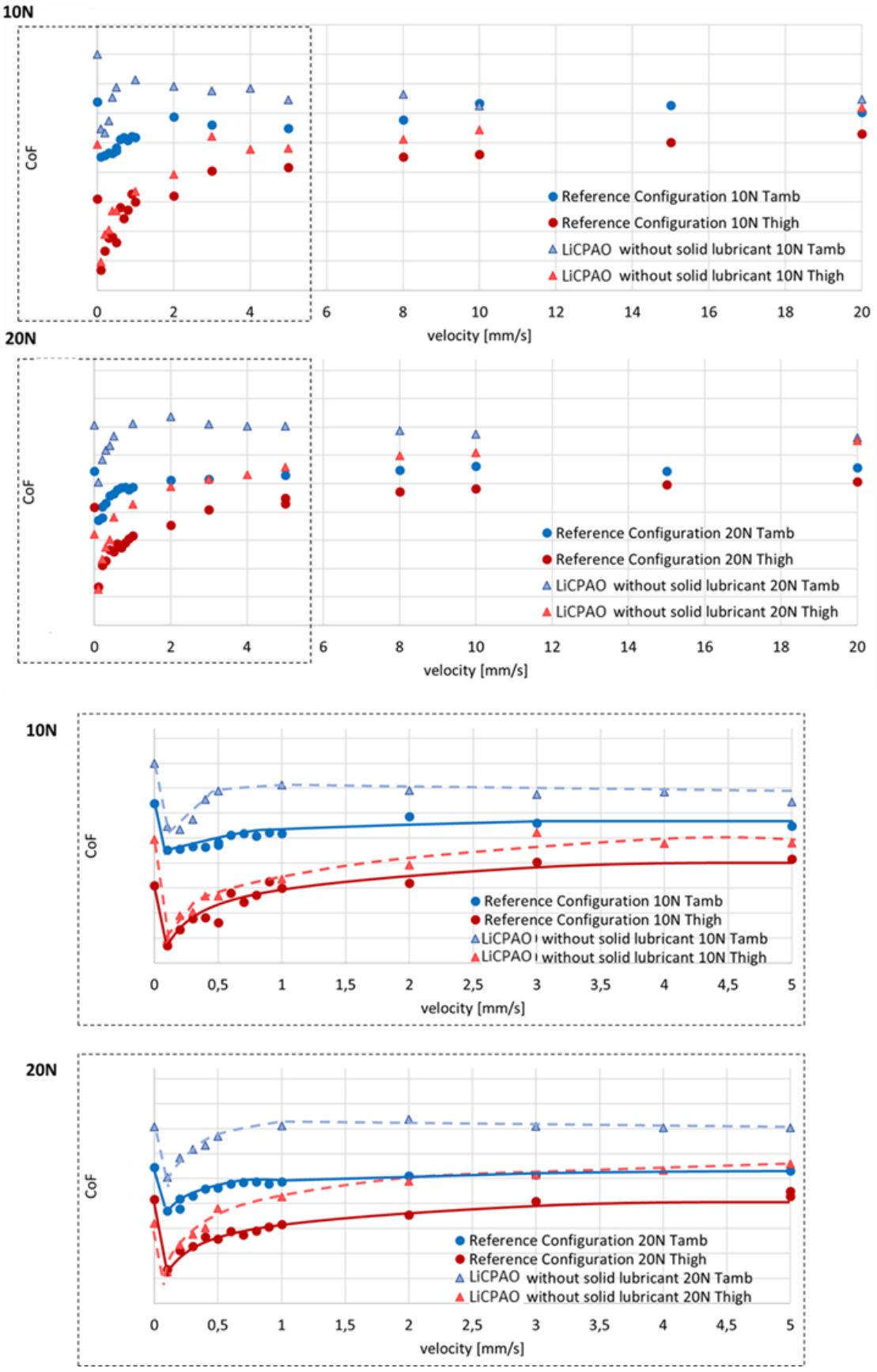

Figure 74: Comparison between the friction coefficient trends of the Reference configuration and the tests performed with the same grease (LiCPAO) without the DLC solid lubricant, as a function of the imposed sliding velocity. The lower images show a detail of the curves within the low velocity range, for 10N and 20N, at both at ambient (25°C) and high (80°C) temperature.

5.3.2. Dry condition

Specific tests in dry conditions have been carried out aiming to observe the role of the DLC coating on the frictional response of the investigated contact, without the presence of the grease. Figure 75 shows the results of the tests in dry conditions, with and without DLC coating.

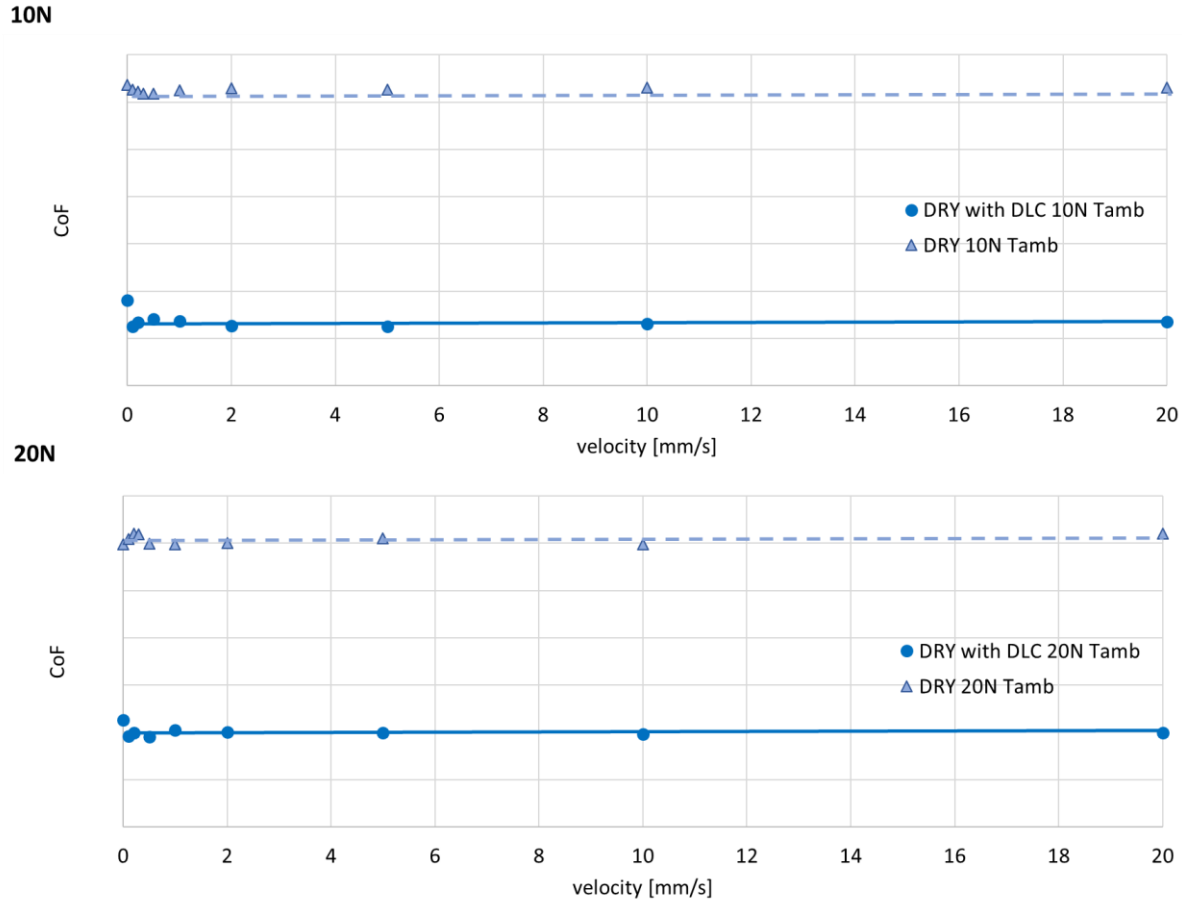

Figure 75: Comparison between the trends of the friction coefficient as a function of the sliding velocity, with and without DLC coating, in dry condition.

The overall frictional response is almost constant with respect to the sliding velocity. Nevertheless, the DLC coating decreases drastically the friction coefficient, with respect to the uncoated samples. As already discussed in Chapter III Section 3.4.3, the formation of a deposit of solid lubrication, on the contact surfaces, has been observed in the case of the tests performed with the DLC solid lubricant. The DLC, on the coated surface sample, creates a third body (DLC particles), which deposits on the counterpart sintered steel, during the sliding, protecting the surface from a premature wear and providing a solid third body that lower the overall friction resistance. The same contribution has been then observed both in dry conditions and with grease lubrication (LiCPAO). The transfer of the solid lubricant leads to a contact that is no longer DLC/Steel, but becomes DLC/DLC after few cycles. Moreover, the tests with DLC coating showed a faster running-in process, with less wear and lower steady-state friction, compared to the same tests

performed on the same specimens without coating. The results are consistent with previous works in literature [90, 122, 135].
All these observations let assume that the retrieved trend of the friction coefficient, with respect to the sliding velocity, within the low velocity range, is not driven by the presence of the DLC, which has an overall effect of decreasing friction. It is then the grease that causes the typical trend at low velocities observed in Figure 74.

5.4. Role of the base Oil in the frictional response

The performance of the base oil (PAO), without additives, has been investigated. The aim is to isolate the influence of the oil, which composes the lithium complex grease analysed in this work, in the observed trends of the friction curves. The results are here compared with the ones obtained by the reference configuration (Figure 76). In both configurations the spring sample is coated with DLC.
Looking at the curves of the base oil (PAO) lubrication, the maximum friction coefficient, which is the static friction coefficient, is following by an exponential decrease as the speed increases, producing a Stribeck-like curve, typical of a lubricating oil [99, 100]. Increasing the sliding velocity, the coefficient of friction becomes stable.
This result confirms that the specific frictional trend, observed within the low velocity range in the reference configuration, is neither caused by the DLC or the oil components, but it is rather an effect of the thickener and the additives.
On the contrary, in the higher speed region, the friction coefficient measured in the greased tests converges with the one obtained with the base oil alone, letting assert that in this region friction is mainly governed by the base oil viscosity.
As reported in the previous cases, also in the case of oil lubrication, there were no significant variations of the friction trends with the variation of the normal load.

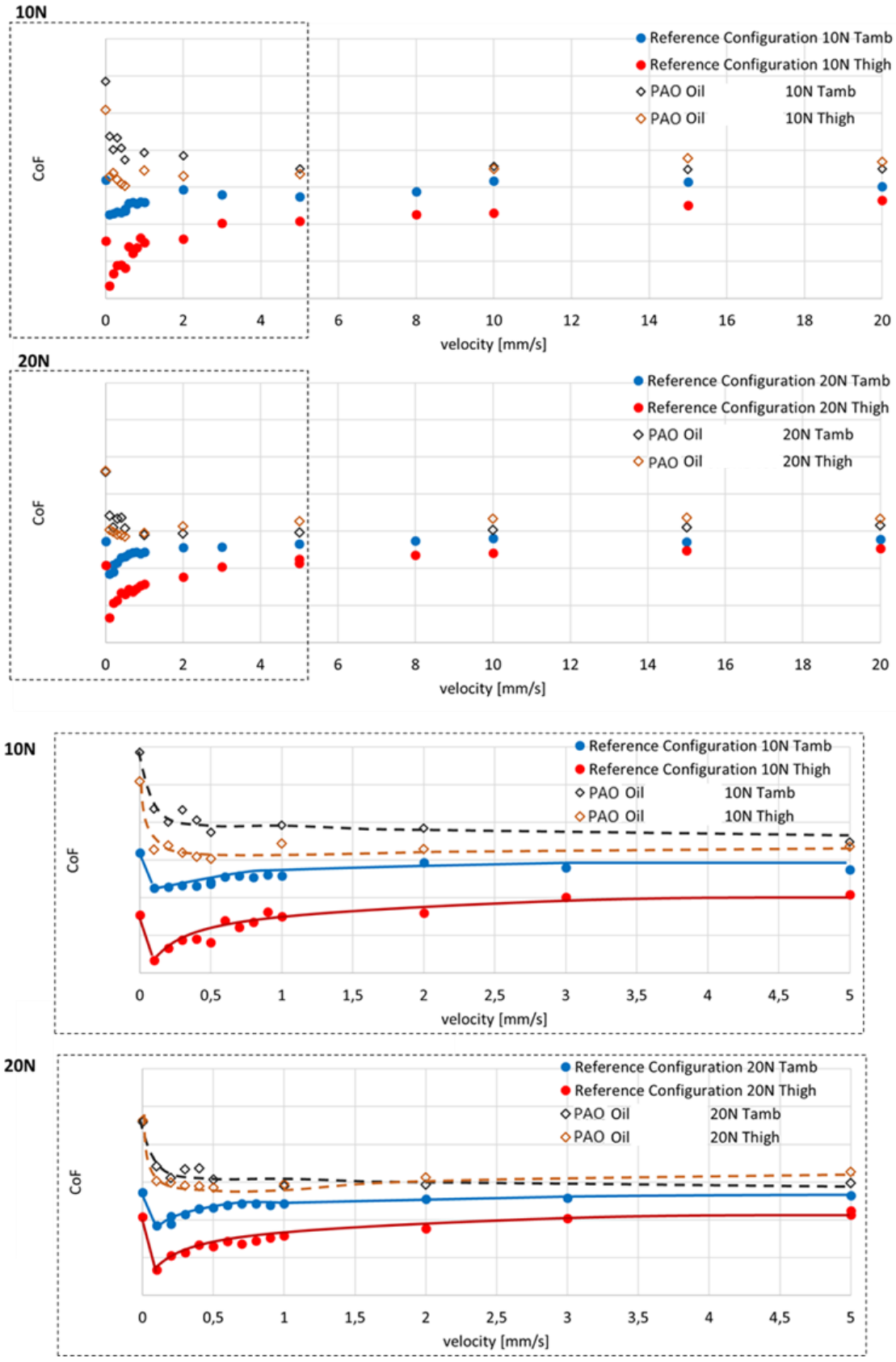

Figure 76: Comparison between the friction coefficient trends and values between the Reference configuration and the tests performed with the PAO oil (with DLC) as a function of the imposed sliding velocity. The lower images show a detail of the curves for 10N and 20N, at both at ambient (25°C) and high (80°C) temperature.

As previously discussed in Section 5.3., also in the case of the oil (PAO), the role of the DLC has the only effect of lowering the friction coefficient. As shown in Figure 77, comparing the tests performed with and without the DLC solid lubrication, the friction coefficient trend of the base oil remains stable. The differences between the two experimental results is only in the friction coefficient values. Again, the frictional behaviour in both cases is represented by the an exponential decrease of the CoF as the speed increases, producing a Stribeck-like curve [99, 100]. As underlined in Figure 77, the static and the dynamic friction coefficient are higher in case of absence of the DLC coating both at ambient and high temperature.

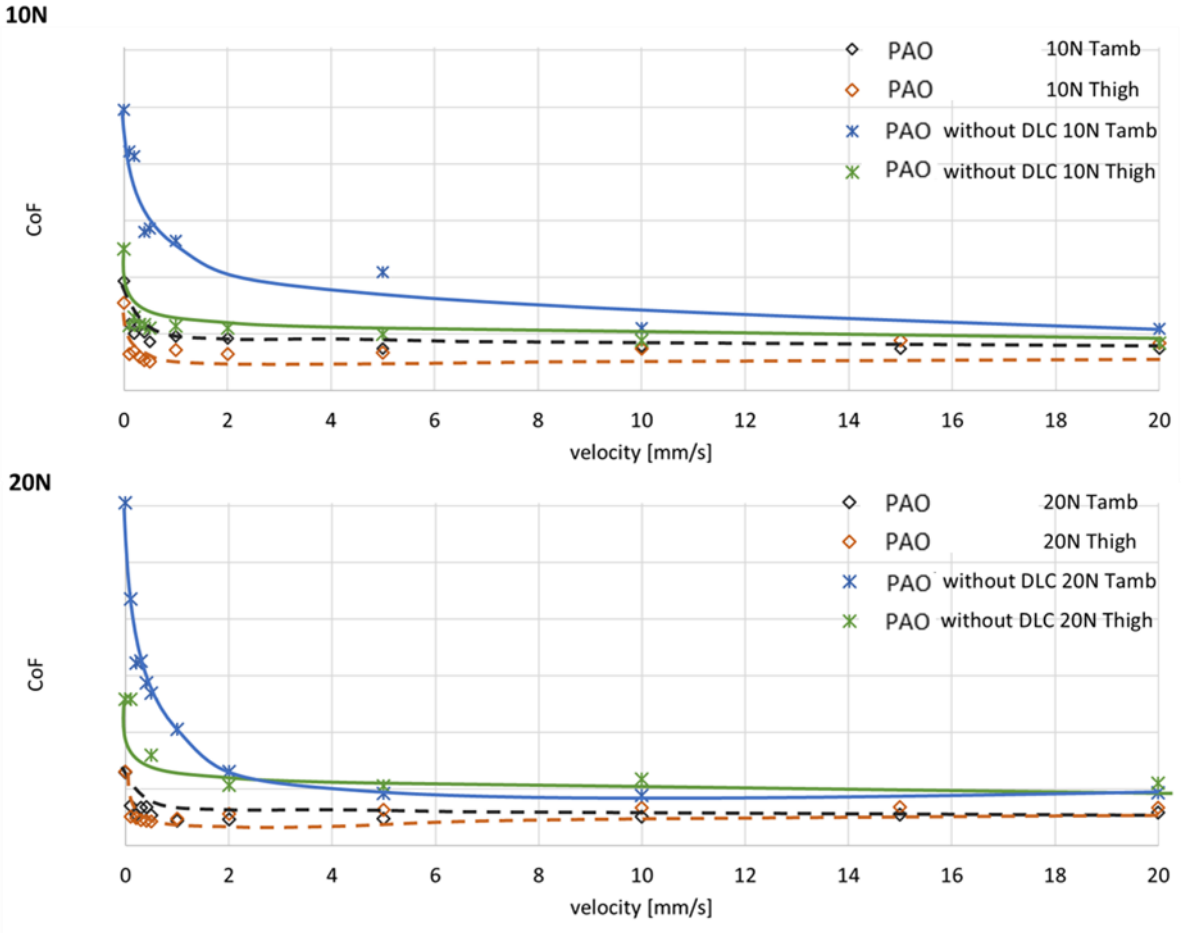

Figure 77: Comparison between the friction coefficient trends and values of the tests performed with the PAO oil, as a function of the imposed sliding velocity, with and without the DLC coating. The upper figure shows the trend and values imposing a normal load equal to 10N and the lower figure imposing a normal load equal to 20N, at both at ambient (25°C) and high (80°C) temperature.

Aiming to understand the role played by the additives, further tests has been then performed with the base oil with the addition of additives and compared in the following section with the different tests performed with and without additives.

5.5. Role of additives in the frictional response

The performance of the PAO oil with the addition of additives has been investigated, aiming to examine the influence of the additives, included in the commercial lithium complex grease, on the frictional trends. The results are shown in Figure 78 and here compared with the ones obtained by the tests performed with the grease (Reference Configuration) and the PAO oil alone.

The presence of additives in the base oil substantially affects and modifies the frictional response. Within the lower velocity range, the trend of the oil with additives get extremely close to the one observed with the grease, in the Reference Configuration. Nevertheless, the higher static friction increases the drop between the static and dynamic one, observed in grease lubrication, which would promote stick-slip instability.

Again, in the high velocity range, where the oil viscosity plays a key role, it is possible to observe a lowering of the friction coefficient with the adding of the additives.

These results are coherent with roles played by the thickener and the additives, both of which decrease the friction coefficient at the lowest velocities (boundary conditions) either affecting the rheology of the lubricant and the physiochemical interaction with the surfaces. When adding the additive to the grease, the same trend is obtained, with moreover and overall decrease of the friction and trend stabilization.

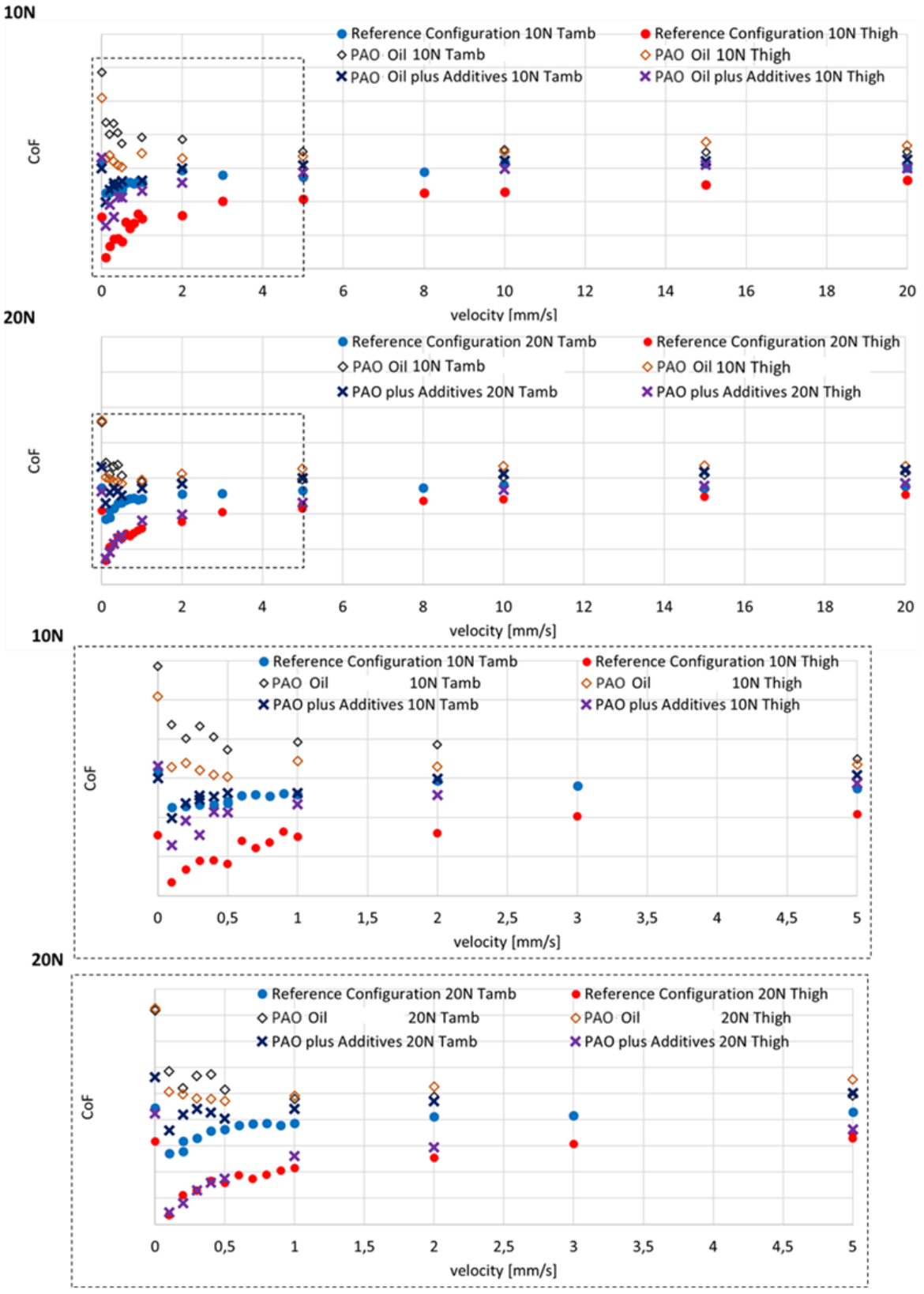

Figure 78: Comparison between the friction coefficient trends, between the Reference configuration, the tests performed with the PAO Oil and the tests performed with the PAO Oil with the additives of the grease, as a function of the imposed sliding velocities. The lower images show a detail of the curves for 10N and 20N, at both at ambient (25°C) and high (80°C) temperature.

About the difference between static and dynamic friction, in presence of additives, both the static and the dynamic friction coefficients are lowered, compared to the PAO Oil or grease alone. A strong decrease in the friction drop is obtained for the oil configuration, because of the strong decrease in the static friction, with respect to the oil. A lower decrease is obtained in the grease configuration, because the static friction is already decreased by the thickener, while the effect of the additive is an overall decrease of the friction, both in static and low velocity dynamic conditions.
Moreover, as previously discussed in Section 5.4., also in the case of the base oil (PAO) whit additives, the DLC has the main effect of lowering the overall friction coefficient.
As shown in Figure 79, comparing the test performed with and without the DLC solid lubricant, it is clear that the DLC coating is lowering all the CoF values. The frictional trend in both cases is equal and the presence of additives in both cases produce a substantial change of the frictional trend comparing to the P Oil trend (without additives) shown in Figure 77.

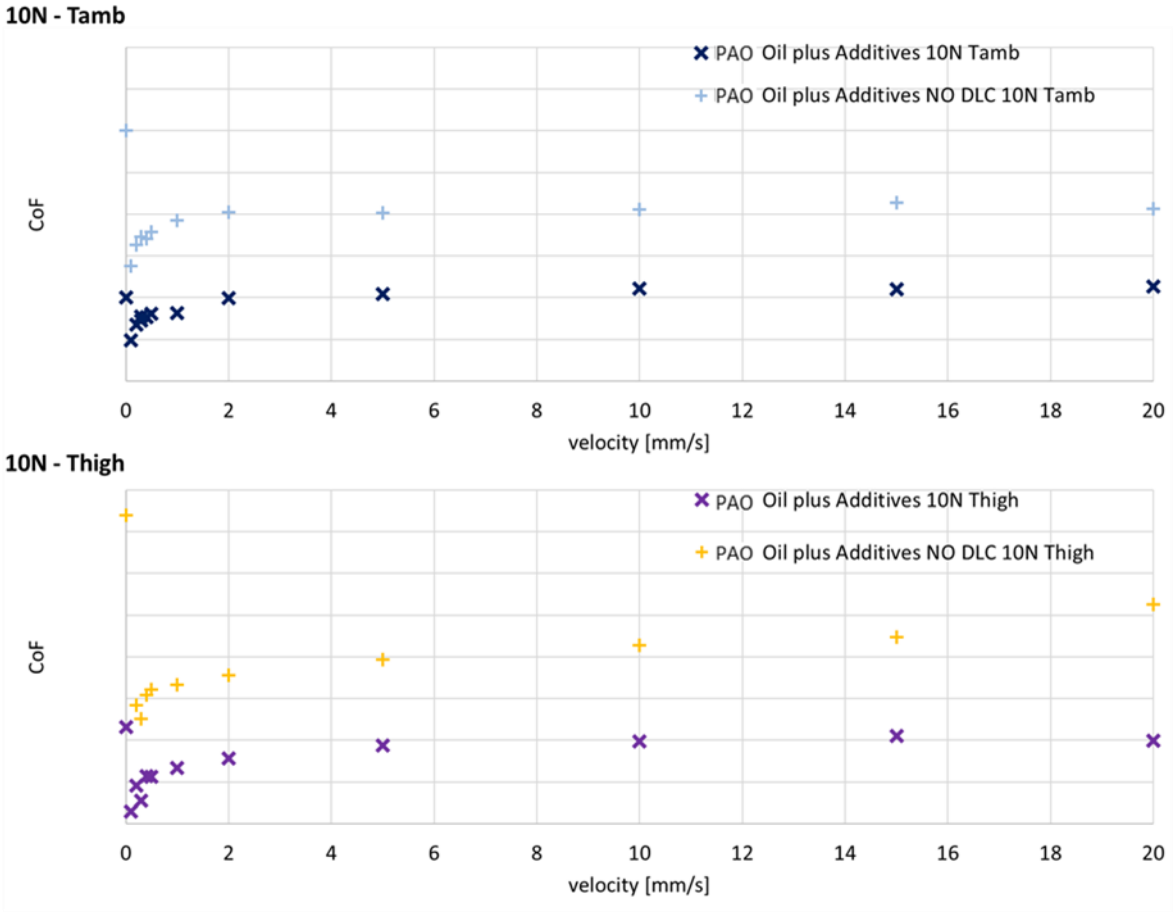

Figure 79: Comparison between the friction coefficient trends and values of the tests performed with the PAO oil of the LiCPAO grease plus Additives as a function of the imposed sliding velocity, with and without the DLC coating on the upper sample. The upper image shows the trend and values imposing a normal load equal to 10N at Ambient Temperature (25°C) and the lower image shows the trend and values imposing a normal load equal to 10N at High Temperature (80°C).

5.6. Concluding remarks

As shown in Chapter IV Section 4.4.3, the root causes of stick-slip instabilities are either a large difference between static and dynamic friction and a negative friction-velocity slope at low velocities. Then, within the low velocity range, critical for such dynamic instabilities, the local frictional contact response has been reproduced and analysed as a function of the different lubricant components. First, the influence of the DLC coating, present in the real brake system, has been analysed and compared to the uncoated case. Then, tests with different combinations of the grease components (i.e. the PAO oil alone), the Lithium Complex thickener and the additives) have been compared too. Markedly different frictional behaviours have been observed under the same operating conditions. It has been then possible to identify some of the relative influences of the lubrication components on the frictional trends, with respect to the imposed velocity.

The following main conclusions can be drawn:

- The DLC coating provide an overall decrease of friction coefficient, compared to the Steel/Steel contact, both in dry and greased conditions. In the case of the dry experimental tests, this difference is notable. The CoF values with DLC are about the 20%-35% of the classical Steel/Steel contact in dry conditions. These results are consistent with previous works in literature [86, 119, 132]. The same conclusions can be observed analysing and comparing the results, obtained with and without the DLC solid lubricant, both in greased and oiled lubrication conditions (Figure 80).

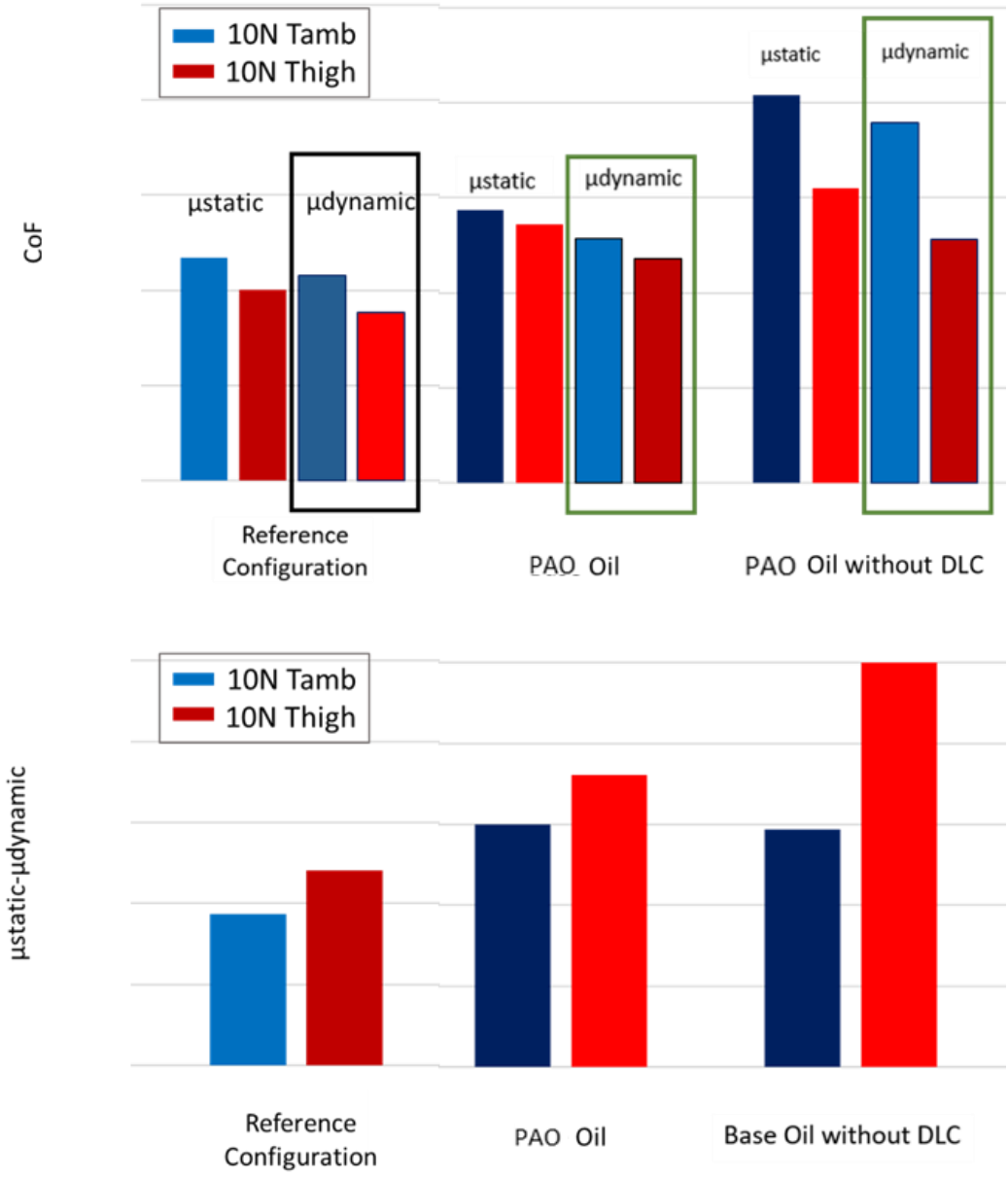

Figure 80: Comparison between the static CoF, dynamic CoF and their difference (µstatic-µdynamic) in both greased and oiled lubrication conditions, with and without DLC, imposing 10N of normal load, at both ambient and high temperature conditions.

- In both lubrication conditions (i.e. grease and base oil), an evident decrease of both the static and the dynamic CoF is underlined in presence of the DLC coating. Comparing the static and the dynamic friction coefficient both at ambient and high temperature, the lowering of the friction coefficients is higher in the case of the base oil. This is due to the role played by the thickener and additives, which already decrease the friction. Moreover, previous works [136, 137] demonstrate that the high friction reduction in case of PAO lubrication is associated with the gradual build-up of a tribofilm with poor friction properties, as shown in Chapter III Section 3.4.3.

- It is confirmed that in greased lubrication, and even in the oil plus additive configuration, a specific friction-velocity trend, with two well distinguished velocity ranges, is observed (high-speed region and the low-speed region). Moreover, in all cases, a high difference between static and dynamic friction coefficients has been observed, mainly due to the drop of the friction coefficient at the lowest velocities (low-speed region).
- In the high-speed region, friction is governed by the oil. Increasing the sliding speed, the friction coefficient of the grease tends in fact to reach the oil behaviour, which follows a Stribeck-like curve. The additives affect the frictional response in this range by a slight lowering of the friction.
- On the contrary, the frictional trend in the low speed region is mainly affected by the presence of the additives and the thickener. The friction coefficient of the greased contact, as well as the one of the oil with additives, shows values, at the lowest velocities, much lower than ones of the base oil alone. Afterwards, the friction increases with the velocity, up to the values of the contact lubricated with the base oil alone.
- The thickener and the additives reduce the static friction coefficient compared to the base oil behaviour, but the difference between static and dynamic friction coefficient (relevant for stick-slip propensity) stays high for both configurations, because of the friction drop at the lowest speeds. A schematic representation of the main trends discussed above is shown in Figure 81.

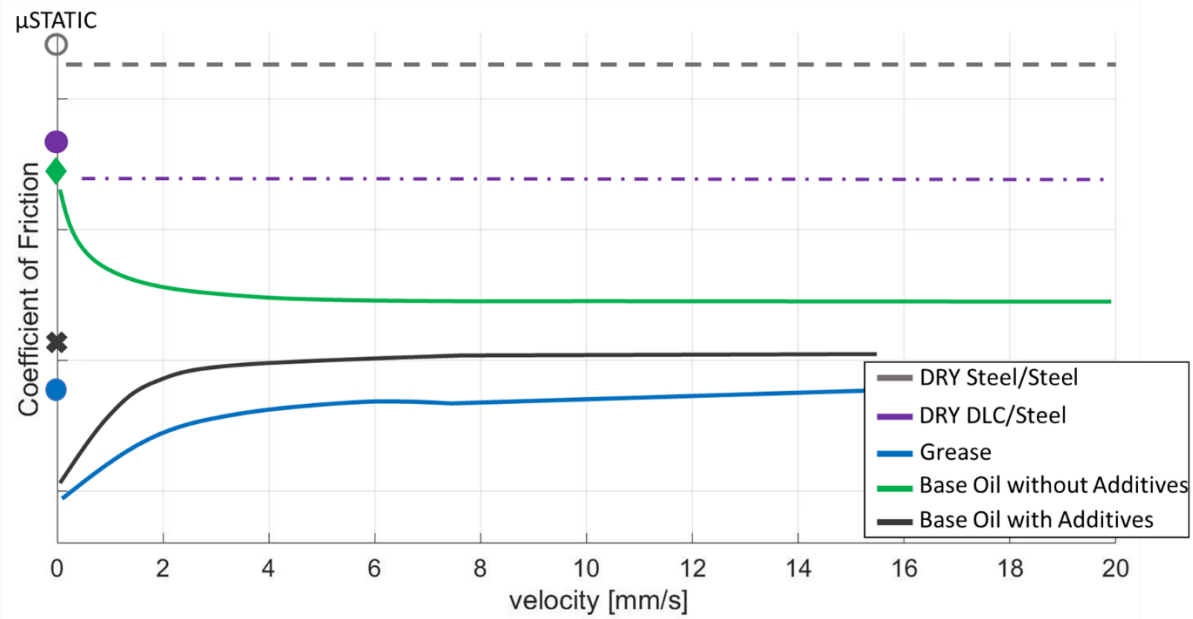

Figure 81: Generalized friction coefficient trends for the dry cases (Steel/steel and DLC/Steel), Lithium Complex grease (LiCPAO) and Synthetic base oil (PAO) whit and without Additives.

- Increasing the temperature, the greased friction coefficient behaviour shows lower values, independently of the tested loads and coatings. This decrease of friction at higher temperature can be associated to both a decrease in oil viscosity and an increase of oil release by the grease matrix, when the temperature increases.

The different observed frictional trends are a macroscopic result of the rheological and physiochemical interactions between the thickener, the additives and the base oil of the grease. It has been observed as the thickener and additive contributions affect mainly the frictional response in static conditions and within the low-velocity range. With respect to the stick-slip propensity, while the thickener and the additives have a positive effect in lowering the static friction coefficient, the decrease of the dynamic friction coefficient in the lower-velocity range can promotes stick-slip, by maintaining a large static-dynamic friction drop. Specific rheological and physiochemical analyses and simulations should be performed in the future to decouple such effects, for different families of greases to ensure the performances on the system stability.

General Conclusions

The presented Ph.D. work has been focused on the study of the stick-slip problem in greased contacts, applying a methodological approach, with both tribological and dynamic analyses, to an industrial case. The investigation has been realized with both experimental campaigns and numerical simulations.

6.1. Original contributions

The main achieved results are here summarized and organized, as the manuscript, in three different main sections: i) the results obtained from the investigations on the entire brake system, from both a tribological and dynamical point of view, to identify the contact instability; ii) the results from the experimental campaigns on the local frictional contact and the numerical simulations of the system response, to highlight the key factor leading to stick-slip; the results on the analysis of the role played by the different lubricant components. The achieved results are discussed from both an industrial and a scientific point of view.

6.1.1. Stick-slip analysis on the entire brake system

During the load descent phase, the widening of the spring assures the braking, thanks to the contact pressure at the greased contact between the fixed cylinder and torsional spring. The operating conditions can induce unwanted noise emissions.
Tribological analyses of the contact surfaces of the brake components, together with the analysis of the acceleration signals, recorded during the instabilities, have been performed on the different brake systems (i.e. different geometries, materials, operating temperatures, velocity and imposed output loads).
The main outcomes can be summarized as follow:

- The noise emission from the brake system is a consequence of stick-slip contact instabilities. The dynamic analysis of the system response, during braking, highlighted a periodic impulsive excitation of the system dynamics, due to the succession of sticking and sliding phases at the greased contact.
- The presence of stick-slip is detected mostly when the internal temperature of the brake system reaches higher values, compared to the ambient one, due to successive working cycles.
- The topological analyses of the different brake systems underlined the presence of characteristic traces of axial movement of the spring. The attempt of the spring to open axially can cause misalignment of the components, modification of the spring stiffness and a localization of the contact pressure. The axial breathing of the spring, during the sick-slip, could be either a cause or an effect of the instability.
- These dynamic and tribological observations were repeatable and characteristic of all the analyzed noisy brakes.

From an industrial point of view, these results are a key point of the performed study. Before this analysis, no clear identification of the origin of the noise in the investigated brake systems was available. Due to the different speeds to which the different brakes are subjected, two different types of noises and consequent phenomena were identified. However, following the analysis, reported in the Chapter II, the stick-slip phenomenon has been identified at the base of both the noise emissions and has been proved that all the brake systems are subjected to the same kind of instability. The performed investigations have led to the assumptions that: i) the stick-slip, observed in the spring-brake systems, is generated at the greased contact between the spring and the drum; ii) it is identified as stick-slip, independently from the geometry, material and boundary conditions of the brake system.

6.1.2. Local contact response and its influence on the dynamic response of the entire brake system

The frictional response of the greased contact has been investigated with respect to the main boundary conditions (velocity, load and temperature), reproducing as close as possible the real contact conditions.
Starting from nominal working conditions, an experimental campaign has been performed to investigate how the frictional behavior of the lubricated contact between spring and drum is affected by different design configurations.
Based on the existing benchmarks of brake systems under production, some main parameters have been tested, including the surface coating of the spring, the drum roughness and the material. In parallel, a numerical lumped model of the entire tubular actuator has been developed and alimented by the data from both the real mechanical system and the experimental frictional tests, aiming identify the key factors affecting the stick-slip propensity of the system. By one side, stiffness, damping and loads have been calculated on the real system, considering all the system components. On the other side, the trends obtained by the frictional experimental tests have been used as input for the numerical simulations. When introducing the frictional behaviours of the reference configuration, both at ambient and high temperature, the results of the numerical simulations show stick-slip at higher temperature, as observed experimentally on the real system. The results obtained by the simulations allowed for asserting that the friction-velocity response of the greased contact plays a key role in destabilizing the system, bringing to the stick-slip instability.

In general, it has been highlighted that:

- For all the tested configurations, the friction coefficient evolution does not follow the typical Stribeck-like curve: the friction coefficient drops drastically at the lowest value of the velocity and then increases until a stabilization. The friction-velocity curve of the greased contact,

characterized by a high difference between the static and the dynamic CoF, and by a negative friction-velocity slope, is at the origin of the appearance of the contact instability. Two regions have been identified in case of grease lubrication: the high-speed range and the low-speed range:
    - The high-speed range does not affect significantly the dynamic response of the system and is mainly driven by the base oil contribution.
    - On contrary, the trend at low-speed range (from 0 to about 1mm/s) has been underlined as more relevant one. When reducing the difference between the static and the dynamic CoF and/or reducing the slope of the curve, an effective decrease of the stick-slip propensity has been observed.
- The friction drop at low velocities is significantly larger at high temperature, compared to ambient temperature, increasing the stick-slip occurrence of the brake system. This increasing in the difference between static and dynamic CoF is due to an overall decreasing of the dynamic friction coefficient values, as the temperature increase. This behaviour is independent of the tested loads and configurations.
- The increasing of the applied normal load leads to an overall decrease of the friction coefficient and a stabilization of the values in the high-speed range.

Moreover, considering the different industrial design configurations some outcomes can be underlined:

- The stiffness and damping have an opposite effect. Increasing the damping or reducing the stiffness the stick-slip propensity is lower. Nevertheless, from an industrial point of view, a substantial modification of C and/or K is not achievable in the design of the brake system , due to the wide range of other functional outputs (e.g. braking torque), which depends from the stiffness and damping of the brake system.
- Considering the others tested parameters (i.e. the honing angle of the drum, the drum material and the solid lubricant used as spring coating) two possible modifications of the reference design have been highlighted as suitable to reduce the stick-slip propensity: the CW coating of the spring and the drum material modification (drum 3). The other tested parameters do not produce significant changes in terms of stick-slip propensity of the system. These results have been confirmed by a parallel design of experiment (D.O.E.) on the brake system. From an industrial point of view, the drum 3 was not considered as a possible design solution because of the high production costs. However, the solid lubricant CW has been recently introduced in the production of the spring-brake system as the best solutions for the spring coating.

6.1.3. Role of the lubricant components on the frictional behavior

The presence of a lubricant at the interface increases the complexity of the phenomenon, from both a tribological and a dynamic point of view. In case of grease lubrication, its complex rheology, function of different components (the thickener, the additives and the base oil), becomes then a key point for the occurrence and evolution of the stick-slip phenomenon, by driving the overall frictional response as a function of the sliding velocity.
In greased lubrication, and even in the oil plus additive configuration, a specific friction-velocity trend, with two well distinguished velocity ranges, has been observed (high-speed region and low-speed region), as previously highlighted. Aiming to understand the role played by the different lubricant components (thickener, oil, additives and solid DLC lubricant) on the frictional response under low sliding velocity conditions, different types of lubrication conditions, corresponding to dry contact, oil lubrication and greased contact (with and without additives), both with and without Diamond-Like-Carbon (DLC) coating, have been tested. The different conclusions listed below:

- The base oil contribution to the frictional behaviour is dominant in the high-speed region. Increasing the sliding speed, the friction coefficient of the grease tends in fact to reach the oil behaviour, which follows a Stribeck-like curve.
- The additives affect the frictional response, in both the high and low speed ranges, leading to different contributions to the local frictional response. In the high-speed range, the additives result in a slight lowering of the friction. On the contrary, in the low-speed region, both the additives and the thickener plays an overwhelmingly role. The friction coefficient of the greased contact, as well as the one of the oil with additives, shows always a behaviour characterized by a high difference between the static and the dynamic CoF and by a negative friction-velocity slope. The CoF values are much lower at the lowest velocities compare to the ones of the base oil alone.
- While the thickener and the additives have a positive effect in lowering the static friction coefficient, the drastic decrease of the dynamic friction coefficient at the lowest velocities can promotes stick-slip, by maintaining a large static-dynamic friction drop.
- As previously asserted, when increasing the temperature, the friction coefficient of the greased contact shows lower values, independently of the tested loads and coatings, and higher differences between static and dynamic CoF are observed. This decrease of friction at higher temperature has been associated to both a decrease in the oil viscosity and an increase of oil release by the grease matrix, when the temperature increases.
- The solid lubricants classified in the DLC-like solid lubricants (i.e. the DLC and the CW) improve the tribological performances of the contact, especially in terms of wear and friction coefficient stability, providing further solid lubrication between the contacting surfaces and creating a

third body on the counter surface, both in dry and lubricated conditions (oil and grease). An evident decrease of both the static and the dynamic CoF is underlined in presence of the DLC coating. Overall, a reduction of the friction drop is observed with the addition of the DLC solid lubrication.

From an industrial point of view, with respect to the stick-slip propensity, the best solution would be a grease that exhibits an overall frictional behaviour constant as a function of the sliding velocity and with a relative low difference between static and dynamic COF. Nevertheless, as demonstrated, the friction curve within the low velocity range is affected by the interaction of all the different components of the lubricant film, and the choice of a suitable lubricant at the contact interface should be done after specific frictional and rheological analyses of the lubricant, to guarantee a better system stability.
In a more general manner, the results if this thesis highlighted the complexity of the local (contact) and global (system) responses involved during the sliding motion between two bodies, and the key role of the lubricant rheology in the evaluation of the stick-slip propensity of the system. Moreover, the present work underlined how a multi-disciplinary approach, including both experimental and numerical analyses, is needed to understand and modify the mechanisms at the origin of the investigated frictional instabilities in greased contacts.

6.2. Future works

As stated above, the results highlighted the complexity of the phenomena and, consequently, allowed to point out some of the main perspectives regarding the futures steps of investigations. Some of the major point of future development are reported in the following:

- The effect other different parameters could be investigated in terms of frictional response. A possible example could be experimental tests on different surface roughness or other drum materials than the drum 3, including porous materials or/and self-lubricating materials. For instance, as previously discussed, the effect of the material properties has led to the reduction of the stick-slip appearance and could be a possible improvement in the design of the brake systems.
- Focusing on the influence of the grease rheology on the frictional behaviour of the contact, and thus on the dynamic response of the system, future works will started with the purpose of decouple the effects of the additives and of the thickener on the overall frictional response of the greased contact. In-depth analyses should be addressed to investigate the rheological and chemical roles of the thickener and the additives in the low-speed range, with the aim of reducing the static-dynamic friction drop. Moreover, further studies are necessary to understand which, among the additives forming the grease LiCPAO, has a more evident positive influence in lowering the static friction coefficient

and which one has a negative effect, lowering the frictional response at the lowest speeds.

- Focusing always the attention on the influence of the grease components on the overall frictional contact behaviour, further works have been started on other greases. The composition and properties of the lubricating film, established at the contact interface, depend on both the grease properties (base oil and thickener type, additives, rheology) and the operating conditions (speed, temperature and normal load). As suggested by previous studies [98], a grease based on a calcium sulfonate complex thickener (CaCMix), such as the , could be a better solution in terms of frictional behaviour in the low-speed range and in high temperature condition, compared to the LiCPAO grease. A preliminary experimental campaign has been performed on this grease, with the presence of the DLC coating on the upper specimen, imposing a normal load equal to 20N, at both ambient and high temperature conditions. The obtained results are shown in Figure 82 and are here compared to the reference configuration (LiCPAO grease and DLC coating on the upper specimen).

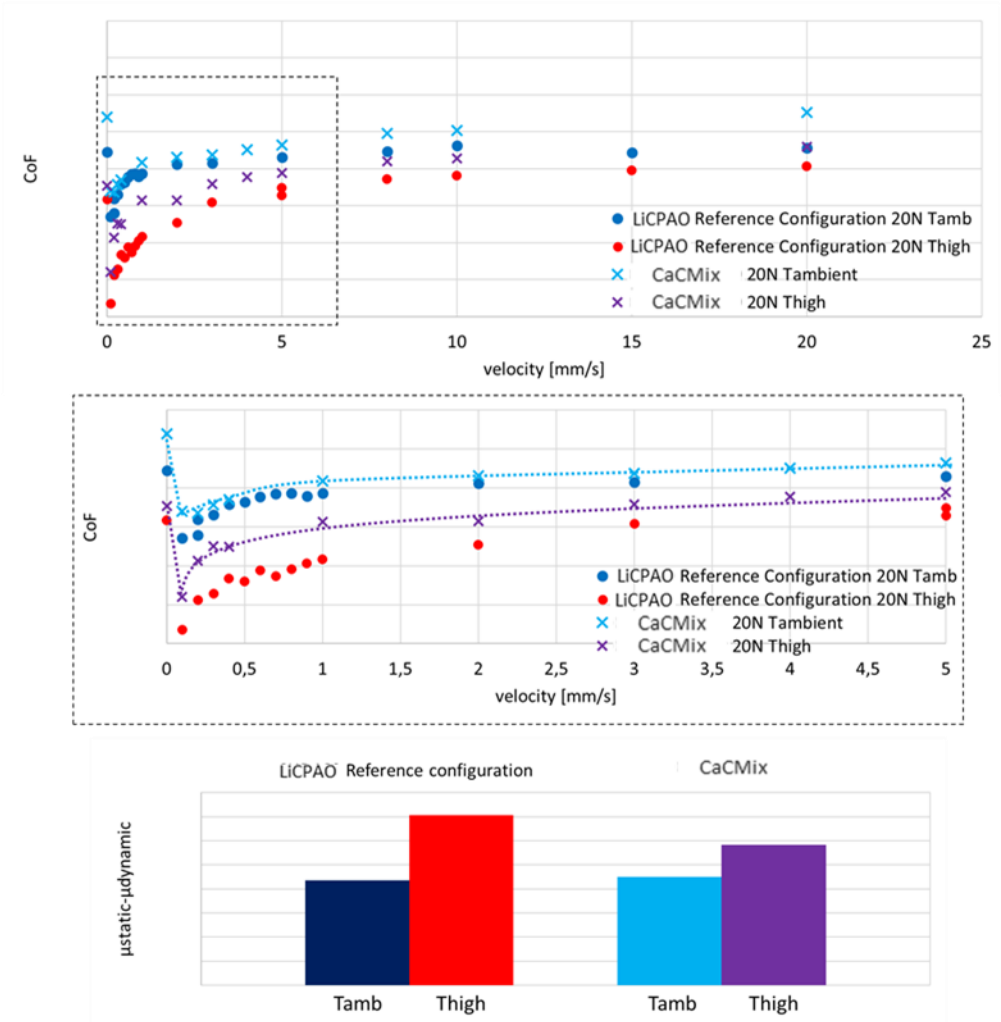

Figure 82: Frictional trend comparison between the Reference configuration (LiCPAO grease) and the tests performed with the CaCMix grease, as a function of the imposed sliding velocities. The lower images show a detail of the curves for 20N and the differences between the static and the dynamic CoF, at both at ambient (25°C) and high (80°C) temperature.

The fictional behaviour of the grease CaCMix shows a more stable trend of the CoF values, compared to the reference configuration of the LiCPAO grease. Moreover, the difference between static and dynamic CoF is lower, both at ambient and high temperature.
However, a sharp difference in the frictional response of the two greases was not observed, identifying again the two different trends within the two different velocity ranges. This is probably due to the presence of the same additives in the two analysed greases or to a similar, but not identical, effect of the thickener.

Again, this preliminary results on a different grease highlight the complexity of the subject and the need for in-depth rheological and physiochemical analyses for distinguish the different physical and chemical mechanisms to be mastered for improving the stability of the frictional contact/system response.

Reference

[1] R.A. Ibrahim, "Friction-Induced Vibration, Chatter, Squeal, and Chaos—Part I: Mechanics of Contact and Friction," *Appl. Mech. Rev.,* vol. 47(7), pp. 209-226, 1994.

[2] J.D. Byerlee, The mechanics of stick-slip, Elsevier, Tectonophysics, 1970.

[3] J-J. Sinou, J.Cayer-Barrioz, H.Berro, "Friction-induced vibration of a lubricated mechanical system," *Tribology International,* vol. 61, pp. 156-168, 2013.

[4] R. Sourain, "Spring brake" SOMFY TECH PROGRAM, Cluses, France, 2020.

[5] *I. Ghezzi, D. Tonazzi, M. Rovere, C. Le Coeur, Y. Berthier, F. Massi, "Tribological investigation of a greased contact subjected to contact dynamic instability",Tribology International, Volume 143, March 2020,.*

[6] V. Popov, Contact Mechanics and Friction, Springer, 2010.

[7] F. P. Tabor, Mechanical Desing Handbook. Friction, Lubrication, and Wear, McGraw-Hill, 2006.

[8] Y. Berthier, "Third-Body Reality – Consequences and Use of the Third-Body Concept to Solve Friction and Wear Problems, Chapter 12," in *Wear: Materials, Mechanisms and Practice*, Gwidon W. Stachowiak, 2015.

[9] Y. Berthier, P. Jacquemard, M.H. Meurisse, "The Third Body Concept: Interpretation of Tribological Phenomena," 1996.

[10] M. Godet, "The third body approach: a mechanical view of wear," *Wear,* pp. 437-452, vol. 100, 1984.

[11] M. Godet, "Third-bodies in tribology," *Wear,* pp. 29-45, vol. 136, 1990.

[12] A. Eleod, F. Oucherif, J. Devecz, Y. Berthier, "Conception of numerical and experimental tools for study of the Tribological Transformation of Surface TTS," *Dowson D. ed. Proccedings of the 25th Leeds-Lyon Symposium on Tribology : Lubrication at the frontier, Elsevier. Tribology Series, 1999,* pp. 673-682, vol. 36, 8-11 septembre 1998.

[13] S. Descartes, Y. Berthier , "Rheology and flows of solid third bodies background and application to an MoS1.6 coating," *Wear,* pp. 546-556, vol. 252, 2002.

[14] Y. Berthier, "Maurice Godet's third body," *In : DOWSON D. ed. Proc. of the 22nd Leeds-Lyon Symposium on Tribology : The third body concept; Amsterdam : Elsevier. Tribology Series, 1996,* pp. 21-30, vol.31, 5-8 septembre 1995, Lyon.

[15] J. Denape, "Third body concept and wear particle behavior in dry friction sliding conditions," *Tribological aspects in modern aircraft industry. Trans Tech Publications,* pp. 1-12, 2014.

[16] F. P. Tabor, D. Bowden, The Friction and Lubrication of Solids, Clarendon Press, 1954.

[17] F. P. Tabor, D. Bowden, Friction and lubrication of solids, Oxford: Clarendon Press, Part I, vol. I, 1950.

[18] G. Lacerra, M. Di Bartolomeo, S. Milana, L.Baillet and E. Chatlet, F. Massi, "Validation of a new frictional law for simulating friction-induced vibrations of rough surfaces," *Tribology International,* vol. 121, pp. 468-480, 2018.

[19] B. Persson, F. Bucher and B. Chiaia, "Elastic contact between randomly rough surfaces: Comparison of theory with numerical results," *Physical Reviews,* 2002.

[20] A. Meziane, L. Baillet, "Non linear analysis of vibrations generated by a contact with friction," *European Journal of Computational Mechanics,* pp. 305-316, 2010.

[21] A. Lazzari, G. Conidi, C. Malmassari, A. Cerutti and F. Massi, "Experimental Evaluation of Brake Pad Material Propensity to Stick-Slip and Groan Noise Emission," *Lubricants,* vol. 6, 2018.

[22] C. Gao, D. Kuhlmann-Wilsdorf, D.D. Makel, "Fundamentals of stick-slip," *Wear,* pp. 162-164, 1139-1149, 1993.

[23] D. Tonazzi,, "Macroscopic frictional contact scenarios and local contact dynamics: at the origins of "macroscopic stick-slip", mode coupling instabilities and stable continuous sliding," INSA, Lyon, 2014.

[24] M. Di Batolomeo, G Lacerra, L Baillet, E Chatelet and F. Massi, "Parametrical experimental and numerical analysis on friction-induced vibrations by a simple frictional system," *Tribology,* vol. 112, pp. 47-57, 2017.

[25] R. J. Wakelin, "Tribology: The friction, lubrication, and wear of moving parts," *Annual Reviews,* vol. 8556, 1974.

[26] H. Kim, N. Kardes, "Chapter 7: Friction and Lubrication," in *Sheet Metal Forming—Fundamentals*, ASM International, 2012, pp. 90-98.

[27] O. Reynolds, "On the theory of lubrication and its application to Mr. Beauchamp Tower's experiments, including on experimental determination of the viscosity of olive oil," *Philos Trans R Soc,* pp. 157-234, 1886.

[28] D. Dowson, G.R. Higginson, Elasto-Hydrodynamic Lubrication, International Series in Materials Science and Technologies, Vol. 23, Pergamon Press Ldt, 1966.

[29] S. M. Hsu, R. S. Gates, "12 - Boundary Lubrication and Boundary Lubricating Films," CRC Handbook of Modern Tribology, 2005.

[30] J. C.J. Bart, E. Gucciardi, S. Cavallaro, "3 - Lubricants: properties and characteristics," in *Biolubricants*, Woodhead Publishing, 2013, pp. 24-73.

[31] M.D. Hersey, Theory and Research in Lubrication: Foundation for future developments, John Wiley & Sons, 1966.

[32] B. Bhushan, Modern Tribology Handbook, CRC Press, 2000.

[33] Q. Xin, "Chapter 10 - Friction and lubrication in diesel engine system design," in *Diesel Engine System Design*, Woodhear Publishing, 2010, pp. 651-758.

[34] N. Hoffmann, M. Fischer, R. Allgaier, L. Gaul, "A minimal model for studying properties of the mode-coupling type instability in friction induced oscillations," *Mechanics Research Communications,* pp. 197-205, vol.2, 2002.

[35] D. Tonazzi, F. Massi, L. Baillet, A. Culla and M. Di Bartolomeo, Y. Berthier, "Experimental and numerical analysis of frictional contact scenarios: from macro stick–slip to continuous sliding," *Meccanica,* Vols. 50, no. 3, pp. 649-664, 2015.

[36] D. Tonazzi, F. Massi, A. Culla, L. Baillet, and A. Fregolent, F. Massi, Y Berthier, "Instability scenarios between elastic media under frictional contact," *Mech. Syst. Signal Process.,* Vols. 40, n. 2, p. 754–766, 2013.

[37] N. Hoffmann, L. Gaul, "Friction Induced Vibrations of Brakes: Research Fields and Activities," *SAE Technical Papers,* 2008.

[38] N. Hoffmann, S. Bieser, L. Gaul, "Harmonic Balance and Averaging Techniques for Stick-Slip Limit-CycleDetermination in Mode-Coupling Friction Self-Excited Systems," *Technische Mechanik,* vol. 24, pp. 185-197, 2004.

[39] H. Keitzel, N. Hoffmann, "Influence of the contact model on the onset of sprag-slip," *Special Issue: GAMM Annual Meeting 2006 – Berlin,* pp. 311-312, Vol. 6, 1, 2006.

[40] A. Meziane, L. Baillet, B. Laulagnet, "Experimental and numerical investigation of friction-induced vibration of a beam-on-beam in contact with friction," *Applied Acoustics,* pp. 843-853, Vol. 71, 9, 2010.

[41] A. Meziane, S. D'Errico, L. Baillet, B. Laulagnet, "Instabilities generated by friction in a pad–disc system during the braking process," *Tribology International,* pp. 1127-1136, Vol. 40, 7, 2007.

[42] N. Hoffmann, "Transient Growth and Stick-Slip in Sliding Friction," *Journal of Applied Mechanics,* 2006, Vol. 73, 4.

[43] F. Massi, O. Giannini, L. Bailet, "Brake squeal as dynamic instability: An experimental investigation," *The Journal of the Acoustical Society of America ,* Vols. 120, 1388, 2006.

[44] A. Akayc, O. Giannini, F.Massia, A. Sestieri, "Disc brake squeal characterization through simplified test rigs," *Mechanical Systems and Signal Processing,* Vols. 23, 8, pp. 2590-2607, 2009.

[45] G. Ouenzerfi, F. Massi, E. Renault, Y. Berthier, "Squeaking friction phenomena in ceramic hip endoprosthesis: Modeling and experimental validation".

[46] P. A. Johnson, H. Savage, M. Knuth, J. Gomberg, and C. Marone, "Effects of acoustic waves on stick–slip in granular media and implications for earthquakes," *Nature,* vol. 451, p. 57–60, 2008.

[47] V. Massimiani, B. Weiland, E. Chatelet, P. Cornuau and F. Massi, "The role of mechanical stimuli on hedonistic and topographical discrimination of textures," *M. Thesis,* vol. 143, 2019.

[48] P. Xing, L. Guobin, H. Gao, G. Wang, "Experimental Investigation on Identifying Friction State in Lubricated Tribosystem Based on Friction-Induced Vibration Signals," *Mechanical Systems and Signal Processing,* p. 138, 2020.

[49] R. D. Whitby, "Stick-slip friction, The frictional properties of a lubricant are critical to ensuring a successful operation," *Wordwide, Tribology & Lubrication Technology,* May 2011.

[50] A. D. Berman, W. A. Ducker, J. N. Israelachv, "Origin and Characterization of Different Stick−Slip Friction Mechanisms," *Langmuir, American Chemical Society ,* Vols. 12, no. 19, pp. 4559-4563, 1996.

[51] F.P. Bowden, D. Tabor, "Friction - An Introduction to Tribology," 1973.

[52] N.L. Kaidanovsky, S.E. Haiken, *Journal of Technical Physics,* 1933.

[53] J-J. Sinou, F. Thouverez, L. Jezequel, "Methods to reduce nonlinear mechanical systems for instability computation.," *Archives of Computational Methods in Engineering,* vol. 11, p. 257–344, 2004.

[54] M. Di Bartolomeo, F. Massi, L. Baillet, A. Culla, and Y. Berthier, "Wave and rupture propagation at frictional bimaterial sliding interfaces: From local to global dynamics, from stick-slip to continuous sliding," *Tribology International,* vol. 52, pp. 117-131, 2012.

[55] R. I. Leine, D. H. Van Campen, A. De Kraker and L. Van Den Steen, "Stick-Slip Vibrations Induced by Alternate Friction Models," *Nonlinear Dynamics ,* vol. 16, p. 41–54, 1998.

[56] N. Hoffmann, "Linear stability of steady sliding in point contacts with velocity dependent and LuGre type friction," *Journal of Sound and Vibration,* pp. 1023-1034, Vol. 301, 3-5, 2007.

[57] V. Prakash, "Frictional Response of Sliding Interfaces Subjected to Time Varying Normal Pressures," *Journal of Tribology,* 1998.

[58] D. Tonazzi, F. Massi, L. Baillet, J. Brunetti and Y. Berthier, "Interaction between contact behaviour and vibrational response for

dry contact system," *Mechanical Systems and Signal Processing,* vol. 110, p. 110–121, 2018.

[59] J. Klein, E. Kumacheva, "Simple liquids confined to molecularly thin layers. I. Confinement-induced liquid-to-solid phase transitions," *J. Chem. Phys.,* vol. 108, 1998.

[60] J. Gao, W. D. Luedtke, D. Gourdon, M. Ruths, J. N., "Frictional Forces and Amontons' Law: From the Molecular to the Macroscopic Scale," *J. Phys. Chem.,* vol. 108, no. 11, pp. 3410-3425, 2004.

[61] J. Le Rouzic, A. Le Bot, J. Perret-Liaudet, M. Guibert, A. Rusanov, L. Douminge, F. Bretagnol and D. Mazuyer , "Friction-Induced Vibration by Stribeck's Law: Application to Wiper Blade Squeal Noise," *Tribology Letters,* vol. 49, p. 563–572, 2013.

[62] B. Armstrong-Helouvry, "Stick-Slip Arising from Stribeck Friction," 1990.

[63] D.P. Soom, A. Hess, "Friction at a Lubricated Line Contact Operating at Oscillating Sliding Velocities," *Journal of Tribology,* vol. 112, pp. 147-152, 1990.

[64] Y. Lei, Y. Leng, "Stick-Slip Friction and Energy Dissipation in Boundary Lubrication," *Physical Review Letters,* 2011.

[65] Y. Lei, Y. Leng, "Force oscillation and phase transition of simple fluids under confinement," *Phys. Rev. Vol. 82, Iss. 4,* 2010.

[66] A. Vanossi, A. Benassi, N. Varini, E. Tosatti, "High-pressure lubricity at the meso- and nanoscale," *Phys. Rev. Vol. 87, Iss. 4,* 2013.

[67] D. Gourdon, J. N. Israelachvili, "Transitions between smooth and complex stick-slip sliding of surfaces," *Phys. Rev. Vol. 68, Iss. 2,* 2003.

[68] R.G. Xu, Y. Len, "Squeezing and stick–slip friction behaviors of lubricants in boundary lubrication," *Proceedings of the National Academy of Sciences Jun 2018, 115 (26) 6560-6565.*

[69] K. N. Elkholy, M. M. Khonsari, "Experimental Investigation on the Stick-Slip Phenomenon in Granular Collision Lubrication," *J. Tribol. Apr 2008, 130(2).*

[70] H. S. Han, K. H. Lee, "Experimental verification of the mechanism on stick-slip nonlinear friction induced vibration and its evaluation method in water-lubricated stern tube bearing," *Ocean Engineering,* pp. 147-161, 2019, vol. 182.

[71] P.A. Thompson, M. O. Robbins, "Origin of Stick-Slip Motion in Boundary Lubrication," *Science,* pp. 792-794, 1990, vol. 250.

[72] Y.S. Tarng, H. E. Cheng, "An investigation of stick-slip friction on the contouring accuracy of cnc machine tools," *International Journal of Machine Tools and Manufacture,* vol. 35 (4), p. 565–576, 1995.

[73] R. Pit, Q.H. Zeng, Q. Dai, B. Marchon, "Experimental study of lubricant-slider interactions," *IEEE Transactions on Magnetics,* pp. 740 - 742, 2003 vol.39.

[74] J-J. Sinou, J. Cayer-Barrioz, H. Berro, "Friction-induced vibration of a lubricated mechanical system," *Tribology International,* vol. 61, p. 156–168, 2013 .

[75] L. Marton, B. Lantos, "Modeling, Identification, and Compensation of Stick-Slip Friction," *IEEE Transactions on Industrial Electronics,* Vols. 54, no. 1, pp. 511-521, 2007.

[76] J. Gao, W. D. Luedtke, U. Landman, "Friction Control in Thin-Film Lubrication," *Journal of Physical Chemistry,* Vols. 102, no. 26, 1998.

[77] A. L. Demirel, S. Granick, "Friction Fluctuations and Friction Memory in Stick-Slip Motion," *Physical Review Letters,* Vols. 77, no. 21, 1996.

[78] G. Gao, "Stick-Slip Motion in Boundary Lubrication," *Tribology Transactions,* vol. 38, 1995.

[79] K. Tanaka , T. Kato , Y. Matsumoto, "Molecular Dynamics Simulation of Vibrational Friction Force Due to Molecular Deformation in Confined Lubricant Film," *Journal of Tribology,* Vols. 125, no. 3, pp. 587-591, 2003.

[80] O. M. Braun, M. Peyrard, "Friction in a solid lubricant film," *Physical Review Letters,* vol. 63, 2001.

[81] P.A. Thompson, G.S. Grest, M.O. Robbins, "Phase transitions and universal dynamics in confined films," *Physical Review Letters,* vol. 3448, 1992.

[82] Y. Lei, Y. Leng, "Stick-Slip Friction and Energy Dissipation in Boundary Lubrication," *Physical Review Letters,* vol. 107, 2011.

[83] J. N. Israelachvili, "18 - Friction and Lubrication Forces," in *Intermolecular and Surface Forces*, Academic Press, 2011, pp. 469-499.

[84] M. Schoen, C.L. Rhykerd, D.J. Diestler, J.H. Cushm, "Shear forces in molecularly thin films," *Science,* vol. 1223, p. 245, 1989.

[85] M. O. Robbins, P. A. Thompson, "Shear flow near solids: Epitaxial order and flow boundary conditions," *Phys. Rev. A,* vol. 6830, p. 41, 1990.

[86] A. A. Batista, J. M. Carlson, "Bifurcations from steady sliding to stick slip in boundary lubrication," *Physical Review E,* Vols. 57, no. 5, 1998.

[87] J. M. Carlson, A. A. Batista, "Constitutive relation for the friction between lubricated surfaces," *Physical Review E,* Vols. 53, no. 4, 1996.

[88] E. Rigaud, D. Mazuyer, J. Cayer-Barrioz, "Interfacial friction law for a circular EHL contact under free sliding oscillating motion," *Tribology Letters,* vol. 51, p. 1:419–430, 2013.

[89] A. Dmitriev, W. Österle,, "The Role of Solid Lubricants for Brake Friction Materials," *Lubricants,* vol. 4, p. 5, 2016.

[90] B. Podgornik, S. Jacobson and S. Hogmark, "DLC coating of boundary lubricated components - Advantages of coating one of the contact

surfaces rather than both or none," *Tribology International,* vol. 36, no. 11, p. 843–849, 2003.

[91] Y. Liu, A. Erdemir, and E. I. Meletis, "Influence of environmental parameters on the frictional behavior of DLC coatings," *Surf. Coatings Technol.,* vol. 94–95, p. 463–468, 1997.

[92] A. Grill, "Tribology of diamondlike carbon and related materials: An updated review," *Surf. Coatings Technol.,* vol. 94–95, p. 507–513, 1997.

[93] Y.R. Jeng, S. Islam, K.T. Wu, A. Erdemir and O. Eryilmaz, "Investigation of Nano-Mechanical and- Tribological Properties of Hydrogenated Diamond Like Carbon (DLC) Coatings," *J. Mech.,* vol. 33, p. 769–776, 2017.

[94] A. Ramalho, J.C. Miranda, "Tribological characterization of electroless NiP coatings lubricated with biolubricants," *Wear,* vol. 263, pp. 592-597, 2007.

[95] L.G. Yu, X.S. Zha, "The friction and wear properties of electroless Ni-polytetrafluoroethylene composite coating," *Thin Solid Films,* vol. 245, pp. 98-103, 1994.

[96] R. Taheri, I.N.A Oguocha, S. Yannacopoulos, "The tribological characteristics of electroless NiP coatings," *Wear,* vol. 249, pp. 389-396, 2001.

[97] X. Zhang, "The effect of Vibrations on the behaviour of Lubricated Elastohydrodinamic Contacts," Department of Engineering and Design, School of Engineering and Informatics, University of Sussex, 2017.

[98] N. De Laurentis, A. Kadiric, P.M. Lugt, P. Cann, "The influence of bearing grease composition on friction in rolling/sliding concentrated contacts," *Tribology International,* vol. 94, p. 624–632, 2016.

[99] H. Cen, P. M. Lugt, and G. Morales-Espejel, "On the Film Thickness of Grease-Lubricated Contacts at Low Speeds," *Tribol. Trans.,* vol. 57, no. 4, pp. 668-678, 2014.

[100] P. Cann, "Understanding grease lubrication," *Tribology Series,* vol. 31, pp. 573-581, 1996..

[101] J. Barauskas, M. Johnsson, F. Tiberg, "Self-Assembled Lipid Superstructures," *Nano Letters,* p. 1615–1619, 2005.

[102] W.H. Bauer, A.P. Finkelstein, S.E. Wiberley, "Flow PropertiesofLithiumStearate-OilModelGreasesasaFunctionofSoapConcentration and Temperature," *ASLE Transactions,* pp. 215-224, 1960.

[103] P. Lugt, "A Review on Grease Lubrication in Rolling Bearings," *Tribology Transactions,* vol. 52, pp. 470-480, 2009.

[104] P.M. Lugt, "Modern advancements in lubricating grease technology," *Tribology International,* vol. 97, p. 467–477, 2016.

[105] L. Salomonsson, G. Stang, B. Zhmud, "Oil/Thickener Interactions and Rheology of Lubricating Greases," *Tribology Transactions,* vol. 50, pp. 302-309, 2007.

[106] A. Neville, A. Morina, T. Haque, M. Voong, "Compatibility between tribological surfaces and lubricant additives—How friction and wear reduction can be controlled by surface/lube synergies," *Tribology International,* vol. 40, no. 10-12, pp. 1680-1695, 2007.

[107] Y. Kanazawa, R. S. Sayles, A. Kadiric, "Film formation and friction in grease lubricated rolling-sliding non-conformal contacts," *Tribology International,* vol. 109, pp. 505-518, 2017.

[108] T. Cousseau, B. Graça, A. Campos, J. Seabra, "Friction torque in grease lubricated thrust ball bearings," *Tribology International,* vol. 44, p. 523–531, 2011.

[109] P.M. Cann, "Grease lubrication of rolling element bearings - role of the grease thickener," *Lubr Sci,* p. 183–196, 2007.

[110] E. Marui, H. Endo, M. Hashimoto and S. Kato, "Some considerations of slideway friction characteristics by observing stick-slip vibration," *Tribology International,* pp. 251-262, 1996, Vol. 29, No. 3,.

[111] L. Wang, H. He, R. Lin, Z. Wu, Q. Wang, B.Yang and R. Chen, "Study on ameliorating friction noise of ABS materials by lubrication," *Polymer Testing,* 2020, Vol. 82.

[112] K. Li, X. Zhang, C. Du, J. Yang, B. Wu, Z. Guo and C. Dong et all, "Friction reduction and viscosity modification of cellulose nanocrystals as biolubricant additives in polyalphaolefin oil," *Carbohydrate Polymers,* pp. 228-235, 2019, Vol. 220.

[113] S. Yamada, K.A. Inomata, E. Kobayashi, et al., "Effect of a Fatty Acid Additive on the Kinetic Friction and Stiction of Confined Liquid Lubricants," *Tribology Letters ,* 2016, Vol. 64, no. 23 .

[114] F. Yang, C. An Tan, F. Chen , "Application of the empirical mode decomposition method to the identification of disc brake squeal," *Proceedings of IMECE2002, ASME International Mechanical Engineering Congress & Exposition,* November 17th, 2002, New Orleans, Louisiana.

[115] E. Lagarde and F. Negrello, "Patent "EP2230415A1 - Spring brake for the actuator of a screen for a building and actuator equipped with such brake," 2010.".

[116] P. Foucher and E. Lagarde, "FREIN II, Logiciel de calcul des ressorts-frein d'intérieur et d'extérieur," SOMFY R&D Center, Cluses, France, 2008.

[117] R. Sourain, "Calcul Pression de Contact," SOMFY TECH PROGRAM, Cluses, France, 2020.

[118] L. K. Johnson, Contact Mechanism, Cambridge University Press, 1985, pp. 84-92, ISBN: 978-0521347969.

[119] S. R. Singiresu, The Finite Element Method In Engineering, 5ed, 2011.

[120] D. Arbtip and S. Kenji, "Inverse adaptation of a hex-dominant mesh for large deformation finite element analysis," *Computer-Aided Design,* p. 427 – 438, 2007, Vol. 39, no. 5.

[121] L. Baillet, T. Sassi, "Mixed finite element formulation in large deformation frictional contact problem," *Revue Européenne des Eléments Finis, Hermès,* pp. 287-304, 2005.

[122] S. Bull, "Tribology of carbon coatings: DLC, diamond and beyond," *Diamond and Related Materials.*

[123] A. M. Wahl, Mechanical Springs, 2nd ed., New York, US: McGraw-Hill, 1963.

[124] A. K. Chopra, Dynamics of structures: Theory and Applications to Earthquake Engineering, New York, US: Prentice Hall, 2012.

[125] M. Popov, "Critical velocity of controllability of sliding friction by normal oscillations in viscoelastic contacts," *Facta Universitatis. Series: Mechanical Engineering,* pp. 335-341, vol. 14, 2016.

[126] M.O. Robbins, P.A. Thompson, "Critical velocity of stick-slip motion," *Science,* p. 253(5022):916, 1991.

[127] A. Papangelo, M. Ciavarella, N. Hoffmann, "Subcritical bifurcation in a self-excited single-degree-of-freedom system with velocity weakening–strengthening friction law: analytical results and comparison with experiments," *Nonlinear Dynamic,* pp. 2037–2046, vol. 90, 2017.

[128] U. Galvanetto, S. R. Bishop, "Dynamics of a Simple Damped Oscillator Undergoing Stick-Slip Vibrations," *Meccanica,* pp. 337–347, vol. 34, 1999.

[129] B. Armstrong-Hélouvry, "Stick Slip and Control in Low-Speed Motion," *EEE Trans. Automat. Contr.,* pp. 1483–1496, vol. 38, no. 10, 1993.

[130] E. Rabinowicz, "The Intrinsic Variables affecting the Stick-Slip Process," *Proceedings of the Physical Society,* 1958.

[131] H. Blok, "Foundamental Aspects of Boundary Friction," *J.Society of Automotive Engineer,* pp. 275, vol. 46, 1940.

[132] L. Tang, X. Zhu, C. Shi, J. Sun, "Investigation of the damping effect on stick-slip vibration of oil and gas drilling system," *Advances in Vibration Engineering,* pp. 79-86, vol. 4, 2016.

[133] M. Rovere, "20170711 - ANALYSE DOE, Identification des sources de bruit," SOMFY SASA, R&D Center, DT Mechanical, Cluses, France, 2017.

[134] *Deutsches Institut für Normung. (2007), Testing of Lubricants—Determination of Shear Viscosity of Lubricating Greases by Rotational Viscosimeter—Part 1: System of Cone/Plate.*

[135] W. Österle, A. Dmitriev, "The Role of Solid Lubricants for Brake Friction Materials," *Lubricants,* 2016, vol. 4, no. 1.

[136] V. Renman, "Tribological testing of DLC coatings for automotive applications," *ISSN: 1650-8297,* p. 19:42, 2012, UPTEC K12 010.

[137] B. Podgornik, J. Vižintin, "Tribological reactions between oil additives and DLC coatings for automotive applications," *Surface and Coatings Technology,* pp. 1982-1989, vol. 200, 2005.

Folio Administratif

THESE DE L'UNIVERSITE DE LYON OPEREE AU SEIN DE L'INSA LYON

NOM : Mme. GHEZZI DATE de SOUTENANCE : 14/12/2020

Prénoms : Ilaria

TITRE : Tribological and Vibro-acoustic Behavior of a Lubricated Contact Subjected to the Stick-Slip Phenomenon: The Case of the Spring-Brake System

NATURE : Doctorat Numéro d'ordre : AAAALYSEIXXXX

Ecole doctorale : MEGA

Spécialité : Génie Mécanique

RESUME :
The main objective of the PhD thesis is the analysis of stick-slip phenomena in lubricated contacts, by merging the physical, experimental and numerical points of view and proposing a novel methodological approach, applied here to an industrial case. Nowadays, in the field of applied mechanics and tribology, one of the most important challenges is the ability to predict and reduce surface damages, failure of machine components and undesirable frictional and dynamic characteristics. In particular, the appearance of friction-induced vibrations at the contact is hardly controllable and can result in high local contact pressure, elevated stresses, system oscillations, discontinuous motion and premature failure [1]. Understanding the conditions for which the system is more predisposed to the stick-slip phenomenon may allow preventing the appearance of such instabilities, and the related vibrations and noise emission. Friction-Induced Vibrations are a phenomenon that engages multiple scientific challenges, due to the complexity of their physics. Focusing the attention on stick-slip phenomena, these are generally characterized by a saw-tooth displacement-time evolution [2]. Each change in the contact parameters influences directly the dynamic and frictional response of the system, due to the mutual influence of the local scale (contact) and the system scale (macroscopic frictional and vibrational response). Moreover, the presence of a lubricant, and in particular of grease, at the contact interface, increases the complexity of the phenomenon, from both a tribological and dynamic point of view. Lubricated systems are supposed to reduce the frictional losses and wear, but they can also collaborate in the appearance of dynamic contact instabilities, due to the friction-velocity characteristics when passing from boundary to mixed contact regimes [3]. The complex rheology of a grease, function of both the matrix, additive and oil responses, becomes then a key point for the occurrence and evolution of stick-slip. Despite the great importance of this phenomenon, from both scientific and industrial points of view, a lack emerges into the literature about stick-slip of lubricated interfaces. The few works are manly focused on molecular dynamics simulations and numerical modelling of the dynamical response of the system. The different role of the grease components, during the sliding, is nowadays still not clear. Nevertheless, the complex rheology of a grease, function of both the thickener, the base oil and the additives, is a key point for understanding and controlling the occurrence and evolution of stick-slip. Moreover, a general approach is needed to account for the coupling between the local phenomena (e.g. lubricated contact response) and the system dynamic response. Aiming to improve the understanding of stick-slip in lubricated contacts, the present Ph.D. work proposes a novel methodological approach to the stick-slip problem of a lubricated contact, referring to a real industrial case, in order to deploy the obtained results in a more realistic and detailed manner. The subject of the investigation is a mechanical brake used in tubular electric actuators [4, 5], which can present frictional instabilities originated at the lubricated contact between the two main brake components. The methodology used is twofold: i) on one hand, experimental tests are carried out to understand the local frictional response of the lubricated contact; ii) on the other hand, a lumped model is created in order to simulate and analyse the system dynamic response. Introducing

the information about the local lubricated contact behaviour (friction law), achieved experimentally, into the numerical model, it is possible to investigate the parameters for which the system is more predisposed to the stick-slip phenomenon and recreate a representative scenario of its appearance. Particular attention has been placed on the analysis of the lubricant rheology, dealing with different types of lubricants and regimes of lubrication, with both oils and greases. The frictional response has been thus related to the different contributions of the grease components (i.e. thickener, base oil and additives) on the rheology at the interface. The obtained local information have been then integrated in the lumped model to evaluate the unstable dynamic response of the entire system (i.e. the stick-slip phenomena) and identify the lubrication parameters that most influence its appearance. The numerical analysis had the dual objective of understanding the role of the local contact response in the system instability and investigating the stick-slip occurrence as a function of the key system parameters. The obtained results allowed to identify the lubrication components, and the respective friction-velocity curves, more favourable for the stick-slip occurrence. Combining the grease rheology evolutions with the stick-slip dynamic response represents a further challenge in both the domains of research. The Ph.D. thesis has been developed in collaboration between the Sapienza University of Rome, Department of Mechanical and Aerospace Engineering (Rome, Italy), the Institut National des Sciences Appliquées (INSA) of Lyon, laboratory LaMCoS (Lyon, France), and the company SOMFY S.A. (Cluses, France).

MOTS-CLÉS : Friction-Induced Vibrations, Stick-Slip, Greased Contact, Tribology, Lubrication

Laboratoire (s) de recherche :
Laboratoire de Mécanique de Contact et des Structures (LaMCoS) UMR CNRS 5259-INSA de Lyon, France
Dipartimento di Ingegneria Meccanica e Aerospaziale (DIMA), La Sapienza-Università di Roma, Italy

Directeurs de thèse:
Yves BERTHIER, Directeur de Recherche, CNRS Lyon
Francesco MASSI, Professor, Università di Roma La Sapienza

Président de jury :

Composition du jury :

Hoffmann, Norbert	Professeur,	Hamburg University of Technology	Rapporteur
Meziane, Anissa	Professeur,	Université Bordeaux	Rapporteur
Fillon, Michel	Directeur de Recherche,	Institut Pprime	Examinateur
Baillet, Laurent	Professeur,	Université Grenoble Alpes-IsTerre	Examinateur
Berthier, Yves	Directeur de Recherche,	CNRS Lyon	Directeur de thèse
Massi, Francesco	Professeur,	La Sapienza – Università di Roma	Directeur de thèse
Le Cœur, Cédric	Ingénieur,	SOMFY SASA	Invité
Tonazzi, Davide	Ph.D.,	La Sapienza – Università di Roma	Invité